TT 64-71325

254p

TRANSLATION

COSMIC RESEARCH

Volume 2 - Number 4 - 1964

FOREIGN TECHNOLOGY DIVISION

AIR FORCE SYSTEMS COMMAND

WRIGHT-PATTERSON AIR FORCE BASE

OHIO

UNEDITED ROUGH DRAFT TRANSLATION

COSMIC RESEARCH

English Pages: 241

S/0293-064-002-004

Akademiya Nauk SSSR

KOSMICHESKIYE ISSLEDOVANIYA

Tom II

Vypusk 4

TABLE OF CONTENTS

APPROXIMATE CALCULATION OF TRAJECTORY FOR ENTRY INTO ATMOSPHERE

V. A. Yaroshevskiy

I

The introduction of certain assumptions characteristic of the basic segment of an atmosphere-entry trajectory makes it possible to reduce the equations of motion to a nonlinear second-order equation. By means of this equation it becomes possible to derive approximate analytical solutions for the flight trajectory and it also becomes possible to analyze the influence of the entry conditions and of the aerodynamic quantities on the most important parameters which are of practical interest, i.e., maximum G-forces, maximum heat flow, etc.

INTRODUCTION

In the literature devoted to problems of returning an artificial satellite, the atmosphere-entry trajectory is frequently divided into three characteristic segments [1].

The first segment, known as the transitional segment, encompasses that part of the trajectory from the descent of the satellite from its initial orbit to entry into the dense layers of the atmosphere. The aerodynamic forces exerted along this segment are not excessively great in comparison with gravitational forces, and they may be regarded as perturbing in nature.

The second basic segment is the most difficult in the sense of aerodynamic load and intensity of heat transfer. It is a characteristic of this segment that the aerodynamic resistance along it considerably ex-

- 1 -

ceeds the projection of the forces of gravity to the velocity-direction line.

The third and final segment is characterized by a rapid growth of the negative angle of trajectory inclination, and here the force of resistance tends to balance the projection of the forces of attraction onto the velocity-direction line.

Occasionally yet another segment — a segment intermediate between the transitional and basic segments — is introduced. In many cases, when the angle of trajectory inclination upon entry into the atmosphere is not excessively small, this segment is not too great in extent and plays no significant role.

Naturally, of greatest interest is the investigation of the main [basic] trajectory segment, since it is precisely here that the acceleration and heat flow attain their maximum values.

In the majority of initial works devoted to an examination of the atmosphere-entry trajectory it was assumed that the angle of trajectory inclination to the local horizon was constant, i.e., a trajectory of spiral shape was assumed. The case c_x = const was considered by Allen and Eggers [2]; the case $c_x = A + B/V^2$ was investigated by Kaepeller and Kuebler [3]; the case $c_x \sim V^n$ was considered by V.Ya. Neyland.

The attempt to refine this solution by introducing the assumption of a constant vertical velocity was made in Reference [4]. The atmosphere-entry trajectories for a flying craft exhibiting lift were considered in References [5, 6].

The main segment of the atmosphere-entry trajectory, with consideration of a change in the angle of trajectory inclination, was examined in References [7-9], as well as independently in a study by the author of the present article, accomplished during the first half of 1959, and providing the basis for the present article.

- 2 -

In these works the problem is reduced to the solution of a non-linear second-order differential equation. An outstanding feature of the present article is the construction of approximate analytical solutions for such an equation, reduced to a simpler form.

The analytical solutions exhibit a lower accuracy than the numerical solutions of the initial equation of motion, but they are nevertheless useful for a number of reasons. They make it possible to ascertain the basic factors affecting the nature of the entry trajectory, they clearly define the structures of various types of trajectories, and they make it possible rapidly to carry out a comparative analysis of aerodynamic loads and thermal regimes. Finally, the reduction of the equations of motion to simplest form facilitates the solution of the variation problem associated with the entry of spacecraft into the atmosphere.

No attempt is made in this article to present systematic data regarding atmosphere-entry trajectories, since such data can be found in the well-known works of Chapman [8, 10, 11].

Nomenclature

V   velocity, m/sec,

H   height, m,

L   range, m,

θ local angle of trajectory inclination, rad,

t   time, sec,

R   radius of planet (Earth), m,

g   acceleration of the force of gravity, m/sec^2,

$dy/dx = -\sqrt{R\lambda}\,\theta,\ c_1 = -\sqrt{R\lambda}\,\theta_{нач},$

ρ density, kg·sec^2/m^4,

λ exponent in density formula, 1/m,

$q = \rho V^2/2 -$ ram pressure, kg/m^2,

- 3 -

G   weight of spacecraft, kg,

$\underline{m}$ mass of spacecraft, $kg \cdot sec^2/m$,

S   characteristic area of spacecraft, m^2,

$\underline{r}$ radius of nose of body, $\underline{m}$,

c_x resistance coefficient,

c_y lift coefficient,

$\sigma_x = c_x S / G$ ballistic parameter, m^2/kg,

$n_x = \sigma_x g$ longitudinal acceleration,

T   temperature, deg. K,

$q_{k.1.}$, $q_{k.t.}$ specific heat flows in presence of laminar or

        [turbulent] boundary layer, $kcal/m^2 \cdot sec$,

Q   total quantity of heat per unit surface, $kcal/m^2$,

$$y = \frac{c_x S}{2m} \sqrt{\frac{R}{\lambda}} \rho - \text{ in case } c_x = \text{const,}$$

$x = \ln V_{кр} / V -$ in case c_x = const,

$dy/dx = -\sqrt{R\lambda}\,\theta, \; c_1 = -\sqrt{R\lambda}\,\theta_{нач},$
$\bar{V} = V / V_{кр}.$

<center>Subscripts</center>

кр = kr = krugovaya skorost' = angular velocity

нач = nach = nachal'noye znacheniye = initial value

к.л. and к.т. = k.l. and k.t. = konvektivnyy laminarnyy and tur-

        bulentnyy = convective heat flow in presence of

        laminar or turbulent boundary layer, respectively

рад = rad = radiatsionny teplovoy potok = radiation heat flow

0 = planetary surface.

The prime denotes differentiation with respect to $\underline{x}$.

I. DERIVATION OF APPROXIMATE EQUATIONS OF MOTION

1. Statement of Problem

    To reduce the equation of motion for a spacecraft along the main

segment of the atmosphere-entry trajectory to its simplest form, we propose that:

a) the planet exhibit an ideal spherical shape, and that the field of gravitation be central.

b) the equatorial velocity of planetary rotation and that of its ambient atmosphere be small in comparison with the velocity of space-craft motion.

c) the altitude at which the main segment of the atmosphere-entry trajectory begins be small in comparison with the planetary radius, i.e., $H \ll R$.

Hence it follows that

$$g = g_0 \left(\frac{R}{R + H} \right)^2 \approx g_0 = \text{const,}$$
$$R + H \approx R = \text{const,}$$
$$V_{\text{кр}} = \gamma \overline{(R + H)g} \approx \gamma \overline{Rg_0} = \text{const.}$$

d) the temperature of the atmosphere be constant, from which it follows that the exponential relationship between density and altitude is as follows:

$$\rho \approx \rho_0 c^{-\lambda H}. \tag{1.1}$$

If the aerodynamic coefficients are functions of the Mach number, it may be held that they are functions only of velocity, since the speed of sound, proportional to the root of the temperature, should be regarded as constant.

e) the angle of trajectory inclination θ is small, $|\theta| \ll 1$, so that $\sin \theta \approx \theta$ and $\cos \theta \approx 1$.

f) for the main segment of the atmosphere-entry trajectory the following inequality be characteristic:

$$|\theta| \ll n_x.$$

g) on examination of the entry of the spacecraft into the atmos-

- 5 -

phere from a virtually circular orbit the following limit initial conditions are assumed:

$$\rho_{\text{нач}} = 0, \quad V_{\text{нач}} = V_{\text{кр}}.$$

Assumption <u>d</u> for the atmosphere of the earth is not sufficiently valid, since even in the range of altitudes from 20 to 80 km the temperature values vary within limits of $\pm 20\%$. As will be shown below, the introduction of this assumption may, in individual cases, introduce an error of the order of $\pm 20\%$ in the determination of the maximum acceleration; however, this error may be corrected.

Assumption <u>e</u> is valid because workable values of maximum acceleration are obtained only for trajectories with small angles of inclination.

The inequality in <u>f</u> is characteristic of the main segment of the atmosphere-entry trajectory. This inequality is equivalent to the assumption pertaining to the relative smallness of the influence exerted by gravitational forces on a change in velocity. In a number of cases the violation of the inequality in <u>f</u> leads to no noticeable error because even in the absence of aerodynamic forces a change in velocity is associated with a change in altitude by the equality

$$\frac{\Delta V}{V} \approx -\frac{g \Delta H}{V^2}.$$

Hence it follows that with values of V of the order of the circular velocity and with ΔH of the order of several tens of kilometers velocity changes only by an order of magnitude of one per cent.

Assumption <u>g</u> is valid because the density ρ along the main segment of the trajectory, where the maximum acceleration and heat-flow values are attained, considerably exceeds the density at the beginning of the main segment. This assumption contradicts assumption <u>f</u> and for this

reason, strictly speaking, the solution for the initial segment of the trajectory is not valid; however, the true solution, as a rule, very rapidly approaches the solution with the limit initial condition $\rho_{nach} = 0$.

2. Evaluation of Certain Assumptions on the Example of a Spiral Trajectory

Let us examine a spiral trajectory $\theta = $ const for $c_x = $ const, $g \approx$ $\approx$ const, holding that $\rho = \rho_0 e^{-\lambda H}$, $V_{max} = \sqrt{Rg_0}$. Then the equation of motion is reduced to the form

$$dz/dH = aze^{-\lambda H} - g,$$ (2.1)

where

$$z = \frac{V^2}{2}, \qquad a = \frac{c_x S \rho_0}{m|\sin\theta|}.$$

Having integrated this equation, we obtain

$$z = \frac{Rg}{2} e^{-(\xi - \xi_{max})} + \frac{g}{\lambda} e^{-\xi} \int_{\xi_{max}}^{\xi} \frac{e^{\eta} d\eta}{\eta},$$ (2.2)

where

$$\xi = \frac{a}{\lambda} e^{-\lambda H}, \qquad \xi_{max} = \frac{a}{\lambda} e^{-\lambda H_{max}}.$$

Let us present this expression in the form

$$z = z_* + \delta z,$$

where

$$z_* = (Rg/2)e^{-\xi}$$ (2.3)

is the solution of Eq. (2.1), derived by neglecting the term g for the limit initial condition $\rho_{nach} = 0$, and δz is a small correction which for small ξ_{nach} can be presented in the form

$$\delta z = \xi_{max} z_*(\xi) + (1.32 + \ln \xi / \xi_{max}) g / \lambda e$$ (2.4)

(the second term in (2.4) is derived through the asymptotic expansion of the integral exponential function).

If we maintain that $z \approx z_*$, the acceleration $n_x = (|\sin \theta| R\lambda / 2)\xi e^{-\xi}$ attains its maximum $\xi = 1$

$$n^{\bullet}_{x\,max} = \frac{|\sin \theta| R\lambda}{2c} \approx 170 |\sin \theta|$$

(for the earth).

It is not difficult to prove that the refined maximum acceleration is attained at $\xi = 1 + O(e)$ and is equal to

$$n_{x\,max} = n^{\bullet}_{x\,max} [1 + e + O(e^2)],$$

where

$$e = \delta z(1) / z_*(1).$$

Hence we obtain that

$$\frac{\delta n_{x\,max}}{n^{\bullet}_{xmax}} \approx \frac{1.32 / \lambda + H_{\text{нач}} - H_*}{R} + \frac{\rho(H_{\text{нач}})}{\rho(H_*)}, \qquad (2.5)$$

where H_* is defined from the condition $\xi = c_x S\rho(H_*) / \lambda m |\sin \theta| = 1$. If, for example, H_{nach} = 100 km, and H_* = 50 km, $\delta n_{x\,max} / n^{\bullet}_{x\,max} \approx 0.01$, i.e., the error is small.

Let us examine what error will be introduced into the definition of $n_{x\,max}$ by the assumption of an isothermal atmosphere, neglecting the term g in (2.1), holding $c_x = c_x(V)$.

Let us write the equation of motion

$$V \frac{dV}{dH} = \frac{c_x(V) V^2 S\rho(H)}{2m |\sin \theta|}, \qquad (2.6)$$

the equation of hydrostatics

$$dp / dH = -\rho(H)g \qquad (2.7)$$

and the equation of the state of the gas

$$p(H) = \rho(H) R_r T(H), \qquad (2.8)$$

where R_g is the gas constant.

From (2.6) and (2.7) we obtain that for small ρ_{nach}

$$\int_{V_{max}}^{V} \frac{dV}{V c_x(V)} - \frac{S}{2G|\sin\theta|} \int_{H_{max}}^{H} g\rho \, dH \approx - \frac{Sp}{2G|\sin\theta|}.$$

Hence

$$V = f(p).$$

The expressions for accelerations and heat flows received by the craft are approximately proportional to

$$\rho^{k} a(V) = \left(\frac{p}{R_r T}\right)^{k} a(V) = \left(\frac{p}{R_r}\right)^{k} a f(p) \frac{1}{T^{k}} = \frac{b(p)}{T^{k}} = \frac{\bar{b}(H)}{T^{k}}. \qquad (2.9)$$

Let us hold that T changes slowly as a function of altitude. In this case we can write: $T = T(\epsilon H)$, where ϵ is a small parameter.

Let the function $b(p) = \bar{b}(H)$ attain its maximum $H = H_*$; $\bar{b}(H_*) = b_{max}$. It is then easy to prove that $\rho^{k} a(V) = \bar{b}(H)/T^{k}(\epsilon H)$ attains its maximum $H = H_* + O(\epsilon)$ and that

$$[\rho^{k} a(V)]_{max} = b_{max}/T^{k}(\epsilon H_*) + O(\epsilon^2). \qquad (2.10)$$

Thus we derive a simple rule for the refinement of the maximum acceleration and heat-flow values obtained on the assumption of an iso-thermal atmosphere. A certain mean value of the temperature $T_{sr} \approx 240^{\circ} K$ corresponds to the "average" value of $\lambda_{sr} \approx 1/7000$ m^{-1}. Let us calculate the maximum magnitude of $\rho^{k} a(V)$ for $T_{sr} = $ const

$$[\rho^{k} a(V)]_{max} = \frac{b_{max}}{T^{k}_{cp}} = A.$$

Let us define the value of H_*, corresponding to b_{max}. The refined value of the maximum magnitude of $\rho^{k} a(V)$ with an accuracy to $O(\epsilon^2)$ is equal to

$$[\rho^{k} a(V)]_{max} = A \left[\frac{T_{cp}}{T(H_*)}\right]^{k}. \qquad (2.11)$$

For example, the value of the maximum acceleration with $\theta = $ const,

- 9 -

c_x = const is equal to

$$n_{x max} \approx 170 |\sin 0| \frac{T_{cp}}{T(H_*)},$$

where H_* is defined from the relationship

$$\frac{c_x S \rho (H_*)}{m \lambda_{cp} |\sin 0|} = 1. \qquad (2.12)$$

Hence we can derive $n_{x\ max}$ as a function of H_*, i.e., in final analysis as a function of σ_x, since the altitude H_* is a function of the magnitude σ_x.

Since the temperature exhibits a maximum value at H = 50 km, the function $n_{x max}(\sigma_x)$ exhibits a minimum. Thus the assumption of an isothermal atmosphere leads to marked errors in the determination of the maximum accelerations and heat flows; however, the result can be corrected, as was indicated earlier. The refinement of the result can be achieved by using the values of λ_* that are not equal to $\lambda_{sr} = (1/7000)$ m^{-1}, but rather to the range of altitudes H ~ H_* of interest to us

$$\lambda_* = - \frac{1}{\rho} \frac{d\rho}{dH} (H_*).$$

3. Derivation of Equation of Motion

If we adopt only assumptions a) and b), the equations of motion are written as follows:

$$\frac{dV}{dt} = - \frac{c_x(M) S \rho(H) V^2}{2m} - g(H)\sin 0, \qquad (3.1)$$

$$V \frac{d\theta}{dt} = \frac{c_y(M) S \rho(H) V^2}{2m} - \cos 0 \left(g(H) - \frac{V^2}{R+H} \right). \qquad (3.2)$$

The kinematic relationships have the following form:

$$dH / dt = V \sin 0, \qquad (3.3)$$

$$dL / dt = VR \cos 0 / (R + H). \qquad (3.4)$$

Introducing additionally assumptions c), d), e), and f), let us

rewrite the system of equations in the following form:

$$\frac{dV}{dt} = -\frac{c_x(V)S}{2m}\rho_0 V^2 e^{-\lambda H},$$ (3.5)

$$V\frac{d\theta}{dt} = \frac{c_y(V)S}{2m}\rho_0 V^2 e^{-\lambda H} - g + \frac{V^2}{R},$$ (3.6)

$$dH / dt = V\theta,$$ (3.7)

$$dL / dt = V.$$ (3.8)

Excluding time, we will obtain

$$\frac{dH}{dV} = -\frac{\theta}{\dfrac{c_x S\rho_0}{2m}Ve^{-\lambda H}},$$

$$V\frac{d\theta}{dV} = -\frac{c_y}{c_x} + \frac{g - \dfrac{V^2}{R}}{\dfrac{c_x S\rho_0}{2m}V^2 e^{-\lambda H}}.$$

Let us represent c_x and c_y in the form of a function of V:

$$c_x = c_x(V), \quad c_y = c_y(V).$$

Let us introduce the dependent variable $\underline{y}$ and the independent variable $\underline{x}$

$$y = \frac{c_x(1)S}{2m}\sqrt{\frac{R}{\lambda}}\rho,$$ (3.9)

$$x = -\int_1^V \frac{c_x(1)dV}{c_x(V)V}.$$ (3.10)

Effecting the substitution of the variables and excluding θ, we will obtain one second-order equation

$$\frac{d^2y}{dx^2} = -\gamma R\lambda \frac{c_y[V(x)]}{c_x(1)} + \frac{\dfrac{1}{V^2(x)} - 1}{y}.$$ (3.11)

The remaining trajectory parameters are defined from the following relationships:

$$\theta = -\frac{1}{\gamma R\lambda}\frac{dy}{dx}.$$ (3.12)

$$n_x = \gamma R\lambda y \frac{c_x[V(x)]}{c_x(1)}V^2(x)$$ (3.13)

$$n_v = \gamma R \lambda \bar{y} \frac{c_v[\bar{V}(x)]}{c_x(1)} \bar{V}^2(x) \tag{3.14}$$

$$t = \frac{1}{\sqrt{g\lambda}} \int_{\lambda}^{x} \frac{dx}{y\bar{V}(x)} \tag{3.15}$$

$$l = \sqrt{\frac{R}{\lambda}} \int_{x_{\text{max}}}^{x} \frac{dx}{y} \tag{3.16}$$

It follows from Relationship (3.12) that the straight-line segments of function y(x) correspond to segments of the trajectory for θ = const.

A simpler and more interesting case from the standpoint of practice is the one in which c_x = const, c_y = const, since along the main segment of the atmosphere-entry trajectory the M(ach) numbers are great and the aerodynamic characteristics of configurations not exceedingly fine are virtually independent of M(ach) number.

The equation of motion in this case is written in the following form:

$$\frac{d^2y}{dx^2} = -\gamma R\lambda \frac{c_v}{c_x} + \frac{e^{2x}-1}{y}. \tag{3.17}$$

Here

$$x = \ln V_{\text{кр}} / V.$$

In the case of descent to the earth it may be held that

$$\lambda \approx (1/7000) \ \text{м}^{-1}, \quad y \approx 1,04 \cdot 10^6 \sigma_x \rho,$$
$$\sqrt{R\lambda} \approx 30, \quad 1/\sqrt{g\lambda} \approx 26,5 \ \text{sec},$$
$$\sqrt{R/\lambda} \approx 212 \ \text{km}, \quad V_{\text{кр}} \approx 7850 \ \text{m/sec}.$$

Let us note that Eq. (3.11) can be made somewhat more complex in order to take into consideration the nonisothermal nature of the atmosphere which, as was shown above, exerts the greatest influence on the accuracy of the results. Thus, for the case c_x = const this equation assumes the following form:

$$\frac{d^2\bar{p}}{dx^2} = -\frac{c_v}{c_x} + \frac{e^{2x}-1}{\bar{\rho}(\bar{p})} \tag{3.18}$$

where

$$\bar{p} = \frac{c_x S}{2G} p, \quad \bar{\rho} = \frac{c_x SR}{2m} \rho = \bar{p} \frac{Rg}{R_r T(\bar{p})},$$

$$x = \ln \frac{V_{\kappa\phi}}{V}, \quad \frac{d\bar{p}}{dx} = -0,$$

$$n_x = \bar{\rho} e^{-2x}, \quad L = R \int_{x_{\text{макс}}}^{x} \frac{dx}{\bar{\rho}},$$

$$t = \sqrt{\frac{R}{g}} \int_{x_{\text{макс}}}^{x} \frac{e^x dx}{\bar{\rho}}.$$

To carry out a comparative evaluation of the thermal regimes along the various atmosphere-entry trajectories, simple approximation formulas for the convective heat fluxes received by the nose of the spacecraft are employed, and in this connection it is held that the nose is spherical in shape.

As a rule, along the main segment of the trajectory it may be held that a flow of a continuous medium is attained.

In the case in which the boundary layer is laminar, the heat flow attains its maximum value at the critical [stagnation] point (the foremost point on the sphere). In the case of large M(ach) numbers, the magnitude of the convection heat flow at the critical [stagnation] point for an isothermal atmosphere may be expressed by the [following] formula for

$$q_{\text{к. л}} = C \rho^{0.5} V^l r^{-0.5},$$

where $3.1 \leqslant l \leqslant 3.25$ ([12]−[15]).

For a comparative analysis the present article uses the formula from [14], which apparently gives a certain exaggerated value for the heat flow upon entry into the earth's atmosphere

$$q_{\text{к. л}} = 8.8 \cdot 10^4 \sqrt{\frac{\rho}{r}} \left(\frac{V}{V_{\kappa\rho}} \right)^{3.25} \text{kcal}/(\text{m}^2/\text{sec}), \quad (3.19)$$

where it is assumed that $V_{kr} = 7850$ m/sec. In the denotations of the

- 13 -

present article for c_x = const this formula is written as follows:

$$q_{\text{к. л.}} = \frac{85 y^{0.5} c^{-3.25x}}{\rho^{0.5} \sigma_x^{0.5}} \ \text{kcal}/(\text{m}^2/\text{sec}). \qquad (3.20)$$

If a turbulent boundary layer is achieved (which is less likely), the convective heat flux attains its maximum value in the section in which passage through the sonic line occurs.

With analogous assumptions the expression for the heat flow is defined by the formula

$$q_{\text{к. т.}} = C \rho^{0.8} V^l r^{-0.2},$$

where $3.19 \leqslant l \leqslant 3.48$ ([16, 17]).

In the present article use is made of the formula [16]

$$q_{\text{к. т.}} = 1.6 \cdot 10^6 \frac{\rho^{0.8}}{r^{0.2}} \left(\frac{V}{V_{\text{кр}}} \right)^{3.19} \ \text{kcal}/\text{m}^2 \text{sec} \qquad (3.21)$$

or

$$q_{\text{к. т.}} = \frac{25 y^{0.8} c^{-3.19x}}{\sigma_x^{0.5} r^{0.2}} \ \text{kcal}/\text{m}^2 \text{sec}. \qquad (3.22)$$

The radiation heat flow from the air heated behind the compression shock is defined by the following formula ([18])

$$q_{\text{рад. в.}} \approx C \rho^k V^l r,$$

where $1.5 \leqslant k \leqslant 1.8, \quad 10 \leqslant l \leqslant 20.$

The role of this type of heat transfer in the case of entry into the atmosphere at circular velocity for spacecraft of dimensions that are not too large is not great.

The radiation heat flow from the spacecraft is defined by the formula

$$q_{\text{рад}} = \varepsilon \sigma T_w^4 \ \text{kcal}/\text{m}^2 \text{sec}, \qquad (3.23)$$

where ε is the emissivity, σ is the Stefan-Boltzmann constant, and T_w is the wall temperature.

If it is maintained that a quasisteady thermal regime is achieved during the course of the flight, the equilibrium wall temperature is determined from the relationship

$$T_w = (q_\text{к} / \varepsilon \sigma)^{1/4}. \tag{3.24}$$

The maximum equilibrium temperature which is defined by the value of the maximum convection heat flow is one of the criteria defining the thermal regime.

Another simple criterion is the value of the total heat flow received per unit of spacecraft surface during the descent

$$Q_\text{к} = \int q_\text{к} dt.$$

Having made use of Formulas (4.3) [sic] and (4.6) [sic], it is not difficult to see that with c_x = const in the case of a descent to the earth

$$Q_{\text{к. з.}} = \frac{2250}{r^{0.5} \sigma_x{}^{0.5}} \int_{x_\text{мах}}^{x} \frac{e^{-2.25x} dx}{y^{0.5}} \ \text{kcal/m}^2, \tag{3.25}$$

$$Q_{\text{к. т.}} = \frac{665}{r^{0.2} \sigma_x{}^{0.8}} \int_{x_\text{мах}}^{x} \frac{e^{-2.19x} dx}{y^{0.2}} \ \text{kcal/m}^2. \tag{3.26}$$

II. BALLISTIC TRAJECTORIES

4. A Ballistic Trajectory with An Initial Angle of Inclination Equal to Zero

In the case $c_y = 0$, $c_x = \text{const}$ the equation of motion assumes a very simple form

$$d^2y / dx^2 = (e^{2x} - 1) / y. \tag{4.1}$$

Let us consider the trajectory for the descent of a satellite into the atmosphere from an orbit decaying under the action of resistance forces. In this case the initial conditions take the following form ([7, 19]):

$$y_0(0) = 0, \quad y_0'(0) = 0.$$

In the vicinity x = 0 Eq. (4.1) changes into the equation yy" = 2x,

having the solution $y = \sqrt{8/3}x^{3/4}$, which satisfies the given initial conditions. Proceeding from this, let us seek a solution of the form

$$y_0 = \sqrt{8/3}x^{3/4}(1 + a_1 x + a_2 x^2 + \dots). \qquad (4.2)$$

Expanding the right-hand part of the equation in series and equating identical powers of x, let us define the coefficients a_i in succession by the recursion formula

$$a_k = \frac{\dfrac{2^k}{(k+1)!} - \dfrac{1}{3}\sum_{m=1}^{k-1}(2m+1)(2m+3)a_m a_{k-m}}{1 + \dfrac{(2k+1)(2k+3)}{3}}. \qquad (4.3)$$

$$a_0 = 1, \quad a_1 = 1/6, \quad a_2 = 1/24,$$
$$a_3 \approx 0{,}0099,$$
$$a_4 \approx 0{,}0021 \text{ etc.}$$

Using this recursion formula, it is possible to prove by induction that

$$|a_n| \leqslant 1/(n+1)^2(1{,}5)^n,$$

i.e., the radius of series convergence is no less than 1.5.

This evaluation is enough to permit utilization of Solution (4.2) for the determination of the maximum accelerations and heat flows over the main segment of the atmosphere-entry trajectory.

With x < 1 we can limit ourselves to three terms (with an error of less than 1%):

$$y_0 \approx \sqrt{8/3}x^{3/4}(1 + x/6 + x^2/24).$$

Hence we can determine the maximum value of the acceleration, differentiating the expression

$$n_x = \sqrt{8R\lambda/3}\left(x^{3/4} + \frac{x^{7/4}}{6} + \frac{x^{11/4}}{24}\right)e^{-2x}$$

with respect to x and solving the equation

$$4x^3 + 9x^2 + 76x - 72 = 0.$$

From this we find that

$$x\big|_{n_{x\,max}} = 0.835 \quad \text{or}\; V\big|_{n_{x\,max}} = 0.434 V_{\text{кр}},$$

$$y\big|_{n_{x\,max}} = 1.45, \quad n_{x\,max} = 0.277\gamma\overline{R\lambda}.$$

For the earth ($\gamma\overline{R\lambda} \approx 30$) it may be held that

$$n_{x\,max} \approx 8.33, \quad \rho\big|_{n_{x\,max}} \approx \frac{1.39 \cdot 10^{-6}}{\sigma_x}.$$

The maximum values of the heat flows as well as the values of the velocity at which these are attained can be determined in analogous fashion:

$$x\big|_{q_{\text{к.л.}\,max}} = 0.237 \;\text{or}\; V\big|_{q_{\text{к.л.}\,max}} = 0.789 V_{\text{кр}},$$

$$y\big|_{q_{\text{к. л. max}}} = 0.197, \quad q_{\text{к. л. max}} = \frac{17.4}{r^{0.5}\sigma_x^{0.5}}\;\text{kcal/m}^2\text{sec},$$

$$x\big|_{q_{\text{к. т. max}}} = 0.4 \;\text{or}\; V\big|_{q_{\text{к. т. max}}} = 0.670 V_{\text{кр}},$$

$$y\big|_{q_{\text{к. т. max}}} = 0.444, \quad q_{\text{к. т. max}} = \frac{3.65}{r^{0.2}\sigma_x^{0.8}}\;\text{kcal/m}^2\text{sec}$$

5. Evaluation of Solution and Limits of Its Applicability

Let us investigate the behavior of the trajectory $y_0(x)$. Let us write the equation for $y - y_0 = \Delta y$

$$\frac{d^2\Delta y}{dx^2} + \frac{\Delta y(c^{2x} - 1)}{y_0(y_0 + \Delta y)} = 0. \qquad (5.1)$$

With small $x > 0$, $y_0 \approx \sqrt{8/3}\, x^{1/2}$, $c^{2x} - 1 \approx 2x$. Since the values of y_0 here are small, even small deviations Δy lead to a large relative error $\Delta y/y_0$. Having substituted the variables $\Delta y/y_0 = z$, $x = e^{x_1}$, we obtain the equation

$$\frac{d^2 z}{dx_1^2} + 2\frac{dz}{dx_1} + \frac{3}{4}\frac{z(2 + z)}{1 + z} = 0,$$

from whose structure it follows that z is oscillatory in nature and decreases in amplitude, i.e., the relative error $\Delta y/y_0$ diminishes.

If this relative error becomes small, Eq. (5.1) becomes a linear equation having solutions

$$z_1 \sim e^{-x_1}\sin\frac{x_1}{\gamma 2}, \quad z_2 \sim e^{-x_1}\cos\frac{x_1}{\gamma 2}$$

or

$$\Delta y_1 \sim \gamma x \sin\frac{\ln x}{\gamma 2}, \quad \Delta y_2 \sim \gamma x \cos\frac{\ln x}{\gamma 2}.$$

With large $\underline{x}$ the linearized equation for the variation Δy is written in the following form

$$\frac{d^2\Delta y}{dx^2} + \frac{e^{2x}-1}{y_0^2}\Delta y = 0. \tag{5.2}$$

Having employed the familiar asymptotic method [20], we can write the approximate solutions for Eq. (5.2) in the form

$$\Delta y_1 \sim \frac{1}{\gamma\omega(x)}\sin\int\omega(x)dx,$$

$$\Delta y_2 \sim \frac{1}{\gamma\omega(x)}\cos\int\omega(x)dx,$$

where

$$\omega(x) = \frac{\gamma\overline{e^{2x}-1}}{y_0}.$$

With $x > 1.5$ the solution y_0 becomes close to e^x, and in this case $\omega(x) \to 1$, i.e., the solutions $y(x)$ close to e^x execute slow undamped oscillations about $\bar{y} \approx e^x$. It is not difficult to see that over the entire range of changes in $\underline{x}$ the variation Δy performs oscillations with non-diminishing amplitudes; however, the ratio $\Delta y/y \sim \Delta H$ always tends to zero. Therefore, the trajectories under consideration are in a certain sense stable.

Let us examine in which range assumptions e) and f) are satisfied.

Let us accept condition $|\theta| < 0.3$ $(\sin\theta \approx \theta, \cos\theta \approx 1)$, as the criterion of fulfillment for assumption e), and let condition $|\theta| < 0.1\, n_x$. serve as the criterion of fulfillment for assumption f).

In accordance with the above we will hold that $y \approx \gamma\overline{8/3}x^1$ for small

$\underline{x}$ and $y \approx e^{\underline{x}}$ for large $\underline{x}$. In this case it is not difficult to derive that for small $\underline{x}$

$$\theta \approx -\gamma 6x / \gamma \overline{R\lambda}, \qquad n_x \approx \gamma \overline{R\lambda} \; \gamma 8/3 \; x^{\prime h},$$

while for a large $\underline{x}$

$$\theta \approx -e^x / \gamma \overline{R\lambda}, \qquad n_x \approx \gamma \overline{R\lambda} \; e^{-x}.$$

Consequently, condition e) is violated for a small velocity ($x > 2.3$, $V < 0.1 \, V_{kr}$), while condition f) is violated in the case of a great velocity ($x < 0.015$, $V > 0.985 \, V_{kr}$) and at a low velocity ($x > 2.3$, $V < 0.1 \, V_{kr}$), i.e., the solution of Eq. (6.1) for initial conditions $y(0) = y'(0) = 0$ correctly reflects the motion of a spacecraft over the main segment of the atmosphere-entry trajectory at $0.985 \, V_{kr} > V > 0.1 \, V_{kr}$.

The attempt to seek the solution $\underline{y}$ in the case of a small nonzero value $y(0) = c_0 > 0$ in the form of a power series with respect to whole-number exponents $\underline{x}$ does not result in success, since the radius of convergence for such a series is very small — of the order of $c_0^{2/3}$. This is easily explained by means of the following: if the solution is extended into the region of negative $\underline{x}$, since $y'' < 0$ when $x < 0$, $y > 0$, the solution $\underline{y}$ with even a small $x^* < 0$ intersects the x-axis along which $y'' = (e^{2x} - 1)/y$ becomes infinity and, consequently, cannot be represented at point x_* by a converging series in powers of $\underline{x}$. Hence, according to the Abel theorem, this solution cannot be represented by such a series even for $x = |x_*| > 0$. This justifies the utilization of the "limit" solution ($y(0) = 0$) expressed by a series which is rapidly convergent over a rather great range.

If the value of c_0 is small, so that assumption f) is satisfied, the solution in the vicinity of $x = 0$ is defined by the formula $y \approx c_0 f(x / c_0^{\prime h})$, where $f_0(\xi)$ serves as the solution of the equation

$$d^2 f / d\xi^2 = 2\xi / f$$

(5.3)

under the initial conditions

$$f(0) = 1, \ f'(0) = 0 \ (\text{Fig. 1}).$$
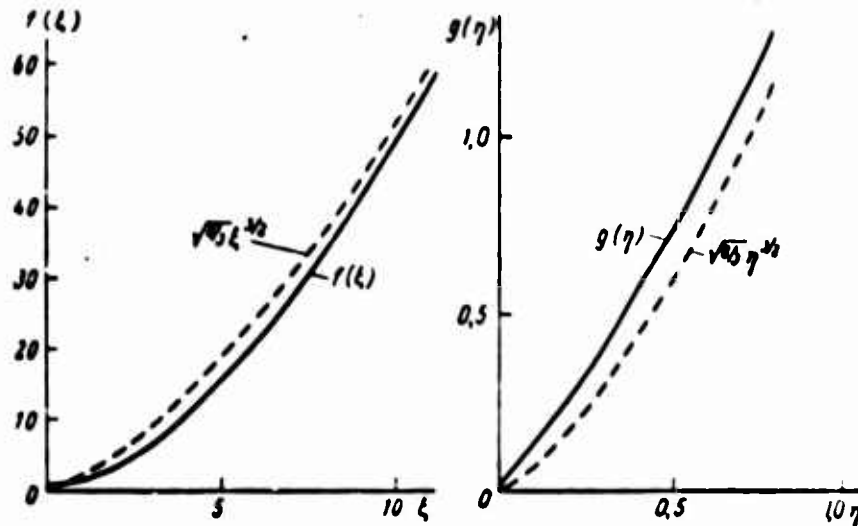
Fig. 1

With $\xi > 7$ $(x > 7c_0^{1/3})$ the function $\underline{f}$ becomes close to $\sqrt{8/3}\,\xi^{3/2}$, i.e., the solution $\underline{y}$ becomes close to y_0 and subsequently remains close to it, since the amplitude of $\Delta y / y_0$ diminishes with increasing $\underline{x}$.

With $x > 7c_0^{1/3}$ the solution Δy may be determined from the solution for the equation in variations (5.2) for the initial conditions

$$\Delta y(7c_0^{1/3}) = -0.11 y_0, \quad \Delta y'(7c_0^{1/3}) = 0.$$

Turning to the expressions for range and time, it is not difficult to prove that in the limit case with $y(0) = 0$ and $x_{nach} = 0$ the integrals (3.15) and (3.16) diverge, which is completely natural — in outer space a space vehicle is in motion for an indeterminately long period of time. Therefore, in calculating range and time it is an absolute necessity to take into consideration the initial value $y(0) = c_0 \neq 0$. Having represented the solution in the form

$$y \approx c_0 / (x / c_0^{1/3}) \qquad \text{for} \qquad x < 7c_0^{1/3}$$
$$y \approx y_0(x) \qquad \text{for} \qquad x > 7c_0^{1/3}$$

we find that for small c_0 and $x > 7c_0^{2/3}$

$$L = \sqrt{\frac{R}{\lambda}} \int_0^z \frac{dx}{v} \approx \sqrt{\frac{R}{\lambda}} \left\{ \int_0^{7c_0^{2/3}} \frac{dx}{c_0 \sqrt{\left(\frac{x}{c_0^{2/3}}\right)}} + \int_{7c_0^{2/3}}^z \frac{dx}{y_0(x)} \right\} \approx$$

$$\approx \sqrt{\frac{R}{\lambda}} \left\{ 2.52\, c_0^{-1/3} - 12.5 + \int_{0.01}^z \frac{dx}{y_0(x)} \right\} \tag{5.4}$$

(for the sake of determinacy the lower limit has been set equal to 0.01, since the solution $y_0(x)$ is valid for $x > 0.015$). An analogous formula is derived for the flight time

$$t \approx \frac{1}{\sqrt{g\lambda}} \left\{ 2.52\, c_0^{-1/3} - 12.5 + \int_{0.01}^z \frac{e^x dx}{y_0(x)} \right\}. \tag{5.5}$$

6. Ballistic Trajectories with An Initial Angle of Inclination Not Equal to Zero

Let us examine the solution of Eq. (4.1) having the initial conditions

$$y(0) = 0, \quad y'(0) = c_1 > 0.$$

If $y(0) = c_0$ is a small quantity not equal to zero, in this case concepts analogous to the previous are applicable and for this reason this problem will not be considered any further.

Let us initially consider the case of $c_1 < 0.7$. In this case it turns out that $x < 0.8c_1^2$ the solution is presented in the form $y = c_1^3 g(x/c_1^2)$, where $g(\eta)$ satisfies the equation

$$d^2g / d\eta^2 = 2\eta / g \tag{6.1}$$

under initial conditions: $g(0) = 0$, $g'(0) = 1$ (Fig. 1).

With $x > 0.8c_1^2$ the solution is close to $y_0(x)$, and $\Delta y = y - y_0$ will be the solution for the equation in variation in variations (5.2) having the initial conditions $\Delta y = 0.12\, y_0$, $\Delta y' = 0$ for $x = 0.8c_1^2$. On the basis of this representation, considering the oscillatory nature of the change Δy, it becomes clear that under certain conditions, when,

in the vicinity of $x = 0.835$, $\Delta y < 0$, the maximum acceleration turns out to be even somewhat smaller than in the case $c_1 = 0$.

The calculation results show that such a reduction, although completely negligible, is attained at $c_1 \approx 0.25$.

Let us further consider the case of "large" $c_1 > 1.2$. The solution for Eq. (4.1) will be sought in the form of the series:

$$y = c_1 x + c_2 x^2 + c_3 x^3 + c_4 x^4 + c_5 x^5 + ..., \tag{6.2}$$

where the coefficients $c_2, c_3,$ c_4 etc. are determined by means of the recursion formula

$$m(m-1)c_m c_1 = \frac{2^{m-1}}{(m-1)!} - \sum_{k=2}^{m-1} c_k c_{m-k+1} k(k-1). \tag{6.3}$$

Hence

$$c_2 = \frac{1}{c_1}, \quad c_3 = \left(1 - \frac{1}{c_1^2}\right)\frac{1}{3c_1},$$

$$c_4 = \left(1 - \frac{2}{c_1^2} + \frac{2}{c_1^4}\right)\frac{1}{9c_1},$$

$$c_5 = \left(3 - \frac{10}{c_1^2} + \frac{17}{c_1^4} - \frac{14}{c_1^6}\right)\frac{1}{90c_1}.$$

We can show that the radius of the convergence of the series is approximately equal to $0.6c_1^2$, i.e., with $c_1 > 1.2$ the series converges in the range in which the accelerations and heat flows attain their maximum values, with the rate of convergence rising with increasing c_1.

In the determination of the maximum magnitude of $q_{k.1.}$ the expansion is also suitable for smaller $c_1 (c_1 \sim 0.5)$.

Since $c_2 = 1/c_1$, with an increase in c_1 the curvature of the trajectory diminishes and the trajectory approaches a spiral $\theta = \text{const}$, considered in [2]. With $c_1 > 3$ (for the earth $|\theta_{nach}| > 6^\circ$) it may be assumed with a sufficient degree of accuracy that along the main segment $y = c_1 x$, i.e., with $c_1 = 3$ the error in the determination of the maximum acceleration amounts approximately to 6%.
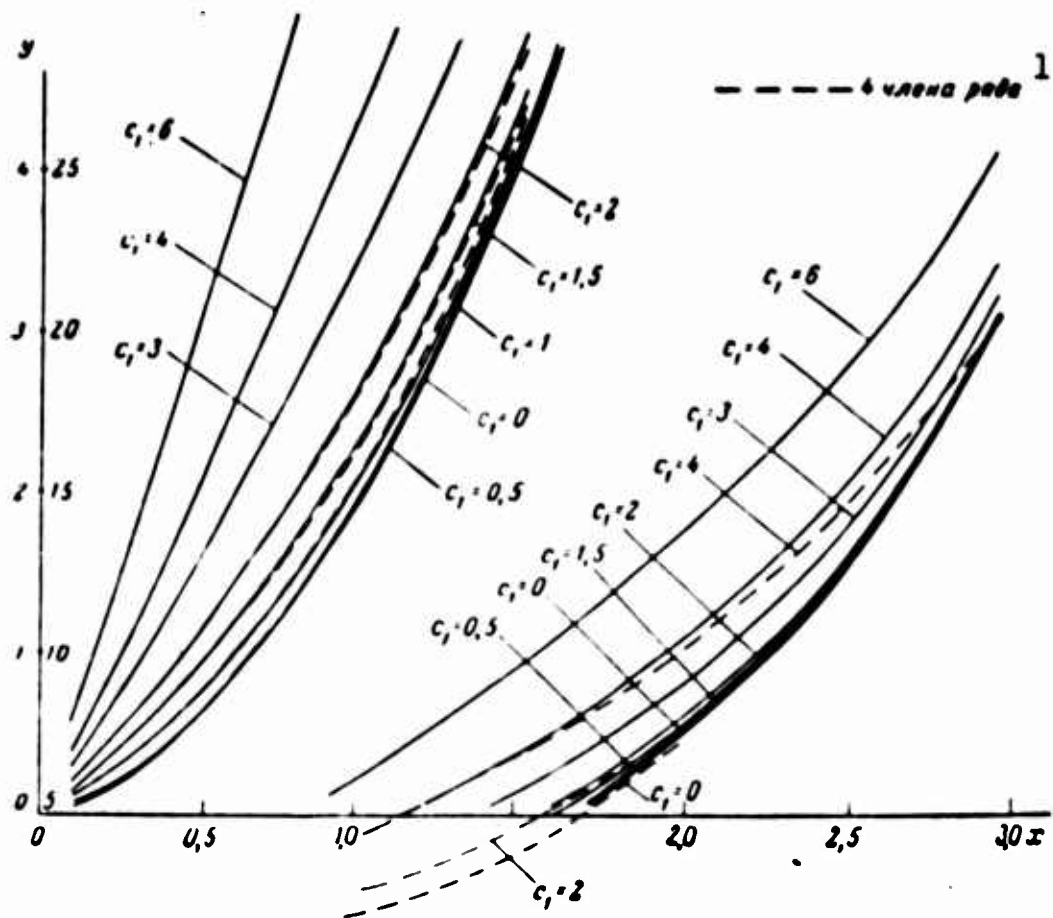
Fig. 2. 1) 4 terms of the series.
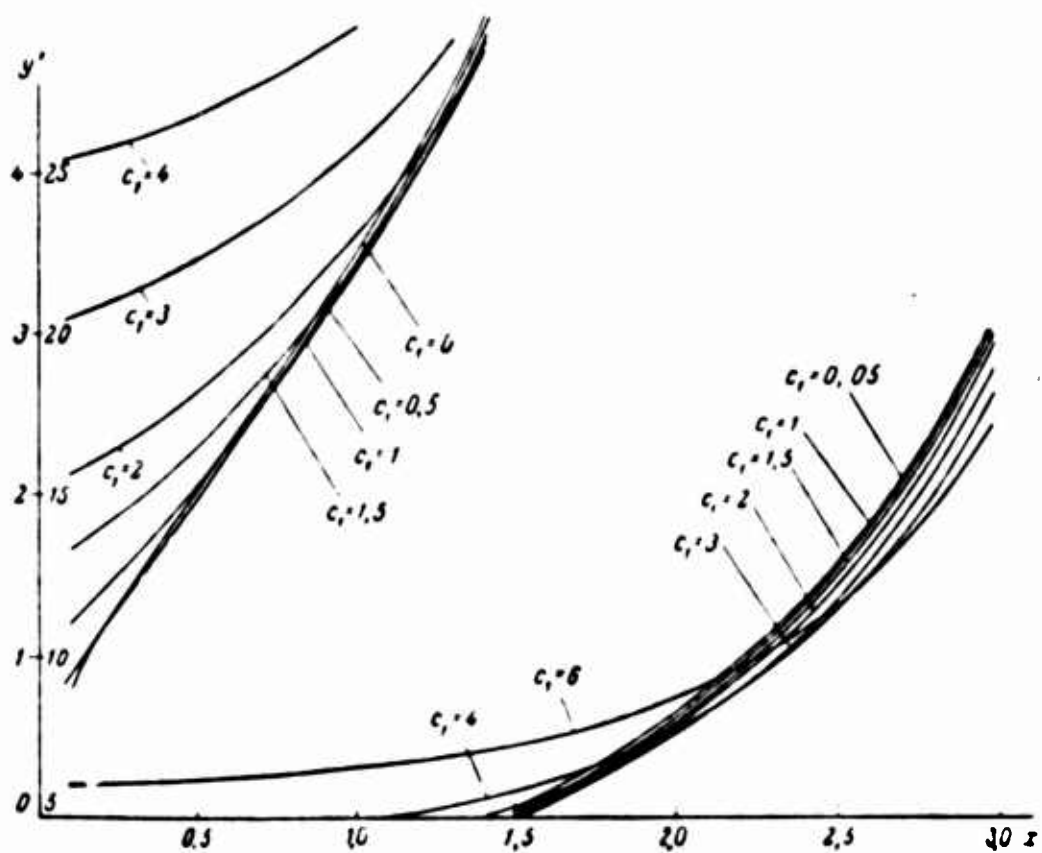
Fig. 3
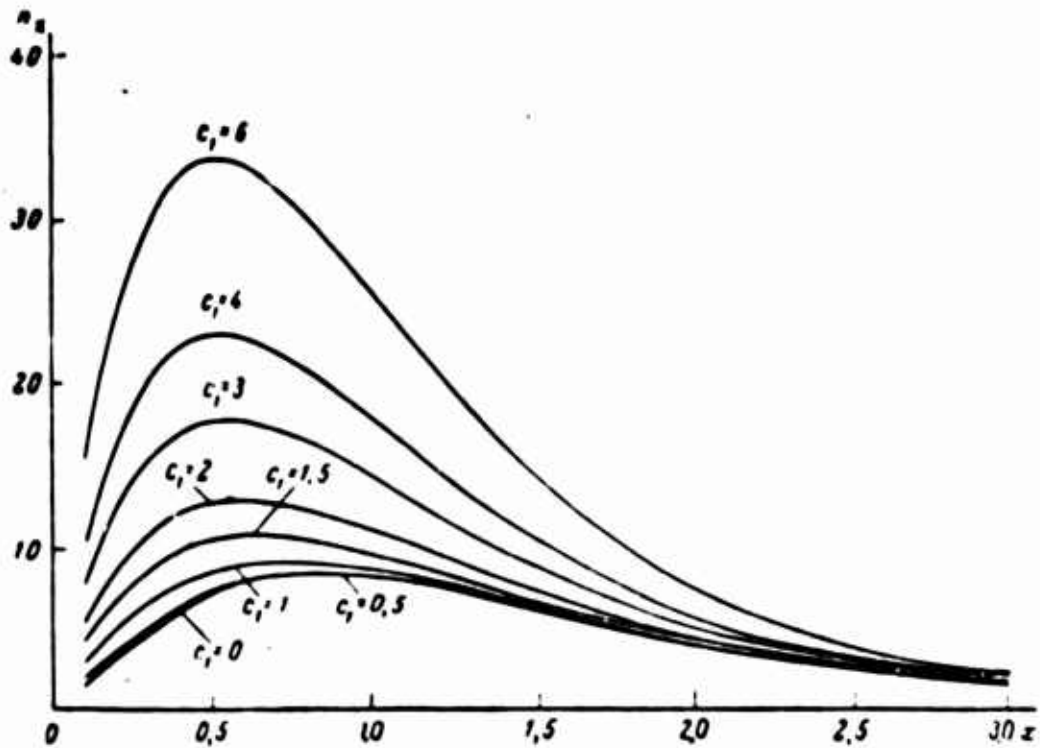
Fig. 4
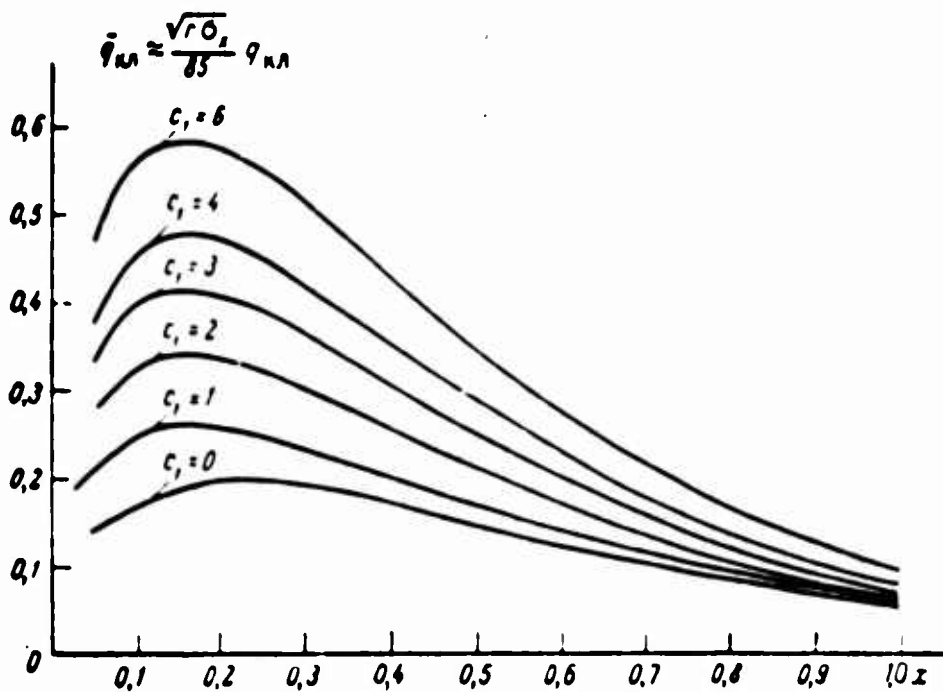
Fig. 5

As an example let us reproduce one of the conclusions in Reference [2], substituting θ by $\sin \theta$ (for large entry angles this difference becomes significant)

$$n_x = \gamma R \lambda e^{-2x} y = \gamma \overline{R \lambda} e^{-2x} c_1 x = R\lambda |\sin \theta| x e^{-2x}.$$

Hence $x|_{n_{x\,max}} = 0.5$ or $V|_{n_{x\,max}} = 0.605 \, V_{кр}$. $n_{x\,max} = \dfrac{R\lambda}{2e} |\sin \theta| \approx$

$\approx 170 |\sin \theta|$ (for the earth).

$$\delta_{\text{кт}} = \frac{r^{0.2} O_d^{0.8} q_{\text{кт}}}{25}$$
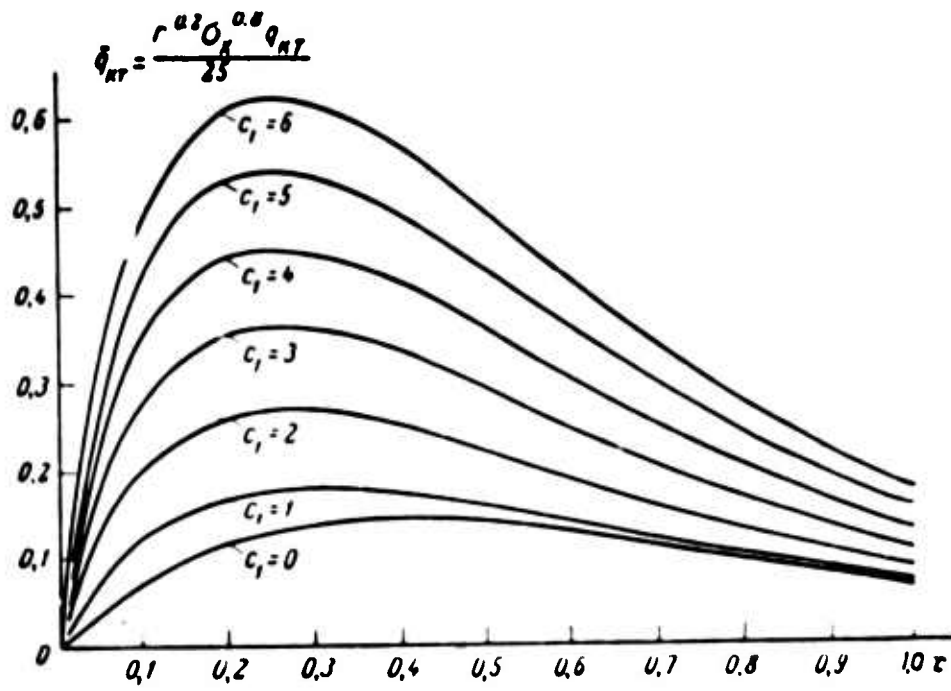
Fig. 6
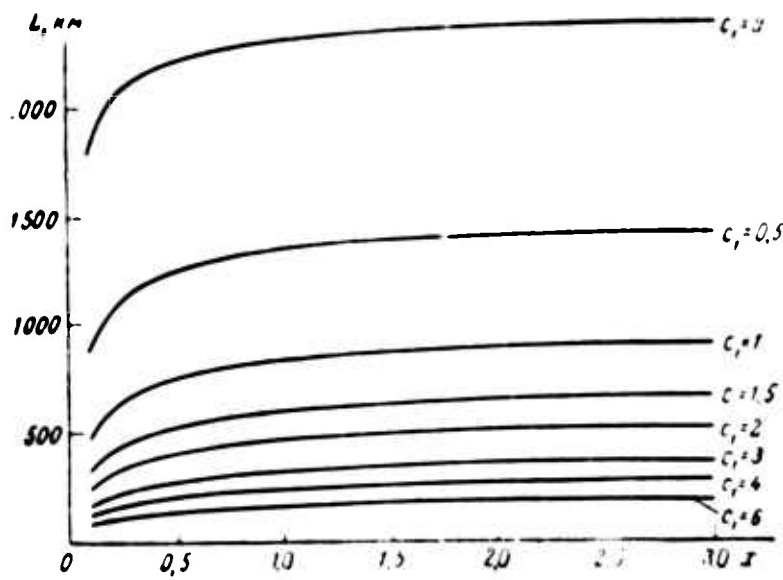
Fig. 7
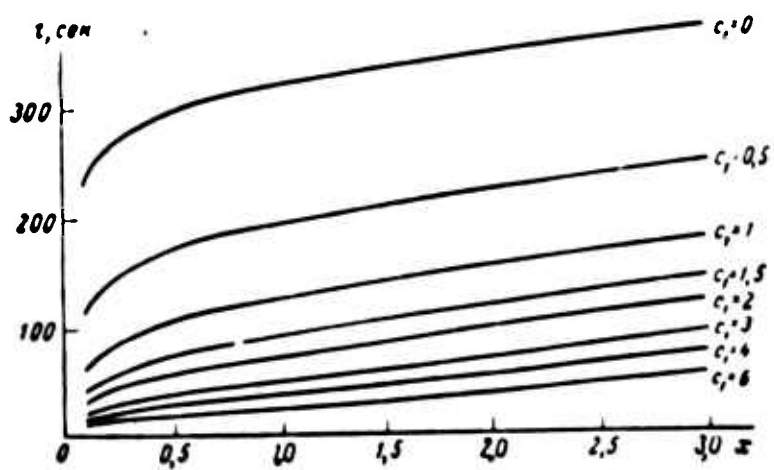
Fig. 8

With $1.2 < c_1 < 3$ it is possible to find the maximum acceleration and the convective heat flow, using the first terms of the expansion in x.

The results of the calculation carried out on a computer for the entire range of values of c_1 are presented in Figs. 2-6; the comparison of these results with the analytical formulas (4.2) and (6.2) is shown in Fig. 2.

Using the limit solution $y = c_1 x$ in the vicinity of $x \sim 0$, we will find that assumption f) is satisfied at $x > 0.01$, i.e., for $V < 0.99\ V_{kr}$.

It can be shown that the range and time of flight in the case of c_1 that are not too small and in the case of small c_0 and x_{nach} are described by the approximation formulas

$$L \approx \sqrt{\frac{R}{\lambda}} \int_{c_0/c_1}^{z} \frac{dx}{y},$$

(6.4)

$$t \approx \frac{1}{\sqrt{g\lambda}} \int_{c_0/c_1}^{z} \frac{e^x\, dx}{y},$$

(6.5)

where y is the solution for Eq. (6.1) in the case of a limit initial condition $y(0) = 0$, $y'(0) = c_1$, i.e., the consideration of the initial conditions, considering the essence of the matter, reduces to the selection of the initial point at which $y(x) = c_0$.

The values for time and range for the case $x_{nach} = 0.01$ are shown in Figs. 7 and 8.

7. The Coefficient of Resistance as An Exponential Function of Velocity

Let $c_x = c_x(V_{kr})(V/V_{kr})^n$. For the sake of convenience let us introduce the functions y and x, somewhat different from those calculated in accordance with the general rule

$$y = n \frac{c_x(V_{kp})S}{2m} \sqrt{\frac{R}{\lambda}} \rho,$$

(7.1)

$$z = \left(\frac{V_{kp}}{V}\right)^n.$$

(7.2)

- 26 -

In this case the equation of motion is written in the following form:

$$\frac{d^2 y}{dx^2} = - \frac{c_y}{c_x(V_{\text{кр}})} \sqrt{R\lambda} + \frac{x^{\frac{2}{n}} - 1}{y}, \qquad (7.3)$$

$$\theta = - \frac{1}{\sqrt{R\lambda}} \frac{dy}{dx}, \qquad (7.4)$$

$$n_x = \gamma R\lambda \cdot \frac{y}{n} x^{-\frac{n+2}{n}}. \qquad (7.5)$$

We will limit ourselves to a consideration of the ballistic trajectories

$$\frac{d^2 y}{dx^2} = \frac{x^a - 1}{y}, \qquad (7.6)$$

$$a = 2/n > 0 \quad \text{for} \quad n > 0.$$

Initially let us consider the case of entry into the atmosphere at a zero angle of inclination for the trajectory

$$y(1) = y'(1) = 0.$$

Let us expand the right-hand part of Eq. (7.6) in a power series with respect to x — 1, which converges at x < 2 and, in analogy to the previous solution, let us seek a solution in the form

$$y = \sqrt{4a/3}(x - 1)^{3/2} [1 + \beta_1(x - 1) + \beta_2(x - 1)^2 + \ldots]. \qquad (7.7)$$

By means of the recursion formula we obtain

$$\beta_1 = \frac{a - 1}{12}, \qquad \beta_2 = \frac{(a - 1)(19a - 43)}{19 \cdot 96},$$

$$\beta_3 = \frac{(a - 1)[19 \cdot 72(a - 2)(a - 3) - 25(a - 1)(19a - 43)]}{9 \cdot 17 \cdot 19 \cdot 256}.$$

In the general case of a noninteger a the radius of convergence for the derived series is not greater than unity. However, in many cases in which a is an integer (n = 2, 1, 2/3, 1/2, ...), the right-hand part of the equation contains a finite number of powers of (x — 1), and Series (7.7) converges within a larger range.

Let us examine in detail two cases:

a) n = 1, α = 2

$$d^2y / dx^2 = (x^2 - 1) / y,$$

$$\beta_1 = i/_{12}, \qquad \beta_2 = -5 / 19 \cdot 96, \qquad \beta_3 = 125 / 9 \cdot 17 \cdot 19 \cdot 256. \qquad (7.8)$$

It is possible to show that the series converges with sufficient speed in any case when x < 5.7, i.e., when V > 0.18 V_{kr}. Considering the three terms in Expansion 7.8), it is possible to write

$$y \approx \sqrt{8/3}(x-1)^{3/2}[1 + (x-1)/12 - (x-1)^2 5/19 \cdot 96]$$

and find the maximum values of acceleration and the heat flow

$$x|_{n_x \, max} = 2.11 \quad \text{or} \quad V|_{n_x \, max} = 0.474 V_{кр},$$

$$x|_{q_{к.\,л.\,max}} = 1.305 \quad \text{or} \quad V|_{q_{к.\,л.\,max}} = 0.765 V_{кр},$$

$$q_{к.\,л.\,max} = \frac{19}{r^{0.5}\sigma_x(V_{кр})^{0.5}} \text{ kcal/m}^2\text{sec},$$

$$x|_{q_{к.\,т.\,max}} = 1.7 \quad \text{or} \quad V|_{q_{к.\,т.\,max}} = 0.59 V_{кр},$$

$$q_{к.\,т.\,max} = \frac{4.6}{r^{0.2}\sigma_x^{0.8}(V_{кр})} \text{ kcal/m}^2\text{sec}$$

b) n = 2, α = 1

$$\frac{d^2y}{dx^2} = \frac{x-1}{y}. \qquad (7.9)$$

The solution is written in the form

$$y = \sqrt{\frac{4}{3}} (x-1)^{3/2},$$

$$x|_{n_x \, max} = 4 \quad \text{or} \quad V|_{n_x \, max} = 0.5 V_{кр},$$

$$n_{x \, max} = 5.62,$$

$$x|_{q_{к.\,л.\,max}} = 1.86 \quad \text{or} \quad V|_{q_{к.\,л.\,max}} = 0.735 V_{кр},$$

$$q_{к.\,л.\,max} = \frac{21}{r^{0.5}\sigma_x^{0.5}(V_{кр})} \text{ kcal/ m}^2\text{sec},$$

$$x|_{q_{к.\,т.\,max}} = 4.04 \quad \text{or} \quad V|_{q_{к.\,т.\,max}} = 0.498 V_{кр},$$

$$q_{к.\,т.\,max} = \frac{6.6}{r^{0.2}\sigma_x^{0.8}(V_{кр})} \text{ kcal/m}^2\text{sec}.$$

Certain results of the calculation carried out by means of the expansions for cases of both negative and positive n are presented in Fig. 9 whence we can see that the maximum value of acceleration diminishes monotonically with increasing n.
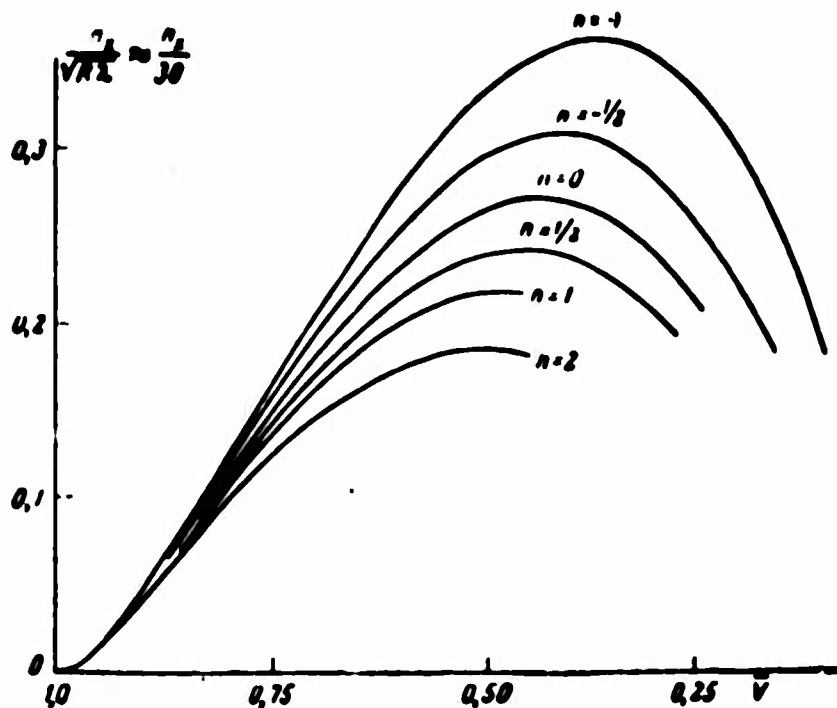
Fig. 9

The case in which the initial angle of trajectory inclination dif-
fers from zero is considered in the same manner as for c_x = const. The
radius of convergence of the derived series is greater, the greater the
entry angle.

Let us cite the first terms of the expansion with respect to x for
the cases $c_x \sim V$ and $c_x \sim V^2$:

a) $n = 1$

$$y = c_1(x - 1) + \frac{(x - 1)^2}{c_1} + \left(1 - \frac{2}{c_1^3}\right)\frac{(x - 1)^3}{6c_1} -$$

$$- \left(1 - \frac{2}{c_1^3}\right)\frac{(x - 1)^4}{9c_1^3} + \frac{\left(25 + \frac{2}{c_1^3}\right)\left(1 - \frac{2}{c_1^3}\right)}{360c_1^3}(x - 1)^5 + \dots \quad (7.10)$$

b) $n = 2$

$$y = c_1(x - 1) + \frac{(x - 1)^2}{2c_1} - \frac{(x - 1)^3}{12c_1^3} + \frac{(x - 1)^4}{36c_1^5} - \frac{17}{1440c_1^7}(x - 1)^5 \dots \quad (7.11)$$

The results of the calculations are presented in Figs. 10 and 11.
The comparison with the results of calculation for the case c_x = const
is presented in Fig. 12. With sufficiently large $c_1 > 3$ it is possible
simply to assume that $y \approx c_1(x - 1)$. In this case, for example, the
acceleration is expressed in the form

- 29 -
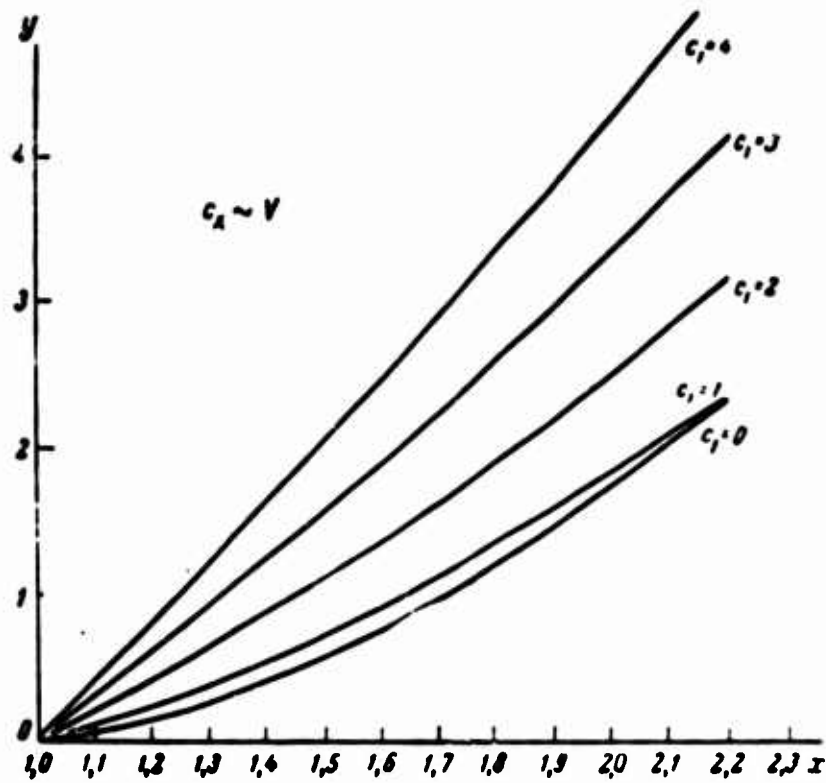
Fig. 10
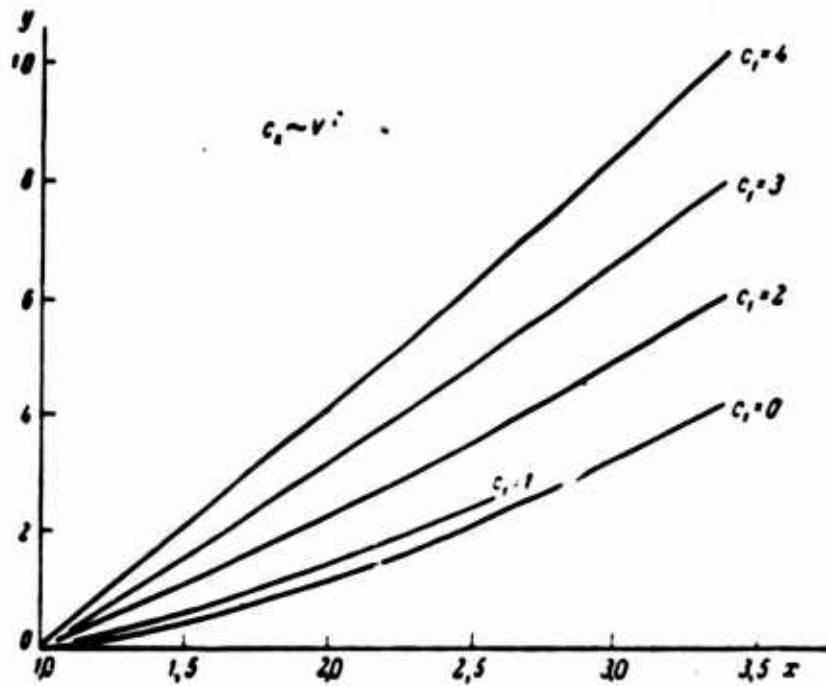
Fig. 11

$$n_z = \sqrt{R}\lambda \frac{yz^{-(n+2)/n}}{n} = R\lambda|\sin\theta|\frac{(x-1)x^{-(r+2)/n}}{n}.$$

The maximum value of acceleration is attained at $x = 1 + n/2$ or with $V = V_{kr}[2/(n+2)]^{1/n}$.

$$n_{z\,max} = \frac{R\lambda|\sin\theta|}{2}\left(\frac{2}{n+2}\right)^{(n+2)/n} \tag{7.12}$$

- 30 -
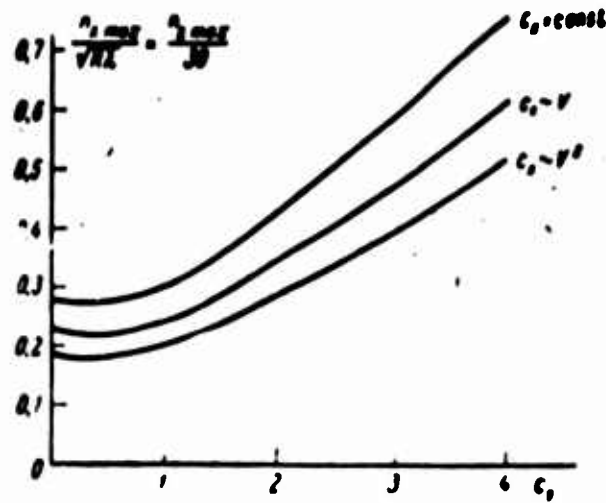
Fig. 12

(this is the result earlier obtained by V.Ya. Neyland).

As we can see, the maximum value of acceleration diminishes with increasing n approximately in identical proportion irrespective of the magnitude of the atmosphere-entry angle. However, the heat flows increase in this case if it is maintained that the values of $\sigma_x(V_{kr})$ are identical in all cases.

8. Determination of the Total Quantity of Heat Received by the Surface of the Craft

In calculating the total quantity of heat received received per unit surface of a ballistic spacecraft having a spherical nose, let us make the following assumptions:

a) We will hold that the convective heat flow can be characterized by the formula

$$q_\kappa = C\rho^k V^l r^{-m}.$$

b) The radiation heat flow from the air heated behind the compression shock can be reglected.

c) Let us hold that the surface of the craft exhibits equilibrium temperature, i.e., given by the equation $q_k = q_{rad}$ until the given maximum T_w is attained. Subsequently, the temperature is regarded as constant and we calculate the integral

$$\int_{t_1}^{t_2} (q_{\scriptstyle н} - q_{pad}|_{T_{w\,max}})\,dt,$$

proportional to the required weight of the heat absorbent (Fig. 13).
In physical terms this corresponds to the melting of the nose of the
craft, the melting point represents $T_{w\ max}$, and the quantity of heat ab-
sorbent is proportional to the weight of the melting material. This
method of evaluating thermal regimes was employed, for example, in Re-
ference [5].
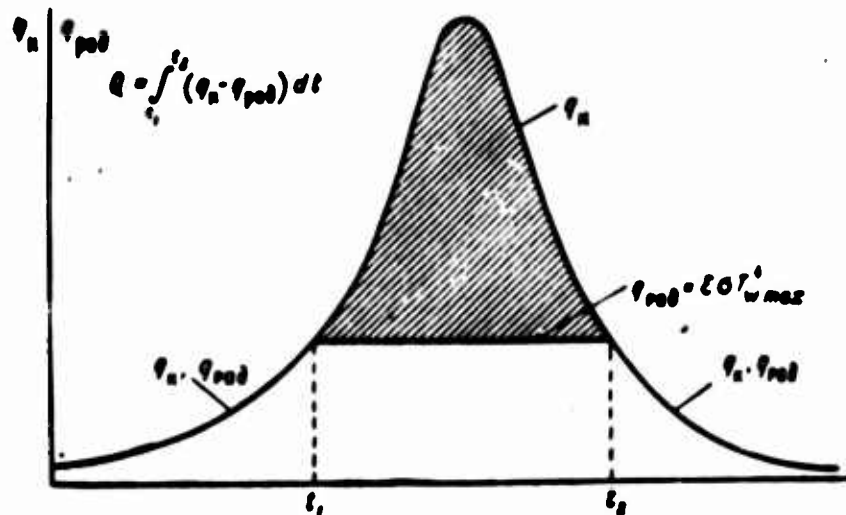
Fig. 13

The calculation was carried out for ballistic trajectories with

$$c_x = \text{const,} \qquad \rho_{нач} = 0, \qquad V_{нач} = V_{кр.}$$

Let us hold that with $|\theta_{нач}| > 6°$ the trajectory may be regarded as spiral,
$\theta = \text{const.}$

Let us consider two cases. The first case corresponds to the lamin-
ar boundary layer and in this case the quantity of heat received at the
critical [stagnation] point of the spherical nose of the craft is calcu-
lated.

We will proceed from Formula (3.20) in our calculations.

Initially let us consider the spiral trajectory

$$y = c_i x = \sqrt{R\lambda}\,|\sin\theta|\,x$$

$$Q = Q_{\text{н. з.}} - Q_{\text{роз}} = \int_{t_1}^{t_2} (q_{\text{н}} - q_{\text{роз}})\,dt =$$

$$= \frac{2270}{r^{0.5}c_i^{0.5}\sigma_x^{0.5}} \int_{x_1}^{x_2} [x^{1/2}e^{-3.25x} - A_*]\frac{e^x}{x}\,dx = \frac{490 f(A_*)}{|\sin\theta|^{2.5}\sigma_x^{0.5}r^{0.5}} \text{ kcal/m}^2. \qquad (8.1)$$

Here

$$A_* = 0.292 \cdot 10^{-13}|\sin\theta|^{-0.5}\sigma_x^{0.5}r^{0.5}T_{w}^{4},$$

and the points x_1 and x_2 are found from the equation

$$x^{0.5}e^{-3.25x} = A_*.$$

Function $f(A_*)$ is shown in Fig. 14. With Formula (8.1) we can trace the influence of the parameters σ_x, $\sin\theta$, $\underline{r}$, $T_{w\text{ max}}$, and ϵ on the total quantity of heat.

For low values of θ_{nach} it is no longer possible to maintain that $\theta = \text{const}$. For this reason here we use the results from the calculation of the ballistic trajectory in accordance with the simplified equation for $c_1 = 0$ and $c_i = 1.5$ $(\theta_{\text{нач}} = 0, \ -3°)$. This makes it possible to construct Q as a function of $|\sin\theta_{\text{nach}}|$ over the entire range of $0 > \theta_{\text{нач}} > -90°$. Certain of the results of the calculation are shown in Figs. 15-17. It is interesting to note that in this case there exists no optimum initial angle of trajectory inclination for which the total quantity of heat would be at a minimum, but rather only a "worst" angle can exist.

The second case corresponds to the turbulent boundary layer on the spherical nose of the craft. In this case, as is well known, the heat flow attains its maximum value in that section in which the velocity is equal to the speed of sound and Formula (3.22) should be employed. Having carried out the computations, analogous to the computations of the previous case, we derive

$$Q = Q_{\text{н.т.}} - Q_{\text{роз}} = \frac{207 g(B_*)}{|\sin\theta|^{0.2}\sigma_x^{0.8}r^{0.2}} \text{ kcal/m}^2.$$
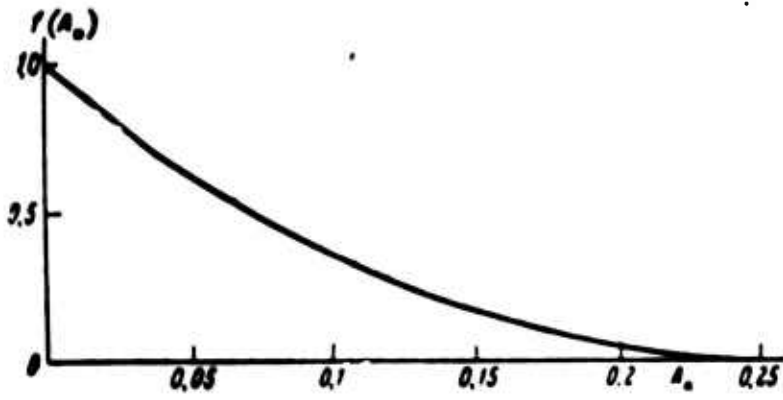
Fig. 14
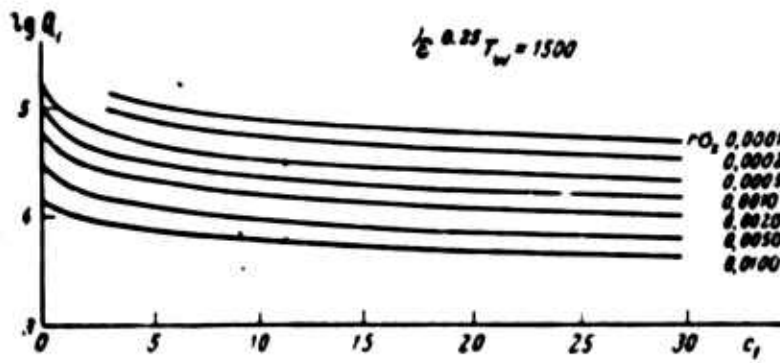
Fig. 15
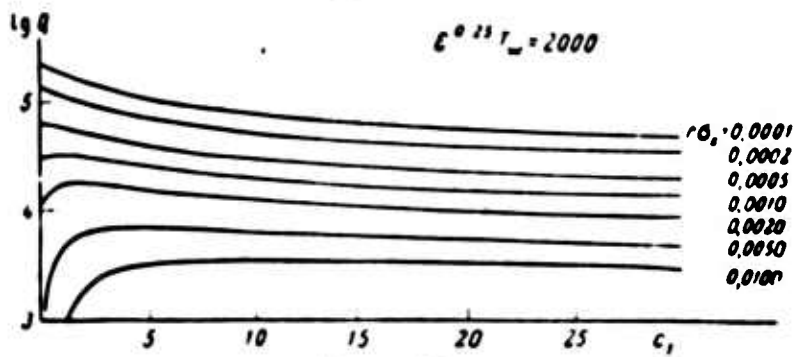
Fig. 16
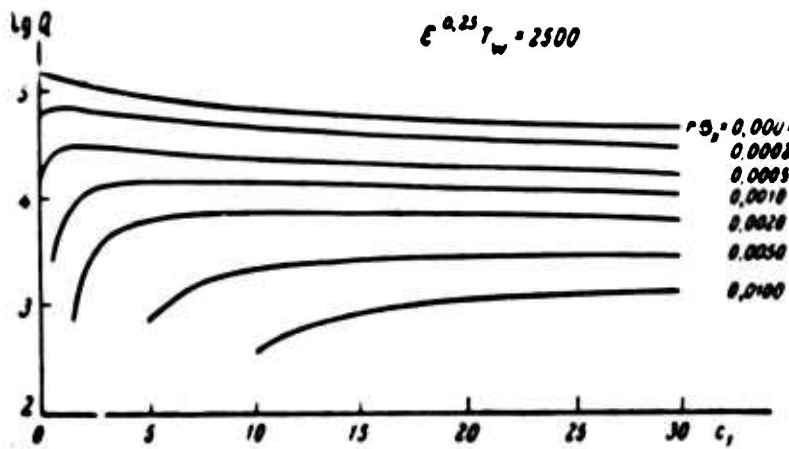
Fig. 17
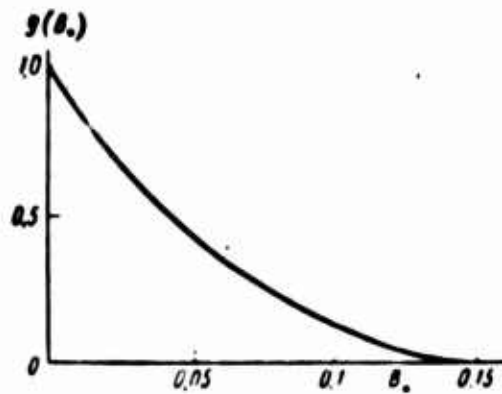
Fig. 18

Here

$$B_* = 0.36 \cdot 10^{-13} |\sin \theta|^{-0.8} r^{0.2} \sigma_x^{0.8} \varepsilon T_w^4.$$

Function $g(B_*)$ is shown in Fig. 18.

If the angle of trajectory inclination upon entry into the atmosphere is great, i.e., the trajectory can be regarded as spiral, but the entry velocity V_{nach} differs from the circular: $V_{нач} \neq V_{кр}$, Formulas (8.1) and (8.2) are transformed in the following manner:

$$Q_{к.д.} - Q_{рад} = \frac{490 \left(\dfrac{V_{нач}}{V_{кр}} \right)^{2.25} f \left[A_* \left(\dfrac{V_{кр}}{V_{нач}} \right)^{2.25} \right]}{|\sin \theta|^{0.5} \sigma_x^{0.5} r^{0.5}} \quad \text{kcal/m}^2$$

$$Q_{к.д.} - Q_{рад} = \frac{207 \left(\dfrac{V_{нач}}{V_{кр}} \right)^{2.19} g \left[B_* \left(\dfrac{V_{кр}}{V_{нач}} \right)^{2.19} \right]}{|\sin \theta|^{0.2} \sigma_x^{0.8} r^{0.2}} \quad \text{kcal/m}^2.$$

Received

27 March 1964

REFERENCES

1. R. Hoglund and J. Thale, ARS Preprint, No. 650-58, 1958.

2. H.J. Allen and A.J. Eggers, NASA Report, 1381, 1959.

3. H.J. Kaepeller and M.E. Kübler, Bericht über den V Internationalen Astronautischen Kongress, Wien [Report on the Fifth International Astronautical Congress, Vienna], R 120, 1955.

4. C. Gazley, Vistas in Astronautics, 1, 8, 1958.

- 35 -

5. A. Ferry, L. Feldman and W. Daskin, Jet Propulsion, 27, No. 11, 1184, 1957.

6. A.J. Eggers, H.J. Allen and S.E. Neice, NASA Report, 1382, 1959.

7. T.K. Nonweiler, Astronautica Acta, 5, No. 1, 40, 1959.

8. D.R. Chapman, NASA TR, NR-11, 1959.

9. A.J. Eggers, Space Technology, Ch. 13, 13, 1959.

10. D.R. Chapman, NASA TR, R-55, 1959.

11. D.R. Chapman and A.K. Kapphahn, NASA TR, R-106, 1961.

12. M.F. Romig, Jet Propulsion, 26, No. 12, 1098, 1956.

13. S. Lees, Jet Propulsion, 261, No. 4, 259, 1956.

14. N.H. Kemp and F.R. Riddell, Jet Propulsion, 27, No. 2, 132, 1957.

15. R.W. Detra, N.H. Kemp, and F.R. Riddell, Jet Propulsion, 27, No. 12, 1256, 1957.

16. M.Sibulkin, Jet Propulsion, 28, No. 8, 548, 1958.

17. M.J. Brunner, Trans. ASME (ser. C), J. Heat. Transfer, 81, No. 3, 223, August, 1959.

18. R.E. Meyerott, Combustion and Propulsion Third Agard Colloq., page 431, March, 1958.

19. F.M. Perkins, Astronautica Acta, 4, No. 2, 113, 1958.

20. A. Erdeyi, Asimptoticheskiye razlozheniya [Asymptotic Expansions], Fizmatgiz [State Publishing House for Physicomathematical Literature], Moscow, 1962.

Manuscript Page No.	[Transliterated Symbols]
8	$r = g = gaz = gas$
9	$cp = sr = sredniy = average$
14	$\text{в} = v = vozdukh = air$

TRACKS OF DIURNAL ARTIFICIAL EARTH SATELLITES

I.V. Aleksakhin, E.P. Kompaniyets and A.A. Krasovskiy

Working formulas are derived for determining the tracks of diurnal artificial earth satellites. The parameters of the tracks are derived and determined as functions of the parameters of the powered segment of the rocket booster's trajectory.

Nomenclature

t time,

τ time segment,

R radius of the earth,

ω_z angular velocity of the earth's rotation,

Ω right ascension,

λ geographic longitude,

φ geocentric latitude,

A azimuth,

i inclination of the orbit,

T period of revolution of the satellite on its orbit,

u latitude argument of satellite.

Subscripts:

$*$ motion on a circular orbit,

e motion on an elliptical orbit,

a, p apogee and perigee of the orbit,

v, n times of passage of the satellite across the ascending and descending nodes of the orbit,

1 time of first starting of booster rocket engine,

2   time of second starting of booster rocket engine,

k   time at end of powered segment of trajectory.

FORMULATION OF THE PROBLEM

An earth satellite is said to be diurnal if its sidereal revolution period is one sidereal day. We shall consider diurnal earth satellites moving on a circular orbit. It follows from the definition that for unperturbed motion, the projection track of the diurnal satellite on the earth's surface will form a closed curve, as was noted at one time in [1, 2].

The problem consists in ascertaining the characteristic peculiarities of those curves, the determination of their parameters and derivation of formulas for calculating the parameters of diurnal-satellite tracks; also, the track parameters as functions of the parameters of the powered trajectory segment.

In deriving the formulas, we shall assume that only the gravitational field of the earth, which is [assumed] Newtonian, acts upon the satellite.

TRACKS OF DIURNAL SATELLITES

Let us examine the position of a satellite at times t_v and t on a circular orbit (Fig. 1). From the spherical triangle formed by the arc segments

$$\Delta u = u, \quad \Delta \varphi = \varphi, \quad \Delta \Omega = \Omega - \Omega_s,$$

we obtain

$$\operatorname{tg} \varphi = \sin \Delta \Omega \operatorname{tg} i, \tag{1}$$
$$\sin \varphi = \sin u \sin i, \tag{2}$$
$$\cos i = \cos \varphi \sin \Lambda. \tag{3}$$

From (1) we find

$$\Delta \Omega = \operatorname{arc} \sin (\operatorname{tg} \varphi / \operatorname{tg} i). \tag{4}$$

During the time $\Delta t = t - t_v$, the earth will turn through an angle
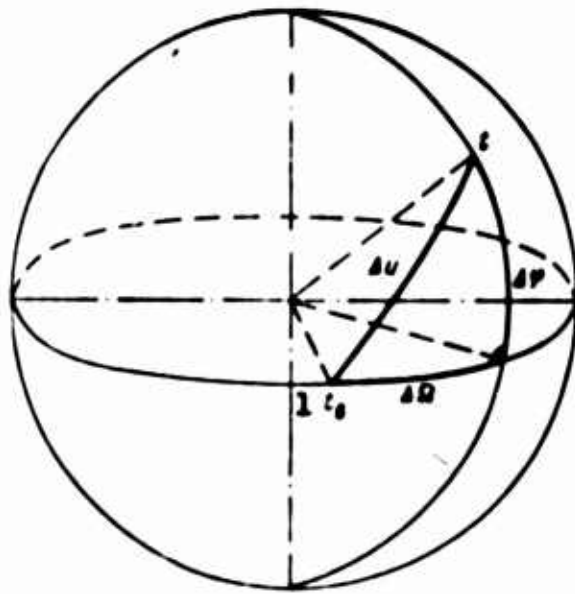
Fig. 1. 1) t_v.

$$\Delta\Omega_3 = \omega_3\Delta t. \tag{5}$$

The time segment Δt is proportional to the arc <u>u</u> and to the satellite's orbital period on a circular orbit

$$\Delta t = (T^\circ / 2\pi)u. \tag{6}$$

From Formula (5) using Relationships (2) and (6), we obtain

$$\Delta\Omega_3 = \frac{\omega_3 T^\circ}{2\pi} \arcsin\left(\frac{\sin\varphi}{\sin i}\right). \tag{7}$$

The change in the satellite's longitude during the time Δt will be

$$\Delta\lambda = \Delta\Omega - \Delta\Omega_3 = \arcsin\left(\frac{tg\,\varphi}{tg\,i}\right) - \frac{\omega_3 T^\circ}{2\pi} \arcsin\left(\frac{\sin\varphi}{\sin i}\right). \tag{8}$$

The current longitude of the satellite is

$$\lambda = \lambda_0 + \arcsin\left(\frac{tg\,\varphi}{tg\,i}\right) - \frac{\omega_3 T^\circ}{2\pi} \arcsin\left(\frac{\sin\varphi}{\sin i}\right). \tag{9}$$

Formula (9) gives a relationship between the longitude and latitude of the satellite's projection onto the earth's surface for a satellite moving on a circular orbit. In the case of a diurnal satellite

$$T^\circ = 2\pi / \omega_3, \tag{10}$$

and Formula (9) assumes the form

$$\lambda = \lambda_0 + \arcsin\left(\frac{tg\,\varphi}{tg\,i}\right) - \arcsin\left(\frac{\sin\varphi}{\sin i}\right). \tag{11}$$

- 39 -

Fig. 2

- 40 -
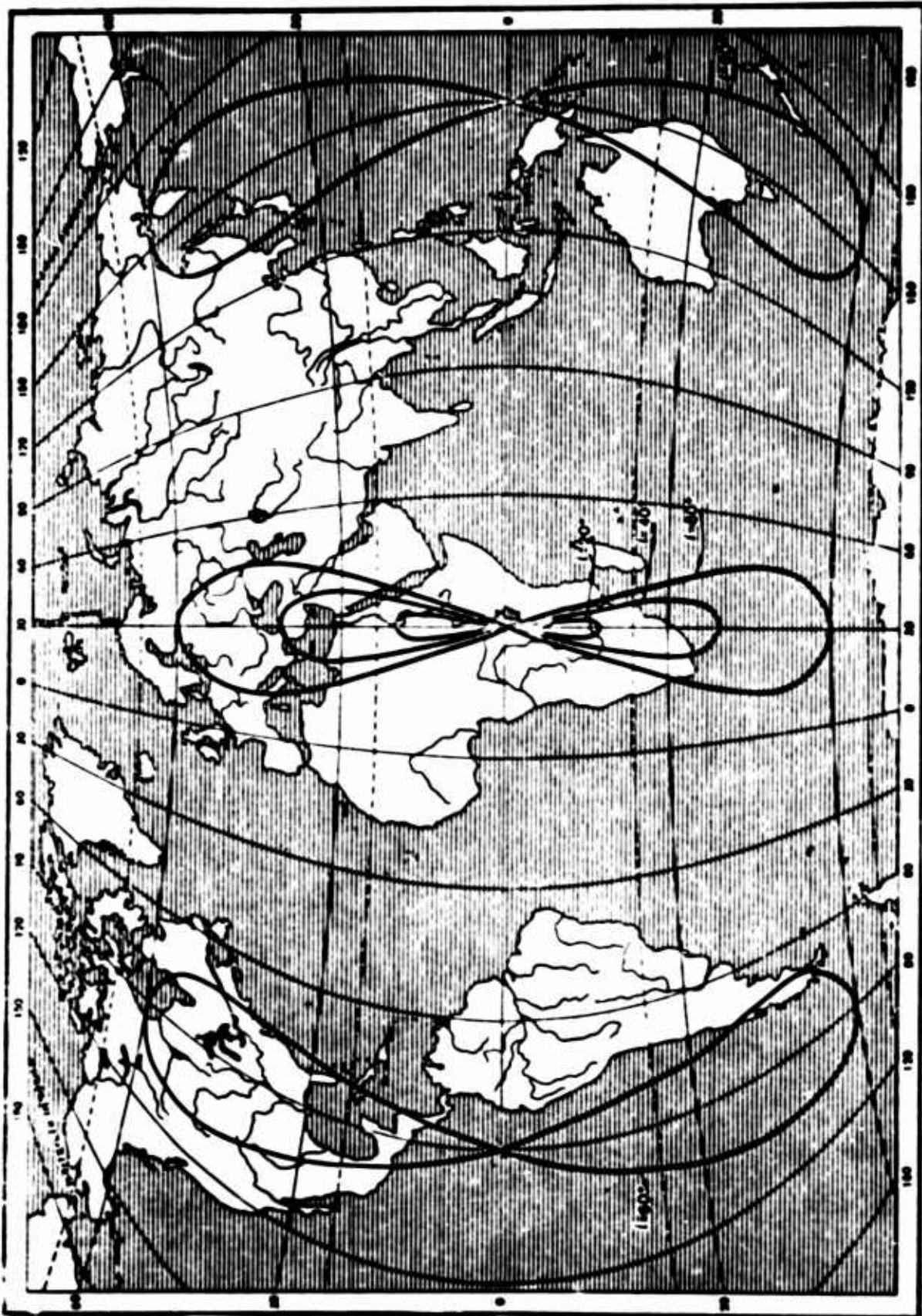
Using Formula (11), it is easy to construct diurnal earth-satellite tracks for specified values of the parameters λ_v and $\underline{1}$. From the results of calculations made for $\lambda_v = 30^\circ E$, $150^\circ E$, $90^\circ W$ and for values of the parameter $\underline{1}$ assigned in the interval $0^\circ \leq 1 \leq 180^\circ$, it follows that the track of a diurnal satellite is a closed double loop or "figure eight," with its center on the Equator (Figs. 2, 3).

Let us note the two limiting cases corresponding to two values of the orbital inclination: $1 = 0$ and 180°. At $1 = 0^\circ$, the diurnal satellite is stationary, remaining above the same point of the Equator at all times. For $1 = 180^\circ$, the diurnal satellite will move westward and pass over every point of the Equator twice each day.
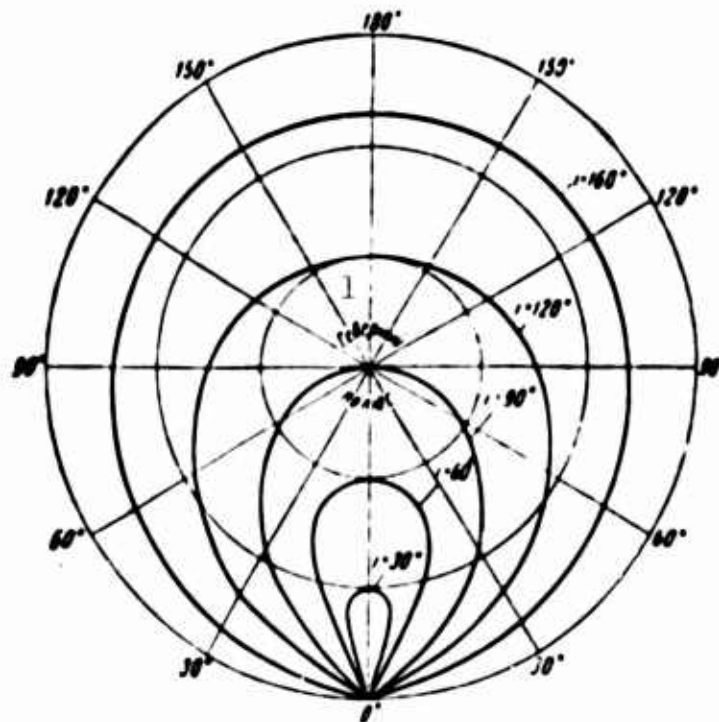
Fig. 3. 1) North Pole.

PARAMETERS OF THE TRACKS

For rough calculations, it is convenient to introduce the following track parameters for diurnal satellites: λ_{ts}, the longitude of the center of the "figure eight"; φ_{max}, the maximum latitude attained in motion along the "figure eight"; $(\Delta\lambda)_{max}$, the largest difference between longitudes reached in motion along the "figure eight."

- 41 -

Let us derive working formulas that enable us to determine these parameters if the parameters $\lambda_к, \varphi_к, A_к$ of the projection of the end of the powered trajectory segment onto the earth's surface are known. Here we shall use the familiar relationship

$$\cos i = \cos \varphi \sin A. \qquad (12)$$

Setting in Expression (11)

$$\lambda = \lambda_к, \quad \varphi = \varphi_к, \quad \lambda_в = \lambda_u \qquad (13)$$

we get

$$\lambda_u = \lambda_к - \arcsin\left(\frac{\operatorname{tg}\varphi_к}{\operatorname{tg} i}\right) + \arcsin\left(\frac{\sin\varphi_к}{\sin i}\right). \qquad (14)$$

It follows from (1) that the maximum latitude value corresponds to the condition

$$\Delta\Omega = \pm 90° \qquad (15)$$

and is equal to

$$\varphi_{max} = \pm i. \qquad (16)$$

To determine the maximum longitude difference in motion along the track, let us decompose the velocity of the satellite's projection over the surface of a nonrotating earth into two components: one with zero azimuth and one with an azimuth of $90°$:

$$V_0 = V \cos A = \omega_э R \cos A, \qquad (17)$$
$$V_{90} = V \sin A = \omega_э R \sin A. \qquad (18)$$

The rotary speed of the point on the earth's surface onto which the satellite projects is equal to

$$V_з = \omega_э R \cos \varphi. \qquad (19)$$

At the moment of crossing the equator, we have from (12)

$$\sin A = \cos i, \qquad (20)$$

and, consequently,

$$V_{90} \leqslant V_з. \qquad (21)$$

Here the equality in Formula (21) applies only for $i = 0°$. It fol-

lows from (21) that at the moment of crossing the Equator, the projection of the satellite onto the surface of a rotating earth will move westward. At the time of attainment of maximum latitude

$$A = 90°, \quad V_{\omega} > V_{s}. \tag{22}$$

The equality obtains in Formula (22) only with $i = 0°$. It follows from (22) that when maximum latitude is reached, the satellite's projection onto the surface of a rotating earth will move eastward.

It is obvious that as the latitude of an artificial earth satellite varies from $0°$ to φ_{max}, the equality

$$V_{\omega} = V_{s}. \tag{23}$$

will obtain at a certain point in time.

At this moment, the difference between the longitude of the satellite's projection onto the earth's surface and the longitude of the center of the "figure eight" reaches its maximum. Let us find it from Condition (23). From (18) and (19), we find

$$\sin A = \cos \varphi. \tag{24}$$

Using Formulas (3), (11), and (24), we can obtain

$$\lambda - \lambda_{u} = \arcsin \sqrt{\frac{\cos i}{1 + \cos i}} - \arcsin \frac{1}{\sqrt{1 + \cos i}}. \tag{25}$$

Consequently, the maximum longitude difference during motion on the track will be

$$(\Delta\lambda)_{max} = 2(\lambda - \lambda_{u}) = 2\left[\arcsin \sqrt{\frac{\cos i}{1 + \cos i}} - \arcsin \frac{1}{\sqrt{1 + \cos i}}\right]. \tag{26}$$

The above applies only for $i \leqslant 90°$. In the case $i > 90°$, Equality (26) is not satisfied, and the projection of the satellite onto the surface of a rotating earth will move continually westward, in such a way that the upper loop of the "figure eight" will enclose the North Pole, and the lower loop the South Pole of the earth (Fig. 3).

From Formula (14), (16), and (26), and from the relationship

$$\cos i = \cos \varphi_{\kappa} \sin A_{\kappa} \qquad (27)$$

it follows that the parameters λ_{ts}, φ_{max}, and $(\Delta\lambda)_{max}$ of the diurnal satellite's track can be determined if the parameters λ_k, φ_k and A_k of the end of the trajectory's powered segment are known. Here the "width" $(\Delta\lambda)_{max}$ and "height" φ_{max} of the "figure eight" do not depend on the longitude of the projection of the end of the powered segment onto the earth's surface, and are determined by the inclination of the orbit (or by the parameters φ_k, A_k). It follows from (14), (16) and (26) that, by varying the longitude and latitude at the end of the powered segment with the orbital inclination held constant, we can change the position of the center of the "figure eight" on the Equator, while keeping its "width" and "height" unchanged.
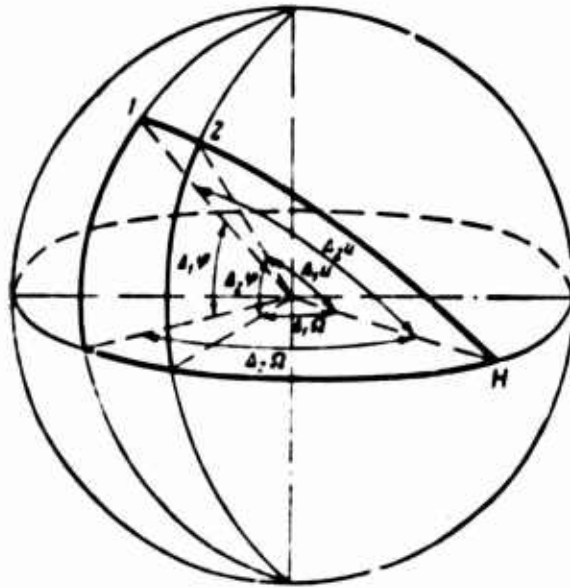
Fig. 4

Let us consider one of the ways in which we can accomplish this without energy losses. It is a known fact that when a diurnal satellite is injected into orbit, it is favorable from a power standpoint to use a "intermittent" powered segment, with the engine operated in two bursts, as follows.

1. Parking the booster rocket at the perigee of a transitional el-

liptical orbit whose apogee height is equal to the altitude of the synchronous diurnal orbit.

2. Motion with the engine off along the transitional ellipse to the region of its apogee.

3. Reignition of the engine in the region of the ellipse apogee and injection into the diurnal orbit.

To change the longitude and latitude at the end of the powered segment, it is convenient to introduce a second "break" on the powered part of the trajectory. The injection scheme will change somewhat when this is done.

1. Parking the booster rocket on an intermediate circular orbit whose altitude is equal to that of the perigee of a transitional elliptical orbit.

2. Motion with the engine off along the intermediate circular orbit for a specified length of time τ_r.

3. Restarting the engine with injection at the perigee of a transitional elliptical orbit.

4. Motion with the engine off along the transitional ellipse to the region of its apogee.

5. Engine started for a third time in the region of the ellipse apogee, with injection into the diurnal orbit.

It is obvious that, by varying the time τ_r of the motion along the intermediate circular orbit, we can change the longitude and latitude at the end of the powered segment without affecting the thrust potential of the rocket booster and holding the inclination of the diurnal orbit unchanged. Let us derive approximate relationships for the parameters at the end of the powered trajectory segment as functions of the time of motion along the intermediate circular orbit. For this purpose, we shall use the following simplifying assumptions: a) when the engine is started

for the second and third times, the thrust impulse is transmitted instantaneously to the booster rocket; b) after the engine is shut off for the first time, the trajectory of the booster rocket lies in the plane of the diurnal orbit.

Let us consider the positions of the booster rocket at the times t_1, t_2, and t_n. Without loss of generality, we shall assume that the times t_1 and t_2 correspond to motion above the northern hemisphere of the earth (Fig. 4).

From the spherical triangles formed by the arcs

$$\Delta_0 u = u_n - u_1, \qquad \Delta_1\varphi = \varphi_1 - \varphi_n, \qquad \Delta_3\Omega = \Omega_n - \Omega_1,$$
$$\Delta_1 u = u_n - u_2, \qquad \Delta_2\varphi = \varphi_2 - \varphi_n, \qquad \Delta_1\Omega = \Omega_n - \Omega_2,$$

we obtain

$$\cos A_1 = -\cos (\Omega_n - \Omega_1) \sin i, \tag{28}$$
$$\cos (u_n - u_1) = \cos (\Omega_n - \Omega_1) \cos \varphi_1, \tag{29}$$
$$\sin \varphi_2 = \sin (u_n - u_2) \sin i, \tag{30}$$
$$\operatorname{tg} (\Omega_n - \Omega_2) = \operatorname{tg} (u_n - u_2) \cos i. \tag{31}$$

The variation of the latitude argument with motion along the intermediate circular orbit is proportional to the time of motion along the intermediate circular orbit:

$$u_2 - u_1 = \frac{2\pi}{T^\circ} \tau_p. \tag{32}$$

Let us determine the coordinates of the booster's projection onto the earth's surface at the time when the engine is started for the second burst. Comparing Expressions (28) and (29), we obtain

$$u_n - u_1 = \arccos \left[\frac{-\cos A_1 \cos \varphi_1}{\sin i} \right]. \tag{33}$$

We find from (32) and (33)

$$u_n - u_2 = \arccos \left[\frac{-\cos A_1 \cos \varphi_1}{\sin i} \right] - \frac{2\pi}{T^\circ} \tau_p. \tag{34}$$

We get the latitude at point 2 by substituting Relationship (34) into Formula (31), which we rewrite in the form

$$\varphi_2 = \arcsin\left[\sin\left(u_n - u_2\right)\sin i\right]. \tag{35}$$

The change in right ascension during the passage from point 1 to point 2 is found by applying Expressions (28) and (30).

$$\Omega_2 - \Omega_1 = \arccos\left[\frac{-\cos A_1}{\sin i}\right] - \operatorname{arc\,tg}\left[\operatorname{tg}\left(u_n - u_2\right)\cos i\right]. \tag{36}$$

The geographic longitude of point 2 is determined by the expression

$$\lambda_2 = \lambda_1 + \left(\Omega_2 - \Omega_1\right) - \omega_3\tau_p. \tag{37}$$

The coordinates of the end of the powered segment at the time of injection into the diurnal orbit can be found from the formulas

$$\lambda_n = \lambda_2 + \pi - \omega_3\frac{T_s}{2}, \quad \varphi_n = \varphi_2 \quad \left(T_s = 2\pi\sqrt{\frac{(r_n + r_a)^3}{2k}}\right). \tag{38}$$

Using Formulas (34)-(38) for assigned λ_1, φ_1 and A_1, we can determine the time τ_r of motion on the intermediate circular orbit that is required to obtain the specified position of the center of the "figure eight" on the Equator.

Received
26 August 1963

REFERENCES

1. A.A. Shternfel'd, Iskusstvennyye sputniki [Artificial Satellites], Gostekhteoretizdat [State Publishing House for Technical and Theoretical Literature], 1958.

2. V. Friedrich, Tech. Session Prepr. Amer. Astronaut. Soc., No. 18, 1959.

Manuscript Page No.	[Transliterated Symbols]
37	з = z = zemlya = earth
37	э = e = ellipticheskiy = elliptical
37	a = a = apogey = apogee

37	п = p = perigey = perigee
37	в = v = voskhodyashchiy = ascending
37	н = n = niskhodyashchiy = descending
38	к = k = konets = end
38	tg = tan = tangent
45	p = r = razryv = discontinuity, break

ON THE POSSIBILITY OF IMPROVING THE ACCURACY OF DETERMINATION OF THE ORBITS OF SPACE VEHICLES BY REDUCING THE INFLUENCE OF CORRELATED ERRORS

A.V. Brykov

The article is devoted to the problem of using statistical methods for processing correlated measurements to determine the actual orbits of space vehicles.

The basic relationships characterizing the effectiveness with which these methods can be applied are ascertained on the simplest example, in which two correlated measurements are reduced.

The possibility, in principle, of making effective use of statistical methods for the evaluation of correlated measurements to determine the orbits of space vehicles is indicated not only in the case in which the probability characteristics of the measurements are exactly known, but also in the case that is of greatest interest from the practical standpoint — that in which they are not known with sufficient certainty.

In conclusion, a quantitative evaluation of the effectiveness of these methods is set forth with reference to an example closely similar to that of determining the orbits of space vehicles.

In launching space vehicles to conduct assigned scientific-research programs, it is necessary, as a rule, to know not only the calculated orbits, but also those actually realized. The elements of the true orbits of space vehicles are required in coordinating the measured data,

predicting motions in the course of the flight, and in solving a number of other problems. Here, the demands made as to the accuracy of the orbital determination may be very high in some cases. Among the problems requiring high-precision determination of the orbits we may encounter, for example, the following:

determination of the density of the atmospheric upper layers from the results of ISZ observations, with the object of constructing a dynamic model of the atmosphere [1, 2];

determining the impact point of a lunar rocket on the surface of the moon from orbital-measurement data [3];

refining the dimensions and figures of celestial bodies in the solar system from the results of observations of space-vehicle flights [4].

It should be noted that the possibility of exact orbit determination from the results of measurements made on short segments of the orbits will considerably expand the range of scientific problems that can be solved with the aid of space vehicles. The accuracy of orbit determination is limited basically by the following three factors:

errors of the measuring systems,

uncertain knowledge of the forces acting on the space vehicle during its flight,

the imperfect state of methods for evaluating the measured information.

In the present paper, these factors will be considered in an analysis of ways to improve the accuracy of orbit determinations only in connection with improvement of the data-reduction methods.

The use of radio-electronic systems as the basic measuring devices for orbital measurements insures the possibility of acquiring a large volume of measurement data, and when the most highly perfected statis-

tical evaluation methods are applied to this, the result may be an orbital determination of rather high accuracy. However, the extensive implementation of such processing methods for determining the orbits of space vehicles encounters a number of difficulties. Foremost among these is that associated with the nature of the errors burdening the measured information. The measurement errors include both weakly correlated, practically independent errors as well as strongly correlated errors.

If the probability characteristics of these errors are known, then the influence of errors of both the first and second types can be reduced significantly by the use of appropriate processing methods under certain conditions, and the very strongly correlated, practically constant errors can be excluded altogether.

Usually, however, the probability characteristics of the measured information, and particularly those of its correlated components, are not known with sufficient certainty. In determining orbits, therefore, we apply techniques based on the classical method of least squares and, consequently, designed for reduction of independent measurements. As a result, strongly correlated measurement-error components determine the accuracy to which the actual orbit is calculated [1].

A second difficulty stems from the presence of error in our knowledge of the forces under which the motion is taking place. Errors in our knowledge of the planetary figures and the astronomical constants, aerodynamic forces, etc. may, for certain types of space vehicles, prove to be decisive for the accuracy with which the actual orbit is calculated. Here, of course, it is not possible to improve the accuracy of the orbit determination substantially by virtue of more perfect evaluation of the measurement data alone. In consequence of this, preference must be given to the classical method of least squares for such types

of orbits.

Finally, the application of orbit-determining techniques based on more highly perfected statistical methods of processing the measured information requires the use of a complex mathematical algorithm and increases the amount of time required for the calculations. We note that these difficulties – apart from the factors related to our ignorance of the probability characteristics – are not of fundamental significance for the problem under consideration and can be surmounted easily. Among other things, most of the quantities whose errors are determined by our inexact knowledge of the forces can be included among the parameters to be determined as a result of the data reduction, or among the parameters to be measured. In the latter case, as will be shown below, they are converted into correlated measurements and their influence on the errors of orbit determination can be partially or totally excluded. As for the complexity and laboriousness of the calculations, this problem is quite solvable at the present advanced state of development of electronic computers. Thus, in view of this last remark, we may consider that the basic obstacle on the path of improving the accuracy of space-vehicle orbit determinations is the presence of strongly correlated errors in the measured information, errors whose probability characteristics are not known with sufficient accuracy.

The task of the present paper consists in indicating the possibility, in principle, of raising the accuracy of space-vehicle orbit determinations by reducing the influence of strongly correlated components of the measurement errors, even when our knowledge of their probability characteristics is limited.

The equations of motion of a space vehicle connect the initial conditions of the motion

$$q_j (j = 1, 2, \ldots, N) \qquad (1)$$

with the measured parameters

$$r_i(i = 1, 2, \ldots, n) \tag{2}$$

by a differential relationship of the form

$$f_i(q_1, q_2, \ldots, q_N, w_1, w_2, \ldots, w_m) = r_i, \tag{3}$$

where $w_\nu(\nu = 1, 2, \ldots, m)$ are certain parameters characterizing the forces in operation.

Suppose that as a result of observations, we have obtained values of the measured parameters distorted by correlated errors:

$$\tilde{r}_i(i = 1, 2, \ldots, n). \tag{4}$$

Then, as we know [1], the determination of the motion's initial conditions can be reduced to solution of a linear system of conditioned equations — a system that, in matrix form, is written as

$$A\Delta q = \Delta r. \tag{5}$$

Here, $\Delta q = \Delta q_{N1}$, $\Delta r = \Delta r_{n1}$ and $A = A_{rN}$ denote, respectively, matrices with elements that are the differences $(\Delta q_j = q_j - q_j^*)$ between the values of the initial conditions of the motion (1) and certain approximate values q_j^* of these conditions; differences $(\Delta r_i = \tilde{r}_i - r_i^*)$ between the parameters (4) and their values as calculated from (3) for $q_j = q_j^*$; and the values of the derivatives of the measured parameters with respect to the initial conditions of the motion $(a_{ij} = \partial r_i / \partial q_j = \partial f_i / \partial q_j)$.

The linear system of conditioned equations (5), which is a relationship between the sought initial conditions of the motion and the correlated measurements that cannot be solved for Δq for n > N, can be solved by statistical methods. One of these methods may be that of processing the dependent measurements, as set forth in [5] — a method developed on the basis of Fisher's maximum plausibility method.

In this case, regardless of the error distribution law, unbiased effective estimates determined by the following matrix relationship apply for the unknown initial conditions:

$$\Delta q = (A^T K^{-1} A)^{-1} A^T K^{-1} \Delta r = Q A^T K^{-1} \Delta r, \qquad (6)$$

where

$$Q = (A^T K^{-1} A)^{-1},$$

and the accuracy of determination of their linear function

$$\varrho = \varphi \Delta q, \qquad (7)$$

where $\varphi = \varphi_{1N}$ is a matrix with elements φ_i, is characterized by the root-mean-square deviation

$$\sigma_\rho = \sqrt{\varphi Q \varphi^T}. \qquad (8)$$

Here $K = K_{nn}$ is the correlation matrix of the measurements being reduced (4).

Use of this method to reduce correlated measurements may not always improve the accuracy as compared with the classical method of least squares. For example, in an analysis of the effect of measurement dependence as reflected in the accuracy of the reduction results [5], a case considered as an example produced the same result with either method over a rather broad range of variation of the strength of the dependence. It is found that to obtain the desired effect of improving the accuracy, it is necessary to satisfy certain conditions imposed on the elements of matrix **A**. To ascertain these conditions and indicate clearly the effectiveness of the correlated-measurement reduction, let us consider the simplest case of reducing excess information: determination of a single quantity ($\Delta q^{(0)}$) from two measurements ($\Delta \bar{r}_1$ and $\Delta \bar{r}_2$).

For such a problem, we shall have

$$\Delta q = \Delta q_N = \Delta q_{11} = \Delta q^{(0)},$$

$$\Delta r = \Delta r_{n1} = \Delta r_{21} = \left\| \begin{array}{c} \Delta r_1 \\ \Delta r_2 \end{array} \right\|,$$

$$A = A_{nN} = A_{21} = \left\| \begin{array}{c} a_1 \\ a_2 \end{array} \right\|,$$

$$K = K_{nn} = K_{22} = \left\| \begin{array}{cc} D_r & K_r \\ K_r & D_r \end{array} \right\|.$$

- 54 -
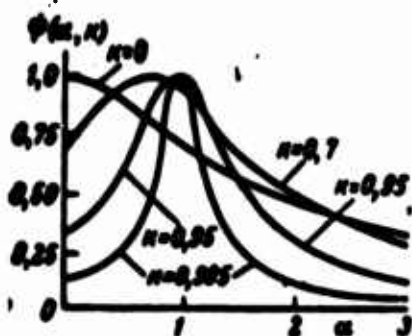
Fig. 1

(it is assumed for simplicity that the measurements are equally accurate). Then the system of conditioned equations takes the form

$$a_1 \Delta q^{(0)} = F_1, \quad a_2 \Delta q^{(0)} = \Delta F_2, \quad (9)$$

and the solution may, on the basis of (6), be written as follows:

$$\Delta q^{(0)} = \frac{(a_1 D_r - a_2 K_r)\Delta F_1 + (a_2 D_r - a_1 K_r)\Delta F_2}{(a_1 D_r - a_2 K_r)a_1 + (a_2 D_r - a_1 K_r)a_2} \cdot (10)$$

Here the accuracy with which $\Delta q^{(0)}$ is determined will be characterized by the root-mean-square deviation

$$\sigma_{\Delta q} = \sqrt{\frac{D_r^2 - K_r^2}{(a_1 D_r - a_2 K_r)a_1 + (a_2 D_r - a_1 K_r)a_2}}. \quad (11)$$

Transforming relationships (10) and (11) in such a way that $\Delta q^{(0)}$ and $\sigma_{\Delta q}$ are expressed in terms of the correlation coefficient $k = K_r / D_r$ and the parameters $\alpha = a_2/a_1$ and $\beta = F_2/\Delta F_1$, we obtain for $a_1 \neq 0$ and $\Delta F_1 \neq 0$

$$\Delta q^{(0)} = \frac{\Delta F_1}{a_1} \frac{(1 - \alpha k) + (\alpha - k)\beta}{(1 + \alpha^2) - 2\alpha k} = \frac{\Delta F_1}{a_1} \chi(\alpha, k, \beta), \quad (12)$$

$$\sigma_{\Delta q} = \frac{\sqrt{D_r}}{a_1} \sqrt{\frac{1 - k^2}{(1 + \alpha^2) - 2\alpha k}} = \frac{\sqrt{D_r}}{a_1} \psi(\alpha, k). \quad (13)$$

For a fixed value of a_1, the errors in the determination of $\Delta q^{(0)}$ may be characterized with an accuracy to within a constant cofactor by the function $\psi(\alpha, k)$. Figure 1 presents a diagram of the variation of this function with the parameter α and the correlation coefficient k. As will be seen from the diagram, the accuracy with which $\Delta q^{(0)}$ is found depends to a high degree on the magnitude of the parameter α. As α varies from 0 to 3, $\psi(\alpha, k)$ diminishes from 1 to 0.28 for k = 0, to 0.13 for k = 0.9 and to 0.06 for k = 0.995. The maximum of the error, which corresponds, as will be seen from (13), to α = k, shifts from values of α = 0 to values of α = 1 and becomes more distinct, without changing in

- 55 -

magnitude, as the correlation coefficient increases. Consequently, the higher the degree of measurement correlation and the greater the difference between the parameter α and that value of it which corresponds to ψ_{max}, the more accurately will $\Delta q^{(u)}$ be determined. For linearly dependent, systematic errors, when $k = 1$ or $k = -1$, it follows from Relationship (13) that there is no error at all in the determination of $\Delta q^{(u)}$ if $\alpha \neq 1$ or $\alpha \neq -1$, respectively, and that the error reaches its maximum for $\alpha = 1$ or $\alpha = -1$. It is this that gives rise to the condition insuring the possibility of reducing or eliminating the correlated-error effect.

Generalizing the results obtained to the case of reducing dependent measurements, in which $N > 1$ and $\dot{n} > N + 1$, we arrive at the conclusion that to ensure a possibility of reducing or eliminating the influence of correlated errors, it is necessary that the elements of the columns of matrix Λ be different. This condition is satisfied at once in problems of determining space-vehicle orbits. As follows from the physical essense of the matrix Λ column elements themselves — elements that are, in this problem, derivatives of the parameters to be measured with respect to the initial conditions of the motion, they will vary essentially along the trajectory [1]. Moreover, it is possible, by appropriate selection of the measurement-point positions relative to the orbit [6], to provide a relationship for them that will be closest to the optimum. Consequently, it may be stated that application of reduction techniques that take measurement dependence into account for determination of space-vehicle orbits may insure an increase in accuracy by reducing or eliminating the influence of correlated measurement errors. For final disposal of the question as to the use of these methods for the case in which errors in our knowledge of the forces are decisive, let us show how these errors can produce errors of measurement. Then,

in accordance with the conclusions derived above, their influence on the accuracy of the orbit determination may be reduced essentially or eliminated altogether.

Let the exact values of the parameters w_ν ($\nu = 1, 2, \ldots, m$) in Relationship (3) be unknown, and assume that we know only their approximate values w_ν^*, so that the error in our knowledge of each parameter $\delta \dot{w}_\nu = w_\nu - w_\nu^*$ is small as compared with the magnitude of the parameter itself. Then on linearization of Relationship (3), the result obtained may be written in the form

$$\sum_{j=1}^{N} \frac{\partial f_i}{\partial q_j} \delta q_j + \sum_{\nu=1}^{m} \frac{\partial f_i}{\partial w_\nu} \delta w_\nu = \delta r_i \quad (i = 1, 2, \ldots, n) \tag{14}$$

or, taking the symbols introduced above into account:

$$\sum_{j=1}^{N} a_{ij} \delta q_j = \delta r_i - \sum_{\nu=1}^{m} \frac{\partial r_i}{\partial w_\nu} \delta w_\nu \quad (i = 1, 2, \ldots, n). \tag{15}$$

It is obvious that the right member of System (15) is a system of $\underline{n}$ random quantities, each of which carries the same errors δw_ν ($\nu = 1, 2, \ldots, m$), whose correlation matrix* we denote by K^W. Then the correlation matrix of the new system of random quantities — let us denote it by K^* — is readily expressed in terms of the assigned matrix K^r and K^W. Obviously, the following relationship will apply for the elements of the matrix K^*:

$$K_{i\mu}^* = K_{i\mu}^r + \sum_{\nu=1}^{m} \sum_{\lambda=1}^{m} \frac{\partial r_i}{\partial w_\lambda} \frac{\partial r_\mu}{\partial w_\lambda} K_{\nu\lambda}^w \quad (i, \mu = 1, 2, \ldots, n). \tag{16}$$

Now if in Expression (15) we replace the random quantities δr_i ($i = 1, 2, \ldots, n$) and δw_ν ($\nu = 1, 2, \ldots, m$) with the particular realizations $\Delta \tilde{r}_i = \tilde{r}_i - r_i^*$ ($i = 1, 2, \ldots, n$) and $\Delta \tilde{w}_\nu = \tilde{w}_\nu - w_\nu^* = w_\nu^* - w_\nu^* = 0$ ($\nu = 1, 2, \ldots, m$), obtained as a a result of measurement, then System (15) becomes the system (5) that we examined earlier, but subject to the additional con-

Fig. 2.

dition that the correlation matrix of the measurements is equal to the matrix K* with elements defined by Relationship (16), i.e., the problem reduces to the case of correlated-measurement reduction examined above.

Up to this point, we have been considering the question as to the possibility of reducing or eliminating the influence of correlated measurement errors in the problem of determining the orbits of space vehicles for the condition that the probability characteristics of the errors are exactly known. But the greatest practical interest attaches to solution of this problem for the case in which our knowledge of the probability characteristics of the measurement errors is limited. To indicate the possibility of solving this problem, let us turn to the elementary example of correlated-measurement reduction examined above. The value of the unknown $\Delta q^{(0)}$ in the presence of measurements $\Delta \tilde{r}_1$ and $\Delta \tilde{r}_2$ is determined by Relationship (10) or (12). Here, if the correlation coefficient $\underline{k}$, which is the fundamental probability characteristic of the measurement errors,* is known with an error δk, then on the basis of (12) the dependence of $\Delta q^{(0)}$ on the error δk can be represented by the following expression:

$$\Delta q^{(0)}(\delta k) = \frac{\Delta \tilde{r}_1}{a_1} \frac{1 + a\beta - (a + \beta)(k - \delta k)}{1 + a^2 - 2a(k - \delta k)} = \frac{\Delta \tilde{r}_1}{a_1} \chi^*(a, k, \beta, \delta k). \qquad (17)$$

To construct the relationship $\Delta q^{(0)}(\delta k)$, on the basis of this expression, it is necessary to know the parameter $\beta = \Delta \tilde{r}_2 / \Delta \tilde{r}_1$, which does not depend on a, but is a function of the correlation coefficient. It is easy to obtain the relationship $\beta(k)$ using the particular realizations given in [5] for the stationary random variable $\Delta r(t)$, which has a zero mathematical expectation, unit dispersion and a normalized correlation function $k(\tau) = e^{-a|\tau|}$. It is obvious that if for a given particular

- 58 -

realization of the random variable its value has been fixed at $\Delta F(t_1) = \Delta F_1 \neq 0$, the ratio of any other value $\Delta F(t_2)$ isolated from the first interval $\tau_1 = t_2 - t_1$, to the first will give the unknown parameter $\beta(\tau_1)$ corresponding to the correlation coefficient $k(\tau_1) = e^{-\alpha\tau_1}$.

Figure 2 shows the relationship $\beta(k)$ for three particular realizations of the random variable $\Delta r(t)$, selected from among the ten particular realizations of [5] in such a way that one of them would assume the largest values (variant $\beta = \beta_1$), another average values (variant $\beta = \beta_2$) and a third the smallest values (variant $\beta = \beta_3$). Since the original random variable $\Delta r(t)$ has a zero mathematical expectation, it follows from (10) that the exact value of the unknown quantity Δq must be equal to zero. Consequently, the value of $\Delta q^{(m)}$, calculated from Formula (12) or (17), is the error of determination of the quantity Δq in a given particular realization of the measurements ΔF_1 and ΔF_2. But since our interest in this problem lies not in the absolute error values, but only in the influence exerted on them by the parameters α, β, k and δk, then it is obvious that it will be sufficient for analysis to consider the variation of the function $\chi^*(\alpha, k, \beta, \delta k)$.

Figure 3 presents curves of the variation of this function with the correlation coefficient for the three variants of the parameter β and three values of α. Here, the curves are given for four values of the errors δk: curves 1 correspond to an error $\delta k = 0$, curves 2 to $\delta k = 0.33\,k$, curves 3 to $\delta k = 0.67k$ and curves 4 to $\delta k = k$. This last case (curve 4) corresponds to reduction of the correlated measurements by the classical method of least squares. Analysis of the curve shown here indicates that for $\alpha = 1$ the results of processing the correlated measurements do not depend on the errors in our knowledge of the correlation coefficient, but are determined entirely by the results of the measurements. In this case, as follows from (12) and (17),

- 59 -
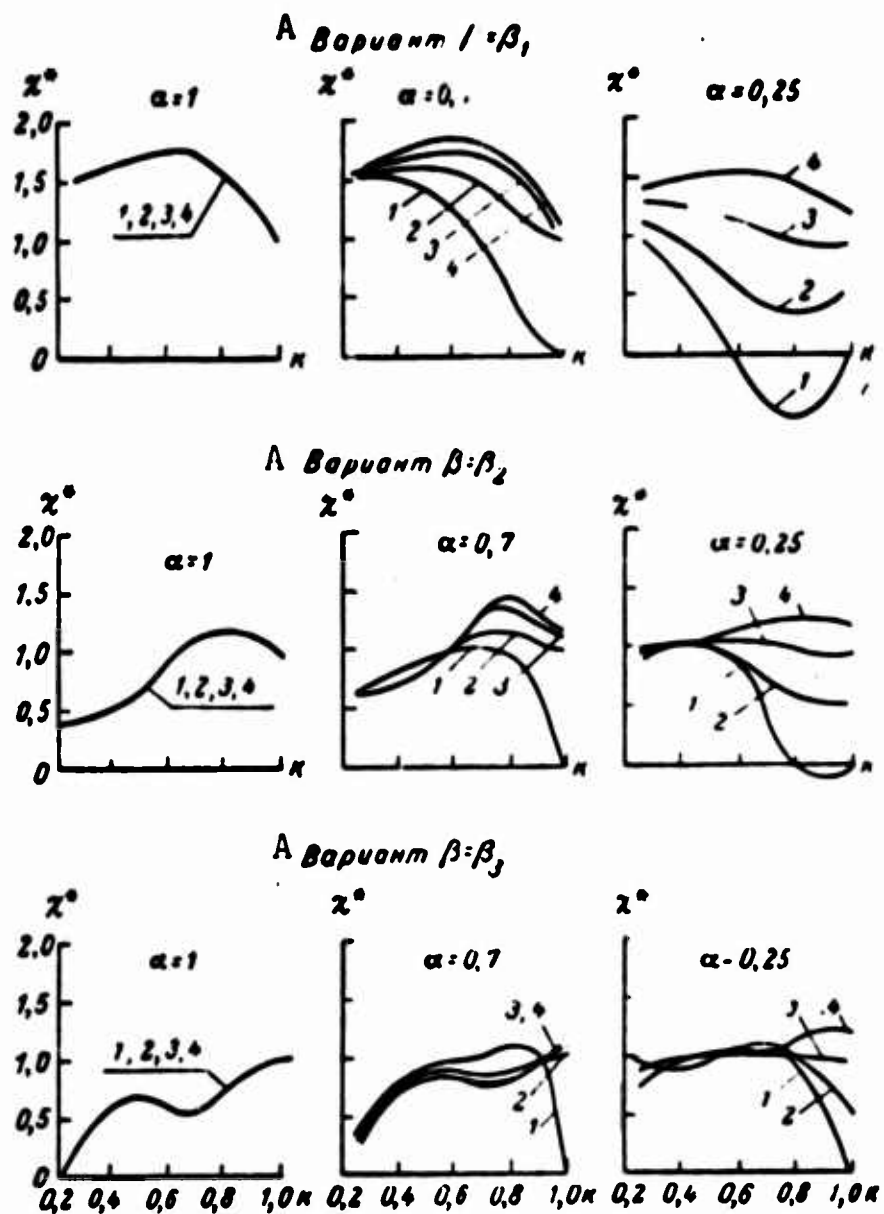
Fig. 3. A) Variant.

$\chi_{k-1}^{*} = 0.5(1+\beta)$. As α diminishes, the difference between the reduction
of the measurements with full ($\delta k = 0$) or partial ($k > \delta k \neq 0$) account
of the dependence and the reduction without consideration of it ($\delta k = k$)
becomes increasingly significant. Thus, for $\alpha = 0.7$, this difference
becomes essential even for $k > 0.3$ for the first β variant, at $k > 0.6$
for the second β variant and at $k > 0.9$ for the third. As α diminishes
further, these limits broaden. For $\alpha = 0.25$, the first β variant gives
an essential difference in the results of reduction for $k \geq 0.25$, the
second for $k > 0.5$ and the third for $k > 0.75$. For values of k smaller
than those indicated above, the curves indicate that the reduction re-

sults practically coincide irrespective of the errors δk. The only exception is a short segment of variation of $\underline{k}$ (from 0.65 to 0.85) for the third β variant, where taking the dependence into account increases the error to 25%. Finally, it is necessary to note the most important peculiarity of reduction of correlated measurements — one that is
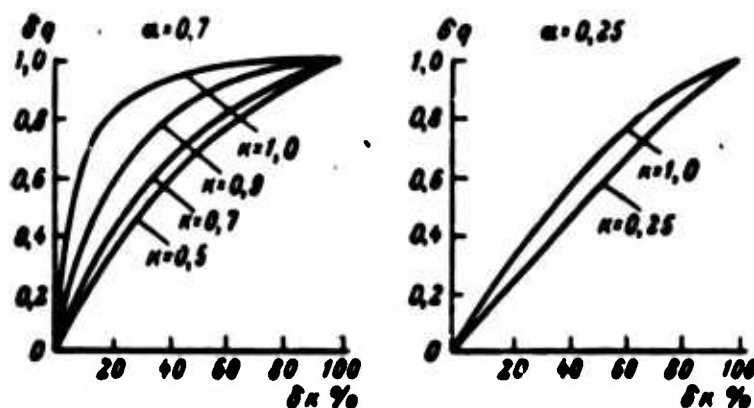
Fig. 4

of fundamental importance for the problem under consideration: this consists in the fact that with diminishing α, the tendency toward reduction of the error as a result of full $(δk = 0)$ or partial $(k > δk \neq 0)$ account of the dependence of the measurements in their reduction manifests with increasing clarity. Thus, for example, for curve 2 $(δk = 0.33k)$, passage from $α = 0.7$ to $α = 0.25$ results for all three β variants, in a diminution of the error by almost half. This tendency is clearly evident from Fig. 4, where the variation of the relative error

$$\delta q(\delta k) = \frac{\Delta q^{(0)}(\delta k) - \Delta q^{(0)}(\delta k = 0)}{\Delta q^{(0)}(\delta k = k) - \Delta q^{(0)}(\delta k = 0)} \tag{18}$$

is shown for the first β variant as a function of the error δk. As will be seen from Relationship (18), $\delta q(\delta k)$ is the ratio of the variation of the error in $\Delta q^{(0)}$ due to the presence of the error δk to its maximum variation, which occurs at the maximum value of the error δk = k, i.e., for reduction of the information by the classical method of least squares. For small α, as will be seen from the diagram shown, even

large errors in the correlation coefficient provide an opportunity for a substantial increase in accuracy, while for large α this possibility is sharply reduced, particularly for values of the correlation coefficient near unity. A qualitatively similar picture also emerges for values of α in excess of unity. If $\alpha > 1$, then the optimum conditions for reduction correspond to large values of α, and the poorest to values of α close to unity. Thus, the results obtained indicate a possibility of improving reduction accuracy even in the presence of errors in our knowledge of the probability characteristics of the measurement errors. Here, this increase will be the greater the more the parameter α departs from unity and the higher the degree of correlation characterizing the measurements.

Generalizing the above result, we arrive at the conclusion that the basic condition for solving the problem posed reduces to the requirement that the column elements of the matrix A be different, i.e., to the same condition as in the case in which correlated measurements with known probability characteristics are being reduced, since this condition admits of full satisfaction in problems of determing space-vehicle orbits, we may definitely conclude that it is possible to improve the accuracy of determination of these orbits by reducing the influence of correlated errors even in cases where their probability characteristics are known only with errors.

From the standpoint of determining space-vehicle orbits, the simple example of correlated-measurement reduction that we have considered above gives only a qualitative characterization of the influence exerted by various factors on the reduction results. To provide some impression of the quantitative side of the problem, let us conclude with some results of reducing correlated measurements for the case in which a single parameter $\Delta q^{(0)}$ is determined from $\underline{n}$ correlated measurements

Δr_i $(i = 1, 2, \ldots, n)$. This problem resembles those in which orbits are determined and may be encountered in practice, for example, in determing the speed of a space vehicle if the direction of that speed and the coordinates of the point at which it is necessary to determine it are known. Particular realizations of a stationary random variable [5] are taken in this problem as the measurement information:

$$\delta r(t) = \gamma \overline{D / \pi} \sum_{k=1}^{m} \gamma \overline{\text{arc tg } \omega_k / \varepsilon - \text{arc tg } \omega_{k-1} / \varepsilon} [\varphi_k \cos \omega_k t + \lambda_k \sin \omega_k t] \qquad (19)$$

with a zero mathematical expectation and a correlation function

$$K_{\delta r}(\tau) = D e^{-\varepsilon |\tau|}, \qquad (20)$$

where ω is the frequency spectrum into which the random variable resolves, D is the dispersion of the random variable, φ and λ are normalized (0.1), mutually independent random numbers, $\tau = t_2 - t_1$ is the difference between two specified points of time within the limits of variation of the random variable being examined and ε is a parameter characterizing the degree of the correlation among the measurements.

Selection of this method for obtaining the measurement information was prompted by the fact that it enables us to obtain information with assigned probability characteristics, and also to obtain, for each particular realization of the random quantities φ_k, λ_k $(k = 1, 2, \ldots, m)$ information characterized by various degrees of dependence, so that we are able to make a comparative analysis of the processing results. In the present problem, we have used the correlation measurements presented in the article [5], measurements that were calculated as follows. From tables of random, normalized (0.1) numbers, ten variants of the numbers φ_k, λ_k were selected at random (from among fifty pairs in each variant), and Formula (19) used with $D = 1$ to calculate particular realizations of the random function $\delta r(t)$. The particular realizations $\Delta r(t)$ in each variant were calculated for three ε values: $\varepsilon_1 = 0.001 \text{ sec}^{-1}$, $\varepsilon_2 =$

- 63 -
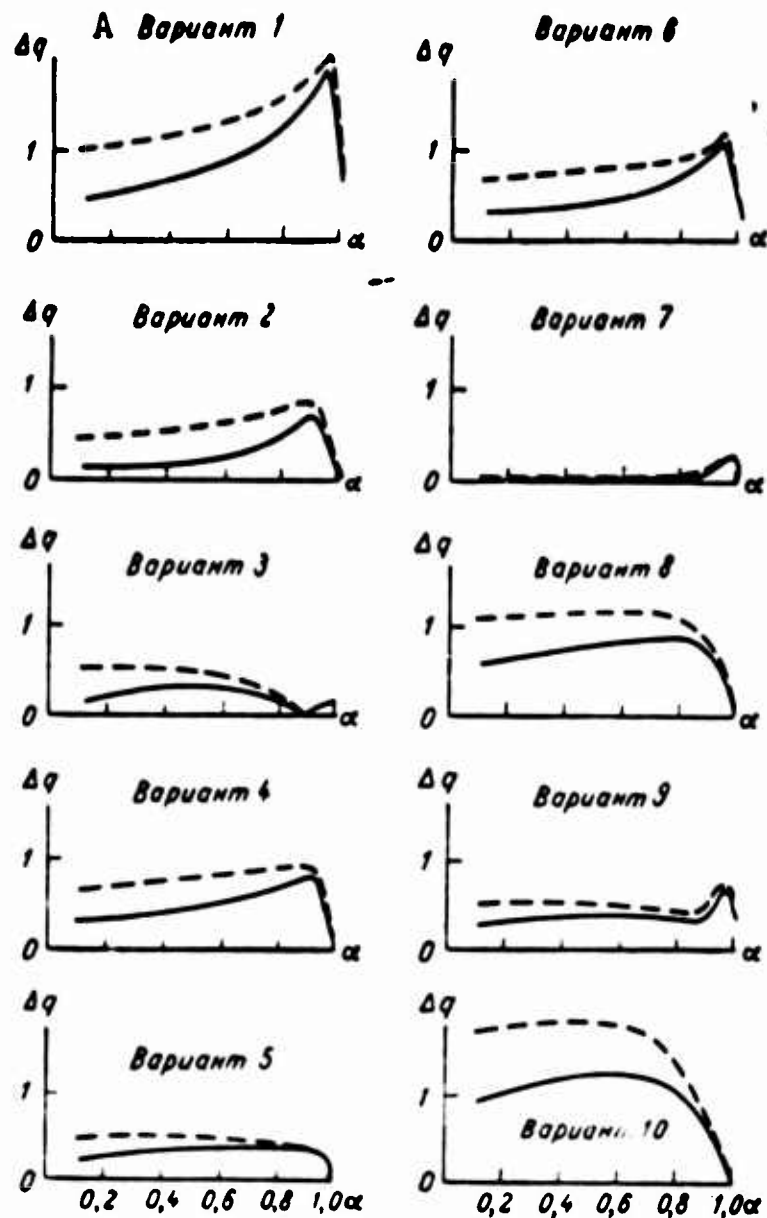
Fig. 5. A) Variant.

= 0.01 sec^{-1} and ε_3 = 0.1 sec^{-1}. The information was evaluated by Relationship (6). Here the following matrices were used: $\Delta q = \Delta q_{Ni} = \Delta q_{ii} = \Delta q^{(0)}$, $\Delta r = \Delta r_{nn} = \Delta r_{ni}$, $A = A_{nN} = A_{ni}$ and $K = K_{nn}$. Moreover, an additional matrix $S = S_{ni} = K^{-1}A$ with elements S_i ($i = 1, 2, \ldots, n$) was introduced, and the solution was written in the form

$$\Delta q^{(0)} = \sum_{i=1}^{n} S_i \Delta \tilde{r}_i \left/ \sum_{i=1}^{n} S_i a_i \right. \tag{21}$$

To permit varying the relationship between the elements of the matrix A over a broad range using the minimum number of parameters, it was assumed that the matrix elements are terms of a geometric progres-

- 64 -
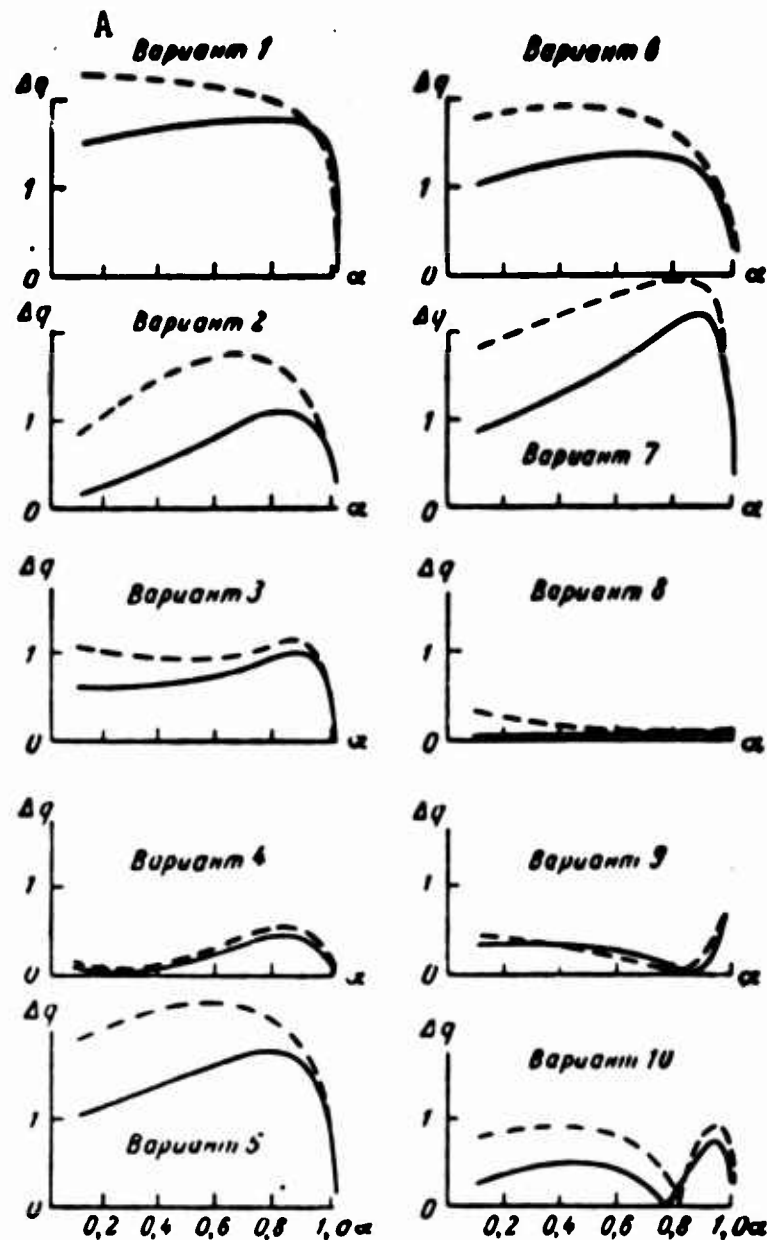
Fig. 6. A) Variant.

sion with a denominator α and, consequently, that $a_i = a_1 a^{i-1}$. If we adopt a constant interval between measurements (Δt = const), then the elements of matrix s are defined by the following finite relationships:

$$S_1 = [(\lambda\alpha - 1) / (\lambda^2 - 1)]a_1,$$
$$S_i = [a^{i-1} / (\lambda^2 - 1)] [\lambda(\alpha - \alpha^{-1}) - (1 + \lambda^2)]a_1 \quad (i = 2, 3, \ldots, n-1), \quad (22)$$
$$S_n = [a^{n-1} / (\lambda^2 - 1)](\lambda\alpha^{-1} - 1)a_1,$$

where $\lambda = e^{-\varepsilon\Delta t}$.

For the case in which the given information is reduced by the classical method of least squares, the solution will, as is regularly seen from (21), assume the form
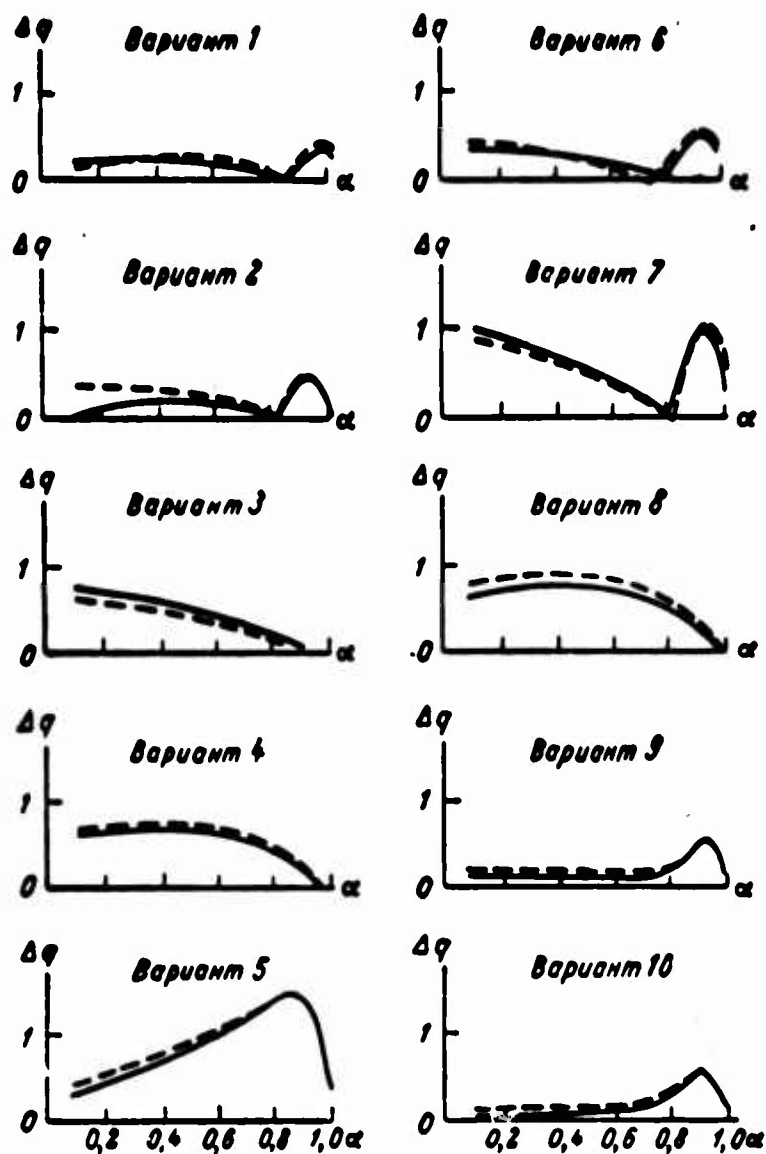
Fig. 7. A) Variant.

$$\Delta q_n^{(v)} = \sum_{i=1}^{n} a_i \Delta \tilde{r}_i \bigg/ \sum_{i=1}^{n} a_i^2. \qquad (23)$$

The results of the calculation are shown in Figs. 5-7 for all ten variants of particular realization of the random function $\delta r(t)$ and for the three values of ε. Here it has been assumed that $\Delta t = 20$ sec, $a_1 = 1$, $n = 90$ and that α varies from 0.1 to 1. The solid line indicates $\Delta q^{(0)}$, and the broken line $\Delta q^{(0)}$ Here, correlation-coefficient values of two neighboring measurements equal to $k_1 = 0.98$; $k_2 = 0.62$; $k_3 = 0.135$, and correlation coefficient values of the first and last measurements equal to $k_1 = 0.165$; $k_2 \approx 0$; $k_3 = 0$ correspond to the values $\varepsilon_1 = 0.001$ sec^{-1}, $\varepsilon_2 = 0.01$ sec^{-1} and $\varepsilon_3 = 0.1$ sec^{-1}.
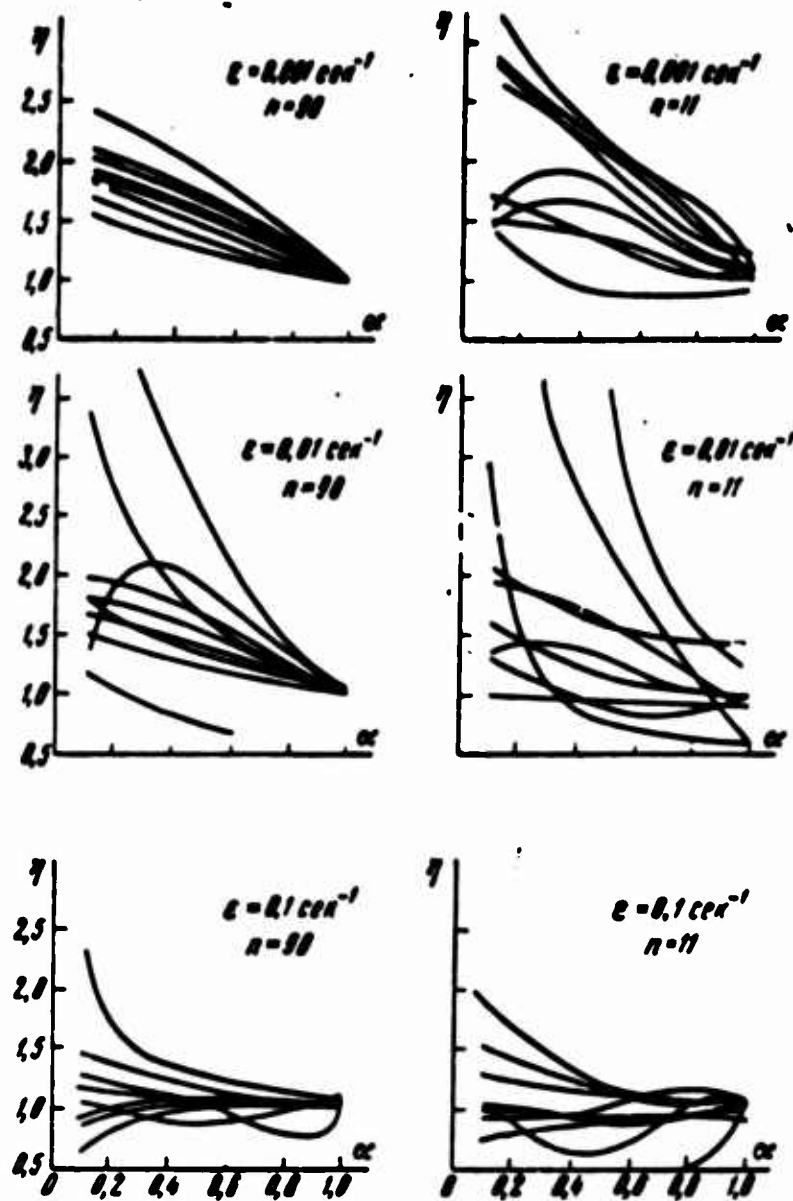
Fig. 8. A) sec^{-1}.

As in the preceding case, the true value of the unknown parameter is
equal to zero here, so that $\Delta \eta^{(i)}$ and $\Delta q_n^{(i)}$ actually represent the error
of the determination of Δq for the given group of measurements. It is
seen from the diagrams shown (see Figs. 5 and 6) that, as a rule, the
error of determination of Δq is considerably smaller if the dependence
is taken into account in the reduction. Here, the error difference in-
creases with diminishing α. For the third variant of ε(see Fig. 7),
when the functional relationship between measurements is very weak,
taking it into account has no substantial effect even for small α. Com-
parison of the results shown in Figs. 5-7 shows that the errors them-

- 67 -

selves, considered over the entire range of variation of α under consideration, are smallest in absolute magnitude in the case of weakly dependent measurements (Fig. 7), and largest for moderate degrees of dependence of the measurements (Fig. 6). In the most strongly correlated measurements (Fig. 5), the errors are somewhat smaller than in the preceding case. This result confirms wnat we said earlier to the effect that statistical processing methods exclude measurements errors the more completely the more closely their dependence approaches the absolutely correlated dependence (linear dependence of errors) or the absolutely noncorrelated dependence (independent errors). Figure 8 presents curves characterizing the variation of the error ratio $\eta = \Delta q_{1r}^{(v)} / \Delta q^{(v)}$ as a function of the parameter α. Curves of $\eta(\alpha)$ are given for n = 90 and for n = 11. Here it was assumed that these eleven measurements were uniformly distributed beginning with the first point at intervals $\Delta t = 160$ sec, i.e., measurements were made at the same time interval as in the case n = 90. The data presented indicate that, as a rule, the coefficient η increases with diminishing α. This means that as α diminishes, processing taking the dependence of the measurements into account becomes more and more advantageous. Here, when a larger number of measurements are utilized (n = 90) and when they are more strongly correlated ($\varepsilon = 0.001$ sec^{-1}), this effect becomes more stable.

In conclusion, we note that the present article has shown only the possibility in principle of improving the accuracy of space-vehicle orbit determination by reducing the influence of correlated measurement errors. It is a first step in an investigation of ways to elevate the accuracy of orbit determination by improving techniques for reducing the measurements. In the next stage of his researches, the author hopes to obtain quantitative evaluations and specific recommendations for various classes of space-vehicle orbits, with consideration of the fact

that various types of orbital measurements whose weights are known only with errors are used as the measurement information.

Received
12 July 1963

REFERENCES

1. P.Ye. El'yasberg and V.D. Yastrebov, In collection entitled "Iskusstvennyye sputniki Zemli" [Artificial Earth Satellites], No. 4. Izd-vo AN SSSR [Academy of Sciences USSR Press], 1960, page 18.

2. P.E. El'yasberg, In collection entitled "Iskusstvennyye sputniki Zemli,"No. 1. Izd-vo AN SSSR, 1958, page 21.

3. L.I. Sedov, In collection entitled "Iskusstveniyye sputniki Zemli," No. 5. Izd-vo AN SSSR, 1960, page 3.

4. I.L. Zhongolovich, Byulleten' ITA [Bulletin of the Institute of Theoretical Astronomy], 7, No. 10, 743, 1960.

5. A.V. Brykov, In collection entitled "Iskusstvennyye sputniki Zemli," No. 16. Izd-vo AN SSSR, 1963, page 124.

6. I.I. Shapiro, Raschet trayektorii ballisticheskikh snaryadov po dannym radiolokatsionnykh nablyudeniy [Calculating the Trajectories of Ballistic Missiles from Radar-Observation Data], IL [Foreign Literature Press], Moscow, 1961.

Manuscript Page No.	[Footnotes]
53	The first subscript designates the number of rows of the matrix, and the second the number of columns.
57	We note that the correlation matrix of the errors δw_v is determined quite dependably in most cases.
58	In the present case, the error in the dispersion is of no significance.

Manu-
script
Page
No.

[Transliterated Symbol]

50   ИСЗ = ISZ = iskusstvennyy sputnik Zemli = artificial earth
        satellite

OPTIMUM REGIMES OF MOTION FOR A POINT OF VARIABLE MASS WITH LIMITED

POWER IN UNIFORM CENTRAL FIELD

V.K. Isayev, V.V. Sonin, B.Kh. Davidson

This article examines regimes of optimum motion for a point of variable mass with limited power in a uniform central field of gravitation, as proposed in Reference [1]. The investigation is based on the maximum principle [2].

There is a discussion of the fundamentals of the qualitative theory of optimum programming of exhaust velocity with consideration of the limits of the range for changes in exhaust velocity, as well as a solution of the problem of synthesizing the optimum control in the absence of influence by limitations on the magnitude of the exhaust velocity.

In References [3-18] an investigation was conducted of the qualitative features of the laws governing the optimum programming of magnitude and direction of the reactive force for a point of variable mass moving in a plane-parallel field; in [3-11] there is a discussion of the case of a constant exhaust velocity, while in [12-18] there is a consideration of the case of limited power.

Let us consider the motion of a point of variable mass in a uniform central gravitational field [1].

The projections of gravitational acceleration onto the Ox- and Ox-axes of a Cartesian coordinate system whose origin O is located at the gravitational center may, for a uniform central field, be written as

follows:

$$g_x = -v^2 x, \quad g_y = -v^2 y, \qquad (0.1)$$

where

$$v^2 = \frac{g(r)}{|r|} = \text{const} > 0.$$

On the basis of Assumption (0.1) a detailed analysis has been carried out in [1] of the structure of optimum control in the motion of a point of variable mass at a constant exhaust velocity.

The present article is a continuation of the investigation into the properties of the optimum motion of the point of variable mass in a uniform central gravitational field.

In the 2nd part there is a discussion of the fundamentals of the qualitative theory of optimum power and exhaust programming for the case of a limited region of changes in the two control parameters; in the 3rd section a solution for the problem of synthesizing the optimum control is presented on the assumption that there are no limitations imposed on the exhaust velocity.

1. STATEMENT OF PROBLEM, SUMMARY OF RESULTS

Let us consider the plane motion of a point of variable mass $m(t) = M(t)/M(0)$ under the action of a jet with a regulated exhaust velocity c and limited power $N = -\dot{M}c^2/2 : 0 \leqslant N \leqslant N(c)_{max}$. Let u and v be projections of the velocity vector onto the Ox- and Oy-axes of a Cartesian coordinate system whose origin O is located at the gravitational center, and let the region of changes in the control inputs (N, c) be given by inequalities of the following form:

$$0 \leqslant N \leqslant N_{max}, \qquad (1.1)$$
$$0 < c_{min} \leqslant c \leqslant c_{max}.$$

Let us introduce the following denotations:

$$u_1 = N / N_{max},$$

$\phi(t)$ is the angle of inclination for the vector of the reactive force $\vec{P} = -\dot{M}\vec{c}$ to the Ox-axis.

Let us introduce the phase vector $x = (u, v, m, x, y) = (z_1, z_2, z_3, z_4, z_5)$ and the control vector $u = (u_1, c, \overline{\phi})$.

The equations of motion for a point of variable mass have the following form [18]:

$$\dot{u} = \frac{Nu_1 \cos \phi}{mc} + g_x(x, y, t), \tag{1.2}$$

$$\dot{v} = \frac{Nu_1 \sin \phi}{mc} + g_y(x, y, t), \tag{1.3}$$

$$\dot{m} = -\frac{Nu_1}{c^2}, \quad \dot{x} = u, \quad \dot{y} = v, \tag{1.4-1.6}$$

where

$$N = 2N_{max} / M_0,$$

g_x, g_y are projections of the acceleration of gravitational forces onto the Ox, Oy axes.

We are interested in the problem of determining control $\vec{u}$, translating System (1.2)-(1.6) from the given initial position $\vec{x}(0) = \vec{x}^0$ to some region $G(\vec{x})$ whose dimensions are smaller than n within an interval of time* t = T (n = 5 is the number of phase coordinates for the plane case), so that a certain functional $S = \sum_{i=1}^{5} c_i z_i(T)$ assumes the maximum value of those possible with Limitations (1.1) or, what is the same, with limitations

$$0 \leqslant u_1 \leqslant 1, \quad 0 < c_{min} \leqslant c \leqslant c_{max}, \tag{1.7}$$

imposed on $\vec{u}$.

The equations of the max-optimum motion of System (1.2)-(1.6) were derived for the stated problem in [18]:

$$\dot{u} = g_x + \begin{cases} 0, \\ -\dfrac{N}{mc_{min}}\dfrac{p_u}{\rho}, \\ \dfrac{Np_u}{2m^2p_m}, \\ -\dfrac{N}{mc_{max}}\dfrac{p_u}{\rho}. \end{cases} \qquad (1.8)$$

$$\dot{v} = g_v + \begin{cases} 0, \\ -\dfrac{N}{mc_{min}}\dfrac{p_v}{\rho}, \\ \dfrac{Np_v}{2m^2p_m}, \\ -\dfrac{N}{mc_{max}}\dfrac{p_v}{\rho}; \end{cases} \qquad (1.9)$$

$$\dot{m} = \begin{cases} 0, \\ -\dfrac{N}{c^2_{min}}, \\ -\dfrac{N}{4p_m^2}\dfrac{\rho^2}{m^2}, \\ -\dfrac{N}{c^2_{max}}; \end{cases} \qquad (1.10)$$

$$\dot{x} = u; \quad \dot{y} = v; \qquad (1.11)-(1.12)$$

$$\dot{p}_u = -p_x; \quad \dot{p}_v = -p_y; \qquad (1.13)-(1.14)$$

$$\dot{p}_m = \begin{cases} 0, \\ -\dfrac{N\rho}{m^2c_{min}} \\ \dfrac{N\rho^2}{2m^3p_m}; \\ -\dfrac{N\rho}{m^2c_{max}}; \end{cases} \qquad (1.15)$$

$$\dot{p}_x = -p_u\dfrac{\partial g_x}{\partial x} - p_v\dfrac{\partial g_v}{\partial x}; \qquad (1.16)$$

$$\dot{p}_v = -p_u\dfrac{\partial g_x}{\partial y} - p_v\dfrac{\partial g_v}{\partial y}. \qquad (1.17)$$

The conditions for attainment of each of the four possible regimes are indicated in the table; the numbers in the table correspond to the sequence of formulas in the right-hand parts of Eqs. (1.8)-(1.10) and (1.15).

1 No режима	2 Условие реализации режима	3 Оптимальные значения управления		1 No режима	2 Условие реализации режима	3 Оптимальные значения управления	
		u_1	c			u_1	c
0 1	$k\rho < Z$ $\rho > 2Z$	0 1	— c_{min}	2 3	$\rho \leq 2Z \leq k\rho$ $Z < k\rho < 2Z$	1 1	$2Z/\rho c_{min}$ c_{max}

1) Regime number; 2) condition for attainment of regime; 3) optimum values of control.

Here we denote:

$$k = \frac{c_{max}}{c_{min}}, \quad Z = -\frac{mp_m}{c_{min}}, \quad \rho = \sqrt{p_u^2 + p_v^2}. \tag{1.18}$$

Having substituted (0.1) into Eqs. (1.16), (1.17), and having integrated (1.13), (1.14), (1.16), (1.17), we will obtain

$$p_u = p_u^0 \cos vt - \frac{p_z^0}{v} \sin vt,$$
$$p_v = p_v^0 \cos vt - \frac{p_v^0}{v} \sin vt. \tag{1.19}$$

According to (1.19), the integral curve $p_v = p_v(p_u)$ is the so-called p-trajectory and represents an ellipse (in the particular case, it represents a circle or segments of two merging straight lines passing through the coordinate origin $p_u = p_v = 0$). Each of the indicated three types of p-trajectories, as demonstrated in [1], corresponds to a completely determinant form of an optimum program of change in the orientation of the reaction-force vector.

The optimum program of change in the inclination of the thrust vector is determined by the relationships [10, 18]

$$\sin \varphi = -\frac{p_v}{\rho}, \quad \cos \varphi = -\frac{p_u}{\rho}. \tag{1.20}$$

We can recommend the following simple method of calculating the trajectories that are close to the optimum. Substituting (1.19) into Eqs. (1.8)-(1.12) and (1.15), we will obtain a system which describes the motion in a Newtonian field of a point of variable mass with control close to optimum. In this case in Eqs. (1.8) and (1.9) g_x and g_y should be replaced by their exact expressions:

$$g_x = \frac{\mu x}{(x^2 + y^2)^{3/2}}, \qquad g_y = \frac{\mu y}{(x^2 + y^2)^{3/2}}, \qquad (1.21)$$

where $\mu = g_0 R_0^2$ is the gravitational constant.

A further simplification may be achieved when the approximate expressions from (0.1) for g_x and g_y are substituted into Eqs. (1.8) and (1.9). In this case System (1.8)-(1.17) will describe the optimum motion of a point in a uniform central gravitational field.

2. OPTIMUM REGIMES OF MOTION FOR A POINT OF VARIABLE MASS WITH LIMITED POWER AND A LIMITED RANGE OF CHANGE IN EXHAUST VELOCITY IN A UNIFORM CENTRAL FIELD

Below there is a discussion of the results obtained in an analysis of the case of a typical characteristic (u_1, c) of the form (1.1). In order to investigate the structure of the optimum control of power and exhaust velocity we employ the method proposed in [10]. According to the table the type of regime* for optimum control $u^* = (u_1, c)$ is a function of the relative places of four curves $\rho(t)$, $k\rho(t)$, $Z(t)$, and $2Z(t)$.

In view of (1.15) $\rho = \rho(p^0, \tau)$ is a periodic function of the dimensionless time $\tau = vt$ with period π [1]. Function $Z(p^0, \tau)$ is a monotonically increasing function in the powered phase where $u_1 = 1$, and it is constant in the coasting phase $(u_1 = 0)$. In other words, Z is a nondiminishing function of τ. In actual fact, let us examine in regimes 1 and 3 (where $c = c_i$, i is min, max) the expression for the derivative

$$\frac{dZ_{1,3}}{d\tau} = -\frac{1}{vc_{min}} (\dot{m}p_m + m\dot{p}_m) = \frac{N(\rho + mp_m/c_i)}{vc_i c_{min} m} = \frac{N\Phi(c_i)}{vc_i c_{min} m}. \qquad (2.1)$$

For regime 2 we find analogously that

$$\frac{dZ_2}{d\tau} = \frac{1}{vc_{min}} \left(\frac{N\rho^2}{4m^2 p_m} p_m - \frac{N\rho^2}{2m^3 p_m} m \right) = -\frac{N\rho^2}{4vm^2 p_m c_{min}}. \qquad (2.2)$$

Bearing in mind that in regime 2 the optimum value of the exhaust velocity c^* satisfies the relationship $c^* = -2mp_m/\rho > 0$, let us rewrite (2.2) in the form:**

- 76 -

$$Z_1' = \frac{N\rho}{2vc^0 c_{min} m}. \tag{2.3}$$

Having taken into consideration the relationship determining the switching function in this regime

$$\theta_2 = \theta(c^0) = \rho + \frac{m p_m}{c^0} - \frac{\rho}{2}, \tag{2.4}$$

on the basis of (2.1)-(2.4) we will obtain the final relationship which is valid for all four regimes:

$$Z' = \frac{N}{vmc_{min}c}\theta(c)u_1. \tag{2.5}$$

Since $N/vmc_{min}c > 0$ and in the active phases $(u_1 = 1)$ $\theta(c) > 0$, $dZ/d\tau \geq \geq 0$, with the equals sign pertaining only to the segments of passive motion $(Z > k\rho)$.

Having made use of the discussed properties of the functions ϑ, ρ, and Z, as well as the table, it is easy to derive the following statements relative to the optimum programming of power u_1 and the exhaust velocity $\underline{c}$. The latter are formulated as functions of the type of $\underline{p}$-trajectory.

Elliptical p-Trajectories

The optimum control of power $u_1(\tau)$ is extremal in nature (i.e., the power can assume only a maximum or minimum value [1, 18]).

In the general case the entire interval of motion can be divided into two sections, depending on the form of power control:

the acceleration segment with continuous control $[0, \tau_1]$ (to the instant τ_1 of the first shutting down of power);

the segment of impulsive control $\tau_1 \leq \tau \leq T$.

Each segment separately may be of as large an extent as we please.

The optimum control of exhaust velocity for each of these segments exibits an essentially different character.

The acceleration segment $0 < \tau < \tau_1$. In the general case three qual-

- 77 -

itatively different zones of optimum programming for the exhaust velocity $c(\tau)$ can be observed on the acceleration segment: in the first of these three intervals — the interval A — the exhaust velocity is maintained at the lower boundary $c(\tau) = c_{min}$; in interval B the magnitude of the exhaust velocity is regulated; the origin of the interval C can be defined as the point at which the upper limit of the exhaust velocity $c = c_{max}$ (Fig. 1) is first attained. Interval A, generally speaking, may be as large as we please. Let $\tau_{01}(1 = - M, \ldots, 0, 1, \ldots, N)$ be a periodic sequence of points, with period π [1], for the minimum convergence of p-trajectories having the coordinate origin $p_u = p_v = 0$ and moreover let τ_{01} be the first point by count of this sequence after the first intersection of the curves $\rho(\tau)$ and $2Z(\tau)$ (see Figs. 1-5), and let τ_{0s} be the first point of this sequence after the first intersection of the curves $k\rho(\tau)$ and $2Z(\tau)$.
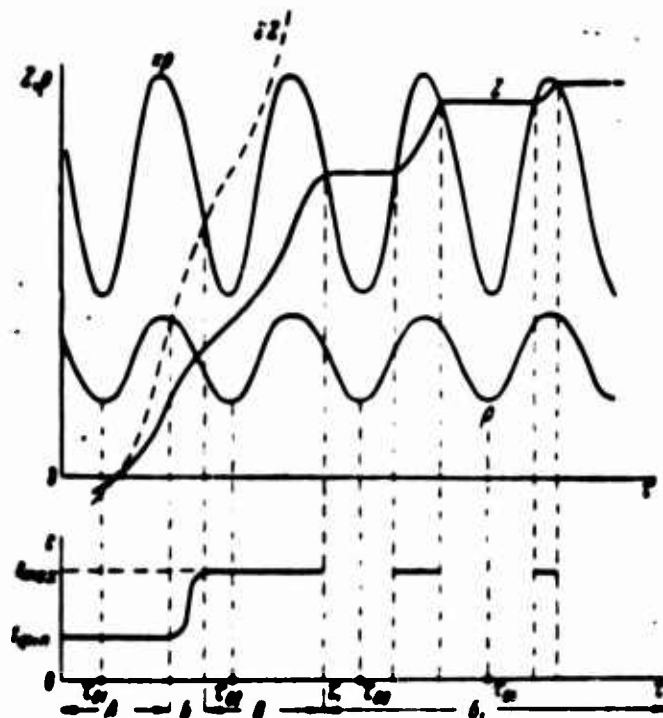
Fig. 1. A = A; Б = B; B = C.

In this case, starting from some instant $\tau = \tau_1^* = \tau_{01} - \xi_1^-$, $0 < \xi_1^- < \pi/2$, the optimum magnitude of the exhaust velocity leaves the lower boundary (τ_1^* is the boundary between intervals A and B of the accel-

eration segment).

In interval 3 the optimum program $c(\tau)$ in the general case is not monotonic. The points at which the exhaust velocity attains a local extremum $(c_1 = c_{ext\,1})$ form a quasiperiodic sequence $\tau_i'' = \tau_{0i} + \delta_i, \delta > 0$ $(i = 1, \ldots, s-1)$ with a period π (Figs. 2-3). Thus in each interval between two intersections of the represented point and the line of apsides of the p-trajectory there is situated only a single peak of the optimum program $c(\tau)$. The sequence of locally extremal values of the exhaust velocity increases monotonically in the second region:

$$c(\tau_{i+1}) > c(\tau_i), \quad (i = 1, \ldots, s-1), \tag{2.6}$$

i.e.,

$$c_{ext}^{i+1} > c_{ext}^{i} \quad (i = 1, \ldots, s-1).$$

This follows directly from the formula $c_{ext}^i = 2Z(\tau_i)c_{min}/\rho(\tau_i)$ $(i = 1, \ldots, s-1)$, which is valid for the point at which, by definition, regime 2 is attained in addition to the above-noted properties of the functions $Z(\tau)$ and $\rho(\tau)$.

Each peak c_{ext}^1 is situated after the passage of the describing point through the pericenter τ_{01} of the p-trajectory, when $\rho'(\tau_i) > 0$. This follows from the relationship

$$c_{ext}^i = \frac{N\rho(\tau_i)}{vm(\tau_i)}\frac{1}{\rho'(\tau_i)}, \tag{2.7}$$

which is satisfied only when $\rho'(\tau_1) > 0$, whence

$$\delta_i > 0 \quad (i = 1, \ldots, s-1). \tag{2.8}$$

Thus with an increase in τ the magnitude of the peak $c_{ext}^i(\tau)$ increases, as does the region $(\tau_{0i} - \xi_i^-, \tau_{0i} + \xi_i^+)$ of its existence (the region in which regime 2 is attained).

It is clear in this case that

$$\xi_i^- < \xi_i^+. \tag{2.9}$$

It is easy to see that with sufficiently large values for the par-
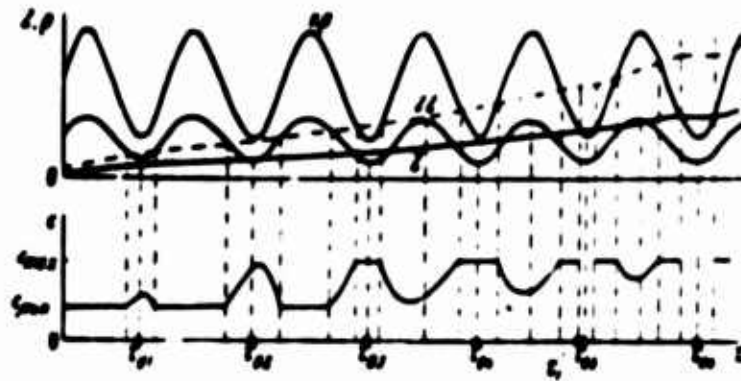
Fig. 2
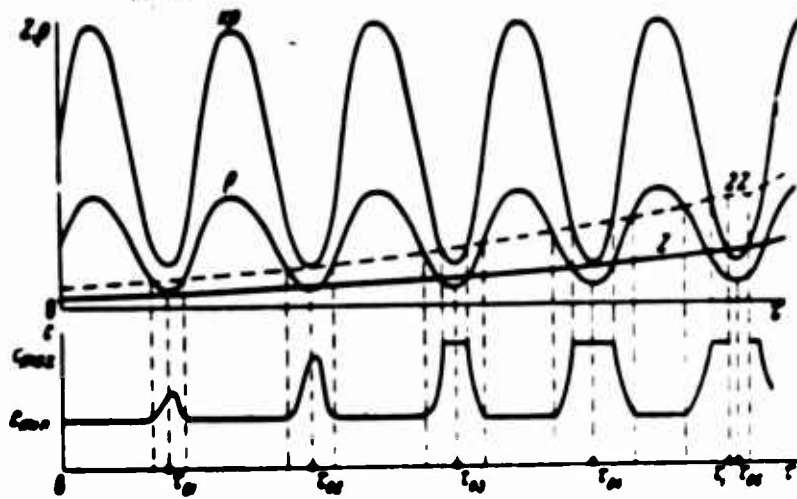
Fig. 3

ameter $\underline{k}$ the interval B is closed solely by regime $2 \ (\xi_i^+ + \xi_{i+1}^- > \pi)$ in this case for the local maximums all of the above-said with regard to c_{ext}^1 is valid, and the points of the local minimums $c = c_{min}^1$ are situated (in view of Formula (2.7) which is also valid here) in front of the apocenters of the $\underline{p}$-trajectory. Each local minimum is smaller in magnitude than the following (Fig. 4).

$$c_{min}^i < c_{min}^{i+1}. \qquad (2.10)$$

With a great energy-liberation value $\tilde{N}$ the optimum program in interval B of the acceleration segment is monotonic with respect to τ (Fig. 1).

Let us now consider the concluding stage of the acceleration segment — interval C. This interval may include segments with regime 2

(Fig. 2), in which case for the local minimums and the points of their distribution all of the above with respect to local minimums in interval B is valid.

The appropriate selection of the parameters $\tilde{N}$ and $\underline{k}$ will make it possible to achieve the monotonicity of the program $c(\tau)$ in this stage as well (Fig. 1).
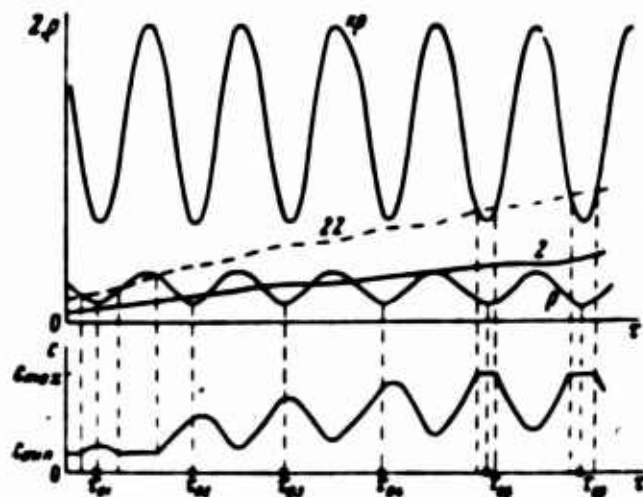
Fig. 4
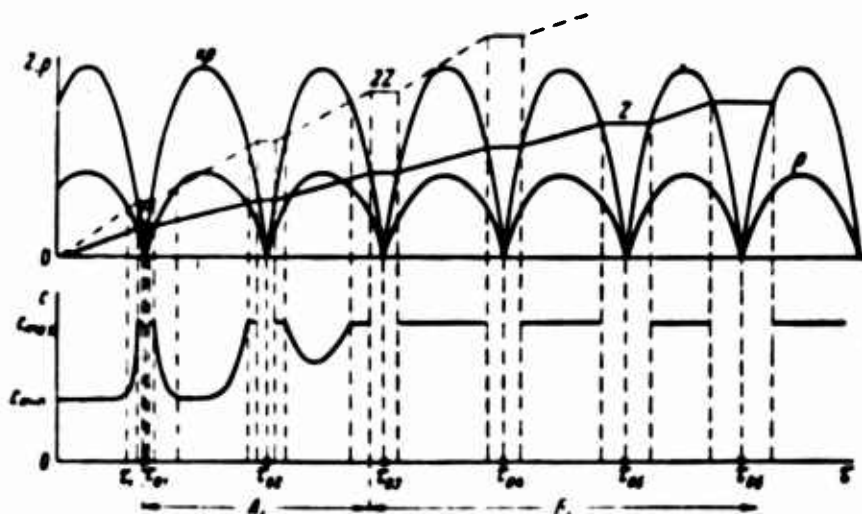
Fig. 5

The segment of continuous control $\tau_1 < \tau < \tau$. After the instant τ_1 of the first shutting down of power an "impulsive" power control regime is established.* In this case regimes with exhaust velocity variable as a function of $\tilde{N}$ and $\underline{k}$, or with constant exhaust velocity $c = c_{max}$, or alternations between the two may be set up on the powered segments.

Thus the segment of impulsive control in the general case contains two qualitatively different intervals: A_1 and B_1, respectively. By convention let us adopt the instant τ_1^* of the intersection of functions Z and $k\rho$ as the origin of the interval B_1, with $Z(\tau) > \rho(\tau), \tau > \tau_1^*$ (in B_1 the combination of regimes 3 and 0 only takes place). The situations which arise in the first somewhat more complex case are considered in the section on "Singular p-trajectories."

For the interval B_1 the results pertaining to the optimum programing of thrust at constant exhaust velocity [1] are valid: the active segments of diminishing length form a sequence with period π. The boundaries of the passive segments $\tau_i^- \leqslant \tau \leqslant \tau_i^+$ are symmetric with respect to the periodic (with period π) sequence of points τ_{0i} ($i = s$, ..., N), corresponding to the pericenters of the p-trajectory:

$$\tau_i^- = \tau_{0i} - \eta_i, \; \tau_i^+ = \tau_{0i} + \eta_i,$$
$$\eta_{i+1} > \eta_i. \tag{2.11}$$

Singular p-trajectories

The optimum control of power u_1 is limited.

The optimum programming of the exhaust velocity is characterized in general by the same features as in the case of elliptical p-trajectories.

The basic difference involves the fact that the exhaust velocity along the acceleration segment — the nondecreasing function τ is the total duration of intervals B and C — is no more than $\pi/2$ (Fig. 5).

With sufficiently low values of $\tilde{N}$ the segment of impulsive control (the concluding stage of optimum motion) opens with the interval A_1 in which the optimum function $c(\tau)$ is a nonmonotonic function of τ (Fig. 5). Any segment of length π from interval A_1 in the general case contains all four types of regimes which follow in the sequence: $0 \rightarrow 3 \rightarrow 2 \rightarrow 1 \rightarrow 2 \rightarrow 3 \rightarrow 0 \rightarrow 3$ etc. With increasing τ the regions occupied by

regime 1 diminish and subsequently disappear entirely.

The sequence of local minimums c_{min}^k in the concluding phase of interval A_1 (attained in regime 2) increases monotonically.

Circular p-trajectorie

The optimum control of power may either be extremal or singular [1, 18].

For the first case the program $c(\tau)$ is a monotonic piecewise-linear function of time consisting in the general case of three segments corresponding to regimes $1 \rightarrow 2 \rightarrow 3$ (i.e., the segments of passive motion are absent).

3. SYNTHESIS OF OPTIMUM CONTROL FOR THE CASE IN WHICH THERE ARE NO LIMITATIONS ON THE MAGNITUDE OF THE EXHAUST VELOCITY

Let us consider the max-optimum motion of a point of variable mass under the action of a reaction stream of limited power $0 \leq N \leq N_{max}$ and with no influence exerted by the limitations imposed on the exhaust velocity.

In the case of a uniform central gravitational field it is possible not only to analyze the qualitative pattern of the optimum regime, but also to derive an exact analytical solution and to carry the synthesis problem pertaining to optimum control to a conclusion.

For this special case let us write a system of equations of optimum motion:

$$\dot{u} = -v^2 x + \frac{Np_u}{2m^2 p_m}, \qquad (3.1)$$

$$\dot{v} = -v^2 y + \frac{Np_v}{2m^2 p_m}, \qquad (3.2)$$

$$\dot{m} = -\frac{N(p_u^2 + p_v^2)}{4m^2 p_m^2}, \qquad (3.3)$$

$$\dot{x} = u, \qquad \dot{y} = v, \qquad (3.4)-(3.5)$$

$$\dot{p}_u = -p_x, \qquad \dot{p}_v = -p_y, \qquad (3.6)-(3.7)$$

- 83 -

$$p_m = \frac{N(p_u{}^2 + p_v{}^2)}{2m^2 p_m}, \qquad (3.8)$$

$$\dot{p}_x = v^2 p_u, \quad \dot{p}_y = v^2 p_v \qquad (3.9)-(3.10)$$

As was shown in [18], System (3.1)-(3.10) decays into systems of equations of motion and equations of mass consumption which are integrated independently of one another. As a matter of fact, for a subsystem consisting of Eqs. (3.3) and (3.8), we can write

$$m^2 p_m = N / 2\gamma, \qquad (3.11)$$

$$m(t)p_m(t) - m(t_0)p_m(t_0) = \frac{\gamma}{2}\int_{t_0}^{t} (p_u{}^2 + p_v{}^2)\,d\xi, \qquad (3.12)$$

where γ is some arbitrary constant. The following serves as a solution for Eqs. (3.6), (3.7), (3.9), and (3.10):

$$p_u = p_u{}^0 \cos v(t - t_0) - \frac{p^0{}_x}{v}\sin v(t - t_0),$$

$$p_v = p_v{}^0 \cos v(t - t_0) - \frac{p^0{}_y}{v}\sin v(t - t_0), \qquad (1.15)$$

where $p_i{}^0 \; (i = u, v, x, y)$ represents the values of the variable p_i at the initial instant of time $t = t_0$.

Equations (3.1), (3.2), (3.6), and (3.7) after simple transformations yield

$$\ddot{x} + v^2 x = 2v[D_4 \cos v(t - t_0) - D_2 \sin v(t - t_0)],$$

$$\ddot{y} + v^2 y = 2v[E_4 \cos v(t - t_0) - E_2 \sin v(t - t_0)], \qquad (3.13)$$

where

$$2vD_2 = (\gamma / v)p_x{}^0, \quad 2vD_4 = \gamma p_u{}^0,$$

$$2vE_2 = (\gamma / v)p_y{}^0, \quad 2vE_4 = \gamma p_v{}^0. \qquad (3.14)$$

The general solution of System (3.13) has the following form:

$$x = [D_1 + D_2(t - t_0)] \cos v(t - t_0) + [D_3 + D_4(t - t_0)] \sin v(t - t_0),$$

$$\qquad (3.15)$$

$$y = [E_1 + E_2(t - t_0)] \cos v(t - t_0) + [E_3 + E_4(t - t_0)] \sin v(t - t_0),$$

where E_i, $D_i (i = 1, \ldots, 4)$ are constants subject to definition on the basis of the boundary conditions.

Let us make use of the derived general relationships for the solu-

tion of the problem pertaining to an overflight of given time T with minimum consumption of mass between two points in space for which the coordinates and velocities have been given. In this case the solution of System (3.1)-(3.10) must satisfy the following boundary conditions (everywhere further on $t_0 = 0$):

$$x(0) = x^0, \quad y(0) = y^0,$$

$$u(0) = u^0, \quad v(0) = v^0, \tag{3.16}$$

$$x(T) = x^1, \quad y(T) = y^1,$$
$$u(T) = u^1, \quad v(T) = v^1,$$
$$m(0) = 1, \quad p_m(T) = -1. \tag{3.17}$$

The second of Conditions (3.17) follows from the fact that the maximizing functional $S(T) = m(T)$.

For the determination of the constants E_1 and D_1 in Relationships (3.15), we have the conditions:

$$x^0 = D_1,$$
$$u^0 = D_2 + vD_3,$$

$$x^1 = D_1 \cos vT + TD_2 \cos vT + (D_3 + TD_4)\sin vT, \tag{3.18}$$
$$u^1 = -vD_1 \sin vT + (\cos vT - vT \sin vT)D_2 + vD_3 \cos vT +$$
$$+ (\sin vT + vT \cos vT)D_4.$$

Analogous relationships exist for E_1:

$$y^0 = E_1,$$
$$v^0 = E_2 + vE_3,$$
$$y^1 = (E_1 + TE_2) \cos vT + (E_3 + TE_4) \sin vT,$$
$$v^1 = -vE_1 \sin vT + (\cos vT - vT \sin vT)E_2 + vE_3 \cos vT + \tag{3.19}$$
$$+ (\sin vT + vT \cos vT)E_4.$$

The determinants of System (3.18) and (3.19) are equal to

$$\Delta = \begin{vmatrix} 1 & 0 & 0 & 0 \\ 0 & 1 & v & 0 \\ \cos vT & T \cos vT & \sin vT & T \sin vT \\ -v \sin vT & \cos vT - vT \sin vT & v \cos vT & \sin vT + vT \cos vT \end{vmatrix} =$$
$$= \sin^2 vT - (vT)^2. \tag{3.20}$$

Δ vanishes only if $vT = 0$. In this case it is clear that $T = 0$ is meaningless and the case $v = 0$ signifies a qualitative change in the system of differential equations and corresponds to the motion for the case in which there is no field, as was considered, for example, in [12], and in [14] for an overflight optimal from the point of view of rapid effect. As a result, the boundary-value problem of (3.13) and (3.16) has the unique solution

$$D_1 = x^0,$$

$$D_2 = \frac{1}{\Delta}[v(\sin vT \cos vT + vT)x^0 + u^0 \sin vT - v(\sin vT + vT \cos vT)x^1 + vTu^1 \sin vT],$$

$$D_3 = \frac{1}{\Delta}[-(\sin vT \cos vT + vT)x^0 - vT^2 u^0 + (\sin vT + vT \cos vT)x^1 - Tu^1 \sin vT],$$

$$D_4 = \frac{1}{\Delta}[vx^0 \sin^2 vT + (vT + \sin vT \cos vT)u^0 - v^2 Tx^1 \sin vT + (\sin vT - vT \cos vT)u^1];$$

(3.21)

$$E_1 = y^0;$$

$$E_2 = \frac{1}{\Delta}[v \sin vT \cos vT + vT)y^0 - \sin^2 vT v^0 - v(\sin vT + vT \cos vT)y^1 + vTv^1 \sin vT],$$

$$E_3 = \frac{1}{\Delta}[-(\sin vT \cos vT + vT)y^0 - vT^2 v^0 + (\sin vT + vT \cos vT)y^1 - Tv^1 \sin vT],$$

$$E_4 = \frac{1}{\Delta}[vy^0 \sin^2 vT + (vT - \sin vT \cos vT)v^0 - v^2 Ty^1 \sin vT + (\sin vT - vT \cos vT)v^1].$$

After the determination from (3.21), (3.22) of the integration constants D_i and $E_i (i = 1, \ldots, 4)$, from Formulas (1.19) we find

$$p_u = \frac{2v}{\gamma}(D_4 \cos vt - D_3 \sin vt), \quad p_v = \frac{2v}{\gamma}(E_4 \cos vt - E_3 \sin vt). \quad (3.23)$$

Having denoted $I^1 = I(T) = \gamma^2 \int_0^T (p_u^2 + p_v^2)dt$ we will obtain:

$$I' = 2v^r \left(T + \frac{1}{2v} \sin 2vT \right) D_i^2 + \frac{2(\cos 2vT - 1)}{v} D_2 D_4 +$$
$$+ \left(T - \frac{\sin 2vT}{2v} \right) D_2^2 + \left(T + \frac{\sin 2vT}{2v} \right) E_i^2 + \frac{2(\cos 2vT - 1)}{v} E_2 E_4 +$$
$$+ \left(T - \frac{\sin 2vT}{2v} \right) E_2^2. \tag{3.24}$$

From (3.12) on the basis of (3.11) it follows that

$$\frac{m^2(t_1) p_m(t_1)}{m(t_1)} - \frac{m^2(t_0) p_m(t_0)}{m(t_0)} = \frac{\gamma}{2} \int_{t_0}^{t_1} (p_u^2 + p_v^2) dt,$$

i.e.,

$$\frac{1}{m(t_1)} - \frac{1}{m(t_0)} = \frac{\gamma^2}{N} \int_{t_0}^{t_1} (p_u^2 + p_v^2) dt. \tag{3.25}$$

Using the boundary conditions (3.17) and Relationships (3.24), (3.25), we will obtain

$$m(T) = \frac{1}{1 + \frac{I'}{N}}, \tag{3.26}$$

$$p_m(0) = - \frac{1}{(1 + I'/N)^2}, \tag{3.27}$$

$$\gamma = - \frac{N}{2} \left(1 + \frac{I'}{N} \right). \tag{3.28}$$

This is actually the conclusion of the solution for the boundary problem (3.1)-(3.10), (3.16), (3.17), since the functions $p_m(t)$ and $m(t)$ are uniquely defined by the familiar constants $p_m(0)$, γ from Relationships (3.11), (3.12).

The derived analytical solution makes it possible in the boundary problem under consideration, to synthesize optimum control. As a matter of fact, the optimum program of thrust-vector orientation is uniquely defined by Relations (1.20) in which in the place of p_u and p_v their values from (3.23) should be substituted. The optimum program for exhaust-velocity regulation is given by the following relationship:

$$c = \frac{p_m(0) + \frac{1}{2\gamma} J(t)}{\mu}. \tag{3.29}$$

In the work by Irving and Blum [13] the problem of selecting the parameter $\tilde{N} = \tilde{N}_*$ was considered from the standpoint of maximizing the payload in the case of fixed boundary conditions.

Following [13], let us make the following assumptions:

1) The terminal mass m_k is composed of the payload m_p, the mass m_b of the empty fuel tanks and their structures, as well as the mass m_s of the powerplant.

2) The mass of the fuel tanks and their structures is a function exclusively of the fuel reserve (it is assumed that the fuel is consumed completely).

3) The mass of the powerplant depends exclusively on the magnitude of the power $\tilde{N}$.

With the above assumptions (boundary conditions (3.16)–(3.17) fixed and assumptions 1)–3) satisfied for each $\tilde{N}$ we can write:

$$m_\kappa = m_s + m_6(1 - m_\kappa) + m_c(\tilde{N}), \tag{3.30}$$

whence

$$m_n = m_\kappa - m_6(1 - m_\kappa) - m_c(\tilde{N}). \tag{3.31}$$

If the following natural condition is now satisfied

$$\partial m_6 / \partial m_\kappa < 0, \tag{3.32}$$

then with an increase in terminal mass there will be a rise in payload for each fixed $\tilde{N}$.

Thus the problem of maximizing m_p in the case of fixed boundary conditions breaks down into two problems:

the problem of seeking out the maximum terminal mass for a given $\tilde{N}$, with $m_k = m_k(T, \tilde{N})$;

the selection from among all $\tilde{N}$ of an $\tilde{N}_*$ that imparts the maximum value to m_p.

Consequently, from the solution of (1.8)-(1.17) for fixed boundary conditions in the maximization of m(T) it is necessary to derive the relationship $m_k = m_k(T, \tilde{N})$, to substitute it into Relationship (3.31), and from this to find $\tilde{N} = \tilde{N}_*$, yielding the maximum for m_p. If $m_k(T, \tilde{N})$ is differentiable with respect to $\tilde{N}$, the extremum should be sought among the roots of the equation*

$$\frac{dm_\text{n}}{d\tilde{N}} = \frac{\partial m_\text{к}}{\partial \tilde{N}} + \frac{\partial m_\text{к}}{\partial T}\frac{\partial T}{\partial \tilde{N}} + \frac{\partial m_\text{б}}{\partial m_\text{к}}\left(\frac{\partial m_\text{к}}{\partial T}\frac{\partial T}{\partial \tilde{N}} + \frac{\partial m_\text{к}}{\partial \tilde{N}}\right) - \frac{dm_\text{c}}{d\tilde{N}} = 0. \qquad (3.33)$$

Since for certain $\tilde{N}$ the boundary problem may have no solution, in addition to the roots of (3.33) it is also necessary to check whether or not a maximum is attained at a limit point from which the boundary problem becomes solvable. In Reference [13] there is discussed the case in which

$$m_\text{б} = K(1 - m_\text{к}), \qquad m_\text{c} = \zeta \tilde{N}, \qquad (3.34)$$

where

$$K = \text{const}, \qquad \zeta = \text{const},$$

and the entire trajectory consists of a segment having a regime of type 2. As was proved in [13], for a problem with a fixed overflight time T it follows from Condition (3.33) that

$$\tilde{N}_* = \sqrt{J/\zeta} - J.$$

Having introduced the notations $\zeta J = C$, we will obtain

$$\tilde{N}_* = C/\zeta - C^2/\zeta,$$

whence

$$(m_\text{n})_\text{max} = [1 - C)^2 - K] / (1 - K). \qquad (3.35)$$

Received
30 May 1963

REFERENCES

1.   G.Ye. Kuzmak, V.K. Isayev and B.Kh. Davidson, Dokl. AN SSSR [Proc. Acad. Sci. USSR], 149, No. 1, 58, 1963.

2.   L.I. Rozonoer, Avtomatika i telemekhanika [Automation and Teleme-
     chanics], I-III, 20, No. 10-12, 1320, 1441, 1561, 1959.

3.   D.Ye. Okhotsimskiy and T.M. Eneyev, Usp. fiz. n. [Achievements in
     the Physical Sciences], 63, 5, 1957.

4.   G. Leitmann, J. Aerospace Sci., 26, No. 9, 586, 1959.

5.   G. Leitmann, J. Aerospace Sci., 27, No. 2, 153, 1960.

6.   G. Leitmann, J. Aerospace Sci., 29, No. 8, 1000, 1962.

7.   G. Leitmann, Variational Problems with Bounded Control Variables.
     Optimization Techniques (G. Leitmann, ed.), Ch. 5, Academic Press,
     N.Y.-London, 1962, page 171.

8.   D.F. Lawden, Aeronaut. Quart., 6, 165, 1955.

9.   A. Miele, Aeronaut. Sci., 24, No. 12, 874, 1957.

10. V.K. Isayev, Avtomatika i telemekhanika, 22, No. 8, 986, 1961.

11. V.K. Isayev, Avtomatika i telemekhanika, 23, No.. 1, 127, 1962.

12. J.H. Irving, Low Thrust Flight: Variable Exhaust Velocity in Gra-
     vitational Fields. Space Technology (H.S. Seifert, ed.), Ch. 10,
     Wiley, 1959, p. 10.

13. J.H. Irving and E.K. Blum, Comparative Performance of Ballistic
     and Low-thrust Vehicles for Flight to Mars. Proc. 2nd. Annual As-
     tronaut. Symposium, II, Vistas in Astronautics, 1959, page 191.

14. G. Leitmann, J. Appl. Mech., 28, Ser. E, No. 2, 171, 1961.

15. G. Leitmann, Prepr. 7th Annual Meet. Amer. Astron. Soc., No. 30,
     61, 1961.

16. C.R. Faulders, ARS Journal, 30, No. 10, 954, 1960.

17. W.G. Melbourne, C.G. Sauer and D.E. Richardson, Interplanetary
     Trajectory Optimization with Power-Limited Propulsion Systems. Proc.
     of the IAS Sympos. in Vehicle Systems Optimization, N.Y., 1961.

18. V.K. Isayev and V.V. Sonin, Avtomatika i telemekhanika, 23, No. 9,
     1117, 1962.

Manu-script Page No.	[Footnotes]
73	The generalization of the problem to the case in which the total motion time is not given in advance but is rather taken from optimum considerations presents no difficulties [2].
76	Problems of optimum control that is singular in the sense of the maximum principle are not considered in the present article.
76	The prime denotes differentiation with respect to τ.
81	The sections in which power is shut off are shown conditionally in corresponding figures as sections with zero exhaust velocity.
89	In problems with fixed T $\partial T/\partial N = 0$.

Manu-script Page No.	[Transliterated Symbols]
88	к = k = konechnaya = terminal
88	б = b = bak = tank
88	c = s = silovoy = powerplant

FASTEST DECELERATION OF THE ROTATION OF AN AXISYMMETRIC SATELLITE

I.V. Ioslovich

In a number of cases the rotation of a satellite about a center of mass is undesirable and may be curtailed by means of a control system. The problem of optimizing this process in terms of rapidity of effect and the synthesizing of a corresponding optimizer was posed in article [1]. It was brought out that for an axisymmetric satellite there arise a number of features associated with the nonuniqueness of the solutions of the variation problem. In this note it is demonstrated that the equations of the variation problem can be integrated for the sections of control constancy and certain facts are presented to characterize the fibering of the phase space by surfaces composed of trajectories.

1. The motion of an axisymmetric satellite under the action of a control system is described in a movable system of coordinates connected with the principal axes of the central ellipsoid of inertia by equations

$$
\begin{aligned}
\dot{x} &= b_1 u_1, \quad |u_i| \leqslant 1, \\
\dot{y} &= Bxz + b_2 u_2, \quad i = 1, 2, 3, \\
\dot{z} &= -Bxy + b_3 u_3,
\end{aligned}
\tag{1.1}
$$

Nomenclature

x, y, z projections of instantaneous angular velocity onto principal axes of inertia;

B a constant defined by the principal moments of inertia;

b_1, b_2, b_3 positive constants characterizing the control system;

u_1, u_2, u_3 control inputs with respect to x, y, z axes;

λ_x, λ_y, λ_z conjugate coordinates of the L.S. Pontryagin maximum principle;

H   the Hamiltonian function of the maximum principle for the prob-
    lem of rapidity of effect;

$$K^2 = \lambda_y^2 + \lambda_z^2, \quad v = y + iz,$$
$$w = \lambda_y + i\lambda_z, \quad w^2 = \lambda_y^2 + i\lambda_z^2,$$
$$b = b_2 \, \text{sgn} \, \lambda_y + ib_3 \, \text{sgn} \, \lambda_z;$$

if the time $\underline{t}$ changes from 0 to T, $\tau = T - t$.

The point with the phase coordinates x_0, y_0, z_0 should be trans-
ferred to position 0, 0, 0 within the shortest possible period of time
T.

In Reference [1] there is presented a derivation of the following
integral by means of the L.S. Pontryagin maximum principle

$$H = \lambda_x b_1 \, \text{sgn} \, \lambda_x + \lambda_y (Bzz + b_2 \, \text{sgn} \, \lambda_y) + \lambda_z (- Bzy + b_3 \, \text{sgn} \, \lambda_z) = C \quad (1.2)$$

and the system of equations for the conjugate coordinate

$$\dot{\lambda}_x = -Bz\lambda_y + By\lambda_z \qquad (1.3)$$

$$\dot{\lambda}_y = Bz\lambda_x \qquad (1.4)$$

$$\dot{\lambda}_z = -Bz\lambda_y. \qquad (1.5)$$

which has the integral $\lambda_y^2 + \lambda_z^2 = K^2$.

The controls have the form

$$u_1 = \text{sgn} \, \lambda_x, \quad u_2 = \text{sgn} \, \lambda_y, \quad u_3 = \text{sgn} \, \lambda_z. \qquad (1.6)$$

If $\lambda_1 = 0$, the corresponding control u_1 is not defined and is
known as unique.

It turns out that there exists an entire region in the phase
space for whose points $\lambda_y = \lambda_z = 0$, $\lambda_x = 1$ when $x < 0$ and $\lambda_x = -1$
when $x > 0$. This region is situated within a certain surface surround-
ing the x-axis and passing through the coordinate origin. This surface,
conventionally referred to as a "cone" in [1], is a switching surface
for the control u_1 and is formed by trajectories which have no switch-
ing points with respect to u_1. The remaining trajectories approach the
"cone" from without and then proceed to the coordinate origin without

sign change with respect to u_1. Within the "cone" there exists a region in which controls u_2 and u_3 are not defined and the variation problem exhibits a nonunique solution. This is explained by the fact that when x_0 is large in comparison with y_0 and z_0, the time required to reduce the y_0 and z_0 coordinates to zero values may prove to be less than $|x_0|/b_1$. For the points lying on the "cone," this time is equal to $|x_0|/b_1$. Unfortunately, the interesting question as to whether or not there exist switching surfaces with respect to u_1, other than the "cone," at the present time has not been subjected to investigation and the general nature of the behavior of the trajectories is not clear.

In addition, there exists a unique control on the rays $|y|/|z| = b_2/b_3$, $x = 0$, where $\lambda_x = 0$, $u_1 = 0$, and the sign changes with respect to u_2 and u_3 does not occur, i.e., $u_2 = -\,\text{sgn}\,y$, $u_3 = -\,\text{sgn}\,z$. The existence of this case of a unique control in Reference [1] is negated as a result of an incorrect analysis.

2. Equations (1.1), (1.4), (1.5) can be written in complex form, introducing the variables $w = \lambda_y + i\lambda_z$ and $v = y + iz$. Moreover, having denoted $b = b_2\,\text{sgn}\,\lambda_y + ib_3\,\text{sgn}\,\lambda_z$, we will obtain equations

$$\dot{w} = -iBxw \tag{2.1}$$
$$\dot{v} = -iBxv + b. \tag{2.2}$$

These equations are easily integrated on those segments on which there is no switching. Having integrated in the opposite direction from the coordinate origin and glueing up the derived solutions, it is possible to construct phase trajectories, solving the synthesis problem. It is thus possible to obtain information about the sign change with respect to u_1, bypassing the integration of Eq. (1.3). For this integral (1.2) should be written in the form

$$|\lambda_x| = C/b_1 - (Bx/b_1)(z\lambda_y - y\lambda_z) - (b_2/b_1)|\lambda_y| - (b_3/b_1)|\lambda_z|. \qquad (2.3)$$

and this will make it possible, after integration of Eqs. (2.1) and (2.2), to show the u_1 switching points.

For the trajectories of the "cone," where by definition there is no u_1 switching, Eqs. (2.1), (2.2) can be immediately integrated. The integration is carried out with respect to the "reciprocal" of the time τ in the halfspace $x > 0$. We have

$$\dot{x} = b_1 \qquad (2.4)$$
$$\dot{y} = -Bxz - b_2 \operatorname{sgn} \lambda_y$$
$$\dot{z} = Bxy - b_3 \operatorname{sgn} \lambda_z \qquad (2.5)$$
$$\dot{\lambda}_y = -Bx\lambda_z$$
$$\dot{\lambda}_z = Bx\lambda_y$$
$$w = w^k e^{iBb_1\tau^2/2} \qquad (2.6)$$
$$v = -e^{iBb_1\tau^2/2} \int_{0}^{\tau} b(\tau) e^{-iBb_1\tau^2/2} d\tau. \qquad (2.7)$$

We can see from Formula (2.6) that the frequency of sign changes with respect to u_2, u_3 increases without limit with increasing τ, and consequently, with increasing $\underline{x}$. Separating Formula (2.7) into real and imaginary parts, it is possible to derive an expression for $\underline{y}$ and $\underline{z}$ in terms of Fresnel integrals and sines and cosines of the argument $Bb_1\tau^2/2$.

3. Having solved the synthesis problem, one usually assumes finite values for the conjugate coordinates $\lambda_x{}^k$, $\lambda_y{}^k$, $\lambda_z{}^k$ and integration is then carried out in the opposite direction from the point 0, 0, 0.

Let us trace the behavior of the trajectories in the upper half-space $x > 0$. The trajectories emanate from point 0, 0, 0 and move upward along the "cone," rotating about the x-axis. Then the last sign change with respect to u_1 occurs, and the trajectories descend from the cone. It is easy to establish that with the last switching $\dot{\lambda}_x < 0$, while for the next-to-last $\dot{\lambda}_x > 0$.

Let us rewrite Expression (1.2) in the form

$$-x\dot{\lambda}_x = C - b_1|\lambda_x| - b_2|\lambda_y| - b_3|\lambda_z|. \qquad (3.1)$$

The quantity $b_2|\lambda_y| + b_3|\lambda_z|$ ranges from $K_{min}(b_2, b_3)$ to $K(b_2^2 + b_3^2)^{1/2}$. Since Integral (3.1) permits of norming, we will hold that $\lambda_x^k = -1$. Then at the coordinate origin we will have

$$C = b_1 + b_2|\lambda_y^k| + b_3|\lambda_z^k|. \qquad (3.2)$$

For all $\lambda_y{}^k$, $\lambda_z{}^k$ satisfying the condition

$$C > K(b_2^2 + b_3^2)^{1/2}, \qquad (3.3)$$

there can be no fulfillment of the inequality

$$-x\dot{\lambda}_x = C - b_2|\lambda_y| - b_3|\lambda_z| < 0. \qquad (3.4)$$

which must occur with the next-to-last sign change with respect to u_1. Consequently, with fulfillment of (3.3) and $\lambda_x{}^k = -1$ the trajectories arrive at the coordinate origin from the $x = 0$ plane, exhibiting no more than a single sign change with respect to u_1.

It is easy to establish that the trajectory for which $\lambda_x{}^k = +1$ and for which Condition (3.3) is satisfied, also exhibits no more than a single sign change with respect to u_1 along the segment from $x = 0$ to the coordinate origin.

REFERENCES

1.   E.B. Lee, ARS. J., 32, No. 6, 981, 1962.

UDK 532.517.2:259.193.2

ANALYSIS OF THE CHEMICAL COMPOSITION OF A LAMINAR MULTICOMPONENT
BOUNDARY LAYER ON THE SURFACES OF BURNING PLASTICS

G.A. Tirskiy

An analysis is given of a possible chemical composition of gases in a boundary layer on the surfaces of structural phenol-formaldehyde-resin-based synthetic materials burning in a dissociated air flow. For typical mixtures, which consist of no fewer than 15–20 components, a calculation is made to determine the effective diffusion coefficients and the corresponding mass-transfer coefficients in the multicomponent gas mixture. For all self-modeling motions in a multicomponent frozen boundary layer, a closeness (equality) theorem is shown to be valid for the effective diffusion coefficients over the entire thickness of the boundary layer for all components possessing close (equal) molecular weights and gas-kinetic parameters and satisfying the boundary conditions $c_1(\infty) = 0$ or $c_1(0) = 0$. It is shown that for plastics based on phenol-formaldehyde-resins, it is generally necessary to introduce at least five essentially different effective diffusion coefficients, and that their introduction enables us to describe the diffusion processes, rate of mass ablation and the temperature and composition on the combustion surface with practical accuracy.

The methods described in the literature for calculating the combustion rates of streamlined surfaces are based on substitution of the multicomponent gas mixture by an effective binary mixture of atoms and

molecules with a single coefficient of binary diffusion of atoms into molecules [1-4]. This model of a binary boundary layer cannot be used in calculating the rate of destruction of structural plastics, when, together w'th the O and N atoms of the air, the boundary layer may simultaneously contain components with low molecular weight (H_2), components with high molecular weight (SiO, CO_2 and components with medium molecular weight $(O_2, N_2, CO, CN, HCN, SiH, C_3)$, all diffusing counter to the O and N atoms. Even for pure dissociated air, when three essentially different binary diffusion coefficients make their appearance, the validity of the binary·boundary-layer model is not obvious.

On the basis of an analysis of the boundary layer's chemical composition when it forms on the surfaces of burning plastics made from phenol-formaldehyde resin and streamlined by dissociated air, it is shown in the present paper that the number of components may run as high as 30-35. If we do not count components whose contents are below 1%, the number of components in the boundary layer will not exceed 15-20. We present for such a mixture a detailed calculation of the effective diffusion coefficients in a frozen boundary layer in the neighborhood of the critical point (line), as defined in [5]. In the process, we prove a theorem of the closeness (equality) of the effective diffusion coefficient over the entire thickness of the boundary layer for all components having molecular weights and gas-kinetic parameters that are closely similar (equal) and satisfying the boundary conditions $c_1(\infty) = 0$ or $c_1(0) = 0$. This theorem remains valid for all self-modeling solutions for the multicomponent boundary layer. Application of this theorem to specific mixtures substantially reduces the number of unknown mass-transfer coefficients, since components with equal effective diffusion coefficients have identical profiles with respect to the concentrations and, consequently, equal mass-tranfer coefficients.

Using the generalized analogies between the mass-transfer coefficients as derived in [5], we shall compute all effective diffusion coefficients at the wall and the ratios of all mass-transfer coefficients. It is shown that the mass-transfer coefficients depend essentially on the boundary conditions, and, in particular, on the degree of dissociation of the air at the outer boundary of the boundary layer. It follows from this that there is not, in the general case, a single binary diffusion coefficient whose introduction might describe with sufficient accuracy the rate of mass ablation, the temperature, and the composition on the combustion front. It is necessary to introduce at least five esssentially different effective diffusion coefficients: $D_M(M =$ $= CO, CN, HCN, SiO, C_2, C_3), D_A(A = O, N), D_{H_2}, D_{CO_2}, D_{O_2}$ — the introduction of which enables us to describe with an accuracy sufficient for practical purposes the processes of diffusion, the rate of mass depletion, the temperature and the composition on the combustion front of a structural plastic.

A formula will be derived for determining the composition of the air on an ideally catalytic nondecomposing wall as a function of the degree of dissociation of the air on the outer boundary of the boundary layer. A comparison of the results obtained by this formula with numerical solutions gives excellent agreement. For a certain range of variation of the external parameters of the problem we derive a formula for the combustion rate of a structural plastic that decomposes without formation of a liquid film, as a function of the degree of dissociation of the air and the composition of the chemical elements in the original plastic. It is shown that graphite possesses the lowest combustion rate as compared with other plastics for identical external streamlining conditions and the same shape of the body.

Using the concept of effective diffusion coefficients, a similar analysis can be carried out for other types of plastics, such as teflon, nylon, organic glass, and others.

1. ANALYSIS OF THE CHEMICAL COMPOSITION OF THE GASES THAT APPEAR ON COMBUSTION OF PLASTICS IN A DISSOCIATED STREAM OF AIR

Structural plastics based on phenol-formaldehyde resins have come into widest application as heat-protective coatings for very high stream temperatures [6-9]. The fillers used to reinforce the resin include cotton cloth (textolite [10]), woven glass or glass fiber (glass textolite [6-10], asbestos (asbotextolite [6-10]), silicon, nylon, terylene, rayon [8] and even magnesium oxide [6].

The percentage content of the phenol-formaldehyde resin $(C_7H_6O)_n$ in the impregnated filler is established in accordance with the intended purpose of the plastic.

On aerodynamic heating of plastics, the "chains" of the resin decay in the solid phase without access of air at 1200-$1400^{\circ}K$ (pyrolysis), with the result that gaseous products with high and low molecular weights are formed; these include H_2, carbon monoxide CO, carbon dioxide CO_2, water vapor H_2O, methyne CH, methylene CH_2, methyl CH_3, methane CH_4, acetylene C_2H_2, ethylene C_2H_4 and numerous other hydrocarbons and radicals.

Apart from the gaseous products, pyrolysis results in formation of a solid coke residue in the form of a rigid, amorphous carbon structure with a high coke content (0.53) [11].

The coke burns in the oxygen and nitrogen of the air and forms other products: cyanide CN, cyanogen C_2N_2. Coke evaporation products: C, C_2, C_3 may form on the surface at high temperatures.

In addition, the following components may be formed as a result of combustion of the coke in the presence of hydrogen: formyl HCO, formal-

dehyde H_2CO, and hydrocyanic acid vapor HCN.

Combination of hydrogen with air yields as products imino NH, amino NH_2, ammonia NH_3, hydrazine N_2H_4, isonitroso HNO and certain others.

Simultaneously with pyrolysis of the resin, a physicochemical transformation also takes place in the filler. Let us consider a case in which the filler is asbestos. Asbestos is completely dehydrated on heating to $900-1000^\circ K$ [12]. On heating to temperatures above $1800^\circ K$, this asbestos residue may enter flow as a result of softening of the asbestos and entrain particles of the coke residue and gases formed on decomposition of the plastic. This is attended by evaporation of silica SiO_2 on the surface, together with its dissociation: $2SiO_2 \rightarrow 2SiO + O_2$. Silicon carbide SiC and silicon dicarbide SiC_2 may form as a result of reaction between silicon and silicon oxide on the one hand, and carbon on the other. Silicon monohydride SiH and silicon mononitride SiN also appear.

Dissociation processes of the air and the combustion products from the plastics also add components to the boundary layer as we move away from the surface: O, N, NO, C, H. Si.

Thus, in the absence of ionization, a boundary layer consisting of no fewer than 30-35 components may, in the general case, form from the five elements O, N, C, H, Si(Mg). In the decomposition of a specific resin under specified flight conditions, however, not all of the gases listed above are present simultaneously in comparable quantities. For example, at surface temperatures higher than $1400^\circ K$ and pressures below 100 bars, there will be practically no CO_2 or hydrocarbons at the surface and in the boundary layer. At temperatures below $2500^\circ K$ and pressures higher than 10^{-3} bar, there will be practically no CN or C_2N_2, etc. In the destruction of textolite, as is indicated by thermochemical analysis, sixteen basic components form: O, N, NO, O_2, N_2, C, C_2, C_3,

CO, CO_2, CN, HCN, H_2O, OH, H, H_2; 11 components form in combustion of graphite,18-19 components in the combustion of asbotextolite, and so forth.

In each specific case, the composition of the gases can be established by consideration of all possible reactions. Without making it our task in this paper to give a detailed analysis of gas composition for the destruction of each specific plastic, we present a calculation of the effective diffusion coefficients for a mixture of gases composed of the five elements O, N, C, H, Si(Mg), using the method of our study [5], in which all binary diffusion coefficients could be broken down into eight groups with equal or nearly binary diffusion coefficients (see Chapter 2). This case covers most mixtures that appear during the destruction of reinforced plastics based on phenol-formaldehyde resins in a dissociated air flow. It will follow from the derivation of these formulas that similar expressions for the effective diffusion coefficients can also be obtained without great effort for more complex gas mixtures.

2. DETERMINATION OF EFFECTIVE DIFFUSION COEFFICIENTS IN THE MOLAR AND MASS DESCRIPTIONS OF DIFFUSION

For a mixture of ideal gases, the kinetic theory of gases and the thermodynamics of irreversible processes [13] give the following expressions for the diffusion vectors $\vec{I}_i$ (we disregard the effect of thermal diffusion as an effect of the second order [14, 15], and the barodiffusion effect drops out by virtue of the approximations of boundary-layer theory):

$$I_i = \rho_i V_i = \rho \sum_{j=1}^{N} \frac{m_i m_j}{m^2} D^*_{ij} \nabla x_j \quad (i = 1, \ldots, N), \quad D^*_{ii} = 0, \qquad (2.1)$$

where the multicomponent diffusion coefficients D^*_{ij} on the basis of the kinetic theory of ideal gases are expressed in first approximation in

terms of the $\frac{1}{2}N(N-1)$ binary diffusion coefficients D_{ij} of the various pairs of components in the mixture, $\vec{V}_1$ is the mass diffusion rate vector of the $\underline{i}\underline{th}$ component, ρ_1, m_1, x_1 are the density, molecular weight and molar (numerical) concentration of the $\underline{i}\underline{th}$ component respectively, ρ is the density of the mixture, $\underline{m}$ is the average molecular weight of the mixture, and N is the number of components in the mixture. Since the coefficients D_{ij}^* are expressed in terms of D_{ij} in the form of $\underline{N}\underline{th}$-order determinants, Expressions (2.1) are not suitable for practical use. Moreover, after substituting Expressions (2.1) in the component diffusion equations, we obtain a system of partial differential equations (in the approximation of boundary-layer theory) that is not solvable for the higher-order derivatives and therefore difficult even for solution on computers.

For these reasons, we shall proceed further from $N-1$ independent Stefan-Maxwell relationships [13]

$$\nabla x_i = \sum_{j=1}^{N} \frac{x_i x_j}{D_{ij}} (V_j - V_i) \qquad (i = 1, \ldots, N),\qquad (2.2)$$

which can be obtained from (2.1) by use of expressions linking the D_{ij}^* through D_{ij} and the identity $\sum_{k=1}^{N} I_k = 0$. The advantage of using Expressions (2.2) consists in the fact they contain only binary diffusion coefficients, which are well known for many component pairs. In the case of a binary mixture (i, j) there exists a unique diffusion coefficient D_{ij} in the molar and mass description of diffusion:

$$I_i^\bullet = -I_j^\bullet = -n D_{ij} \nabla x_i, \quad I_i = -I_j = -\rho D_{ij} \nabla c_i, \qquad (2.3)$$

where

$$I_i^\bullet = n_i(v_i - v^\bullet) = n_i V_i^\bullet, \quad I_i = \rho_i(v_i - v) = \rho_i V_i,$$

$$v^\bullet = \sum_{k=1}^{N} x_k v_k, \quad v = \sum_{k=1}^{N} c_k v_k, \quad c_i = \frac{m_i}{m} x_i, \quad x_i = \frac{n_i}{n}, \qquad (2.4)$$

$$n = \sum_{k=1}^{N} n_k.$$

Here, $\vec{I_1}^*$ is the molar diffusion-flux vector, $\vec{I_1}$ is the mass diffusion-flux vector, n_1 is the number of moles of the ith component per unit of volume, $\vec{v_1}$ is the average statistical velocity of component 1 and $\vec{v_1}^*$ and $\vec{v}$ are, respectively, the averaged molar and averaged mass velocities of the mixture.

In determining the effective diffusion coefficients in a multicomponent mixture, we shall presently see that we must distinguish the effective diffusion coefficients for the molar description of diffusion from the effective diffusion coefficients in the mass description.

Since only the projections of the diffusion vectors onto the normal to the surface, i.e., onto the y-axis, are required in the approximation of boundary-layer theory, we shall henceforth operate only with the projections, denoting them by the same letters, but in lightface type. Then Relationships (2.2) may be presented in the form

$$I_i^* = -nD_i^* \frac{\partial x_i}{\partial y} \quad (i = 1, \ldots, N), \tag{2.5}$$

where the effective diffusion coefficients D_i^* for the molar description of diffusion will be defined from one of the following three formulas:

$$\frac{1}{D_i^*} = \sum_{j=1}^{N} \frac{x_j}{D_{ij}}\left(1 - \frac{I_j^*}{I_i^*}\right) = \sum_{j=1}^{N} \frac{x_j}{D_{ij}} \frac{v_j - v_i}{v_i - v^*} = \sum_{j=1}^{N} \frac{1}{D_{ij}}\left(x_j - x_i \frac{I_j^*}{I_i^*}\right). \tag{2.6}$$

Hence the defined diffusion coefficient for an ith component in a multicomponent mixture depends not only on the composition and the binary diffusion coefficients, but also on the ratios of all other flows $I_k^*(k \neq 1)$ to the flow I_1^*.

For certain particular cases of diffusion, the dependence of D_i^* on the flows can be dispensed with. Let us consider some of these.

1. All binary diffusion coefficients are equal (or nearly equal): $D_{1j} = D$. Then it follows from (2.6) that

$$D_i^\bullet = D_{ij} = D \qquad (i = 1, \ldots, N). \qquad (2.7)$$

2. Let us consider a mixture in which the components 2, 3, ..., N move at the same speed (or are at rest): $v_1 \neq v_2 = v_3 = \ldots = v_N.$ Then it follows from (2.6) that

$$\frac{1 - x_1}{D_1^\bullet} = \sum_{j=2}^{N} \frac{x_j}{D_{1j}}, \quad D_i^\bullet = D_{i1} \quad (i = 2, \ldots; N) \qquad (2.8)$$

The corresponding molar flows may be written in the form

$$I_1^\bullet = - nD_1^\bullet \frac{\partial x_1}{\partial y} \qquad (2.9)$$

$$I_i^\bullet = - nD_{i1} \frac{\partial x_i}{\partial y} = x_i \left(\sum_{j=2}^{N} \frac{x_i}{D_{1j}} \right)^{-1} \frac{\partial x_1}{\partial y} \quad (i \neq 1). \qquad (2.10)$$

The expression for $D_1^\bullet$ in this case was obtained earlier by Wilke [16].

3. In the case in which one of the mixture components moves at a velocity much higher than those of the remaining components, then Formula (2.9) applies for this component, while Formulas (2.10) remain valid for the other components.

Let us now pass to determination of the effective diffusion coefficients D_1 for the mass description of diffusion. Using the relationships

$$c_i = (m_i / m) x_i \qquad (i = 1, \ldots, N)$$

it is easy to derive the Stefan-Maxwell analogue for the mass-concentration gradients from (2.2):

$$\nabla c_i = \sum_{j=1}^{N} \frac{c_i x_j}{D_{ij}} (V_j - V_i) - \sum_{h=1}^{N} c_h \sum_{j=1}^{N} \frac{c_i x_j}{D_{hj}} (V_j - V_h) \quad (i = 1, \ldots, N) \qquad (2.11)$$

Instead of the vector relationships (2.11), we shall henceforth operate with their projections onto the y-axis and denote the vector projections by the same symbols, but in lightface type. Then Relationships may be presented in the form

$$I_i = -\rho D_i (\partial c_i / \partial y) \quad (i = 1, \ldots, N),$$ (2.12)

where the effective diffusion coefficients B_1 in the mass diffusion description will be determined from one of the following three formulas:

$$\frac{1}{D_i} = \sum_{j=1}^{N} \frac{z_j}{D_{ij}} \left(1 - \frac{V_j}{V_i}\right) + \sum_{k=1}^{N} c_k \sum_{j=1}^{N} \frac{z_j}{D_{kj}} \frac{V_j - V_k}{V_i} =$$

$$= \sum_{j=1}^{N} \frac{z_j}{D_{ij}} \frac{v_i - v_j}{v_i - v} + \sum_{k=1}^{N} c_k \sum_{j=1}^{N} \frac{z_j}{D_{kj}} \frac{v_j - v_k}{v_i - v} =$$ (2.13)

$$= \sum_{j=1}^{N} \frac{z_j}{D_{ij}} \left(1 - \frac{c_i}{c_j} \frac{I_j}{I_i}\right) + \sum_{k=1}^{N} c_k \sum_{j=1}^{N} \frac{z_j}{D_{kj}} \left(\frac{c_i}{c_j} \frac{I_j}{I_i} - \frac{c_i}{c_k} \frac{I_k}{I_i}\right).$$

Let us again consider particular cases in which the coefficients D_1 do not depend on the flows.

1. All binary diffusion coefficients are equal (or nearly equal): $D_{ij} = D$ Then we obtain at once from (2.13)

$$D_i = D_{ij} = D \quad (i = 1, \ldots, N).$$ (2.14)

2. The components 2, 3, ..., N move at the same average speed (or are at rest): $v_1 \neq v_2 = v_3 = \ldots = v_N$. Then it follows from (2.13) that

$$\frac{1 - c_1}{D_1} = \sum_{j=2}^{N} \frac{z_j + z_1 c_j - c_1 z_j}{D_{1j}} = \sum_{j=2}^{N} \frac{z_j \left[1 + \frac{x_1}{m}(m_j - m_1)\right]}{D_{1j}}.$$ (2.15)

$$\frac{1}{D_i} = \frac{m}{m_1} \frac{1}{D_{1i}} + \sum_{j=2}^{N} \frac{z_j \left(1 - \frac{m_j}{m_1}\right)}{D_{1j}} = \frac{z_1}{D_{1i}} + \sum_{j=2}^{N} \frac{z_j m_j}{m_1} \left(\frac{1}{D_{1i}} - \frac{1}{D_{1j}}\right) (i \neq 1).$$ (2.16)

From comparison of Formulas (2.8) with the corresponding Formulas (2.15) and (2.16), it follows that in this case the effective diffusion coefficients in the molar and mass descriptions of diffusion generally differ from one another. It is easily proven, that, for example, in the boundary layer around the critical point (line) in the absence of homogeneous chemical reactions, the Wilke condition:

$v_1 \neq v_2 = v_3 = \ldots = v_N$ necessarily results in equality of all binary dif-

fusion coefficients, so that then Formulas (2.8) will coincide with Formulas (2.15) and (2.16), giving: $D_1^* = D_1 = D_{1j} = D$ for all components. Hence the use of Formulas (2.8) or (2.15) and (2.16) for the effective diffusion coefficients together with (2.5) or (2.12) and the corresponding diffusion equations for solution of problems of convective mass transfer will result, in the general case of diffusion, in a violation of the law of mass conversation in the basic equations of motion.

3. If for a component $\underline{i}$ in some region of the flow $c_i \to 0$, but $I_i \neq 0$, then we obtain from the third formula of (2.13) in this region

$$1/D_i = \sum_{j \neq i} x_j/D_{ij}. \tag{2.17}$$

4. Finally, we might indicate mixtures such that the effective diffusion coefficients for some components are calculated explicitly without restrictions on the diffusion velocities. Suppose that all binary diffusion coefficients can be broken down into two groups, for example,

$$D_{MM}(M = O_2, N_2, CO, CN, HCN) \text{ and } D_{MCO_2} \tag{2.18}$$

or D_{MM} and D_{MH_2}, where in each group the binary diffusion coefficients are close (equal) to one another. From the second definition (2.13) for this case, applying

$$V_{CO_2}^{\cdot} = \frac{m}{m_M} V_{CO_2} = \frac{1 - x_{CO_2}}{1 - c_{CO_2}} V_{CO_2}$$

we obtain

$$\frac{1}{D_M} = \frac{1 - x_{CO_2}}{D_{MM}} + \frac{x_{CO_2}}{D_{MCO_2}} + \left(\frac{1}{D_{MM}} - \frac{1}{D_{MCO_2}}\right) \frac{m}{m_M} \frac{c_{CO_2} V_{CO_2}}{c_M V_M} c_M. \tag{2.19}$$

$$D_{CO_2} = D_{MCO_2}. \tag{2.20}$$

I.e., in this case the effective diffusion coefficient for $CO_2(H_2)$ is equal to its own binary diffusion coefficient for the pair $CO_2, M(H_2, M)$

It follows from the definitions (2.13) (see also Formula (2.19)) that in the general case, the effective diffusion coefficients D_i can be calculated only after solution of the diffusion equations, when we have found the diffusion flows $I_i(c_iV_i)$. I.e., the coefficients D_i will depend, generally speaking, on the determining parameters of the specific problem. If a generalized analogy between the mass-transfer coefficients $z_i'(0) = 1/(c_{ie} - c_{i0})(\partial c_i/\partial y)_{y=0}$, where $c_{ie} - c_{i0}$ is the concentration gradient across the boundary layer, has been established for the specific problem, then we can calculate the effective diffusion coefficients at the wall from (2.13). This generalized analogy can be obtained readily for a frozen flow, when the corresponding problem for the boundary layer can be reduced to ordinary differential equations. For example, we have [5] for a boundary layer in the neighborhood of the critical point (line)

$$\left(\frac{c_iV_i}{c_jV_j}\right)_0 = \frac{c_{ie} - c_{i0}}{c_{je} - c_{j0}}\left(\frac{D_{i0}}{D_{j0}}\right)^{0.6}, \quad 0.25 < S_{i0} < 5, \quad S_i = \mu/\rho D, \quad (2.21)$$

on an impermeable wall,

$$\left(\frac{c_iV_i}{c_jV_j}\right)_0 = \frac{c_{ie} - c_{i0}}{c_{je} - c_{j0}}\frac{D_{i0}}{D_{j0}} \quad (2.22)$$

on a permeable wall for a moderate influx of mass $(-n\varphi(0) = 0.2-0.6, \ 0.3 < S_{i0} < 3)$ and

$$\left(\frac{c_iV_i}{c_jV_j}\right)_0 = \frac{c_{ie} - c_{i0}}{c_{je} - c_{j0}}\left(\frac{D_{i0}}{D_{j0}}\right)^2 \quad (2.23)$$

for an intense air blast approaching the flow-detachment regime $(-n\varphi(0) \approx 1, \ 0.6 < S_{i0} < 1.4)$.

Here $\varphi(0)$ is the value of the stream function at the wall and $S_{i0} = (\mu/\rho D_i)_0$ is the generalized Schmidt number also at the wall. Formulas (2.21)-(2.23) were obtained both analytically [5], using asymptotic integration of the diffusion equations for $S_i \to \infty$, and by numeri-

cal integration of the equations of the binary boundary layer with variable properties in the neighborhood of the critical point (line) and on a plate (at a Mach number smaller than two) being blasted by six different gases (hydrogen, helium, argon, carbon dioxide, air and mercury vapor). Formula (2.22) can be presented in the form

$$A_{ij} = \left(\frac{D_j}{D_i}\frac{c_iV_i}{c_jV_j}\right)_e \frac{c_{je}-c_{jo}}{c_{ie}-c_{io}} - 1. \tag{2.24}$$

TABLE 1

He		CO₂		He		CO₂	
$\varphi(0)$	A_{ij}	$\varphi(0)$	A_{ij}	$\varphi(0)$	A_{ij}	$\varphi(0)$	A_{ij}
−0.2	0.884	−0.25	0.97	−0.4	1.067	−0.75	1.08
−0.3	0.989	−0.5	1.02	−0.5	1.117		

Table 1 presents the value of A_{1j} for blasting with helium and the value of A_{1j} for blasting with carbon dioxide in air for the case of a critical-line neighborhood with a temperature factor $T_0/T_r = 0.5$ $(S_t = 1,\ S_i = \mu/\rho D_{ij})$. It follows from this table that Formula (2.22) or (2.24) is satisfied for a moderate influx to within $\pm$ 10%. The analogy (2.21) is confirmed nicely in the theory of heat exchange on an impermeable wall [17].

The generalized analogies between the mass-transfer coefficients (2.21)-(2.23) remain valid with the same accuracy also for a boundary layer with arbitrary longitudinal pressure gradient [18].

3. CALCULATION OF EFFECTIVE DIFFUSION COEFFICIENTS IN THE MASS DESCRIPTION OF DIFFUSION FOR CERTAIN GAS MIXTURES

Using the generalized analogies (2.21)-(2.23), the effective diffusion coefficients at the wall can be computed explicitly for a given specific gas mixture. Let us perform these calculations in application to mixtures that appear on heterogeneous combustion of plastics in a dissociated air stream (see Chapter 1). As follows from Tables 2 and 3, which were compiled on the basis of data on the interaction-force par-

ameters for the Lennard-Jones potential [19], the binary diffusion co-
efficients for the gas mixtures examined in Chapter I can be broken
down into eight groups:

$$D_{MM}(M = O_2, N_2, NO, CO, CN, HCN, HNO, HCO, H_2CO, N_2H_4, SiH, C_2,$$
$$C_3, C_4H_2, C_3H_4 \text{ etc.})$$

$$D_{AM}(A = O, N), D_{MSiO} \text{ (or } D_{MCO}), D_{MH}, D_{ASiO}, D_{AH}, D_{H,SiO}, D_{AA}. \quad (3.1)$$

where the binary diffusion coefficients in each group differ from one
another by no more than 2-5%, with the exception of the coefficients
D_{MC_2} and D_{MC_3}, which differ from one another by 12-12%. Since the gas-
kinetic parameters are at present known very approximately for the
molecules C_2 and C_3 and these molecules can appear in noteworthy quan-
tities only under conditions approaching those at which graphite boils
and, furthermore, it follows from the equilibrium condition [20] that
$c_{C_3} \approx 0.1 c_{C_2}$, we shall not introduce the supplementary group D_{MC_2} of bi-
nary diffusion coefficients, even though it would not be particularly
difficult to calculate the effective diffusion coefficients in this
case as well. Moreover, the boiling state of graphite (of coke) will
not be reached in practice when plastics are destroyed, and the C_2 and
C_3 vapors will be present in negligible quantities at the wall and in
the boundary layer. It follows from the equilibrium condition for the
graphite vapor above the solid phase [20] that $c_C < c_{C_2}$, i.e., carbon
atoms are present in small quantities. For example, with p_e = 10 bars
and T_0 = 4590°K, c_C = 0.0391, c_{C_2} = 0.1376, c_C = 0.7633; with p_e =
= 10^{-2} bar and T_0 = 3390°K c_C = 0.055, c_C = 0.115, c_{C_3} = 0.830, etc.

Thus, Case (3.1) will cover a mixture consisting of no fewer than
25 components. In practice, this case will cover the majority of mix-
tures that appear during the destruction, in a dissociated stream of
air, of the structural plastics most commonly used as heat-protective

TABLE 2*

The Table gives values of $\sqrt{\frac{1}{m_i}+\frac{1}{m_j}} \cdot \dfrac{\pi}{(\sigma_i+\sigma_j)\,\overline{\Omega}^{(11)}\,(\tau_{ij})}$ for two temperature values (upper number T = 2000°K and lower number for T = 4000°K).

1) Air.

TABLE 3*

*The Table gives values of $\sqrt{\frac{1}{m_i} + \frac{1}{m_j}} \cdot \frac{10^0}{(e_i + e_j) \, \Gamma \, \Omega^{(ll)}{}^*(\tau_{ij})}$ for two temperature values (upper figure for $T = 8000\,°K$ and lower for $T = 12,000\,°K$). 1) Air

coatings. Then omitting the cumbersome intermediate displays, we obtain from the definition (2.13) the following expressions for the reciprocal effective diffusion coefficients in the boundary layer for Case (3.1):

$$
\frac{1}{D_M} = \sum_{j=1}^{N} \frac{z_j}{D_{Mj}} + \left\{ \left(\frac{m}{m_A} c_{SiO} - z_{SiO} \right) B_{SiO} + \left(\frac{m}{m_A} c_{H_2} - z_{H_2} \right) B_{H_2} + \right.
$$

$$
+ \frac{m}{m_M} \left(\frac{1}{D_{MM}} - \frac{1}{D_{AM}} \right) + c_{H_2} \left[\left(\frac{m}{m_M} - \frac{m}{m_A} \right) \left(\frac{1}{D_{MM}} - \frac{1}{D_{MH_2}} \right) - \right.
$$

$$
\left. - \left(\frac{m}{m_M} - \frac{m}{m_{H_2}} \right) \left(\frac{1}{D_{MM}} - \frac{1}{D_{AM}} \right) \right] + c_{SiO} \left[\left(\frac{m}{m_M} - \frac{m}{m_A} \right) \left(\frac{1}{D_{MM}} - \frac{1}{D_{MSiO}} \right) - \right.
$$

$$
\left. \left. - \left(\frac{m}{m_M} - \frac{m}{m_{SiO}} \right) \left(\frac{1}{D_{MM}} - \frac{1}{D_{AM}} \right) \right] \right\} \frac{c_O V_O + c_N V_N}{V_M} +
$$

$$
+ \left\{ \left[\frac{m}{m_{SiO}} (c_O + c_N) - (z_O + z_N) \right] B_{SiO} + \left(\frac{m}{m_{SiO}} c_{H_2} - z_{H_2} \right) B_{H_2,SiO} + \right.
$$

$$
+ \left(\frac{1}{D_{MM}} - \frac{1}{D_{AM}} \right) \left(\frac{m}{m_M} - \frac{m}{m_{SiO}} \right) (c_O + c_N) + \left(\frac{1}{D_{MM}} - \frac{1}{D_{MSiO}} \right) \left[\frac{m}{m_M} - \right.
$$

$$
\left. - (c_O + c_N) \left(\frac{m}{m_M} - \frac{m}{m_A} \right) \right] - c_{H_2} \left(\frac{1}{D_{MM}} - \frac{1}{D_{MSiO}} \right) \left(\frac{m}{m_M} - \frac{m}{m_{H_2}} \right) +
$$

$$
\left. + c_{H_2} \left(\frac{1}{D_{MM}} - \frac{1}{D_{MH_2}} \right) \left(\frac{m}{m_M} - \frac{m}{m_{SiO}} \right) \right\} \frac{c_{SiO} V_{SiO}}{V_M} +
$$

$$
+ \left\{ \left[\frac{m}{m_{H_2}} (c_O + c_N) - (z_O + z_N) \right] B_{H_2} + \left(\frac{m}{m_{H_2}} c_{SiO} - z_{SiO} \right) B_{H_2,SiO} + \right.
$$

$$
+ \left(\frac{1}{D_{MM}} - \frac{1}{D_{AM}} \right) \left(\frac{m}{m_M} - \frac{m}{m_{H_2}} \right) (c_O + c_N) + \left(\frac{1}{D_{MM}} - \frac{1}{D_{MH_2}} \right) \left[\frac{m}{m_M} - \right.
$$

$$
- (c_O + c_N) \left(\frac{m}{m_M} - \frac{m}{m_A} \right) - c_{SiO} \left(\frac{1}{D_{MM}} - \frac{1}{D_{MH_2}} \right) \left(\frac{m}{m_M} - \frac{m}{m_{SiO}} \right) +
$$

$$
\left. + c_{SiO} \left(\frac{1}{D_{MM}} - \frac{1}{D_{MCO_2}} \right) \left(\frac{m}{m_M} - \frac{m}{m_{H_2}} \right) \right\} \frac{c_{H_2} V_{H_2}}{V_M}
$$

$$
(M = O_2, N_2, NO, CO, CN, HCN, C_2, C_3)
$$

$$\frac{1}{D_{\text{ЖО}}} = \frac{1}{D_{\text{МЖО}}} + z_{\text{К}}\left(-\frac{1}{D_{\text{М ЖО}}} - \frac{1}{D_{\text{МЖО}}}\right) + (1 - z_{\text{НО}})\left(\frac{1}{D_{\text{ММ}}} - \frac{1}{D_{\text{МЖО}}}\right) +$$

$$+ (z_0 + z_{\text{Н}})\left(\frac{1}{D_{\text{АЖО}}} - \frac{1}{D_{\text{МЖО}}}\right) + (z_{\text{ЖО}}c_{\text{К}_1} - c_{\text{ЖО}}z_{\text{К}_1})B_{\text{К.ЖО}} +$$

$$+ [z_{\text{ЖО}}(c_0 + c_{\text{Н}}) - c_{\text{ЖО}}(z_0 + z_{\text{Н}})]B_{\text{ЖО}} + \left(\frac{1}{D_{\text{ММ}}} - \frac{1}{D_{\text{АМ}}}\right)\left(\frac{m_i}{m_{b\text{М}}} - \right.$$

$$\left. - \frac{m}{m_{\text{ЖО}}}\right)c_{\text{ЖО}}(c_0 + c_{\text{Н}}) + \left(\frac{1}{D_{\text{ММ}}} - \frac{1}{D_{\text{ММ}_1}}\right)\left(\frac{m_i}{m_{\text{М}}} - \frac{m}{m_{\text{ЖО}}}\right)c_{\text{ЖО}}c_{\text{К}_1} -$$

$$- (1 - c_{\text{ЖО}})\left(\frac{1}{D_{\text{ММ}}} - \frac{1}{D_{\text{МЖО}}}\right)\left[\frac{m_i}{m_{i\text{М}}} - (c_0 + c_{\text{Н}})\left(\frac{m}{m_{\text{М}}} - \frac{m}{m_{\text{А}}}\right) - c_{\text{К}_1}\left(\frac{m}{m_{\text{М}}} - \right.\right.$$

$$\left.\left. - \frac{m}{m_{\text{К}_1}}\right)\right] + \left\{\left(\frac{m}{m_{\text{А}}}c_{\text{К}_1} - z_{\text{К}_1}\right)B_{\text{К}_1} + \left(\frac{m}{m_{\text{А}}}c_{\text{ЖО}} - z_{\text{ЖО}} - \frac{m}{m_{\text{А}}}\right)B_{\text{ЖО}} +\right.$$

$$+ \left(\frac{1}{D_{\text{ЖМ}}} - \frac{1}{D_{\text{АМ}}}\right)\left[\frac{m}{m_{\text{М}}} - c_{\text{ЖО}}\left(\frac{m}{m_{\text{М}}} - \frac{m}{m_{\text{ЖО}}}\right) - c_{\text{К}_1}\left(\frac{m}{m_{\text{М}}} - \frac{m}{m_{\text{К}_1}}\right)\right] -$$

$$- (1 - c_{\text{ЖО}})\left(\frac{1}{D_{\text{ММ}}} - \frac{1}{D_{\text{МЖО}}}\right)\left(\frac{m}{m_{\text{М}}} - \frac{m}{m_{\text{А}}}\right) +$$

$$+ c_{\text{К}_1}\left(\frac{1}{D_{\text{ММ}}} - \frac{1}{D_{\text{ММ}_1}}\right)\left(\frac{m}{m_{\text{М}}} - \frac{m}{m_{\text{А}}}\right)\frac{c_0 V_0 + c_{\text{Н}}V_{\text{Н}}}{V_{\text{ЖО}}} +$$

$$+ \left\{\left(\frac{m}{m_{\text{К}_1}}c_{\text{ЖО}} - z_{\text{ЖО}} - \frac{m}{m_{\text{К}_1}}\right)B_{\text{К,ЖО}} + \left[\frac{m}{m_{\text{К}_1}}(c_0 + c_{\text{Н}}) - (z_0 + z_{\text{Н}})\right]B_{\text{К}_1} +\right.$$

$$+ \left(\frac{1}{D_{\text{ЖМ}}} - \frac{1}{D_{\text{АМ}}}\right)\left(\frac{m}{m_{\text{М}}} - \frac{m}{m_{\text{К}_1}}\right)(c_0 + c_{\text{Н}}) - (1 - c_{\text{ЖО}})\left(\frac{1}{D_{\text{ММ}}} - \frac{1}{D_{\text{МЖО}}}\right) \times$$

$$\times \left(\frac{m}{m_{\text{М}}} - \frac{m}{m_{\text{М}}}\right) + \left(\frac{1}{D_{\text{ЖМ}}} - \frac{1}{D_{\text{ММ}_1}}\right)\left[\frac{m}{m_{\text{М}}} - (c_0 + c_{\text{Н}})\left(\frac{m}{m_{\text{М}}} - \frac{m}{m_{\text{А}}}\right) - \right.$$

$$\left.\left. - c_{\text{ЖО}}\left(\frac{m}{m_{\text{М}}} - \frac{m}{m_{\text{ЖО}}}\right)\right]\right\}\frac{c_{\text{Н}}V_{\text{Н}_1}}{V_{\text{ЖО}}} \tag{3.2}$$

$$\frac{1}{D_{\text{К}_1}} = \frac{1}{D_{\text{ММ}_1}} + z_{\text{ЖО}}\left(\frac{1}{D_{\text{К,ЖО}}} - \frac{1}{D_{\text{ММ}_1}}\right) + (1 - \dot{z}_{\text{К}_1})\left(\frac{1}{D_{\text{ММ}}} - \frac{1}{D_{\text{ММ}_1}}\right) +$$

$$+ (z_0 + z_{\text{Н}})\left(\frac{1}{D_{\text{АК}_1}} - \frac{1}{D_{\text{ММК}_1}}\right) + (z_{\text{К}_1}c_{\text{ЖО}} - c_{\text{К}_1}z_{\text{ЖО}})B_{\text{К,ЖО}} +$$

$$+ [z_{\text{К}_1}(c_0 + c_{\text{Н}}) - c_{\text{К}_1}(z_0 + z_{\text{Н}})]B_{\text{К}_1} + \left(\frac{1}{D_{\text{ЖМ}}} - \frac{1}{D_{\text{АМ}}}\right)\left(\frac{1}{m_{\text{М}}} - \frac{1}{m_{\text{Н}}}\right) \times$$

$$\times (c_0 + c_{\text{Н}})c_{\text{К}_1} + \left(\frac{1}{D_{\text{ЖМ}}} - \frac{1}{D_{\text{МЖО}}}\right)\left(\frac{m}{m_{\text{М}}} - \frac{m}{m_{\text{К}_1}}\right)c_{\text{ЖО}}c_{\text{К}_1} - (1 - c_{\text{К}_1}) \times$$

$$\times \left(\frac{1}{D_{MM}} - \frac{1}{D_{MM_i}}\right)\left[\frac{m}{m_M} - (c_O + c_N)\left(\frac{m}{m_M} - \frac{m}{m_A}\right) - c_{SiO}\left(\frac{m}{m_M} - \frac{m}{m_{SiO}}\right)\right] +$$

$$+ \left\{\left(\frac{m}{m_A}c_{SiO} - x_{SiO}\right)B_{SiO} + \left(\frac{m}{m_A}c_{M_i} - x_{H_i} - \frac{m}{m_A}\right)B_{H_i} + \left(\frac{1}{D_{MM}} - \frac{1}{D_{AM}}\right) \times\right.$$

$$\times \left[\frac{m}{m_M} - c_{SiO}\left(\frac{m}{m_M} - \frac{m}{m_{SiO}}\right) - c_{H_i}\left(\frac{m}{m_M} - \frac{m}{m_{H_i}}\right)\right] - (1 - c_{H_i}) \times$$

$$\times \left(\frac{1}{D_{MM}} - \frac{1}{D_{MH_i}}\right)\left(\frac{m}{m_M} - \frac{m}{m_A}\right) + c_{SiO}\left(\frac{1}{D_{MM}} - \frac{1}{D_{MSiO}}\right)\left(\frac{m}{m_M} - \frac{m}{m_A}\right)\right\} \times$$

$$\times \frac{c_O V_O + c_N V_N}{V_{M_i}} + \left\{\left(\frac{m}{m_{SiO}}c_{H_i} - x_{H_i} - \frac{m}{m_{SiO}}\right)B_{H_i SiO} + \left[\frac{m}{m_{SiO}}(c_O + c_N) -\right.\right.$$

$$- (x_O + x_N)\Big]B_{SiO} + \left(\frac{1}{D_{MM}} - \frac{1}{D_{AM}}\right)\left(\frac{m}{m_M} - \frac{m}{m_{SiO}}\right)(c_O + c_N) - (1 - c_{H_i}) \times$$

$$\times \left(\frac{1}{D_{MM}} - \frac{1}{D_{MM_i}}\right)\left(\frac{m}{m_M} - \frac{m}{m_{SiO}}\right) + \left(\frac{1}{D_{MM}} - \frac{1}{D_{MSiO}}\right)\left[\frac{m}{m_M} - \left(\frac{m}{m_M} - \frac{m}{m_A}\right) \times\right.$$

$$\times (c_O + c_N) - c_{H_i}\left(\frac{m}{m_M} - \frac{m}{m_{H_i}}\right)\Big]\bigg\}\frac{c_{SiO}V_{SiO}}{V_{H_i}}$$

$$\frac{1}{D_O} = \frac{1}{D_{AM}} + c_O\left(x_{SiO} - c_{SiO}\frac{m}{m_M} + x_{H_i} - c_{H_i}\frac{m}{m_M}\right)\left(\frac{1}{D_{MM}} - \frac{1}{D_{AM}}\right) +$$

$$+ x_N\left(\frac{1}{D_{AA}} - \frac{1}{D_{AM}}\right) + x_{SiO}\left(\frac{1}{D_{ASiO}} - \frac{1}{D_{AM}}\right) + x_{H_i}\left(\frac{1}{D_{AH_i}} - \frac{1}{D_{AM}}\right) +$$

$$+ (c_{SiO}x_O - c_O x_{SiO})B_{SiO} + (c_{H_i}x_O - c_O x_{H_i})B_{H_i} +$$

$$+ c_O c_{SiO}\left(\frac{m}{m_M} - \frac{m}{m_A}\right)\left(\frac{1}{D_{MM}} - \frac{1}{D_{MSiO}}\right) + c_O c_{H_i}\left(\frac{1}{D_{MM}} - \frac{1}{D_{MH_i}}\right)\left(\frac{m}{m_M} - \frac{m}{m_A}\right) +$$

$$+ \left[\frac{m}{m_A}B_A + \left(c_{H_i}\frac{m}{m_A} - x_{H_i}\right)B_{H_i} + \left(c_{SiO}\frac{m}{m_A} - x_{SiO}\right)B_{SiO} +\right.$$

$$\left(\frac{1}{D_{MM}} - \frac{1}{D_{MSiO}}\right)\left(\frac{m}{m_M} - \frac{m}{m_A}\right)c_{SiO} + \left(\frac{1}{D_{MM}} - \frac{1}{D_{MH_i}}\right)\left(\frac{m}{m_M} - \frac{m}{m_A}\right)c_{H_i} +$$

$$+ \left(\frac{1}{D_{MM}} - \frac{1}{D_{AM}}\right)\left(x_{SiO} + x_{H_i} - \frac{m}{m_M}c_{SiO} - \frac{m}{m_M}c_{H_i} + \frac{m}{m_A}\right)\Big]\frac{c_N V_N}{V_O} +$$

$$+ \left\{\left[(c_O + c_N - 1)\frac{m}{m_{H_i}} - (x_O + x_N)\right]B_{H_i} + \left(c_{CO_i}\frac{m}{m_{H_i}} - x_{CO_i}\right)B_{H_i SiO} +\right.$$

$$+ \left(\frac{1}{D_{MM}} - \frac{1}{D_{AM}}\right)\left(\frac{m}{m_M} - \frac{m}{m_{H_i}}\right)(c_O + c_N - 1) + \left(\frac{1}{D_{MM}} - \frac{1}{D_{MH_i}}\right)\left[\frac{m}{m_M} -\right.$$

$$-(c_0 + c_N)\left(\frac{m}{m_M} - \frac{m}{m_A}\right)\Bigg] + c_{MO}\left(\frac{1}{D_{MM}} - \frac{1}{D_{MSO}}\right)\left(\frac{m}{m_M} - \frac{m}{m_{H_1}}\right) -$$

$$- c_{MO}\left(\frac{1}{D_{MM}} - \frac{1}{D_{MH}}\right)\left(\frac{m}{m_M} - \frac{m}{m_{SO}}\right)\Bigg\}\ \frac{c_{H_1} V_{H_1}}{V_0} +$$

$$+ \Bigg\{\Bigg[(c_0 + c_N - 1)\frac{m}{m_{SO}} - (z_0 + z_N)\Bigg] B_{SO} + \left(c_{H_1}\frac{m}{m_{SO}} - z_{H_1}\right) B_{H,SO} +$$

$$+ \left(\frac{1}{D_{MM}} - \frac{1}{D_{AM}}\right)\left(\frac{m}{m_M} - \frac{m}{m_{SO}}\right)(c_0 + c_N - 1) + \left(\frac{1}{D_{MM}} - \frac{1}{D_{MSO}}\right)\Bigg[\frac{m}{m_M} -$$

$$- (c_0 + c_N)\left(\frac{m}{m_M} - \frac{m}{m_A}\right)\Bigg] + c_{H_1}\left(\frac{1}{D_{MM}} - \frac{1}{D_{MH_1}}\right)\left(\frac{m}{m_M} - \frac{m}{m_{SO}}\right) -$$

$$- c_{H_1}\left(\frac{1}{D_{MM}} - \frac{1}{D_{MSO}}\right)\left(\frac{m}{m_M} - \frac{m}{m_{H_1}}\right)\Bigg\}\frac{c_{SO} V_{SO}}{V_0},$$

where

$$\frac{1}{D_{MM}} - \frac{1}{D_{AM}} = \frac{0,285}{D_{MM}} = \frac{0,400}{D_{AM}}, \qquad \frac{1}{D_{MM}} - \frac{1}{D_{MH_1}} = \frac{0,723}{D_{MM}} = \frac{2,61}{D_{MH_1}}$$

$$\frac{1}{D_{MM}} - \frac{1}{D_{MSO}} = -\frac{0,173}{D_{MM}} = -\frac{0,147}{D_{MSO}} \qquad \frac{1}{D_{ASO}} - \frac{1}{D_{AM}} = \frac{0,108}{D_{ASO}} = \frac{0,124}{D_{AM}} \qquad (3.3)$$

$$\frac{1}{D_{AH_1}} - \frac{1}{D_{MH_1}} = -\frac{0,215}{D_{AH_1}} = -\frac{0,176}{D_{MH_1}}, \qquad \frac{1}{D_{AH_1}} - \frac{1}{D_{MSO}} = -\frac{4,10}{D_{AH_1}} = -\frac{0,804}{D_{MSO}}$$

$$\frac{1}{D_{AA}} - \frac{1}{D_{AM}} = -\frac{0,355}{D_{AA}} = -\frac{0,262}{D_{AM}}$$

$$B_{SO} = \frac{1}{D_{MM}} - \frac{1}{D_{AM}} + \frac{1}{D_{ASO}} - \frac{1}{D_{MSO}} = -\frac{0,088}{D_{MM}} = -\frac{0,123}{D_{AM}} =$$

$$= -\frac{0,109}{D_{ASO}} = -\frac{0,0745}{D_{MSO}}$$

$$B_{H_1} = \frac{1}{D_{MM}} + \frac{1}{D_{AH_1}} - \frac{1}{D_{AM}} - \frac{1}{D_{MH_1}} = \frac{0,236}{D_{MM}} = \frac{1,035}{D_{AH_1}} = \frac{0,331}{D_{AM}} = \frac{0,853}{D_{MH_1}}$$

$$B_{H,SO} = \frac{1}{D_{MM}} + \frac{1}{D_{H,SO}} - \frac{1}{D_{MSO}} - \frac{1}{D_{MH_1}} = \frac{0,160}{D_{MM}} = -\frac{0,552}{D_{H,SO}} = \qquad (3.4)$$

$$= -\frac{0,136}{D_{MSO}} = -\frac{0,577}{D_{MH_1}}$$

$$B_A = \frac{1}{D_{AM}} + \frac{1}{D_{AM}} - \frac{1}{D_{AA}} - \frac{1}{D_{MM}} = -\frac{0,008}{D_{MM}} = -\frac{0,137}{D_{AM}} = -\frac{0,186}{D_{AA}}$$

since, according to Tables 2 and 3   ..ave, in virtual independence
of temperature

$$\frac{D_{MM}}{D_{AM}} = \frac{D_{N,O}}{D_{N,N}} = 0.715, \qquad \frac{D_{MM}}{D_{MH_2}} = \frac{D_{N,CO}}{D_{N,M_2}} = 0.277,$$

$$\frac{D_{MM}}{D_{AH_2}} = \frac{D_{N,CO}}{D_{NM_2}} = 0.228, \qquad \frac{D_{AH_2}}{D_{AM}} = \frac{D_{NH_2}}{D_{N,N}} = 3.135,$$

$$\frac{D_{AH_2}}{D_{MH_2}} = \frac{D_{NH_2}}{D_{N,M_2}} = 1.215, \qquad \frac{D_{AM}}{D_{MH_2}} = \frac{D_{N,N}}{D_{N,M_2}} = 0.3875,$$

$$\frac{D_{MM}}{D_{MSiO}} = \frac{D_{N,CO}}{D_{N,SiO}} = 1.173, \qquad \frac{D_{ASiO}}{D_{AM}} = \frac{D_{NSiO}}{D_{N,N}} = 0.892, \qquad (3.5)$$

$$\frac{D_{HA_2}}{D_{MSiO}} = \frac{D_{NH_2}}{D_{N,SiO}} = 5.10, \qquad \frac{D_{AA}}{D_{AM}} = \frac{D_{NO}}{D_{N,N}} = 1.355,$$

$$\frac{D_{MM}}{D_{ASiO}} = \frac{D_{N,CO}}{D_{NSiO}} = 0.800, \qquad \frac{D_{AM}}{D_{MSiO}} = \frac{D_{N,N}}{D_{N,SiO}} = 1.645,$$

$$\frac{D_{ASiO}}{D_{MSiO}} = \frac{D_{NSiO}}{D_{N,SiO}} = 1.466, \qquad \frac{D_{MM}}{D_{H,SiO}} = \frac{D_{N,CO}}{D_{H,SiO}} = 0.290.$$

In deriving Formulas (3.2), it was assumed that

$$m_A = m_O = m_N. \qquad (3.6)$$

In the last analysis, however, the assumption (3.6) will not be
reflected in the calculation of the effective diffusion coefficients
at the wall, since the concentration of atoms at the wall is equal to
zero (see Formulas (3.21) below). Further, we have taken advantage of
the fact that the molecular weights of all components with the sub-
script M are nearly equal (equal).

An expression for $1/D_N$ is obtained from the last formula for $1/D_O$
by replacing therein x_O and c_O by x_N and c_N, respectively. In deriving
Formulas (3.2), the notation has been shortened in the atom group
(Symbol A), with only the O and N left. If it is necessary to
account for other components with diffusion properties similar to those
of atoms, such as CH_2, HO, H_2O, NH and others (see Tables 2 and 3), then
formulas for the $1/D_M$, $1/D_{SiO}$ and $1/D_{H_2}$ of such a mixture will be obtain-

ed from Formulas (3.2) if $c_0 + c_N$ in these formulas is replaced by $c_0 + c_N + c_{CH_2} + c_{HO} + \ldots$, $x_0 + x_N$ by $x_0 + x_N + x_{CH_2} + x_{HO} + \ldots$ and $c_0 v_0 + c_N v_N$ by $c_0 v_0 + c_N v_N + c_{CH_2} v_{CH_2} + c_{HO} v_{HO} + \ldots$.

In the formula for $1/D_0$, x_N should be replaced by $x_N + x_{CH_2} + x_{HO} + \ldots$, $c_0 + c_N$ by $c_0 + c_N + c_{CH_2} + c_{HO} + \ldots$, $x_0 + x_N$ by $x_0 + x_N + x_{CH_2} + x_{HO} + \ldots$ and $c_N v_N$ by $c_N v_N + c_{CH} v_{CH} + c_{HO} v_{HO} + \ldots$.

Expressions for $1/D_N$, $1/D_{CH}$, $1/D_{HO}$, ... will be obtained from the formula for $1/D_0$ by cyclical replacement of the subscripts O, N, CH, HO ...

From Formulas (3.2), we can obtain expressions for the effective diffusion coefficients of a number of important particular cases. For example, for the case of combustion of graphite in dissociated air at temperatures in the boundary layer above $1400^\circ K$ and pressures $p_e < 100$ bars, i.e., when the presence of CO_2 may be disregarded, we obtain

$$\frac{1}{D_0} = \frac{1}{D_{AM}} + (x_N + x_C)\left(\frac{1}{D_{AA}} - \frac{1}{D_{AM}}\right) + $$
$$+ \frac{m}{m_A}\left(\frac{1}{D_{AM}} - \frac{1}{D_{AA}}\right)\frac{c_N v_N + c_C v_C}{V_0},$$

$$\frac{1}{D_N} = \frac{1}{D_{AM}} + (x_C + x_0)\left(\frac{1}{D_{AA}} - \frac{1}{D_{AM}}\right) + $$
$$+ \frac{m}{m_A}\left(\frac{1}{D_{AM}} - \frac{1}{D_{AA}}\right)\frac{c_C v_C + c_0 v_0}{V_N},$$

$$\frac{1}{D_C} = \frac{1}{D_{AM}} + (x_0 + x_N)\left(\frac{1}{D_{AA}} - \frac{1}{D_{AM}}\right) + $$
$$+ \frac{m}{m_A}\left(\frac{1}{D_{AM}} - \frac{1}{D_{AA}}\right)\frac{c_0 v_0 + c_N v_N}{V_C},$$

$$\frac{1}{D_M} = \frac{1 - x_0 - x_N - x_C}{D_{MM}} + \frac{x_0 + x_N + x_C}{D_{AM}} + \quad (3.7)$$
$$+ \frac{m}{m_M}\left(\frac{1}{D_{MM}} - \frac{1}{D_{AM}}\right)\frac{c_0 v_0 + c_N v_N + c_C v_C}{V_M},$$
$$(M = O_2, N_2, NO, CO, CN, C_2, C_3).$$

$$\frac{m}{m_{\text{M}}} = \frac{1 - x_{\text{O}} - x_{\text{N}} - x_{\text{C}}}{1 - c_{\text{O}} - c_{\text{N}} - c_{\text{C}}}. \qquad (3.8)$$

Before calculating the effective diffusion coefficients at the wall, let us demonstrate that the following theorem applies. All components with nearly equal (equal) molecular weights and gas-kinetic parameters $\sigma_i^2 \Omega^{(1,1)*}(\tau_{ij})$ satisfying the boundary conditions

$$(c_{\text{M}})_e = 0 \qquad (3.9)$$

(for example, M = CO, CN, HCN, HNO, HCO, H_2CO, N_2H_4, SiH, C_2, C_3, C_2H_2, C_2H_4 and so forth), or

$$(c_i)_0 = 0 \qquad (3.10)$$

(for example, $i = O_2$, NO or $i = O$, N) have nearly equal (equal) effective diffusion coefficients through the entire thickness of the boundary layer.

For the proof, let us introduce the dimensionless diffusion mass flow X_1 and the concentration ratio z_{M} for the Mth component from the formulas

$$X_{\text{M}} = \frac{I_{\text{M}}}{(c_{\text{M}})_0 \sqrt{\beta \mu_0 \rho_0}}; \quad c_{\text{M}} = (c_{\text{M}})_0 + [(c_{\text{M}})_e - (c_{\text{M}})_0] z_{\text{M}}(\eta), \qquad (3.11)$$

where $\mu_0 \rho_0$ is the product of the coefficient of viscosity by the density under the conditions at the wall, β is the velocity gradient of the inviscid flow at the critical point (line) and η is a dimensionless variable related to the normal coordinate $\underline{y}$, which is reckoned with reference to the moving front (if destruction is taking place) by the relationship [21]

$$\eta = \left(\frac{\beta}{\mu_0 \rho_0}\right)^{1/2} \int_0^y \rho \, dy.$$

In these variables, the equations for the effective Schmidt numbers $S_{\text{M}} = \mu / \rho D_{\text{M}}$ will be, according to the first formula of (3.2) for $1/D_{\text{M}}$,

$$S_M X_M = l z'_M - X_M \sum_{j=1}^{N} \frac{x_j}{S_{Mj}} + \frac{\mu}{\rho} \{\ldots\} (X_0 + X_N)(1 - z_M) +$$
$$+ \frac{\mu}{\rho} \{\ldots\} X_{S1O}(1 - z_M) + \frac{\mu}{\rho} \{\ldots\} X_{H,}(1 - z_M), \quad l = \frac{\mu \rho}{\mu_0 \rho_0}, \quad (3.12)$$

where the subscript M runs through all components indicated in the condition of the theorem, the curly brackets $\{\ldots\}$ in (3.12) signify the corresponding expressions appearing in curly brackets in the first formula of (3.2) for $1/D_M$ and

$$X_0 = (c_0)_0 X_0, \quad X_N = (c_N)_0 X_N, \quad X_{S1O} = (c_{S1O})_0 X_{S1O}, \quad X_{H,} = (c_{H,})_0 X_{H,}.$$

The corresponding diffusion equations in these variables will be [21]

$$X'_M + n \varphi(\eta) z'_M = 0, \quad (3.13)$$

where n = 1 is the two-dimensional case, n = 2 is the axisymmetric case and $x^2 \varphi(\eta)$ is a function proportional to the stream function. It is necessary to solve the system (3.12) and (3.13) for the sought functions z_M and X_M for the boundary conditions

$$z_M(0) = 0, \quad z_M(\infty) = 1. \quad (3.14)$$

To prove the theorem, it is sufficient to show that the boundary-value problem (3.12)-(3.14) does not depend on the subscript M. The sum in (3.12) may be represented in the form

$$\sum_{j=1}^{N} \frac{x_j}{D_{Mj}} = \frac{1 - x_0 - x_N - x_{CH} - \ldots}{D_{MM}} + \frac{x_0 + x_N + x_{CH,}}{D_{AM}}, \quad (3.15)$$

from which it follows that the sum (3.15) does not depend on the subscripts M, since D_{MM} and D_{AM} for any M are nearly equal (equal) by the condition of the theorem. For the same reason, the expressions in curly brackets do not depend on the subscripts M. The boundary conditions (3.14) are also the same for all M. Hence all functions z_M and X_M will satisfy the same equations and boundary conditions, i.e., they coincide identically. But then the effective Schmidt numbers

$$S_M = l(z'_M / X_M) \tag{3.16}$$

will also be independent of the subscript M. Q.E.D. If the components satisfy the boundary conditions (3.10), then instead of the system (3.12) we shall have

$$S_i X_i = l z_i' = X_i \sum_{j=1}^{N} \frac{x_j}{D_{ij}} - \frac{\mu}{\rho} \{\ldots\} (X_0 + X_N) z_i -$$
$$- \frac{\mu}{\rho} \{\ldots\} X_{SiO} z_i - \frac{\mu}{\rho} \{\ldots\} X_H z_i, \qquad X_i = - \frac{I_i}{(c_i)_e \sqrt{\beta \mu_0 \rho_0}}.$$

Equations (3.13) and the boundary conditions (3.14) remain unchanged. From this it again follows that the effective diffusion coefficients for components with nearly equal (equal) diffusion properties that satisfy the boundary conditions (3.10) are equal through the entire thickness of the boundary layer.

Similarly, we might prove the theorem that for O and N atoms, which satisfy the boundary conditions $(c_A)_0 = 0$, the effective diffusion coefficients are nearly equal (equal) over the entire thickness of the boundary layer.

It is readily seen that the theorem proven above also remains valid for all self-modeling solutions to the equations of a multicomponent boundary layer. It follows at once from these results that the mass-transfer coefficients $z'_i(0) = c'_i(0) / (c_{ie} - c_{i0})$ are equal for all components satisfying the conditions of the theorem, i.e.,

$$\frac{c_i'(0)}{c_j'(0)} = \frac{c_{ie} - c_{i0}}{c_{je} - c_{j0}}. \tag{3.17}$$

This fact substantially reduces the number of mass-transfer coefficients that we seek. For example, for the mixture considered in Chapter 1, it is necessary to find, instead of 30–35 mass-transfer coefficients, only six mass-transfer coefficients: $z'_M(0)$ (M = CO, CN, HCN, HNO, HCO, H_2CO, N_2H_4, SiH, C_2, C_3, C_2H_2, C_2H_4 etc.), $z'_A(0)$ (A = CH, CH_2, CH_4, HO, H_2O, NH etc.), and $z'_{SiO}(0)$, $z'_{H_2}(0)$, $z'_{O_2}(0) = z'_{NO}(0)$, $z'_O(0) = z'_N(0)$.

The mass-transfer coefficient for molecular nitrogen need not be found, since this coefficient and the concentration c_{N_2} can be found from the identity $c_{N_s} = 1 - \sum\limits_{k \neq N_s} c_k.$ To find the remaining unknown quantities $z'_i(0)$, we calculate the effective diffusion coefficients at the wall. Here we shall assume that complete recombination of the atoms of the air and complete consumption of the oxygen take place at the wall. Then Formulas (3.2) at the wall, using the boundary conditions

$$(c_O)_0 = (c_N)_0 = (c_{O_2})_0 = (c_{NO})_0 = 0, \ |c_O V_O|_0, \ |c_N V_N|_0, \ |c_{O_2} V_{O_2}|_0,$$
$$|c_{NO} V_{NO}|_0 < \infty \tag{3.18}$$

and the relationship

$$\left(\frac{m}{m_M}\right)_0 = \left(\frac{1 - x_{H_2} - x_{SiO}}{1 - c_{H_2} - c_{SiO}}\right)_0 \tag{3.19}$$

will assume the simpler form

$$\frac{1}{D_M} = \frac{1}{D_{MM}}\left[1 + x_{SiO}\left(\frac{D_{MM}}{D_{MSiO}} - 1\right) + x_{H_2}\left(\frac{D_{MM}}{D_{MH_2}} - 1\right)\right] +$$

$$+ \left\{\left(\frac{m}{m_A}c_{SiO} - x_{SiO}\right)B_{SiO} + \left(\frac{m}{m_A}c_{H_2} - x_{H_2}\right)B_{H_2} + \frac{m}{m_M}\left(\frac{1}{D_{MM}} - \frac{1}{D_{AM}}\right) +\right.$$

$$+ c_{H_2}\left[\left(\frac{m}{m_M} - \frac{m}{m_A}\right)\left(\frac{1}{D_{MM}} - \frac{1}{D_{MH_2}}\right) - \left(\frac{m}{m_M} - \frac{m}{m_{H_2}}\right)\left(\frac{1}{D_{MM}} - \frac{1}{D_{AM}}\right)\right] +$$

$$+ c_{SiO}\left[\left(\frac{m}{m_M} - \frac{m}{m_A}\right)\left(\frac{1}{D_{MM}} - \frac{1}{D_{MSiO}}\right) - \left(\frac{m}{m_M} - \frac{m}{m_{SiO}}\right)\left(\frac{1}{D_{MM}}\right.\right.$$

$$\left.\left.\left. - \frac{1}{D_{AM}}\right)\right]\right\}\frac{c_O V_O + c_N V_N}{V_M} + \left\{\left(\frac{m}{m_{SiO}}c_{H_2} - x_{H_2}\right)B_{H_2,SiO} +\right.$$

$$+ \frac{m}{m_M}\left(\frac{1}{D_{MM}} - \frac{1}{D_{MSiO}}\right) + c_{H_2}\left[\left(\frac{m}{m_M} - \frac{m}{m_{SiO}}\right)\left(\frac{1}{D_{MM}} - \frac{1}{D_{MH_2}}\right) -\right.$$

$$\left.\left. - \left(\frac{m}{m_M} - \frac{m}{m_{H_2}}\right)\left(\frac{1}{D_{MM}} - \frac{1}{D_{MSiO}}\right)\right]\right\}\frac{c_{SiO} V_{SiO}}{c_M V_M}c_M + \left\{\left(\frac{m}{m_{H_2}}c_{SiO} - x_{SiO}\right)B_{H,SiO} +\right.$$

$$+ \frac{m}{m_M}\left(\frac{1}{D_{MM}} - \frac{1}{D_{MH_2}}\right) + c_{SiO}\left[\left(\frac{m}{m_M} - \frac{m}{m_{SiO}}\right)\left(\frac{1}{D_{MM}} - \frac{1}{D_{MH_2}}\right)\right] -$$

$$- \left(\frac{m}{m_{\mathrm{M}}} - \frac{m}{m_{\mathrm{SiO}}} \right) \left(\frac{1}{D_{\mathrm{MM}}} - \frac{1}{D_{\mathrm{MH_2}}} \right) \Big) \Big] \Big\} \frac{c_{\mathrm{H_2}} V_{\mathrm{H_2}}}{c_{\mathrm{M}} V_{\mathrm{M}}} \, c_{\mathrm{M}}$$

$$(\mathrm{M} = \mathrm{O_2, \ N_2, \ NO, \ CO, \ CN, \ HCN, \ C_2, \ C_3}), \tag{3.20}$$

$$\frac{1}{D_{\mathrm{SiO}}} = \frac{1}{D_{\mathrm{MM}}} \left[1 + x_{\mathrm{SiO}} \left(\frac{D_{\mathrm{MM}}}{D_{\mathrm{MSiO}}} - 1 \right) + x_{\mathrm{H_2}} \left(\frac{D_{\mathrm{MM}}}{D_{\mathrm{SiOH_2}}} - \frac{D_{\mathrm{MM}}}{D_{\mathrm{MSiO}}} \right) \right] +$$

$$+ (x_{\mathrm{SiO}} c_{\mathrm{H_2}} - c_{\mathrm{SiO}} x_{\mathrm{H_2}}) B_{\mathrm{H_2 SiO}} + \left(\frac{1}{D_{\mathrm{MM}}} - \frac{1}{D_{\mathrm{MH_2}}} \right) \left(\frac{m}{m_{\mathrm{M}}} - \frac{m}{m_{\mathrm{SiO}}} \right) c_{\mathrm{SiO}} c_{\mathrm{H_2}} -$$

$$- (1 - c_{\mathrm{SiO}}) \left(\frac{1}{D_{\mathrm{MM}}} - \frac{1}{D_{\mathrm{MSiO}}} \right) \left[\frac{m}{m_{\mathrm{M}}} - c_{\mathrm{H_2}} \left(\frac{m}{m_{\mathrm{M}}} - \frac{m}{m_{\mathrm{H_2}}} \right) \right] +$$

$$+ \left\{ \left(\frac{m}{m_{\mathrm{A}}} c_{\mathrm{SiO}} - x_{\mathrm{SiO}} \right) B_{\mathrm{SiO}} + \left(\frac{m}{m_{\mathrm{A}}} c_{\mathrm{H_2}} - x_{\mathrm{H_2}} \right) B_{\mathrm{H_2}} + \frac{m}{m_{\mathrm{M}}} \left(\frac{1}{D_{\mathrm{MM}}} - \frac{1}{D_{\mathrm{AM}}} \right) +$$

$$+ c_{\mathrm{H_2}} \left[\left(\frac{m}{m_{\mathrm{M}}} - \frac{m}{m_{\mathrm{A}}} \right) \left(\frac{1}{D_{\mathrm{MM}}} - \frac{1}{D_{\mathrm{MH_2}}} \right) - \left(\frac{m}{m_{\mathrm{M}}} - \frac{m}{m_{\mathrm{H_2}}} \right) \left(\frac{1}{D_{\mathrm{MM}}} - \frac{1}{D_{\mathrm{AM}}} \right) \right] +$$

$$+ c_{\mathrm{SiO}} \left[\left(\frac{m}{m_{\mathrm{M}}} - \frac{m}{m_{\mathrm{A}}} \right) \left(\frac{1}{D_{\mathrm{MM}}} - \frac{1}{D_{\mathrm{MSiO}}} \right) - \left(\frac{m}{m_{\mathrm{M}}} - \frac{m}{m_{\mathrm{SiO}}} \right) \left(\frac{1}{D_{\mathrm{MM}}} - \frac{1}{D_{\mathrm{AM}}} \right) \right] +$$

$$+ \frac{m}{m_{\mathrm{A}}} \left(\frac{1}{D_{\mathrm{AM}}} - \frac{1}{D_{\mathrm{ASiO}}} \right) - \frac{m}{m_{\mathrm{M}}} \left(\frac{1}{D_{\mathrm{MM}}} - \frac{1}{D_{\mathrm{MSiO}}} \right) \Big\} \frac{c_{\mathrm{O}} V_{\mathrm{O}} + c_{\mathrm{N}} V_{\mathrm{N}}}{c_{\mathrm{SiO}} V_{\mathrm{SiO}}} c_{\mathrm{SiO}} +$$

$$+ \left\{ \left(\frac{m}{m_{\mathrm{H_2}}} c_{\mathrm{SiO}} - x_{\mathrm{SiO}} \right) B_{\mathrm{H_2 SiO}} + \frac{m}{m_{\mathrm{M}}} \left(\frac{1}{D_{\mathrm{MM}}} - \frac{1}{D_{\mathrm{MH_2}}} \right) + \right.$$

$$+ c_{\mathrm{SiO}} \left[\left(\frac{m}{m_{\mathrm{M}}} - \frac{m}{m_{\mathrm{H_2}}} \right) \left(\frac{1}{D_{\mathrm{MM}}} - \frac{1}{D_{\mathrm{MSiO}}} \right) - \left(\frac{m}{m_{\mathrm{M}}} - \frac{m}{m_{\mathrm{SiO}}} \right) \left(\frac{1}{D_{\mathrm{MM}}} - \frac{1}{D_{\mathrm{MH_2}}} \right) \right] +$$

$$+ \frac{m}{m_{\mathrm{H_2}}} \left(\frac{1}{D_{\mathrm{MH_2}}} - \frac{1}{D_{\mathrm{H_2 SiO}}} \right) - \frac{m}{m_{\mathrm{M}}} \left(\frac{1}{D_{\mathrm{MM}}} - \frac{1}{D_{\mathrm{MSiO}}} \right) \Big\} \frac{c_{\mathrm{H_2}} V_{\mathrm{H_2}}}{c_{\mathrm{SiO}} V_{\mathrm{SiO}}} c_{\mathrm{SiO}},$$

$$\frac{1}{D_{\mathrm{H_2}}} = \frac{1}{D_{\mathrm{MH_2}}} + x_{\mathrm{SiO}} \left(\frac{1}{D_{\mathrm{H_2 SiO}}} - \frac{1}{D_{\mathrm{MH_2}}} \right) + (1 - x_{\mathrm{H_2}}) \left(\frac{1}{D_{\mathrm{MM}}} - \frac{1}{D_{\mathrm{MH_2}}} \right) +$$

$$+ (x_{\mathrm{H_2}} c_{\mathrm{SiO}} - c_{\mathrm{H_2}} x_{\mathrm{SiO}}) B_{\mathrm{H_2 SiO}} + \left(\frac{1}{D_{\mathrm{MM}}} - \frac{1}{D_{\mathrm{MSiO}}} \right) \left(\frac{m}{m_{\mathrm{M}}} - \frac{m}{m_{\mathrm{H_2}}} \right) c_{\mathrm{SiO}} c_{\mathrm{H_2}} -$$

$$- (1 - c_{\mathrm{H_2}}) \left(\frac{1}{D_{\mathrm{MM}}} - \frac{1}{D_{\mathrm{MH_2}}} \right) \left[\frac{m}{m_{\mathrm{M}}} - c_{\mathrm{SiO}} \left(\frac{m}{m_{\mathrm{M}}} - \frac{m}{m_{\mathrm{SiO}}} \right) \right] +$$

$$+ \left\{ \left(\frac{m}{m_{\mathrm{A}}} c_{\mathrm{SiO}} - x_{\mathrm{SiO}} \right) B_{\mathrm{SiO}} + \left(\frac{m}{m_{\mathrm{A}}} c_{\mathrm{H_2}} - x_{\mathrm{H_2}} - \frac{m}{m_{\mathrm{A}}} \right) B_{\mathrm{H_2}} + \right.$$

$$+ \left(\frac{1}{D_{\mathrm{MM}}} - \frac{1}{D_{\mathrm{AM}}} \right) \left[\frac{m}{m_{\mathrm{M}}} - c_{\mathrm{SiO}} \left(\frac{m}{m_{\mathrm{M}}} - \frac{m}{m_{\mathrm{SiO}}} \right) - c_{\mathrm{H_2}} \left(\frac{m}{m_{\mathrm{M}}} - \frac{m}{m_{\mathrm{H_2}}} \right) \right] -$$

$$- (1 - c_{\mathrm{H_2}}) \left(\frac{1}{D_{\mathrm{MM}}} - \frac{1}{D_{\mathrm{MH_2}}} \right) \left(\frac{m}{m_{\mathrm{M}}} - \frac{m}{m_{\mathrm{A}}} \right) + c_{\mathrm{SiO}} \left(\frac{1}{D_{\mathrm{MM}}} - \frac{1}{D_{\mathrm{MSiO}}} \right) \times$$

$$\times \left(\frac{m}{m_M} - \frac{m}{m_A} \right) \Big\} \frac{c_O V_O + c_N V_N}{c_{H_2} V_{H_2}} c_{H_2} + \Big\{ \left(\left(\frac{m}{m_{SiO}} c_{H_2} - x_{H_2} - \frac{m}{m_{SiO}} \right) B_{H_2 SiO} - \right.$$

$$- (1 - c_{H_2}) \left(\frac{1}{D_{MM}} - \frac{1}{D_{MH_2}} \right) \left(\frac{m}{m_M} - \frac{m}{m_{SiO}} \right) + \left(\frac{1}{D_{MM}} - \frac{1}{D_{MSiO}} \right) \times$$

$$\times \left[\frac{m}{m_M} - c_{H_2} \left(\frac{m}{m_M} - \frac{m}{m_{H_2}} \right) \right] \Big\} \frac{c_{SiO} V_{SiO}}{c_{H_2} V_{H_2}} c_{H_2},$$

$$\frac{1}{D_O} = \frac{1}{D_N} = \frac{1}{D_A} = \frac{1}{D_{AM}} \left[1 + x_{SiO} \left(\frac{D_{AM}}{D_{ASiO}} - 1 \right) + x_{H_2} \left(\frac{D_{AM}}{D_{AH_2}} - 1 \right) \right],$$

$$\frac{1}{D_{O_2}} = \frac{1}{D_{NO}} = \frac{1}{D_{MM}} \left[1 + x_{SiO} \left(\frac{D_{MM}}{D_{MSiO}} - 1 \right) + x_{H_2} \left(\frac{D_{MM}}{D_{MH}} - 1 \right) \right]$$

That is to say, for those components whose concentrations at the wall are zero, while their mass diffusion flows are other than zero, the effective diffusion coefficients at the wall are calculated explicitly in terms of binary diffusion coefficients and composition. The expressions for the remaining diffusion coefficients include the ratios of the corresponding diffusion flows at the wall, which can be expressed by means of the generalized analogies (2.21)-(2.23). Then we obtain an algebraic system of equations for determination of the coefficients D_i at the wall. Let us solve this system for the case of moderate blasting (analogy (2.22)) and in its absence (2.21). We note at the outset that it follows from comparison of Formulas (3.2) for $1/D_M$ with the formula for $1/D_{SiO}$ that the effective coefficients D_M (M = CO, CN, HCN, etc.) differ from the diffusion coefficient D_{SiO} by no more than 10%. Hence for the sake of simplicity in the displays, we shall include D_{SiO} in the coefficients D_M. Then, applying (3.22) and (3.5), we obtain from (3.20) the following final expressions for the effective diffusion coefficients at the wall:

$$D_A = D_O = D_N = \frac{D_{AM}}{1 - 0{,}681 x_{H_2}}, \qquad D_{O_2} = D_{NO} = \frac{D_{MM}}{1 - 0{,}724 x_{H_2}},$$

$$D_{H_2} = D_{MH_2}\left[1 + \frac{m}{m_M}(0{,}747 + 0{,}201 c_{H_2})\frac{c_{Ae}}{1 - 0{,}681 x_{H_2}}\right];$$

$$D_M = D_{MM}\cdot\left[\frac{1 - 2{,}62\,\dfrac{m}{m_M}c_{H_2}}{1 - 0{,}724 x_{H_2}} + \right.$$

$$\left. + \frac{(0{,}400 + 0{,}185 c_{H_2} - 0{,}141 x_{H_2} - 0{,}039 x_{H_2} c_{H_2})\,\dfrac{m}{m_M}\,\dfrac{c_{Ae}}{1 - 0{,}681 x_{H_2}}}{1 - 0{,}724 x_{H_2}}\right],$$

$$\tag{3.21}$$

$$\frac{m}{m_M} = \frac{1 - x_{H_2}}{1 - c_{H_2}} \quad (M = CO,\ CN,\ HCN,\ SiO,\ HNO,\ HCO,\ H_2CO,\ N_2H_4,$$

$$SiH,\ C_2,\ C_3,\ C_2H_2,\ C_2H_4),\qquad c_A = c_O + c_N.$$

It follows from analysis of these formulas that during burnout of plastics with a 50% (or smaller) content of phenol-formaldehyde resin, when the hydrogen concentration in the condensed phase amounts to $c_{H_2}^{(1)} < 0{,}03-0{,}05$, and is even smaller in the boundary layer $c_{H_2} < 0{,}01$ $(x_{H_2} < 0{,}13-0.15)$, the effective diffusion coefficients for the pyrolysis and combustion products of the plastic will depend chiefly on the degree of dissociation $(c_A)_e$ of the air at the outer boundary of the boundary layer. Here, if we disregard the influence of the small quantity of hydrogen in Formulas (3.21), then we shall have in approximation (to within 3%)

$$D_H = D_{MH}(1 + 0{,}747 c_{Ae});$$

$$D_M = D_{MM}(1 + 0{,}399\,c_{Ae}),$$

i.e., the effective coefficients for the combustion products (molecules) vary in the interval

$$D_{MM} \leqslant D_M \leqslant D_{AM}. \tag{3.22}$$

For the mixture under consideration, therefore, four essentially different effective diffusion coefficients appear: $D_A (A = O, N)$, $D_M (M = CO, CN, HCN, SiO, HNO, HCO, H_2CO, N_2H_4, SiH, C_2, C_3, C_2H_2, C_2H_4$ etc.)

$$D_{O_2} = D_{NO}, \ D_{H_2}.$$

If we take into account the presence of a small quantity of hydrocarbons, CH, CH_2 and HO, H_2O, NH, etc, then still another effective diffusion oefficient makes its appearance. For the case (3.7), the effective diffusion coefficients at the wall, taking into consideration the boundary conditions (3.18) and $(c_{CO})_e = (c_{CN})_e = (c_C)_e = (c_{C_1})_e = (c_{C_1})_e = 0$, and (3.5) will be

$$D_A = D_O = D_N = \frac{D_{AM}}{1 - 0{,}262 x_C}, \qquad D_{O_2} = D_{NO} = \frac{D_{MM}}{1 - 0{,}285 x_C},$$

$$D_C = \frac{D_{AM}}{1 + 0{,}262 \dfrac{m}{m_A} \dfrac{c_{Ac}}{1 - 0{,}262 x_C}}, \qquad \frac{m}{m_M} = \frac{1 - x_C}{1 - c_C}, \qquad (3.23)$$

$$D_M = D_{MM} \frac{1 + 0{,}285 \dfrac{m}{m_M} \left(c_{Ac} \dfrac{D_A}{D_{MM}} - c_C \dfrac{D_C}{D_{MM}} \right)}{1 - 0{,}285 x_C} \qquad (M = CO,\ CN,\ C_2,\ C_3).$$

It follows from these formulas that if the group of components possesses only approximately equal (equal) molecular weights and gas-kinetic parameters, but these components satisfy different boundary conditions: $(c_O)_0 = (c_N)_0 = 0$, $(c_C)_e = 0$, then the effective diffusion coefficients for them will differ.

Let us now present an example in the which the effective diffusion coefficients at the wall are calculated by application of the analogy (2.21) for the case of a dissociated five-component air: O, N, NO, O_2, N_2. We obtain from (3.7) and the boundary conditions (3.18), less the condition for O_2,

$$D_O = D_N = D_{AM}, \qquad D_{NO} = D_{MM}, \qquad (3.24)$$

$$\frac{D_O}{D_{O_2}} = \frac{D_O}{D_{O_2 N_2}} \left[1 + \left(1 - \frac{D_{O_2 N_2}}{D_{OO_2}} \right) \frac{c_O V_O + c_N V_N}{c_{O_2} V_{O_2}} c_{O_2} \right]. \qquad (3.25)$$

Using the analogy (2.21), where we denote the exponent 0.6 by $\underline{k}$, we obtain instead of (3.25) an equation for determining the effective diffusion coefficient for O_2:

$$\frac{D_O}{D_{O_2}} = \frac{D_{AM}}{D_{O_2}} = \frac{D_{AM}}{D_{O_2N_2}} \left[1 + \left(1 - \frac{D_{O_2N_2}}{D_{OO_2}} \right) \frac{(c_A)_e (c_{O_2})_0}{(c_{O_2})_e - (c_{O_2})_0} \left(\frac{D_{AM}}{D_{O_2}} \right) \right]^k . \qquad (3.26)$$

TABLE 4

$(c_A)_e$		0	0,231	0,5	0,75	1
$\left(\frac{D_O}{D_{O_2}} \right)_0$	$k = 0,6$	1,399	1,291	1,179	1,086	1
	$k = 0,8$	1,399	1,286	1,173	1,082	1
	$k = 1,0$	1,399	1,281	1,167	1,078	1
	$k = 1,5$	1,399	1,268	1,152	1,070	1
	$k = 2,0$	1,399	1,254	1,139	1,063	1

We shall assume that all of the oxygen at the outer boundary of
the boundary layer is dissociated; then we get from (3.26)

$$\left(\frac{D_{AM}}{D_{O_2N_2}} = \frac{D_{OO_2}}{D_{O_2N_2}} = 1,399 \right), \text{ see Tables 2 and 3}$$

$$\frac{D_O}{D_{O_2}} = 1,399 \left[1 - 0,285 (c_A)_e \left(\frac{D_O}{D_O} \right)^k \right], \quad c_{Ae} \geqslant 0,231. \qquad (3.27)$$

For complete dissociation of the air at the outer boundary of the
boundary layer, we shall have from (3.26) and (3.27) $D_O = D_{O_2} = D_{AM}$.
In the absence of dissociation, $D_{O_2} = D_{O_2N_2}$. For the intermediate cases,
it follows from Table 4, which has been drawn up on the basis of the
solution to Equation (3.27), that

$$1 \leqslant \frac{D_O}{D_{O_2}} \leqslant \frac{D_{AM}}{D_{O_2N_2}} = 1,399$$

for any exponent k > 0 and, moreover, that variation of k in the inter-
val from 0.6 to 2 has practically no effect on the accuracy with which
the effective diffusion coefficient is determined (variation of k
through a factor of 3.5 affects the solution by no more than 3% for all
values of $(c_A)_e$). This circumstance enables us to use Analogy (2.22) in
determining the effective diffusion coefficients at the wall when the
latter is being destroyed, and to do so for a broad range of variation
of the blasting parameter $-n\varphi(0) > 0$. The approximate value of the blast-
ing parameter $n\varphi(0)$ can always be found before solving the problem (see

Chapter 4).

If the effective diffusion coefficients have already been deter-
mined, then we can use the generalized analogies (2.21)-(2.23) to find
the ratios of all mass-transfer coefficients to one another. To find
the last mass-transfer coefficient, it is necessary to solve any of the
N diffusion equations

$$[(l/S_i)z_i']' + n\varphi(\eta)z_i' = 0, \; z_i(0) = 0, \; z_i(\infty) = 1. \qquad (3.28)$$

This equation was solved numerically for variable $\underline{l}$ and S_1 for the
case of a binary boundary layer with various gases being blown in over
a wide range of variation of the external parameters, jointly with the
impulse and heat-inflow equations; it was also solved with the parame-
ter $\underline{l}$ variable and the number S_1 constant. Approximation of these nu-
merical solutions gives [21]

$$z'_i(0)S_{i0}^{-1} = 0,570(1 + 0,34b)l_e^{0,44-0,04b}S_{i0}^{-0,6} + 0,67a(1 + 0,2a),$$
$$b = n - 1, \quad a = n\varphi(0) < 0, \quad 0,3 < S_{i0} < 3. \qquad (3.29)$$

For $-\alpha < 0.5$, the deviation of Formula (3.29) from the numerical
solutions does not exceed 3-4%. For $-\alpha \approx 1$, the error may reach 10%.
Actual calculation of the generalized Schmidt numbers S_{10} shows that
they are of the order of ordinary Schmidt numbers as calculated from
the binary diffusion coefficient [22]. Hence Formula (3.29) can also
be used for a multicomponent boundary layer with substitution therein
of the corresponding generalized Schmidt number S_{10}. Application of the
integral method of solution to the problem (3.28), using the linear
profiles for concentration and velocity, gives

$$z_i'(0)S_{i0}^{-1} = [z_i'(0)S_{i0}^{-1}]_0 + (1 - {}^1\!/_3 S_{i0}^{-2(1-k)})\,a, \qquad (3.30)$$

where $[z_i'(0)S_{i0}^{-1}]_0$ is the value of the mass-transfer coefficient for $\alpha =$
$= 0$ and $\underline{k}$ is the exponent in the generalized analogies (2.21)-(2.23).
For the analogy (2.22), $S_{10}^{-\frac{2}{3}(1-k)} = 1$ and the additive term in (3.30)

will coincide with the additive term governed by forcing the inflow in Formula (3.29), if we disregard the small linear term of the order of α^2.

The method of asymptotic integration [5] also gives a value for the mass-transfer coefficient $z_i'(0)$ closely similar to that from Formula (3.29).

For mixtures in which the heat capacities of the components are closely similar, or if components with sharply divergent capacities appear, but do so in small concentrations (for example H_2 and $c_{H_2} < 0.01$), then application of Formulas (2.21)-(2.23) to the heat-transfer coefficient gives a generalized analogy between heat and mass transfer. In this case, therefore, the problem of finding the heat- and mass coefficients in a multicomponent boundary layer in the neighborhood of the critical point (line) will be solved. Utilization of these results will enable us to reduce any problem of heterogeneous combustion (with a finite or infinite rate of reaction advance) to the solution of the corresponding system of finite transcendental equations for the concentrations, temperature at the combustion front and the blasting parameter α (combustion rate) [22].

4. EXAMPLES

1. As our example, let us consider the problem of determining the composition of the air on an impermeable ideally catalytic wall in the neighborhood of the critical point (line) when the wall temperature is held rather low, so as to satisfy the boundary conditions

$$(c_0)_\bullet = (c_{NO})_\bullet = (c_N)_\bullet = 0, \ |c_0 V_0|_\bullet, \ |c_N V_N|_\bullet, \ |c_{NO} V_{NO}|_\bullet < \infty. \quad (4.1)$$

In the boundary layer, however, the flow will be regarded as frozen. The law of conservation of the element O on the impermeable wall is written in the form

$$c_0 V_0 + c_{0_2} V_{0_2} + \frac{8}{15} c_{NO} V_{NO} = 0. \quad (4.2)$$

- 129 -

The law of conservation of the element N is a corollary of (4.2) and the identities

$$\sum_{k=1}^{N} c_k = 1, \quad \sum_{k=1}^{N} c_k V_k = 0.$$

Using the analogies (2.21) and Conditions (4.1), we can transform Relationship (4.2) as follows:

$$(c_0)_e - (c_0)_0 + \left(\frac{D_0}{D_{0_2}}\right)_e^{0.6} \left[(c_0)_0 + \frac{8}{15} (c_{NO})_0 \left(\frac{D_{NO}}{D_0}\right)_0^{0.6} \right] \qquad (4.3)$$

where, in accordance with the boundary conditions (4.1) and Formulas (2.17), we have, virtually irrespective of wall temperature (see Tables 2, 3):

$$\left(\frac{D_{NO}}{D_0}\right)_0 = \frac{D_{0,N_2}}{D_{00_2}}. \qquad (4.4)$$

For the ratio of the effective diffusion coefficients D_0/D_{0_2}, we find, applying (4.1) and (2.21) to Formula (3.25):

$$\left(\frac{D_0}{D_{0_2}}\right)_e = \frac{D_{00_2}}{D_{0,N_2}} \left[1 + \left(1 - \frac{D_{0,N_2}}{D_{00_2}}\right) \frac{(c_A)_e (c_{0_2})_e}{(c_0)_e - (c_{0_2})_e} \left(\frac{D_0}{D_{0_2}}\right)_e^{0.6} \right]. \qquad (4.5)$$
$$(c_A)_e = (c_0)_e + (c_N)_e.$$

We note that for complete dissociation of the air at the outer boundary of the boundary layer, when $(C_A)_e = 1$, $(c_{0_2})_e = 0$, it follows from (4.5) that $D_0 = D_{0_2} = D_{00_2}$. Then, according to (4.3), we get $(c_{0_2})_0 = (c_{0_2})_e$, i.e., there are no changes in chemical composition at the wall. For $(c_A)_e < 1$ we get from Equations (4.3), (4.4) and (4.5)

$$\left(\frac{D_0}{D_{0_2}}\right)_e = \frac{D_{00_2}}{D_{0,N_2}} \left[1 - \left(1 - \frac{D_{0,N_2}}{D_{00_2}}\right) \frac{(c_A)_e (c_{0_2})_e}{(c_0)_e + {}^{8}/_{15} (c_{NO})_e \left(\frac{D_{0,N_2}}{D_{00_2}}\right)_e^{0.6}} \right] \qquad (4.6)$$

where the concentration of molecular oxygen at the wall $(c_{0_2})_0$ must be found from the transcendental equation

$$(c_{0_2})_0 = (c_{0_2})_e + \left(\frac{D_{00_2}}{D_{0,N_2}}\right)_0^{0.6} \times$$

$$\times \left[1 + \left(1 - \frac{D_{0,N_2}}{D_{00_2}}\right) \frac{(c_A)_e(c_0)_0}{(c_0)_e + {}^9/_{16}(c_{N0})_e\left(\frac{D_{0,N_2}}{D_{00_2}}\right)^{0.6}}\right] \times$$

$$\times \left[(c_0)_e + {}^9/_{16}(c_{N0})_e\left(\frac{D_{0,N_2}}{D_{00_2}}\right)_0^{0.6}\right] \qquad (4.7)$$

The solution of this last equation may be presented with suffi-cient accuracy in the form

$$(c_{0_2})_0 = \frac{(c_{0_2})_e + \left(\frac{D_{00_2}}{D_{0,N_2}}\right)_0^{0.6}\left[(c_0)_e + {}^9/_{16}(c_{N0})_e\left(\frac{D_{0,N_2}}{D_{00_2}}\right)_0^{0.6}\right]}{1 + 0.6\left(1 - \frac{D_{0,N_2}}{D_{00_2}}\right)\left(\frac{D_{00_2}}{D_{0,N_2}}\right)_0^{0.6}(c_A)_e}. \qquad (4.8)$$

From this it follows that for $(c_0)_e = 0$, $(c_{0_2}) = (c_{0_2})_e$ and no changes in the concentration of the element O take place at the wall. The maximum value of the O_2 concentration at the wall will occur at $(c_0)_e = 0.231$ and will be equal to $(c_{0_2})_0 = 0.280$. As $0.231 < c_{Ae} \to 1$, the separating effect will be weakened and it will tend to zero as $(c_A)_e \to 1$. This is a consequence of the obvious fact that for $(c_A)_e > 0.231$ at the outer boundary of the boundary layer, atomic nitrogen, which has the same elevated diffusivity as oxygen atoms, begins to make its appearance.

The comparison given in [5] between Formulas (4.6) and (4.8) and the numerical solutions shows a difference no greater than 2% in the concentration of components and the effective diffusion coefficients at the wall.

2. Using the results of Chapters 2 and 3, the task of finding the concentrations of the components at the wall and the combustion rate of the plastic can be reduced to solution of a finite system of transcen-dental equations if we know the temperature of the wall. Indeed, if, for example, the components O, O_2, NO, N, N_2, CO, CN, HCN, H, H_2, C,

C_2, C_3, SiO, CO_2 are present in the boundary layer and the components N_2, H_2, CN, HCN, CO, SiO, CO_2, C, C_2, C_3 are present at the combustion surface, then the laws of conservation of the elements C, O, H and SiO (SiO may be regarded as an element if it is assumed that SiO does not react with other components at the combustion front) at the front, taking Analogy (2.22) and the boundary conditions

$$(c_0)_e = (c_H)_e = (c_{HO})_e = (c_{O_1})_e = (c_H)_e = 0,$$
$$|c_0 V_0|_e, \ |c_H V_H|_e, \ |c_{HO} V_{HO}|_e, \ |c_{O_1} V_{O_1}|_e < \infty,$$
$$(c_{CO})_e = (c_{CH})_e = (c_{CO_1})_e = (c_{HCH})_e =$$
$$= (c_C)_e = (c_{C_1})_e = (c_{C_1})_e = (c_{H_1})_e = (c_{BIO})_e = 0$$

(4.9)

into account, can be written in the form

$$-\xi = \frac{{}^{9}/_{11}\left(\frac{D_{CO_1}}{D_M}\right)_e c_{CO} + {}^{9}/_7 c_{CO} + {}^{9}/_6 c_{HCH} + {}^{9}/_{13} c_{CH} + \left(\frac{D_0}{D_M}\right)_e c_0 + c_{O_1} + c_{O_1}}{{}^{9}/_{11} c_{CO_1} + {}^{9}/_7 c_{CO} + {}^{9}/_6 c_{HCH} + {}^{9}/_{13} c_{CH} + c_0 + c_{O_1} + c_{O_1} - c_0^{(1)}} =$$

$$= \frac{{}^{9}/_{11}\left(\frac{D_{CO_1}}{D_M}\right)_e c_{CO} + {}^{9}/_7 c_{CO} - (c_0)_e\left(\frac{D_0}{D_M}\right)_e - (c_{O_1})_e\left(\frac{D_{O_1}}{D_M}\right)_e}{{}^{9}/_{11} c_{CO_1} + {}^{9}/_7 c_{CO} - c_0^{(1)}} =$$

$$= \frac{\left(\frac{D_{H_1}}{D_M}\right)_e c_{H_1} + {}^{9}/_{37} c_{HCH}}{c_{H_1} + {}^{9}/_{37} c_{HCH} - c_H^{(1)}} = \left(\frac{D_{BIO}}{D_M}\right)_e \frac{c_{BIO}}{c_{BIO} - c_{BIO}^{(1)}}, \quad \sum_{h=1}^{N} c_h = 1.$$

(4.10)

In Equations (4.10), the quantities $c_i^{(1)}$ denote the concentrations of the corresponding chemical elements in the condensed phase, and the auxiliary parameter — $\xi = n\varphi(0)(S_M)_0 [z_i'(0)]^{-1}$ is connected with the dimensionless stream function at zero $n\varphi(0) = \alpha$ by the relationship (see Formula (3.29))

$$-\frac{\alpha}{L_e^4} = \frac{0{,}570(1 + 0{,}34b)}{(S_M)_e^{0.6} L_e^{0.06 + 0.06b}} \frac{\xi}{1 + 0{,}67(1 + 0{,}2\alpha)\xi}.$$

(4.11)

The ratios of the effective diffusion coefficients at the wall should be taken from Formulas (3.21). If to Equations (4.10) we add combustion-equilibrium conditions (or any other conditions that correspond to a finite rate of the heterogeneous reactions)

$$\frac{c_{CO_2}}{c_{CO_2}} = \frac{11}{198} \, pm \, 10^{-(\ldots)} \qquad 500 < T < 1400^\circ K,$$

$$0.2771 \frac{c_{HCN}}{\gamma c_{N_2} c_{H_2}} = 10^{(\ldots)}, \qquad \frac{c_{CN}}{\gamma c_{N_2}} = \frac{13}{\gamma pm} 10^{(\ldots)}, \qquad (4.12)$$

$$c_C = f_1(T), \qquad c_{C_2} = f_2(T), \qquad c_{O_2} = f_3(T),$$

where functions f_1, f_2, and f_3 are known [20], then this battery of equations may be regarded as a system of eleven equations for determination of the ten concentrations c_{CO_2}, c_{CO}, c_{HCN}, c_{CN}, c_C, c_{C_2}, c_C c_{H_2}, c_{SiO}, and c_{N_2} at the wall and the parameter ξ, which depends on three parameters: the temperature T_0 at the combustion front, the pressure p_e at the critical point (line) and the degree of dissociation of the air $(c_A)_e$ at the outer boundary of the boundary layer. To determine the temperature T_0 at the combustion front, it is necessary to invoke the condition of energy conservation on the combustion front [22]. Then the mass rate of combustion will be defined from the formula

$$- \rho_1 D = \sqrt{\beta \mu_e \rho_e} \, \frac{a}{l_e^{1/2}}, \qquad \beta = \left(\frac{du_e}{dx}\right)_{x=0}. \qquad (4.13)$$

We present here a particular solution of this system.

For wall temperatures $1400 \leq T \leq 3000^\circ K$ and $p_e > 10^{-3}$ bar at the combustion front, there will be practically none of the components C, C_2, C_3, CO, CN, HCN. Then we obtain for this region of temperatures and pressures, using (4.10),

$$- \xi = \frac{^3/_7 c_{CO}}{^3/_7 c_{CO} - c_C^{(1)}} = \frac{^4/_7 c_{CO} - k_e}{^4/_7 c_{CO} - c_O^{(1)}} = \frac{(D_H/D_M)_e c_{H_2}}{c_{H_2} - c_H^{(1)}}, \qquad (4.14)$$

$$k_e = (D_O/D_M)_e (c_O)_e + (D_O/D_M)_e (c_{O_2})_e. \qquad (4.15)$$

From this,

$$c_{CO} = \frac{k_e c_C^{(1)}}{^3/_7 k_e + ^4/_7 c_C^{(1)} - ^3/_7 c_O^{(1)}}, \qquad \xi = \frac{k_e}{^4/_8 c_C^{(1)} - c_O^{(1)}},$$

$$c_{H_2} = \xi \frac{c_H^{(1)}}{(D_H/D_M)_e + \xi}.$$

- 133 -

If in Formulas (3.21) we disregard the weak influence of the small hydrogen concentration on the effective diffusion coefficients, we obtain

$$k_e = \frac{0.231 + (D_{AM}/D_{MM} - 1)(c_0)_e}{1 + (D_{AM}/D_{MM} - 1)(c_A)_e}, \qquad (D_{N_i}/D_M)_e = 3.62 \cdot \frac{1 + 0.747(c_A)_e}{1 + 0.399(c_A)_e}$$

Finally, using (4.11) and (4.13), we obtain a finite formula for the mass rate of combustion:

$$\frac{\rho_i D}{\gamma \beta \mu_e \rho_e} = \frac{0.570(1 + 0.34b)}{4^{0.06 + 0.06b}(S_M)_e^{0.6}} \frac{\xi}{1 + 0.67(1 + 0.2a)\xi}, \qquad (4.16)$$

where

$$(S_M)_e = \frac{0.75}{1 + 0.369(c_A)_e}, \qquad \xi = \frac{k_e}{^4/_x c_0^{(1)} - c_0^{(1)}}$$

From this it is evident that the combustion rate depends essentially on the degree of dissociation $(C_A)_e$ of the air at the outer boundary of the boundary layer:

$$(\rho_i D)_{(C_A)_e = 0.231} = 1.399 (\rho_i D)_{(C_A)_e = 0}.$$

It also follows from Formula (4.16) that the mass rate of combustion of a plastic not containing oxygen (i.e., graphite) will be lowest, given identical external streamlining conditions and identical body shapes. On the other hand, given the condition of equilibrium combustion, maximum ablation will occur on a material whose elementary composition approaches the condition $c_C^{(1)} = {}^3/_4 c_0^{(1)}$, if we consider that no CO_2 is formed. On plastics based on phenol-formaldehyde resins, as a rule, $c_0^{(1)} > {}^3/_4 c_0^{(1)}$, i.e., it is necessary to have an additional influx of oxygen from the air for complete combustion of the coke (graphite).

REFERENCES

1. L. Linz, Collection entitled "Gazodinamika i teploobmen pri nalichii khimicheskikh reaktsiy" [Gas Dynamics and Heat Transfer in the Presence of Chemical Reactions], IL [Foreign Literature

Press], Moscow, 1962, page 13.

2. S.M. Scala, A Study of Hypersonic Ablation. Tenth International Astronautical Congress 29 August - 5 Sept. 1959. London.

3. G.A. Tirskiy, Zh. vychisl. matem. i matemat. fiz. [Journal of Computer Mathematics and Mathematical Physics], 1, No. 5, 884, 1961.

4. G.A. Tirskiy, Prikl. mekhan. i tekhn. fiz. [Applied Mechanics and Technical Physics], No. 6, 54, 1961.

5. G.A. Tirskiy, Dokl. AN SSSR [Proceedings of the Academy of Sciences USSR], 155, No. 6, 1278, 1964.

6. Plastmassy — naiboleye teplostoykiy material pri ochen' vysokikh temperaturakh (obzor) [Plastics — The Most Thermostable Materials at Very High Temperatures (Survey)], Vopr. raketn. tekh. [Problems of Rocket Engineering], No. 4, 1960, page 58.

7. Plastmassy v raketnoy tekhnike (obzor) [Plastics in Rocket Engineering (Survey)]. Vopr. raketn. tekhn., No. 7, 1961, page 55.

8. Plastmassy v raketnoy tekhnike (obzor). Vopr. raketn. tekhn., No. 8, 1961, page 3.

9. G. Sutton, JAS/S, 27, No. 5, 1960.

10. Ya.L. Shugal, V.V. Baranovskiy, Sloistyye plastiki [Laminated Plas'ics], Goskhimizdat [State Publishing House for Chemical Literature], Leningrad, 1933.

11. I.P. Losev and G.S. Petrov, Khimiya iskusstvennykh smol [Chemistry of Synthetic Resins], Goskhimizdat, Leningrad, 1951.

12. P.N. Sokolov and V.Ye. Shneyder, Asbest [Asbestos], 2nd Edition, Moscow, 1959.

13. Dzh. Girshfelder, Ch. Kertiss and R. Berd, Molekulyarnaya teoriya gazov i zhidkostey [Molecular Theory of Gases and Liquids], IL, 1961.

14. I. Prigogine and R. Buess, Acad. Roy. Belg., 38, Ser. 5, 711, 1952.

15. D. Girshfelder, Collection entitled "Problemy dvizheniya golovnoy chasti raket dal'nego deystviya" [Problems of the Motion of Nose Cones of Long-Range Rockets], IL, Moscow, 1959, page 343.

16. C.R. Wilke, Chem. Engineering Progress, 46, No. 2, 95, 1950.

17. L.Khouart, Sovremennoye sostoyaniye aerodinamiki bol'shikh skorostey [Contemporary State of High-Speed Aerodynamics], II, IL, Moscow, 1956, page 308.

18. B.I. Reznikov and G.A. Tirskiy, Obobshchennaya analogiya mezhdu koeffitsiyentami massoobmena v laminarnom mnogokomponentnom pogranichnom sloye s proizvol'nym gradientom davleniya [Generalized Analogy Between the Coefficients of Mass Transfer in a Laminar Multicomponent Boundary Layer with Arbitrary Pressure Gradient], In preparation.

19. A. Poger and A. Svehl, Estimated Viscosities and Thermal Conductivities of Gases at High Temperatures. NASA TR, R-132, 1963.

20. L.D. Gurvich et al. Termodinamicheskiye svoystva individual'nykh veshchestv [Thermodynamic Properties of Individual Substances], II, Izd-vo AN SSSR [Academy of Sciences USSR Press], 1962.

21. G.A. Tirskiy, Prikl. mekhan. i tekhn. fiz. [Applied Mathematics and Technical Physics], No. 5, 39, 1961.

22. G.A. Tirskiy, Dokl. AN SSSR [Proceedings of the Academy of Sciences USSR], 156, No. 4, 756, 1964.

HYDROMAGNETIC AND THERMODYNAMIC PATTERN OF A MAGNETIC STORM

V.P. Shabanskiy

This article deals with the pattern of a magnetic storm. The shock wave that is propagated from the sun through the interplanetary gas (or by means of a solar corpuscular stream) intensively heats the interplanetary gas in the vicinity of the terrestrial magnetosphere. In this event the magnetosphere, subjected to the pressure of the corpuscular stream, heats up with considerably less intensity as a result of the existence within the sphere of a strong magnetic field. The virtual adiabatic compression of the magnetosphere during this period coincides with the first phase of the storm.

With passage of time the magnetosphere is heated up by noncolliding magnetohydrodynamic waves which form at the boundary of the magnetosphere.

As the effective temperatures are evened out in the magnetosphere and the stream, the magnetosphere experiences an expansion despite the fact that the pressure in the stream may not diminish. In this case the relative expansion of the magnetosphere considerably exceeds the initial compression.

The quantity of energy transferred by the hydromagnetic waves during the period of the expansion process is adequate for the establishment (or reinforcing) of the ring current which is responsible for the main phase of the storm.

1. MODEL OF STORM

A magnetic storm begins on the earth with the arrival of a solar corpuscular stream. This is intended to refer to the augmentation of the solar wind. A pronounced augmentation of the solar wind causes a storm exhibiting a sudden onset. It is possible to evaluate the rate of propagation for the perturbation from the sun to the earth by compar-

ing the instant of the sudden onset with a solar flare preceding the magnetic storm. This rate is of the order $3 \cdot 10^7 - 10^8$ cm·sec^{-1}. The "Explorer X" launched in March of 1961 beyond the limits of the terrestrial magnetosphere disclosed a directed stream of pro·ons with an energy of 500 ev [1]. This corresponds exactly with a rate of $3 \cdot 10^7$ cm·sec^{-1}. The stream of protons fluctuated about a mean value of $3 \cdot 10^8$ cm^2·sec^{-1} which for the density of the plasma yields 10 protons and electrons per cm^3. Certain data indicated that the temperature of the stream was of the order $10^5 - 10^6$°K. Toward the end of the flight a magnetic storm was recorded, and during this period the "Explorer X" detected both an increase in density and an increase in proton energy. Similar results were obtained with other rockets and satellites, launched beyond the limits of the magnetosphere: the "Mariner II" [2] and "Lunik-2" and "Lunik-3" [3], the rocket sent to Venus [4], and "Explorer XII."

The most natural assumption would be that the sudden onset of the storm should be ascribed to the arrival of a shock wave propagated from the sun through the interplanetary plasma (or ascribed to an unperturbed supersonic corpuscular stream — a solar wind). Despite the fact that the mean·free path of individual particles in interplanetary plasma is greater than the distance from the sun to the earth, because of the presence of a magnetic field the width of the front in the solar wind in such noncolliding plasma may be considerbly less than the mean free path and is defined by the Larmor proton radius. With B ~ 10^{-5} gauss protons with an energy of 500 ev exhibit a Larmor radius of the order of 10^8 cm. The duration of the increase in the horizontal component of the magnetic field at the surface of the earth — a period of time of the order of a single minute — indicates the slope of the perturbation front producing the sudden onset. This time coincides exactly

with the time required for the passage of a stream moving at a velocity of 10^8 cm·sec^{-1} through the region occupied by the terrestrial magnetosphere, this region exhibiting linear dimensions of the order of 10^{10} cm. Therefore the width of the stream front should not exceed 10^{10} cm. It is difficult to conceive a plasma cloud moving from the sun to have such a sharp front in each case of a storm with a sudden onset. At the same time, the hypothesis of a shock wave with a sharp front corresponds to the observed pattern.

Having attained the region occupied by the terrestrial magnetosphere, the shock wave is partly reflected from it and in part it passes through the magnetosphere. Prior to the arrival of the shock wave responsible for the sudden onset, the magnetosphere was surrounded by a region of elevated density on the daylight side behind the shock-wave front (fixed relative to the earth) formed by the unperturbed supersonic solar wind flowing into this region. The arriving perturbation will experience partial reflection at the boundary of this region, increasing in the region the jump in density, pressure, temperature, and in the interplanetary magnetic field frozen into the solar plasma. As a result, the stream behind the surface of the reflected wave, directly interacting with the magnetosphere, becomes more dense, hotter, and less supersonic.

The first phase of a magnetic storm associated with an increase in the horizontal component of the magnetic field at the surface of the earth may be explained by a reduction in the volume of the magnetosphere as a result of additional compression brought about by an increase in pressure in the gas surrounding the magnetosphere; it is through this gas that the shock wave from the sun passed. In this case it is tacitly assumed that the shock wave, having passed through the magnetosphere, will not heat up the plasma of the magnetosphere. Only

in this case will the magnetosphere be compressed by the action of the pressure in the gas surrounding the magnetosphere, this pressure having been elevated by the shock wave. Such a situation indeed follows from the theory of magnetohydrodynamic shock waves. In the transition to a medium exhibiting a larger magnetic field (i.e., of lower compressibility) the jump in pressure and density at the shock-wave front diminishes. Since on the average the magnetic field of the magnetosphere is considerably greater in magnitude than the magnetic fields of interplanetary space, the magnetosphere (with the exception, perhaps, of its outermost parts) is heated considerably less by the shock wave than the ambient interplanetary gas. The compression of the magnetosphere under the action of the external pressure may be regarded as an adiabatic process.

The first phase of a magnetic storm with a sudden onset on the average lasts from 2 to 8 hours, after which the main phase of the storm begins, during which period a reduction in the horizontal component of the magnetic field at the surface of the earth in the middle and lower latitudes is observed. In this case the effect of the reduction of the field during the period of the main phase proves to be several fold more intense than the effect of the increase in the field during the first phase of the storm. This fact cannot be comprehended within the framework of the simple hypothesis of a reduction in the external pressure in the solar wind, as a result of which the expansion of the magnetosphere and, consequently, the reduction of the horizontal component of the field at the surface of the earth should not exceed the effect of the initial compression. Moreover, a great many phenomena contradict the hypothesis of an attenuation of the solar stream during the 2-3 days after the onset of a storm, and particularly the great duration (up to 10 days) of the Forbush decay in cosmic radiation, produced

by this stream. Therefore the model of a storm must make it possible to have the main phase occur under conditions of even more elevated external pressure.

It is possible to imagine that during the first phase and during the first half of the main phase of a storm there occurs an evening out of temperatures between the comparatively cold magnetosphere and the interplanetary gas surrounding the magnetosphere, heated by the shock wave. In this case the reference to the temperature of the interplanetary gas should be understood to refer to a certain effective temperature of the turbulent nonuniformities in the space between the fixed front of the reflected wave and the boundary of the magnetosphere – a region with a regular magnetic field. It would be most natural to assume that the energy carriers are the hydromagnetic waves generated at the boundary of the magnetosphere by the nonuniformities of the stream. The magnetosphere as a whole (or at least its internal region, if the pressure of the solar wind continues to increase) begins to expand during the process of temperature leveling. In order for this expansion in the case of a nondiminishing external pressure to result in a significant reduction in the horizontal component it is necessary for the relative expansion in the internal regions of the magnetosphere to be greater than in the external regions. The existence of a region of elevated plasma density around the earth (the geocorona) with a sharp drop in density at a distance of 3.5 earth radii [5] should result in the partial reflection of the hydromagnetic waves propagating from the surface of the magnetosphere at the boundary of the region exhibiting the elevated density, and consequently, it should result in more intense heating and expansion of the plasma at this boundary.

Thus it is possible to imagine the following pattern for the course of a storm. A shock wave from the sun intensely heats up the interplane-

tary plasma and weakly heats the gas of the magnetosphere. The passage of the wave through the magnetosphere corresponds to the sudden onset of a storm. The elevated pressure of the interplanetary plasma behind the front of the shockwave leads to virtually adiabatic compression of the comparatively cold magnetosphere. Then there occurs a slower process of temperature leveling between the magnetosphere and interplanetary gas. This process is accompanied by an expansion of the entire magnetosphere or of its internal region. In this case there is a reduction in the horizontal component of the magnetic field at the earth in the middle and lower latitudes. An estimate of the time required to transfer the energy from the magnetosphere stream by hydromagnetic waves, this energy adequate for the reduction of the horizontal component of the field at the equator, is presented in Section 2. The heated magnetosphere even prior to the complete leveling out of the temperatures expands at constant external pressure to dimensions exceeding the dimensions of the magnetosphere in an unperturbed state. As will be demonstrated in Section 3, this occurs because the density of the gas of the magnetosphere on the average is considerably greater than the density of the stream plasma.

2. HEATING OF MAGNETOSPHERE BY HYDROMAGNETIC WAVES

Let us consider a case of perpendicular shock waves, i.e., waves propagated in a direction perpendicular to the magnetic field. For rarefied plasma

$$8\pi P / B^2 \ll 1,$$
(1)

where B is the field strength and $P = nkT$ is the gas pressure; the perpendicular shock waves dissipate with the condition [6]

$$M > 1 + \tfrac{3}{4}(8\pi P / B^2)^{1/2},$$
(2)

where $M = u_1/s_a$ is the Mach magnetic number, u_1 is the velocity of the wave front, $s_a = B/4\pi\rho)^{1/2}$ is the Alfven velocity, and ρ is the density

- 142 -

of the frozen-in plasma. This condition is equivalent to the condition $v > v_t$, where v_t is the thermal velocity of the electrons, and $\underline{v}$ is the electron velocity perpendicular to the magnetic field in the plane of the wave front. The beam instability which arises in this case develops along the length

$$l \sim (c/\omega_0)(B^2/8\pi P)^{1/2}, \tag{3}$$

where $\underline{c}$ is the speed of light, and $\omega_0 = (4\pi e^2 n/m_e)^{1/2}$ is the plasma electron frequency. The quantity $\underline{l}$ defines the width of the front of the noncolliding perpendicular shock wave. With a density $n \sim 10^3$ cm^{-3} the ratio $c/\omega_0 \sim 5 \cdot 10^4$ cm, and $B^2/8\pi P$ at a distance of about 3.5 earth radii from the center of the earth is of the order of 10^3 for cold ($\varepsilon \sim kT \sim 1$ ev) and of the order of one for heated ($\varepsilon \sim 10^3$ ev) magnetospheric plasma. Therefore $\underline{l}$ ranges from $5 \cdot 10^7 - 5 \cdot 10^4$ cm, indicating that noncolliding shock waves can exist in a magnetosphere exhibiting characteristic dimensions of $10^9 - 10^{10}$ cm. The heating of the plasma from an energy of 1 ev to 10^3 ev per particle of a distance of about 3.5 earth radii from the earth's center, where the density $n \sim 10^3$ is adequate for the creation of the ring current of westerly direction that is responsible for the reduction in the horizontal component of the field during the main phase of the magnetic storm by 100-200 γ.

From the conditions of continuity at the front of the shock wave the expression for the velocity of the front relative to the nonmoving medium in front of the wave front may be written in the following form:

$$u_1^2 = [(P_1\eta)/\rho_1] \cdot [(a+1)/a] \cdot [1 + a(a+2)\beta], \tag{4}$$

where

$$\eta = (P_2 - P_1)/P_1, \quad a = (\rho_2 - \rho_1)/\rho_1 = (B_2 - B_1)/B_1$$

are the relative jumps in pressure and density at the front of the shock wave, $\beta = B_1^2/8\pi P_1$, with the subscript 1 pertaining to the medium

- 143 -

before the front and 2 pertaining to the medium behind the front of the wave.

For a weak shock wave ($\alpha \ll 1$) and a rarefied plasma ($\beta \gg 1$) we will have

$$M = u_1 / s_n = 1 + {}^3/_4 u. \tag{5}$$

Therefore Condition (2) reduces to the condition imposed on the amplitude of the magnetic field in the wave

$$a = \delta B / B > (8\pi P / B^2)^{1/2}. \tag{6}$$

We can see from (6) that for dissipation the amplitude of the wave should not be too small.

In order to evaluate the heating time let us use the formula for the irreversible changes occuring in the weak shock wave [7]

$$\delta U = -(\delta x)^3 / 12 (\partial^2 P^* / \partial x^2)_s, \tag{7}$$

where δU is the energy liberated at the front of a weak wave per 1 g of mass, S is the entropy, and $x = 1/\rho$ is the specific volume,

$$P^* = P + B^2 / 8\pi = P + A^2 / 8\pi x^2, \tag{8}$$

and $A = B/\rho =$ const (the condition of being frozen on both sides of the front). Since δU is a quantity having the third order of smallness with respect to the jump in density, the relationship between P and $\underline{x}$ on both sides of the front may be taken into consideration in zero order, i.e., we hold S = const. Then the adiabatic curve $P x^\gamma =$ const, where γ is the specific-heats ratio c_p / c_v, together with (8) defines the equation of state for the "gas-magnetic field" system in the variables P*, x. Having substituted $P =$ const $x^{-\gamma}$ into (7), we will have

$$\delta U / U = \delta T / T = \{(\gamma - 1) u^3 / 12\} \cdot \{(\gamma + 1)\gamma + 0(B^2 / 8\pi P)\}. \tag{9}$$

For a rarefied plasma the change in energy per single heavy particle with mass $\underline{m}$ is equal to

$$\delta \varepsilon = m \delta U = {}^1/_4 m s_n^2 a^3, \tag{10}$$

where it has been taken into consideration that $U = P/\rho(\gamma - 1)$.

Given an oscillation frequency of ν the velocity and characteristic heating time will, respectively, be equal to

$$d\varepsilon/dt = \tfrac{1}{4} m s_a^2 \alpha^2 \nu, \quad t \sim 4\varepsilon/m s_a^2 \alpha^2 \nu. \tag{11}$$

If we assume $n \sim 10^3$ cm^{-3}, $\varepsilon \sim 10^3$ ev, $s_a^2 \simeq 2 \cdot 10^{15}$ cm$^2 \cdot$sec^{-2} for a distance $L \sim 3.5$ earth radii, we will have

$$t \sim 2/\alpha^2 \nu. \tag{12}$$

The time calculated from the sudden onset to the arrival of the maximum of the main phase (to the end of heating) may cover a wide range, i.e., from several hours to days ($4 \cdot 10^3$ sec $< 6 < 10^5$ sec). This yields the limits within which the perturbation parameters are confined: $2 \cdot 10^{-5}$ sec $< \alpha^3 \nu < 4 \cdot 10^{-4}$ sec. For example, with $\alpha \sim 10^{-1}$ it is necessary to have field oscillations with a period of a minute, and with $\alpha \sim 3 \cdot 10^{-1}$ half-hourly oscillations are required. At the moment it is not known whether or not such oscillations exist in the magnetosphere.

It should be pointed out that the given mechanism is effective for the cold component of a plasma. With regard to the particles in the belts, since their energy considerably exceeds 10^3 ev, their heating is a considerably slower process. In particular this pertains to the protonosphere detected during the observations conducted by the "Explorer XII" and consisting of protons exhibiting energies in excess of 10^2 kev [8]. If the density recorded by "Explorer XII" of protons with energies from 150 kev to 4.5 Mev is actually that great, as maintained in [8] ($n \sim 0.5$ cm^{-3} at the maximum of the proton belt at $L \sim 3.5$), the main energy must be contained precisely by that component of the plasma of the magnetosphere. However, the mass of the gas is determined by the cold component ($n \sim 10^3$ cm^3). Although this specific medium, strictly speaking, requires a special approach to clarify the behavior of shock

waves, the above-cited formulas are approximately valid if it is maintained that the Alfven velocity in [11] is governed by the cold component (n ~ 10^3 cm^{-3}), while the energy and pressure are defined by protons exhibiting energies in hundreds of kev. As calculated in [9], the ring current of the protonosphere reduces the horizontal component of the magnetic field at the equator at the equator by 40 γ. Consequently, in order to explain the main phase the protonosphere must be heated 2-3 times. As can be seen from (11), the time needed to heat the protonosphere is greater by more than two orders of magnitude than the time required to heat the cold component to 10^3 ev. The same can be said about the storm-attenuation phase, which for the protonosphere will be considerably more prolonged. Moreover, Condition (6) makes possible the dissipation of the waves in the noncolliding plasma and calls for the existence of amplitudes somewhat too large, since for the protonosphere $B^2/8\pi P$ ~ 6 [8]. Thus from the standpoint of the considered mechanism, the cold plasma particles of the magnetosphere, heated by hydromagnetic waves, are responsible for the reduction of the field during the main phase of the storm. However, this does not preclude the possibility of the protonosphere serving as a constant external force for the reduction of the horizontal component at the surface of the earth by an order of magnitude of 40 γ.

3. RELATIONSHIP BETWEEN THE AMPLITUDES OF THE FIRST AND MAIN STORM PHASES

Let us now examine another aspect of the problem: is it possible as a result of heating, for the cold magnetosphere, initially compressed by a shock wave, to expand under conditions of constant external pressure to dimensions greater than the nonperturbed value? For a rough qualitative consideration of the processes of magnetosphere compression and expansion during the course of a storm we need not take into consi-

deration the fact that in the nonperturbed state there already exists within the magnetosphere a constant ring current stretching the lines of force in the direction from the surface of the earth and reducing the horizontal component of the field, i.e., it is possible to assume that prior to the onset of the storm the pressure of the plasma within and without the magnetosphere is identical. In this case the pressure on the plasma from the side of the magnetic field in nonperturbed state will be equal to zero. The relative compression of the magnetosphere results in the first phase of the storm, whereas the extension of the magnetosphere produces the main phase. In this case, in terms of the approach to the problem, the magnetosphere should here be understood to refer to the region that is most active in causing the changes in the field at the surface of the earth, i.e., the region bounded by magnetic shells with $L \sim 3$–5. The volume and, consequently, the magnitude of the field at the surface of the earth, thus defined as the magnetosphere, is defined in the various phases of the storm by the relationship of the gas pressures on the two sides of the conventional boundary of the magnetosphere and the magnetic pressure. Let us assume the pressure directed into the magnetosphere as the positive pressure from the side of the magnetic field, i.e., the pressure which appears with an increase in the volume of the magnetosphere. For a magnetic pressure P_B we can assume the simplest linear relationship with respect to the volume V, and namely

$$P_B = K(V - V_0) / V_0, \tag{13}$$

where V_0 is the unperturbed volume and K is a positive coefficient of proportionality, expressed in the units of pressure.

During the first phase (the compressed state) volume V_1 and the gas pressure P_1 for the magnetosphere are defined by equations

- 147 -

$$P_1 = P_0(V_0/V_1)^\gamma, \tag{14}$$

$$P_1 = P_c + K(V_1 - V_0)/V_0, \tag{15}$$

where P_0 is the pressure of magnetosphere prior to perturbation and P_c is the pressure during the perturbation in the corpuscular stream behind the front of a fixed reflected wave. These equations describe the quasisteady state of the magnetosphere directly after the sudden onset and reflect the rapid process of the leveling out of pressures (Eq. (15)) and the transfer of energy (the adiabatic curve (14)), delayed in comparison with the aforementioned process. Prior to perturbation the pressure in the corpuscular stream in our assumptions was obviously $P_{0c} \sim P_0$.

Let us assume that P_c is comparable with P_0, and $K \gg P_c$, P_0. The last condition indicates the greater elasticity of the lines of force and the limited relative change in the volume of the magnetosphere. With these assumptions the solution for System (14)-(15) yields

$$\Delta V_1/V_0 = (V_1 - V_0)/V_0 = -(P_c - P_0)/K, \tag{16}$$

$$\Delta P_1/P_0 = (P_1 - P_0)/P_0 = \gamma(P_c/K)(P_c - P_0)/P_0. \tag{17}$$

The change in temperature (from the equation of state for an ideal gas)

$$\Delta T/T_0 = (T_1 - T_0)/T_0 = [(P_c - P_0)(\gamma P_c - P_0)]/KP_0. \tag{18}$$

Let us now consider the main phase of the storm. From the instant of the onset of the main phase, there occurs a slow isothermal expansion of the magnetosphere during the process of the leveling out of temperatures between the cold magnetosphere and the interplanetary gas heated by a shock wave, this leveling out being accomplished by means of transferring energy from the corpuscular stream of the magnetosphere by means of hydromagnetic waves. The expansion will continue until the temperature T_2 of the magnetosphere becomes equal to the effective temperature of the ambient plasma (the regions behind the front of the

reflected wave). The final state of the magnetosphere (P_2, V_2, T) is described by equations

$$P_2 V_2 / P_1 V_1 = T / T_1, \tag{19}$$

$$P_2 = P_c + K[(V_2 - V_0) / V_0]. \tag{20}$$

It may be held that $V_1 \sim V_0$; $T_1 \sim T_0$. In this case, assuming $K \gg P_c$, P_0 we will have, in first approximation,

$$\Delta V_2 / V_0 = (V_2 - V_0) / V_0 = (T P_0 - P_c T_0) / (K T_0 - P_0 T) = \\ = P_c / K(n / n_c - 1), \tag{21}$$

where $\underline{n}$ and n_c are the number of particles per unit volume in the magnetosphere and the corpuscular stream, respectively. Having carried out a comparison with (16), we see that the ratio of volumes for the main and first phases will equal

$$\Delta V_2 / \Delta V_1 = -P_c / (P_c - P_0)(n / n_c - 1). \tag{22}$$

Since the average density of the gas in the magnetosphere exceeds the average density of the stream, this ratio in terms of absolute magnitude is greater than 1, i.e., the expansion of the magnetosphere during the main phase of the storm and, consequently, the proportional reduction in the horizontal component of the field at the equator exceeds the effect of compression during the first phase. A similar qualitative relationship is always encountered.

Thus a rough but essentially correct model confirms the thought expressed earlier to the effect that the expansion of the active region of the magnetosphere and the main phase of the storm are not associated with the exit of the earth from the corpuscular stream or a region of elevated pressure, but may occur within the body of the stream itself with a nonattenuating pressure P_c. Moreover, the expansion of the active region may occur in the case of an increasing P_c. This is well illustrated by observations [10] with "Explorer XII" dur-

ing the storm of 30 September 1961, when a shift in the outer boundary of the magnetosphere toward the earth from the daylight side from a distance of 10 to 8 earth radii was observed during the main phase, and this indicated that there was an additional increase in the pressure in the stream. In this case, apparently, the ground stations failed to record any unique features at this instant on the magnetograms, e.g., a pronounced increase in the horizontal component, which might have been expected. It should be pointed out that the effect of the additional compression of the magnetosphere boundary during the period of the main phase should have appeared with the shift of the sharp boundary of the outer radiation belt of electrons with energies of 10-100 kev to the higher latitudes; however, there are no data in [11] from "Injun I" for the indicated storm.

We can see from (21) that for various storms exhibiting identical amplitudes of field increase at the equator during the period of the first phase (identical P_c in the streams) the reduction of the field during the period of the main phase is all the greater, the lower the density n_c of the stream, i.e., the greater the density n_c in the corpuscular stream, the more intense the first phase of the storm, the more rarefied and "hotter" the stream, and the more intense the main phase. The absence of a first phase in certain storms may also be interpreted as the passage of the earth from a more dense cold region to a less dense hotter region of the stream, given the equality of pressures in these regions. In this case, the temperature of the stream behind the front of a fixed shock wave reflected from the magnetosphere should be understood to refer to a certain effective temperature for the motion of plasma and magnetic nonuniformities.

In conclusion let us deal with the problem of the energy balance of stream and storm. It is a widely held opinion that the energy of

the corpuscular stream is inadequate for maintenance of a storm. The maximum energy supplied by the stream during the time $\underline{t}$ of the storm may be evaluated as

$$A_c = 2m_p v_0^2 n_c \pi L^2 r_0^2 t \sim 5 \cdot 10^{28} \text{ ergs} \tag{23}$$

with a stream velocity of $v_0 \sim 5 \cdot 10^7$ cm·sec^{-1}, a density $n_c \sim 10$ cm^{-3}, an effective cross section of the magnetosphere $\pi L^2 r_0^2$ (where $L \sim 10$, r_0 is the radius of the earth), and $t \sim 10^5$ sec. The energy expended on the heating of the plasma of the magnetosphere in the development of the ring current during the main phase is of the order of

$$A = n \varepsilon V \sim 10^{21} \text{ergs} \tag{24}$$

with $n \sim 10^3$ cm^{-3}, $\varepsilon \sim 10^3$ ev, and an active-region volume of $V \sim 10^{27}$ cm^3.

If we take into consideration that the main phase develops against a background (particularly in the high latitudes) of half-hourly oscillations with an amplitude larger than the regular component of magnetic-field reduction, it perhaps becomes necessary to raise the estimate of energy A by an order or even two of magnitude. In this case the ratio A_c/A remains of the order of $5 \cdot 10^2 - 5 \cdot 10^3$. If we take into consideration that prior to the flow past the magnetosphere the stream is heated behind the front of the wave reflected from the magnetosphere and that the region behind the front of the wave is turbulent, and that in actual fact interaction of the hot stream with the magnetosphere is not limited by section with $L \sim 10$, but that there occurs a section over the entire magnetosphere extended away from the sun which, according to data from "Explorer X," is considerably greater than $L \sim 10$, we can assume that the coefficient of energy transformation from the stream to the magnetosphere is in no case less than $10^{-2} - 10^{-3}$, which is fully adequate for energy balance.

Of the role of magnetic fields frozen into the stream we can say the following in so far as this pertains to the transformation of energy from the stream to the magnetosphere. The greatest of the observed field values of the order 10-50 γ show that the field energy may be greater than the thermal energy of a supersonic stream before the front of a reflected wave, but it is smaller than the energy of directed motion. It is precisely for this reason that the magnetic fields which possibly extend over great distances are incapable effectively of raising the coefficient of transformation, since even in the assumption of virtually laminar flow of a corpuscular stream past the magnetosphere the effective cross section of the magnetosphere should not experience a noticeable increase, because the magnetic field with an energy smaller than the energy of the directed motion of the stream is incapable of imparting to the magnetosphere the momentum of the stream particles moving relative to the disk $L \approx 10$ with great impact parameters.

REFERENCES

1. B. Rossi, J. Phys. Japan, Suppl. A2, 615, 1962.

2. M. Neugebauer and S. Snyder, Science, 138, No. 3545, 1095, 1962.

3. K.I. Gringauz, V.V. Bezrukikh, V.D. Ozerov and R.Ye. Rybchinskiy, Dokl. AN SSSR [Proc. Acad. Sci. USSR] 131, 1301, 1960.

4. K.I. Gringaus, XIII Intern. Astr. Congress, Washington, D.C., Oct., 1961.

5. K.I. Gringaus, Collection entitled "Iskusstvennyye sputniki zemli" [Artificial Satellites of the Earth], Issue 12. Izd-vo AN SSSR [Acad. Sci. USSR Press], 1962, page 105.

6. R.Z. Sagdeev, Proceedings of the Symposium on Electromagnetics

and Fluid Dynamics of Gaseous Plasma. April, 1961, Brooklyn, page 443.

7.   F. Hoffman and E. Teller, Phys. Rev., 80, 692, 1950.

8.   L.R. Davis, Aeroplane and Astronautics, 102, 127, 1962; Trans. Amer. Geophys. Union, 43, 211, 1962.

9.   S.I. Akasofu, J.C. Cain and S. Chapman, J. Geophys. Res., 67, 2645, 1962.

10. W.G.V. Resser, J. Geophys. Res., 68, 3131, 1963.

11. B. Maehlum and B.J. O'Brien, J. Geophys. Res., 68, 997, 1963.

ON THE FINE STRUCTURE OF THE THERMAL-EMISSION SPECTRUM OF THE EARTH'S ATMOSPHERE

K.Ya. Kondrat'yev and Yu.M. Timofeyev

The difficulties encountered in studying the composition and structure of the earth's atmosphere from measured data on the spectral distribution of the outgoing radiation obtained by means of satellites are discussed. Calculations are made to determine the contours of isolated emission lines of various intensities at various heights in the atmosphere. The variation in the line contours with altitude is analyzed under the conditions of standard atmospheric layering. Phenomena of line "inversion" and "splitting" are detected. The importance of investigating the fine structure of the atmosphere's emission spectrum to solve "inverse" problems of atmospheric spectroscopy is pointed out with reference to the samples considered.

*   *   *

During recent years, study of the earth's atmosphere with the aid of rockets and satellites has been developing vigorously. Here it is obvious that direct measurements of composition and structural parameters of the atmosphere can be made only at high altitude. The properties of the atmosphere's lower layers can be studied by means of satellites only when indirect techniques are employed (as regards the necessity of using satellites for such purposes, this is dictated by the effort to obtain information on the properties of the atmosphere on the planetary scale). It is most natural to use information on the radiation field of the earth as a planet in elaborating such methods, since the quantitative characteristics of the radiation field that can be measured by apparatus aboard a satellite are determined to an essential

degree by the composition and structure of the atmosphere. This applies particularly to the thermal radiation of the atmosphere, which, in turn, is determined by the distributions of temperature at the atmospheric components emitting the thermal radiation.

This has been the occasion for the appearance, in recent times, of a considerable number of papers devoted to the problem of interpreting spectral measurements of the thermal radiation of the earth as a planet with the object of obtaining data on the vertical distribution of temperature and the absorbing components of the atmosphere [1]. The same also applies to investigations of the atmospheres of other planets (and, in particular, to the problem of detecting life on other planets).

One of the basic difficulties in determining the structural parameters (including temperature) of the atmosphere from spectral thermal-measurement data consists in the fact that, on the one hand, the emission spectrum of the atmosphere has an exceptionally complex structure characterized in many cases by the presence of line and absorption-band overlapping. On the other hand, contemporary measurement technique does not permit us to resolve the fine structure of the spectrum under the conditions of satellite measurements (the chief obstacle consists in inadequate sensitivity of existing infrared receivers). Given such a situation, the problem of interpreting the measurement data is complicated in the extreme. Let us imagine, for example, that measurements of the spectral energy distribution have been obtained in the region of a highly intense absorption band (for example, the carbon-dioxide band at 15 μ).

In this case, a spectral instrument of low resolving power is capable of measuring no more than the distribution of energy in the radiation spectrum of an ideal black body at a temperature equal to the

temperature of the gas, so that even qualitative interpretation of the measurement results — identification of the emitting gas — is possible here. In other, simpler cases (weak and nonoverlapping absorption bands), the problem of interpreting the measurement data becomes somewhat easier. Nevertheless, considerable difficulties will be inevitable in attempts to interpret the data of any measurements that "blur" the fine structure of the emission spectrum. Only measurements made with instruments of high resolution, instruments of capable of resolving the fine structure of the spectrum, can deliver data that admit of completely correct interpretation. With this in mind, the authors have calculated the contours of isolated spectral lines at various altitudes in the atmosphere with the object of ascertaining circumstances of importance for the interpretation of measurement data on the fine structure of the atmospheric emission spectrum.

The intensity of ascending monochromatic atmospheric thermal radiation $I_\nu(p)$ at a level $\underline{z}$ to which the pressure $\underline{p}$ corresponds can be calculated from the following familiar formula [2]:

$$I_\nu(p) = \int_{p_0}^{p} E_\nu(T(\xi)) \frac{dP_\nu}{d\xi} d\xi + E_\nu(T(p_0)) P_\nu(p_0, p),$$ (1)

$$P_\nu(p_i, p) = \exp\left[-\frac{\sec\vartheta}{g} \int_{p_i}^{p} k_\nu(\xi) q(\xi) d\xi\right].$$

Here $E_\nu(T)$ is the intensity of monochromatic radiation from an ideal black body at the frequency ν and the temperature T; $P_\nu(p_i, p)$ is the monochromatic transmission function; p_0 is the pressure at the level of the earth's surface; p_i is the pressure at the level ξ; ϑ is the sighting direction angle reckoned from the nadir; $\underline{g}$ is the acceleration of gravity; k_ν is the mass absorption coefficient; $\underline{q}$ is the relative concentration of the emitting gas (calculated per unit mass of air).

Under the conditions prevailing in the earth's atmosphere of alti-

tudes up to 30 km, the contours of the spectral lines may be regarded as Lorentz contours:

$$k_v = \frac{S\alpha}{\pi}((v-v_0)^2 + \alpha^2)^{-1} \quad \left(S = \int_0^\infty k_v d_v\right),\qquad (2)$$

where S is the total intensity of the lines, v_0 is the frequency corresponding to the center of the line, and α is the line half-width, which depends on pressure:

$$\alpha = \alpha_0(p/p_0),\qquad (3)$$

where α_0 is the half-width of the line at $p = p_0$. Although, as we know, the half-width is also a function of temperature, this may be taken into account in the present case (for normal vertical temperature gradients in the atmosphere) by substituting for (3) the relationship

$$\alpha = Ap^n.\qquad (4)$$

Here A is a constant; n varies in the interval from 0.9 to 1.1. In the calculations whose results are to be presented below, we have assumed $\alpha_0 = 0.07155 \text{ cm}^{-1}$.

Generally speaking, the dependence on temperature should be taken into account for the line intensities; it is defined by the formula

$$S = S_0f(T) = S_0(T_0/T) \exp\{[(E_V + E_R)/k](1/T_0 - 1/T)\}.\qquad (5)$$

where S_0 is the intensity of a line of the rotational/vibrational absorption band at the temperature $T = T_0$ and E_V and E_R are, respectively the vibrational and rotational energies of the molecule in the lower state.

In a number of cases, however, the temperature dependence of line intensity is found for all practical purposes to be negligible, since the factor 1/T and the exponential factor in Formula (5) compensate one another. It is just such cases that are considered below. We also note that we limited ourselves to consideration of spectral lines of carbon dioxide. This is essential, in particular, from the standpoint

- 157 -

of the fact that the relative volume concentration of carbon dioxide in the atmosphere may be regarded as constant at 0.03%.

Taking the assumptions that we have made into account, together with (2) and (3), it is not difficult to derive a formula for the transmission function:

$$P_\nu(p_0, p) = \left[\frac{(\nu - \nu_0)^2 + \left(\frac{a_0 p}{p_0}\right)^2}{(\nu - \nu_0)^2 + a_0^2} \right]^{-\eta} \quad \left(\eta = \frac{1}{2} \frac{S p_0 C}{\pi a_0 \rho_0 g}\right). \qquad (6)$$

where ρ_0 is the density of the atmosphere at the level of the earth's surface. The following values of η were adopted for the specific calculations: $\eta_1 = 1772$, $\eta_2 = 177.2$, and $\eta_3 = 17.72$. The limiting values of η correspond to cases of weak and strong absorption lines. The calculations were based on layering corresponding to the standard atmosphere: ARDC = 59 [3]. The line contours were calculated up to an altitude of 50 km with an altitude step of 10 km, and apply for radiation in the direction of the vertical to the earth's surface. Not only the Lorentz, but also the Doppler broadening of the spectral lines was taken into account in the layer above 30 km (calculations showed that the assumption of a purely Lorentzian contour for the 30-km level results in errors of calculation of the radiation intensity not exceeding 8%).· The data on the line contours were taken from Reference [4]. In this case, the transmission function may be calculated by the formula

$$P_\nu(p_0, p) = e^{-\tau_\nu(p)},$$

$$\tau_\nu = 2\pi\gamma \int_{a_1}^{a_2} H(a, \omega)\, da, \quad \gamma = \frac{S_0 p_0 C}{2\pi^{3/2} \rho_0 g a_0}, \quad a = \sqrt{\ln 2}\,\frac{a}{a_d}, \quad \omega = \sqrt{\ln 2}\,\frac{\nu - \nu_0}{a_d}, \qquad (7)$$

where a_1 and a_2 correspond to the boundaries of the layer under consideration, a_d is the Doppler half-width of the lines, C is the volume concentration of carbon dioxide and $H(a, \omega)$ is a known (calculated) function.

It is not difficult to understand that the shape transformations undergone by the spectral lines at various levels in the atmosphere are due primarily to the following factors: the variation of temperature with altitude, the line intensities and the dependence of the line half-widths on pressure. The influence of these factors may be traced in Figs. 1-3, which represent the intensity variations of the ascending thermal radiation within the limits of an isolated spectral line at various levels and at various values of the parameter γ (the line intensity). As we see, the contours of the spectral emission lines may be classified into three categories in the case under consideration.

Fig. 1. Intensity of ascending radiation as a function of frequency at the level z = 20 km. A) I_ν, ergs/(sec-cm^2-cm-cm^{-1}); B) $\nu - \nu_0$, cm^{-1}.
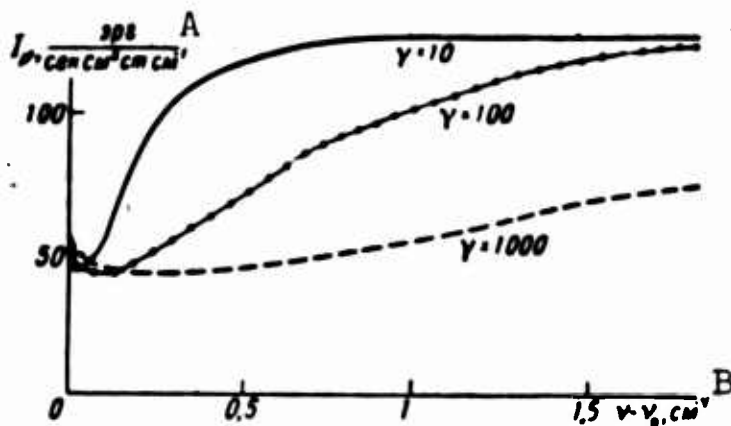
Fig. 2. Intensity of ascending radiation as a function of frequency at the level z = 30 km. A) I_ν, ergs/(sec-cm^2-cm-cm^{-1}); B) $\nu - \nu_0$, cm^{-1}.

1. The intensity of the ascending radiation is minimal at the center of the line and increases in the direction of the line skirts (Fig.

1). A similar phenomenon of line "inversion" is observed in cases in which the underlying layers of the atmosphere are warmer, as is the case, for example, at the level z = 20 km. It is natural that the most distinct "inversion" effect should appear in the case of weak lines (γ = = 10), when the layers of the atmosphere situated at great distances from the level under consideration make a considerable contribution to the radiation in the region of the skirts of the line.

2. The intensity of the ascending radiation is at its maximum at the center of the line and diminishes toward the skirts (Fig. 3). In this case, the emission line is similar to an absorption line, a possibility provided that the underlying layers of the atmosphere are cooler (as we know, the temperature maximum is situated at the 50-km level).

3. The intensity of the ascending radiation varies little as a function of frequency. Such a situation arises either in the case of highly intense lines (Fig. 1-3, curves for γ = 1000), or in the presence of a rather extensive isothermal layer below the level under consideration. Therefore it is obvious that in any case in which the radiation does not depend on frequency, we may judge of the temperature of the corresponding isothermal layer from the intensity of the radiation (in a region of intense lines, this is a thin layer of the atmosphere adjacent to the level being examined). It is interesting to note in this connection that it was precisely this idea that was used to determine the temperature of the lower stratisphere from measurements of the outgoing radiation at the center of the carbon dioxide absorption band (wavelength interval from 14-16 μ) made with the American weather satellite "Tyros VII."

The shape of the spectral-line contour at the 30-km level is quite peculiar (Fig. 2). In this case, we observe "fine structure" in the spectral line: with increasing distance from the center of the line,
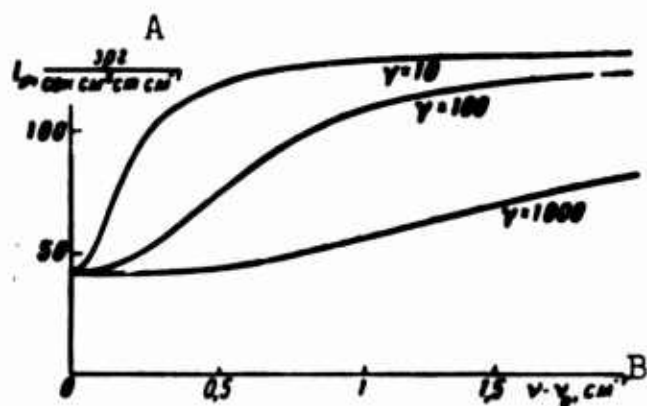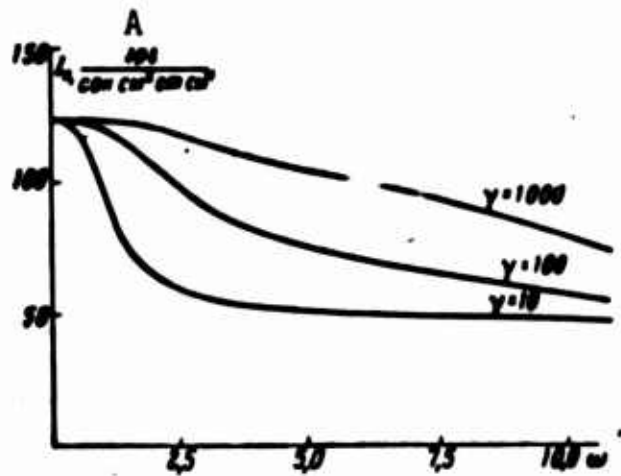
Fig. 3. Intensity of ascending radiation as a function of frequency at the level z = 50 km. A) I_ν, ergs/(sec-cm^2-cm-cm^{-1}.
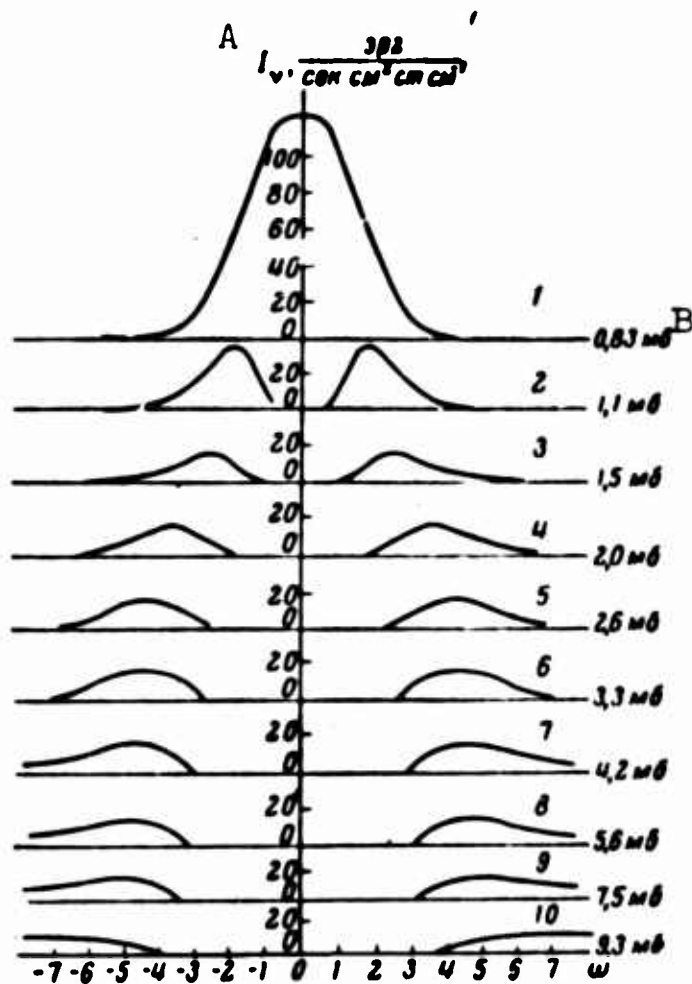
Fig. 4. Contribution of various layers of the atmosphere to ascending radiation at the level z = 50 km; γ = 100. A) I_ν, ergs/(sec-cm^2-cm-cm^{-1}; B) mb.

the radiation intensity first diminishes slightly and then rises sharply. The line appears to be split into two parts: a weak ("normal") line near $\nu = \nu_0$ and a strong ("inverted") line at a certain distance from $\nu = \nu_0$. Such a dependence of the radiation in the line on frequency is

- 161 -
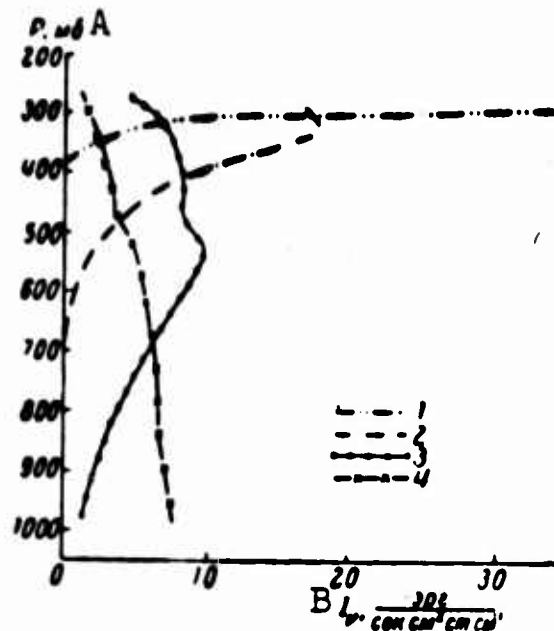
Fig. 5. Contribution to ascending radiation at altitude $z = 20$ km as a function of altitude of the layer ($\gamma = 1000$). $\nu - \nu_0$: 1) 0.2862 cm^{-1}; 2) 0.7155 cm^{-1}; 3) 1.431 cm^{-1}; 4) 2.862 cm^{-1}. A) P, mb; B) I_ν, ergs/(sec-cm^2-cm-cm^{-1}).

determined completely by the singularities of the vertical temperature distribution (temperature drop in the troposphere, isothermy in the lower stratosphere and inversion in the upper stratosphere).

It was noted earlier that the dependence of the line half-width on pressure has a substantial influence on the transformation of the spectral-line contours. This is manifested in the fact that with increasing altitude (diminishing pressure), the spectral lines become narrower. It is found as a result that, at sufficiently high altitudes, where the lines are extremely narrow, the chief contribution to the radiation in the frequency regions remote from the center of the line is made by the radiation of the line skirts, which is generated at lower levels, or even by radiation from the earth's surface. Obviously, the profiles of the emission lines are found to be highly complex in such a situation.

The "mechanism" by which the spectral-line contour is shaped in the atmosphere can be followed in Fig. 4, which represents the results

of a calculation of the contributions made by various layers of the atmosphere situated in the altitude range from 20-50 km to the intensity of the ascending radiation at the 50-km level for a parameter $\gamma = 100$. Clearly discernible here is the fact that shaping of the emission-line skirts is determined by the radiation of atmospheric layers remote from the level under consideration.

This conclusion is also represented in Fig. 5, wh'~h characterizes contribution to the intensity of the ascending radiation at the level $z = 20$ km as a function of the altitude of the emitting layer ($\gamma = 1000$). It is natural that in the frequency region close to the center of the line, the ascending radiation is governed by radiation from layers of the atmosphere bounding the level being studied. As we move into the region of the line skirts, however, the contribution made by radiation from remote layers increases steadil; and the neighboring layers become less important. At great distances from the center of the line, the fraction of radiation arriving from below increases monotonically with increasing depth of the layer. Under such conditions, the influence of the earth's surface also begins to make itself felt to a considerable degree.

The calculations examined above indicate that even in the simplest possible case, that of an isolated spectral line, its contour experiences a highly complex transformation in the atmosphere. This means that averaging, which smooths the fine structure of the emission spectrum, may make it exceedingly difficult (or, strictly speaking, make it impossible) to interpret the experimental data. It must be stressed once again that experimental investigations of the emission-spectrum fine structure offer the greatest promise for solution of "inverse" problems of the physics of planetary atmospheres.

REFERENCES

1. K.Ya. Kondrat'yev, Meteorologicheskiye sputniki [Weather Satellites], Gidrometeoizdat [State Publishing House for Hydrometeorological Literature], 1963.

2. K.Ya. Kondrat'yev, Luchistyy teploobmen v atmosfere [Radiant Heat Transfer in the Atmosphere], Gidrometeoizdat, 1956.

3. K.Ya. Kondrat'yev, Meteorologicheskiye issledovaniya s pomoshch'yu raket i sputnikov [Meteorological Research with the Aid of Rockets and Satellites], Gidrometeoizdat, 1962.

4. D.W. Posener, Austral. J. Phys., 12, No. 2, 1959.

SCATTERING OF LIGHT IN A SPHERICAL ATMOSPHERE. III

I.N. Minin, V.V. Sobolev

The present article, as was the case in the previous articles [1, 2], contains a study of the scattering of light in the atmosphere of a planet, with consideration of the curvature of the atmospheric layers. It is assumed that the coefficient of absorption diminishes exponentially with altitude. Expressions have been derived for the optical distances in the atmosphere. An approximate solution has been found for the problem of the scattering of light in an atmosphere bounded by a reflecting surface. The found solution has been used to calculate: 1) the brightness of a planet close to the terminator; 2) the brightness of the zenith when viewed from the surface of the earth for various zenith distances of the sun.

In the present article, as in the previous articles [1, 2], the problem of the diffusion of radiation in the atmosphere of a planet illuminated by solar rays is considered. The curvature of the atmospheric layers is taken into consideration in this case. In [1] the basic equations for the problem were derived, and in [2] their solution for the case in which the coefficient of absorption is constant in the atmosphere was found. Below we introduce the assumption that the coefficient of absorption diminishes exponentially with altitude. For this case the problem will be solved in first approximation. It is the intention in the following to refine the derived solution.

Basic equations. As before, we will hold that a planet of radius R is illuminated by parallel solar rays producing an illumination of an area perpendicular to these rays that is equal to πS. The distance of

any point in the atmosphere from the center of the planet will be denoted by r and the angle between the radius vector and the direction to the sun is denoted by ψ.

Let $J(r, \psi)$ be the mean intensity of the diffuse emission at the point having coordinates r and ψ. In [1] for purposes of determining the magnitude of $J(r, \psi)$ the following approximate equation has been derived:

$$\Delta J - [a'(r) / a(r)] / \partial J / \partial r = a^2(k^2 J - f), \qquad (1)$$

$$k^2 = (3 - \lambda x_1)(1 - \lambda), \qquad (2)$$

$$f = \lambda S / 4[3 + (1 - \lambda)x_1]e^{-T}, \qquad (3)$$

where Δ is the Laplace operator; x_1 is the first coefficient in the expansion of the scattering indicatrix $x(\gamma)$ for the Legendre polynomial; λ is the albedo of the scattering particle; T is the optical distance from the sun to the given point in the atmosphere.

Let us assume that the coefficient of absorption diminishes exponentially with altitude, i.e.,

$$a(r) = a(R)e^{-(r - R)/H_0}, \qquad (4)$$

where H_* is the altitude of a uniform atmosphere. In this case Eq. (1) assumes the form

$$\frac{\partial^2 J}{\partial r^2} + \left(\frac{2}{r} + \frac{1}{H_0}\right)\frac{\partial J}{\partial r} + \frac{1}{r^2 \sin \psi}\frac{\partial}{\partial \psi}\left(\sin \psi \frac{\partial J}{\partial \psi}\right) = a^2(k^2 J - f), \quad (5)$$

$$T = a(r) \int_{r \cos \psi}^{\infty} e^{-\frac{1}{H_0}(\sqrt{r^2 \cos^2 \psi + s^2} - r)} ds. \qquad (6)$$

Subsequently, in the cited equations in the place of r we will use another variable — the optical depth τ — equal to

$$\tau = \int_{r}^{\infty} a(r') dr' = a(r) H_0. \qquad (7)$$

The optical thickness of the atmosphere, denoted by τ_0, is equal to

$$\tau_0 - \int_R^\infty \alpha(r)\,dr = \alpha(R)H_*.\qquad(8)$$

Boundary conditions must also be associated with Eq. (5). As was shown in [2], at the outer edge of the atmosphere (when $\tau = 0$) we have

$$J = \frac{2}{3 - \lambda z_1}\left[\frac{\partial J}{\partial \tau} - \frac{\lambda S}{4}z_1\cos\psi\right],\qquad(9)$$

while at the inner boundary (with $\tau = \tau_0$):

$$(1 - A)J = \frac{2}{3 - \lambda z_1}(1 + A)\left[-\frac{\partial J}{\partial \tau} + \frac{\lambda S}{4}e^{-T(\tau_0,\psi)}z_1\cos\psi\right] + ASe^{-T(\tau_0,\psi)}\cos\psi.\qquad(10)$$

Here A denotes the albedo of the planet surface. It is clear that $T(\tau_0, \psi) = \infty$ when $\psi > \pi/2$.

Definition of the function $T(\tau, \psi)$. For the problem under consideration the quantity $T(\tau, \psi)$ is of great significance, representing the optical path of the solar rays in the atmosphere to the point having coordinates τ, ψ. This magnitude is defined by Formula (6). We will now simplify this formula, taking advantage of the fact that the altitude of a uniform atmosphere is considerably smaller than the radius of the planet. Initially we will hold that $\psi \leq \pi/2$. In this case Formula (6) can be rewritten in the following form

$$T = \alpha(r)\int_r^\infty e^{-\frac{r'-r}{H_*}}\frac{r'\,dr'}{\sqrt{r'^2 - r^2\sin^2\psi}}.\qquad(11)$$

Assuming here that $r' = r + H_*x$, we will obtain

$$T = \alpha(r)H_*\int_0^\infty e^{-x}\frac{(r + H_*x)\,dx}{\sqrt{r^2\cos^2\psi + 2rH_*x + H_*^2x^2}}\qquad(12)$$

Having used Formula (7) and having denoted $\tau/\tau_0 = u$, we will find that

$$T(\tau, \psi) = \tau b(u, \psi),\qquad(13)$$

where

$$b(u, \psi) = \int_0^\infty e^{-s} \frac{1 + \frac{H_0}{r} s}{\sqrt{\left(1 - \sin\psi + \frac{H_0}{r} s\right)\left(1 + \sin\psi + \frac{H_0}{r} s\right)}} ds, \quad (14)$$

$$\frac{r}{H_0} = \frac{R}{H_0} - \ln u. \quad (15)$$

When $H_* \ll r$ the function $b(u, \psi)$ can be expanded in series

$$b(u, \psi) = b_0(u, \psi) + b_1(u, \psi) + \ldots, \quad (16)$$

where

$$b_0(u, \psi) = \frac{1}{\sqrt{1 + \sin\psi}} \int_0^\infty e^{-s} \frac{ds}{\sqrt{1 - \sin\psi + \frac{H_0}{r} s}} \quad (17)$$

and

$$b_1(u, \psi) = \frac{1 + 2\sin\psi}{2(1 + \sin\psi)^{3/2}} \frac{H_0}{r} \int_0^\infty e^{-s} \frac{s\, ds}{\sqrt{1 - \sin\psi + \frac{H_0}{r} s}}. \quad (18)$$

Having introduced the denotation

$$a = r / H_0 (1 - \sin\psi), \quad (19)$$

in the place of (17) and (18) we find

$$b_0(u, \psi) = g(a) \sec \psi, \quad (20)$$

$$b_1(u, \psi) = \left[1 + \left(\frac{1}{2a} - 1 \right) g(a) \right] \frac{1 + 2\sin\psi}{2(1 + \sin\psi)^3} \cos\psi, \quad (21)$$

where

$$g(a) = 2\sqrt{a}\, e^a \int_{\sqrt{a}}^\infty e^{-t^2} dt. \quad (22)$$

Let us note that when $a \gg 1$ for the calculation of $g(a)$ we can use the expansion

$$g(a) = 1 - 1/2a + 3/(2a)^2 - \ldots. \quad (23)$$

Therefore with angles ψ not close to $\pi/2$ we obtain in approximate terms $T = \tau \sec \psi$. From (20) and (21) it follows that

$$b_0\left(u, \frac{\pi}{2}\right) = \sqrt{\frac{\pi r}{2H_0}}, \quad b_1\left(u, \frac{\pi}{2}\right) = \frac{3}{8} \frac{H_0}{r} b_0\left(u, \frac{\pi}{2}\right). \quad (24)$$

- 168 -

It is clear that the quantity $2T(\tau, \pi/2) = 2\tau b(u, \pi/2)$ represents the complete optical path of a solar ray in the atmosphere, reaching the greatest optical depth τ.

If $\psi > \pi/2$, for $T(\tau, \psi)$ we will have

$$T(\tau, \psi) = 2T(\tau_1, \pi/2) - T(\tau, \pi - \psi), \qquad (25)$$

where τ_1 is the greatest optical depth in the atmosphere for the solar ray under consideration. Having used Expression (13) for $T(\tau, \psi)$ and having denoted $u_1 = \tau_1/\tau_0$, in the place of (25) we will obtain

$$b(u, \psi) = 2(u_1/u)b(u_1\pi/2) - b(u, \pi - \psi). \qquad (26)$$

For u_1, taking into consideration (15) and (19), we will find

$$\ln u_1/u = a = (1 - \sin\psi)(R/H_* - \ln u). \qquad (27)$$

Table 1 shows the values of the function $b(u, \psi)$ for various values of u and ψ. During the calculations it was assumed that $R/H_* = 800$ (this is approximately the situation for the earth). Since the quantity H_*/R is very small, only the first term was taken in Expansion (16), i.e., the function $b_0(u, \psi)$ was actually calculated. Let us note that when $\psi \leq \pi/2$ at the upper edge of the atmosphere, the function $b_0(u, \psi)$ is equal to $b_0(0, \psi) = \sec\psi$.

TABLE 1

The Value of the Function $b(u, \psi)$

ψ \ u	0	10^{-5}	10^{-4}	10^{-3}	10^{-2}	10^{-1}	1
80°	5.76	5.59	5.59	5.59	5.58	5.58	5.58
82	7.18	6.81	6.81	6.81	6.80	6.80	6.80
84	9.57	8.76	8.75	8.75	8.73	8.73	8.73
86	14.3	12.0	12.0	12.0	12.0	12.0	12.0
87	19.1	14.7	14.7	14.7	14.7	14.7	14.7
88	28.6	18.7	18.7	18.7	18.7	18.7	18.7
89	57.3	25.0	24.9	24.9	24.9	24.9	24.9
90	∞	35.7	35.7	35.6	35.6	35.5	35.4
91	∞	55.8	55.7	55.7	55.5	55.3	
92	∞	98.4	98.1	97.8	97.4	97.0	
93	∞	203	202	201	200	198	
94	∞	504	500	496	493	489	
96	∞	6 080	5 990	5910	5830		
98	∞	19 200	18 800				

The most interesting conclusion which follows from Table 1 involves the fact that the function $b(u, \psi)$ for the given value of ψ vir-

tually does not change. Only in the uppermost layers of the atmosphere, in the case of extremely small values of $\underline{u}$, does this function increase with altitude. The same conclusion may be drawn on the basis of Formula (27) from which we can see that the quantity $\underline{a}$ and u_1/u for large R/H_* and not excessively small $\underline{u}$ are virtually independent of $\underline{u}$.

Thus the function $T(\tau, \psi)$ with an accuracy adequate for many applications may be represented in the form of the product of the optical depth τ and the quantity $\underline{b}$ which is a function exclusively of ψ and plays the role of a "generalized secant." This markedly simplifies the theory of the scattering of light in a planetary atmosphere.

It should be pointed out that the problem of the optical distances in the atmosphere has been considered earlier in a number of works. Of these particular attention should be given to the articles by V. G. Fesenkov [3] and Lenoble and Sekera [4], in which the exponential law was adopted for the drop in the coefficient of absorption with altitude. In [4] the equation for the transfer of radiation in a spherical atmosphere was also derived, and the authors propose to undertake a detailed examination of this equation.

Solution of problem in first approximation. The sought function $J(\tau, \psi)$ is defined by Eq. (5) with boundary conditions (9) and (10). If the altitude of a uniform atmosphere is considerably smaller than the radius of the planet, Eq. (5) may be rewritten in the form

$$\frac{\partial^2 J}{\partial r^2} + \frac{1}{H_*}\frac{\partial J}{\partial r} + \frac{1}{R^2}\frac{\partial^2 J}{\partial \psi^2} = \alpha^2(k^2 J - 1). \qquad (28)$$

Having introduced the denotation $R\alpha(R)d\psi = dt$, in the place of (28) we obtain

$$\frac{\partial^2 J}{\partial t^2} + \left(\frac{\tau_0}{\tau}\right)^2 \frac{\partial^2 J}{\partial t^2} = k^2 J - 1. \qquad (29)$$

In making the transition from (5) to (28) or (29) we essentially

make the assumption that the atmosphere consists of plane-parallel layers. This assumption is usual in the theory of the scattering of light in atmospheres of planets. It is clear that this assumption may be accepted in the given case, since its validity is a function only of the structure of the atmosphere, and not of the manner in which the atmosphere is illuminated.

It is usual in the theory of the scattering of light in planetary atmospheres also to hold that $T = \tau$ sec ψ, where ψ = const in the entire atmosphere as a result of which no derivative with respect to ψ is included in the equation to which the considered problem is reduced. The indicated additional assumptions may be regarded as acceptable only when the angles ψ are far from $\pi/2$. In general, these assumptions may not be made, and in the derivation of Eqs. (28), (29) they are omitted.

However, as the first approximation to the solution of the problem in Eq. (29) we have nevertheless eliminated the term containing the derivative with respect to $\underline{t}$, leaving the expression for $\underline{f}$ without change, i.e., we will assume that the atmospheric layers are illuminated at each point by solar rays just as in the case of a spherical case. In this case Eq. (29) assumes the form

$$d^2J/d\tau^2 = k^2J - f, \qquad (30)$$

where $\underline{f}$ is given by Formula (3), while T is given by the formulas considered in detail above.

For the derivation of Solution (29) to the function defined by Eq. (30) it will subsequently be necessary to add a certain correction factor. It is clear that for angles ψ not close to $\pi/2$ this correction factor will be small. When, however, the angle ψ is close to $\pi/2$, the correction factor will apparently be significant. However, for the time being we will not find this correction factor and the function $J(\tau, \psi)$ defined by Eq. (30), will be accepted as the first rough solution for

the problem.

The solution of Eq. (30) has the form

for $\lambda < 1$

$$J = Ce^{k\tau} + De^{-k\tau} - \frac{1}{2k}\int_0^\tau f(\tau')[e^{k(\tau-\tau')} - e^{-k(\tau-\tau')}]d\tau', \qquad (31)$$

for $\lambda = 1$

$$J = C + D\tau - \int_0^\tau f(\tau')(\tau - \tau')d\tau'. \qquad (32)$$

Here C and D are constants defined by the boundary conditions (9) and (10).

If the function $J(\tau, \psi)$ is known, then the formulas cited in [1, 2] can be used to find the intensity of radiation at any given point in theatmosphere. Below the intensities of radiation are determined for two cases which are of particular interest from the standpoint of practical applications.

Brightness of planet close to the terminator. Let us assume that a planet is surrounded by an atmosphere of infinitely great optical thickness. Proceeding from the fact that J does not increase with $\tau \to \infty$, for the constant C included in Formula (31), we find

$$C = \frac{1}{2k}\int_0^\infty f(\tau)e^{-k\tau}d\tau. \qquad (33)$$

For the sake of simplicity let us hold that the scattering of light in the atmosphere is isotropic. Then, from the boundary condition (9) (for $x_1 = 0$) we obtain

$$D = -[(3 - 2k) / (3 + 2k)]C \qquad (k = \sqrt{3(1-\lambda)}). \qquad (34)$$

Substituting (33) and (34) into (31) leads to the following expression for J:

$$J = \frac{1}{2k}\int_0^\infty \left[e^{-k|\tau-\tau'|} - \frac{3-2k}{3+2k}e^{-k(\tau+\tau')} \right] f(\tau')d\tau'. \qquad (35)$$

Let us find the distribution of the brightness of a planet along

the equator of intensity. Let θ be the angle between the radius vector and the direction to an observer. If the thickness of a uniform atmosphere is small in comparison with the radius of the planet, it may be held that along a beam passing through the atmosphere to the observer the angles θ and ψ do not change. In this case the intensity of radiation from the atmosphere will be equal to

$$I(\theta, \psi) = \lambda \int_{0}^{\infty} \left[J(\tau, \psi) + \frac{S}{4} e^{-T(\tau, \psi)} \right] e^{-\tau \sec \theta} \sec \theta \, d\tau. \qquad (36)$$

Having substituted (35) into (36) and having used Formula (3) (for $x_1 = 0$), we obtain

$$I(\theta, \psi) = \frac{\lambda S}{4} \int_{0}^{\infty} e^{-T-\tau \sec \theta} \sec \theta \, d\tau +$$

$$+ \frac{3}{4} S \frac{\lambda^2}{1 - k^2 \cos^2 \theta} \left(\frac{2 + 3 \cos \theta}{2k + 3} \int_{0}^{\infty} e^{-T-k\tau} d\tau - \cos \theta \int_{0}^{\infty} e^{-T-\tau \sec \theta} d\tau \right). \qquad (37)$$

If we hold that the quantity T is represented by Formula (13) and $\underline{b}$ is a function only of ψ, then instead of (37) we will have

$$I(\theta, \psi) = \frac{\lambda S}{4} \frac{1}{1 + b \cos \theta} +$$

$$+ \frac{3}{4} S \frac{\lambda^2}{1 - k^2 \cos^2 \theta} \left(\frac{2 + 3 \cos \theta}{2k + 3} \frac{1}{b + k} - \frac{\cos^2 \theta}{1 + b \cos \theta} \right). \qquad (38)$$

The following quantity in Formula (38)

$$I_1(\theta, \psi) = \frac{\lambda S}{4} \frac{1}{1 + b \cos \theta} \qquad (39)$$

represents the intensity of radiation governed by first-order scattering.

Let us note that the sum of the angles ψ and θ (or their difference) is equal to the phase angle, i.e., to the angle at the planet between the directions to the sun and to the earth.

Table 2 presents the values of the quantities I and I_1 defined by Formulas (38) and (39) for a phase angle of 90° (in units of 10^{-3} S). The calculations have been carried out for the case of pure scattering

- 173 -

($\lambda = 1$). For purposes of comparison the values of the quantity I_* have also been given, this quantity having been defined by Formula (38) for $b = \sec \psi$, i.e., representing the intensity of the radiation found from the conventional theory (without consideration of the curvature of the atmospheric layers).

It might be thought that Venus has an atmosphere of great optical thickness. Measurements of the brightness of Venus close to the terminator were carried out by N.P. Barabashev [5]. A comparison of his results with those cited in Table 2 shows that the calculated brightness of the planet behind the terminator diminishes considerably more rapidly than the brightness that was measured. Probably this divergence can be explained by the imperfection of the theory. At the same time it should be borne in mind that the observation data are not reliable, since the phenomenon of photographic irradiation affects the observed brightness of the planet [6].

TABLE 2

Brightness of Planet Close to Terminator

ψ	I_1	I	I_*	ψ	I_1	I	I_*
80°	38.5	148	145	90	6.85	21.7	0
82	32.2	120	113	91	4.42	13.6	0
84	25.8	92.6	82.9	92	2.52	7.71	0
86	19.2	65.8	54.6	93	1.24	3.76	0
87	15.9	52.7	40.7	94	0.505	1.52	0
88	12.7	41.6	26.8	96	0.0425	0.127	0
89	9.65	31.0	13.3	98	0.0133	0.0396	0

Zenith brightness. Let us assume that the atmosphere is of finite optical thickness τ_0 and touches a surface having albedo A. We will also hold that pure scattering of light takes place in the atmosphere ($\lambda = 1$). In this case for the quantity J we must take Formula (32).

In the determination of constants C and D from the boundary conditions (9) and (10) we assume that $x_1 = 0$. In particular, this pertains to the isotropic scattering and to the Rayleigh scattering indicatrix.

- 174 -

With the above-indicated boundary conditions we find that $C = 2D/$
$/3$, and

$$\left[\frac{4}{3} + (1 - A)\tau_0\right]D = (1 - A)\int_0^{\tau_0} f(\tau)(\tau_0 - \tau)d\tau +$$

$$+ \frac{2}{3}(1 + A)\int_0^{\tau_0} f(\tau)d\tau + AS e^{-T(\tau_0, \psi)}\cos\psi. \qquad (40)$$

The last term in Formula (40) is equal to zero when $\psi > \pi/2$.

Knowing the magnitude of J makes it possible to determine the intensity of radiation in the atmosphere. In particular, it is possible to find the zenith brightness in the case of observation from the surface of the planet. Having denoted the brightness by $I(\psi)$ (the angle ψ is the solar zenith distance), we have

$$I(\psi) = \int_0^{\tau_0} J(\tau, \psi)e^{-\omega\tau}d\tau + I_1(\psi), \qquad (41)$$

where $I_1(\psi)$ is the zenith brightness governed by the first-order scattering and equal to

$$I_1(\psi) = x(\psi)\frac{S}{4}\int_0^{\tau_0} e^{-T(\tau, \psi)-\omega\tau}d\tau. \qquad (42)$$

Having substituted (32) into (41), we find

$$I(\psi) = D(\tau_0 - 1/3 + 1/3 e^{-\omega}) +$$

$$+ \int_0^{\tau_0} f(\tau)(1 - \tau_0 + \tau - e^{-\omega\tau})d\tau + I_1(\psi). \qquad (43)$$

The function $f(\tau)$ in (43) is defined by Formulas (3) and (13). In the case under consideration ($\lambda = 1$) we have

$$f(\tau) = \sqrt[3]{}_4 S e^{-b\tau}. \qquad (44)$$

As before, we will hold that $\underline{b}$ is a function only of ψ. Therefore with the substitution of (44) into (43) we obtain

$$I(\psi) = D\left(\tau_0 - \frac{1}{3} + \frac{1}{3}e^{-\omega}\right) +$$

$$+ \frac{3S}{4b}\left[\left(1 + \frac{1}{b}\right)\left(1 - e^{-b\tau_0}\right) - \tau_0 - \frac{b}{b-1}\left(e^{-\omega} - e^{-b\tau_0}\right)\right] + I_1(\psi). \qquad (45)$$

- 175 -

TABLE 3

Values of I_0 and ΔI

ψ	I_0	ΔI A=0,2	ΔI A=0,8	ψ	I_0	ΔI A=0,2	ΔI A=0,8
		$\tau_0 = 0,1$				$\tau_0 = 0,3$	
80°	18,2	3,3	7,4	80°	30,2	12,8	22,6
82	17,2	2,9	6,0	82	26,2	11,0	18,4
84	15,8	2,4	4,8	84	21,6	8,9	14,4
86	13,7	2,0	3,4	86	16,2	6,6	10,3
87	12,3	1,7	2,8	87	13,3	5,4	8,4
88	10,6	1,4	2,2	88	10,4	4,3	6,5
89	8,60	1,10	1,70	89	7,72	3,19	4,85
90	6,35	0,80	1,18	90	5,38	2,20	3,35
91	4,12	0,52	0,78	91	3,40	1,39	2,12
92	2,34	0,29	0,44	92	1,92	0,78	1,17
93	1,14	0,14	0,21	93	0,931	0,379	0,705
94	0,458	0,057	0,087	94	0,375	0,152	0,232
96	0,0362	0,0048	0,0072	96	0,0312	0,0128	0,0195
98	0,0119	0,0016	0,0022	98	0,00975	0,00398	0,00600

The substitution of (44) into (40) yields

$$\left[\frac{4}{3} + (1-A)\tau_0\right]D = \frac{3S}{4b}\left[(1-A)\left(\tau_0 - \frac{4}{b} + \frac{1}{b}e^{-b\tau_0}\right) + \right.$$
$$\left. + \frac{2}{3}(1+A)(1 - e^{-b\tau_0}) + \frac{4}{3}Ae^{-b\tau_0}b\cos\psi\right],\qquad(46)$$

while for the quantity $I_1(\psi)$ we now have

$$I_1(\psi) = x(\psi)\frac{S}{4}\frac{e^{-\tau_0} - e^{-b\tau_0}}{b-1}.\qquad(47)$$

Quantity $I(\psi)$ is conveniently presented in the form

$$I = x(\psi)I_0 + \Delta I,\qquad(48)$$

where I_0 is the intensity governed by the first-order scattering in the case of a spherical scattering indicatrix, and ΔI is the intensity due to scatterings of higher orders. The quantity I_0 is defined by Formula (47) when $x(\psi) = 1$, and ΔI is found from Formula (45).

Table 3 shows the values of I_0 and ΔI (in units of 10^{-3} S) as functions of the solar zenith distance ψ for various magnitudes of the atmospheric optical thickness τ_0. The quantity ΔI is given for two values of the albedo of the planet's surface ($A = 0.2$ and $A = 0.8$), approximately corresponding to summer and winter conditions.

From Table 3 we can see that the relative role of higher-order scatterings changes little with a change in the solar zenith distance.

TABLE 4

Zenith Brightness for Rayleigh Scattering Indicatrix

φ	τ₀ = 0,1		τ₀ = 0,3	
	$A = 0,3$	$A = 0,6$	$A = 0,3$	$A = 0,6$
80°	17,3	21,4	36,2	45,8
82	16,0	19,2	31,0	38,6
84	14,4	16,7	25,3	30,6
86	12,2	13,7	18,9	22,4
87	11,0	12,1	15,6	18,4
88	9,33	10,2	12,1	14,3
89	7,54	8,14	9,00	10,6
90	5,56	5,95	6,26	7,39
91	3,62	3,87	3,94	4,67
92	2,04	2,19	2,20	2,61
93	1,00	1,07	1,08	1,41
94	0,402	0,432	0,435	0,515
96	0,0338	0,0362	0,0364	0,0432
98	0,0107	0,0113	0,0114	0,0134

However, no great importance should be given to this conclusion, since it is based on an approximate theory.

Table 4 shows the values of the total zenith brightness calculated according to Formula (48) with utilization of Table 3 for the Rayleigh scattering indicatrix. As is well known, the zenith brightness for various zenith distances of the sun was determined by observation in many works (see, for example, [7]). A comparison of the calculated and observed values of zenith brightness shows that in general they agree with one another. However, let us postpone a detailed comparison of theory with observation until the theory is refined.

Conclusion. As was stated, the theory of the scattering of light in a spherical atmosphere that we discussed above is rather approximate. However, it can be refined by bearing in mind the term in Eq. (29) that we discarded. An even more exact solution to the problem can be derived by considering the integral equation which describes the diffusion of radiation in a spherical atmosphere — the equation constructed by us in Reference [8]. The results of the numerical solution of this equation will be presented in a separate report.

In the equation for the transfer of radiation that we have used in

this work we have not taken into consideration the refraction of radiation. However, consideration of refraction apparently should be carried out only in a consideration of first-order scatterings for angles ψ close to $\pi/2$. In consideration of scatterings of higher order the refraction can probably be neglected, as it is neglected in the conventional theory for the scattering of light in planetary atmospheres (without taking into consideration the curvature of the atmospheric layers).

The authors express their gratitude to Ye.B. Babkova and L.P. Savitskaya for the calculations that were made for this article.

REFERENCES

1. V. V. Sobolev, I. N. Minin. Sb. "Iskusstvennyye sputniki Zemli," vyp. 14. Izd-vo AI SSSR, [Collection entitled "Artificial Satellites of the Earth," Issue 14. Academy of Sciences USSR Press], 1962, page 7.

2. I. N. Minin, V. V. Sobolev. Kosmicheskiye issledovaniya [Cosmic Research], 1, No. 2, 227, 1963.

3. V. G. Fesenkov. Astron. zh. [Astronomy Journal], 32, No. 3, 265, 1955.

4. J. Lenoble, Z. Sekera. Proc. Nat. Acad. Sci. USA, 47, No. 3, 372, 1961.

5. N. P. Barabashev. Issledovaniye fizicheskikh usloviy na Lune i planetakh. Izd-vo Khar'k. gos. un-ta [Investigation of Physical Conditions on the Moon and on Planets. Publishing House of the Kharkov State University], 1952.

6. V. V. Sharonov. Priroda planet. Fizmatgiz [The Nature of Planets.

Physics-Mathematics Press], 1958.

7. G.V. Rozenberg. Sumerki [Twilight], Fizmatgiz, 1963.

8. I.N. Minin, V.V. Sobolev. Astron. zh., 40, No. 3, 496, 1963.

THE DAYLIGHT LUMINESCENCE OF THE UPPER LAYERS OF THE

TERRESTRIAL ATMOSPHERE IN THE 1.25μ REGION

N.M. Gopshteyn, V.I. Kushpil'

This article presents the results obtained in the measurement of the brightness of the terrestrial atmosphere in the near infrared region of the spectrum at altitudes below 30 km. A significant increase in the brightness of the upper layers of the atmosphere was observed in the region of 1.25μ in comparison with the adjacent sections of the spectrum. The intensity of the observed luminescence is not a function of altitude and azimuth. Concepts pertaining to the possible causes of the luminescence are formulated.

A number of works [1] have recently been published and these have been devoted to the photochemical reactions in the upper layers of the terrestrial atmosphere. In this connection it is regarded as useful that we report certain of the results obtained in the measurements of the brightness of scattered radiation at altitudes below 30 km, these measurements having been carried out in 1956 by means of balloons, and it was at this time that an anomalously high brightness was encountered in the spectral region around 1.25μ.

The measurements were carried out in the near infrared region by means of a self-recording photoelectric spectralphotometer. The separation of individual sections of the spectrum was achieved by means of interference light filters. A germanium photodiode in conjunction with a tube amplifier was used as the emission receiver. After amplification the signal was rectified by a synchronous detector and recorded on a

strip of photo-sensitive paper by means of a mirror galvanometer.
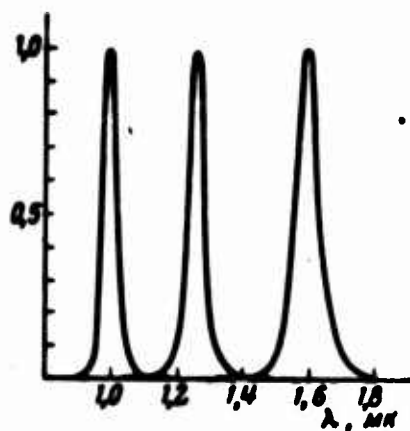
Fig. 1. Relative spectral sensitivity of instrument for various filters.

The relative spectral sensitivity of the instrument for the selected light filters is shown in Fig. 1.

The calibration of the instrument was carried out on the basis of a white diffusely scattering surface illuminated by an incandescent bulb with a tungsten filament. The distribution of the energy in the spectrum of the bulb was taken from [2], while the illumination of the white surface was changed by altering the distance between the surface and the bulb.

The minimum brightness recorded by the instrument at a signal-to-noise ratio of 2 was as follows:

Wavelength, μ	1	1.25	1.59
Brightness, $w \cdot cm^{-2} \cdot \mu^{-1} \cdot ster^{-1}$.	$3 \cdot 10^{-7}$	$2 \cdot 10^{-7}$	$3 \cdot 10^{-8}$.

During the measurements the photometer was directed at the sky at an angle of 30° to the horizon. The field of view amounted to 2°. As a result of the rotation of the instrument about the vertical axis a 30° small-circle [almucantar] section of the sky was viewed. The position of the photometered section of the sky was determined with respect to the sun and the horizon line by means of a panoramic camera with a field of view of 240°. On the basis of the photographs produced by this camera it was also possible to determine whether or not clouds or other extraneous items entered the field of view of the photometer.

Below we present the results of the measurements obtained from two flights. In the first flight (23 September 1956) an altitude of 30 km was attained; on the second flight (9 October 1956) the altitude of 20 km was attained.
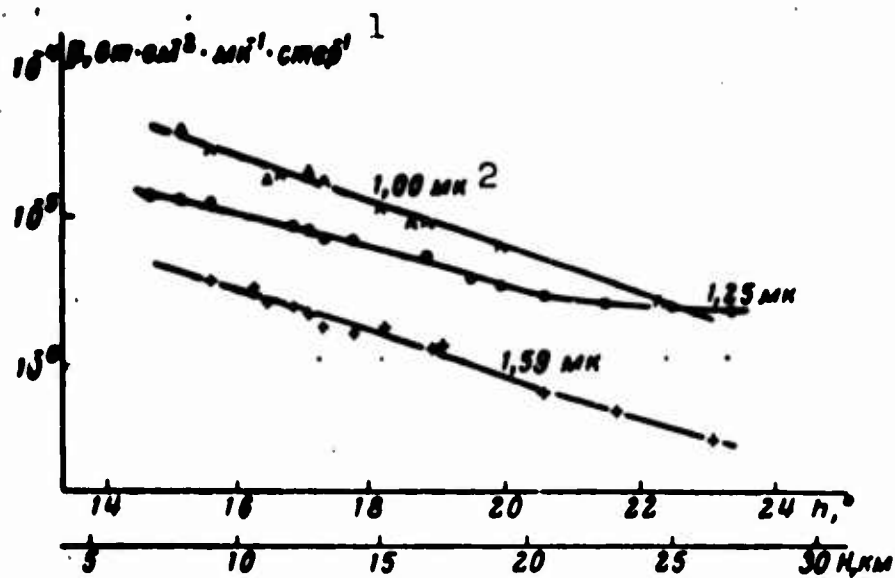
Fig. 2. Measurements of brightness on 23 September 1956 for points in the sky having an azimuth ξ with respect to the sun equal to 150-180°. The scattering angles φ = 115-125°; H is the altitude at the instant of measurement; h is the height of the sun above the horizon. 1) $w \cdot cm^{-2} \cdot \mu^{-1} \cdot ster^{-1}$; 2) μ.
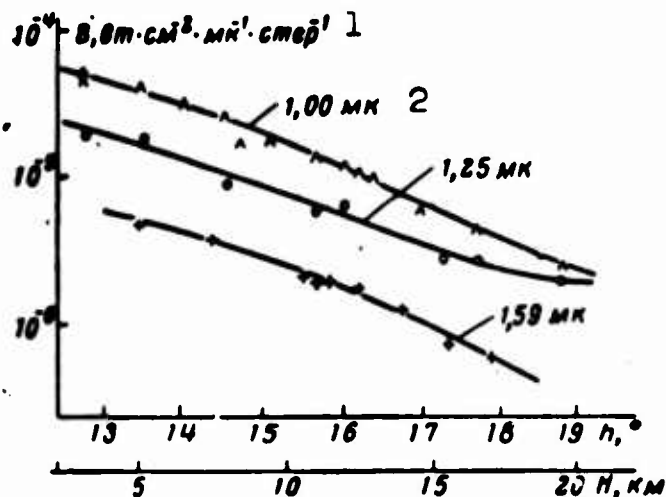
Fig. 3. Measurements of brightness on 9 October 1956. The denotations are the same as in Fig. 2. 1) $w \cdot cm^{-2} \cdot \mu^{-1} \cdot ster^{-1}$; 2) μ.

On the first flight the ascent lasted approximately two hours and the instrument was positioned for approximately one hour at the maximum altitude. For this reason at a level of 30 km there are measurements for the sun at heights of 24 to 30°.

The relationship between brightness and altitude for wavelengths of 1.00, 1.25, and 1.59 μ is presented in Figs. 2 and 3. From these figures we can see that on 9 October 1956 the brightness at altitudes

- 182 -

of 5-8 km was close to that observed on 23 September 1956, while at higher altitudes it diminishes somewhat more rapidly. However, the over-all shape of the curves remains similar; the observed difference is due to the change in meteorological conditions. In both cases for wavelengths of 1.00 and 1.59 μ the brightness diminishes monotonically with altitude, whereas for 1.25 μ, beginning with an altitude of 18-19 km, brightness ceases to diminish and approaches a certain limit equal to $2-2.5 \cdot 10^{-6} w \cdot cm^{-2} \cdot \mu^{-1} \cdot ster^{-1}$.

Fig. 4. Spectral relationships in terms of measurements taken on 23 September 1956. Azimuth $\xi = 105-150^0$. 1) H = 6 km; h = 14^0; 2) H = 10 km; h = 16^0; 3) H = 14 km; h = 18^0; 4) H = 18 km; h = 19.5^0; 5) H = 22 km; h = 21^0; 6) H = 26 km; h = 23^0; 7) H = 29 km; h = 24^0. A) $w \cdot cm^{-2} \cdot \mu^{-1} \cdot ster^{-1}$; B) μ.
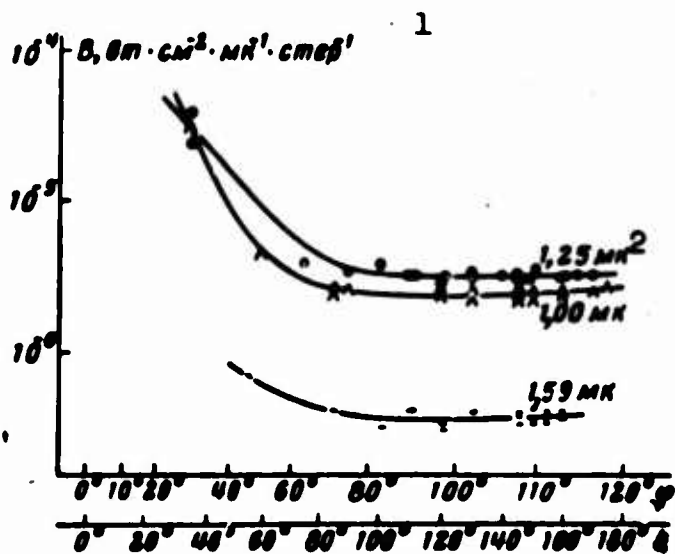
Fig. 5. Absolute indicatrices with respect to measurements taken on 23 September 1956. H = 29-30 km; h = $29-30^0$; ξ is the azimuth of the mea-

sured point and φ is the scattering angle. 1) $w \cdot cm^{-2} \cdot \mu^{-1} \cdot ster^{-1}$; 2) μ.

This phenomenon appears more clearly if we present the result in the form of a spectral relation of sky brightness for various altitudes (Fig. 4). It is seen clearly that at wavelengths of 1.00 and 1.59 μ the brightness diminishes with altitude, while in the case of 1.25 μ, beginning with an altitude of 22 km, brightness virtually does not diminish.

If at an altitude of 19-20 km the results of the measurements for the two days differ on a wavelength of 1.25 μ by no more than 20%, then for the wavelengths of 1.00 and 1.59 μ the brightness on 23 September 1956 differs from that measured on 9 October 1956 by a factor of almost two.

It is interesting to trace the relationship between brightness and the angle of scatter. Figure 5 shows the absolute indicatrices of scattering for the same spectral sections. No significant difference in the shape of the indicatrix for various wavelengths is observed.

The absence of a change in luminescence at 1.25 μ with altitude indicates that the source of this luminescence is found above 30 km. The observed phenomenon cannot be explained by reflection or scattering of solar light by any clouds in the upper atmosphere, since this assumption would make it impossible to explain the specifics of the spectrum (Fig. 4).

The effect may apparently be caused by luminescent or photochemical reactions in the upper atmosphere under the influence of solar radiation. The circumstance that the brightness considerably exceeds (by a factor of 375) the brightness of night-sky luminescence indicates the significant role played by the sun in the origin of the luminescence observed on 1.25 μ, whereas the daylight brightness on 1.59 μ at an altitude of 30 km is greater than that at night by a factor of only 50

- 184 -

[3].

REFERENCES

1. Collection entitled Issledovaniya verkhney atmosfery s pomoshch'yu raket i sputnikov. Korotkovolnovoye i korpuskulyarnoye izlucheniye Solntsa i ikh vozdeystviye na verkhnyuyu atmosferu Zemli [Investigations of the Upper Atmosphere with Rockets and Satellites. Short-wave and Corpuscular Radiation from the Sun and their Effect on the Upper Atmosphere of the Earth], edited by G.S. Ivanov-Kholodnoy, IL [Foreign Literature Press], Moscow, 1961.

2. W.E. Forsythe and E.Q. Adams, J. Optical. Soc. Amer., 35, No. 2, 108, 1945.

3. V.I. Morov, Astron. zh. [Astronomy Journal], 37, No. 1, 123, 1960.

EFFECT OF HIGH-ENERGY PROTONS ON SEMICONDUCTOR NUCLEAR-RADIATION DETECTORS

L. S. Brykina, B. M. Golovin, A. P. Landsman, B. P. Osipenko
and O. P. Fedoseyeva

The action of high-energy protons on surface-barrier silicon nuclear-radiation detectors is studied. Data are obtained on the dependence of pulse amplitude, the signal/noise ratio and energy resolution as functions of the radiation dose that has been received by the detector. A working model developed earlier is used for estimation of the lifetimes of such detectors in the earth's radiation belts.

The present paper represents a partial report of research done by the authors into the effect of high-energy protons on semi-conductorized instruments, and contains a preliminary communication concerning changes that take place in certain properties of semiconductor detectors when they are bombarded by protons with energies around 650 Mev.

Specimen surface-barrier detectors made from n-type silicon with a resistivity of 200-500 ohms·cm and resolutions varying from 1 to 3% in the registration of alpha-particles with energies of 4.8 Mev were subjected to bombardment.

The process on which series production of these devices will be based was used in preparing the detectors.

The pulse amplitude, capacitances, energy resolution, back current and noise level of the detectors were studied during the experiments as functions of the doses received.

In all, 14 specimens were bombarded. The intensity of the proton

beam was determined from the activation of aluminum foil (in the reaction $Al^{27}(p,3pn)Na^{24}$) placed in the same position as the detectors. The measurements made showed that the proton-beam intensity varied from $1.7 \cdot 10^8$ to $6 \cdot 10^8$ protons·cm^{-2} between different bombardment sessions. The maximum dose received by the detectors in this study was around $2 \cdot 10^{13}$ protons·cm^{-2}.

To permit comparison of our data with the results of other authors [1, 2], which were obtained on bombardment of semiconductor detectors with neutrons having energies of 14 Mev, reference is made to the results of our paper [3]. In this study, the energy-dependence of the detrimental effect of the nuclear particles on silicon photoelectric cells was calculated on the assumption that the detrimental effect of the nuclear radiation is determined by the quantity of energy expended per unit time in the specimen on the formation of displaced atoms.

According to the results of this study, the damage to the specimens as a result of bombardment with neutrons having an energy T_n and protons with an energy T_p will be the same if the relationship

$$D_p(T_p)W_p(T_p) = D_n(T_n)W_n(T_n), \qquad (1)$$

is satisfied; here D_n and D_p are the neutron and proton radiation doses received by the specimen, respectively, and W_n and W_p are the detrimental effects due to the neutrons and protons.
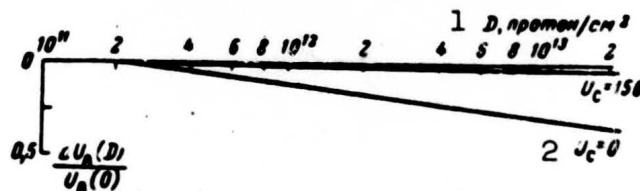
Fig. 1. Amplitude of pulse generated by counter on excitation by alpha particles with energy of 4.8 Mev as a function of radiation dose that has been received by the counter. 1) D, protons/cm^2; 2) $U_s = 0$.

It can be stated on the basis of this relationship that the same changes in the characteristics of the specimens that were observed when
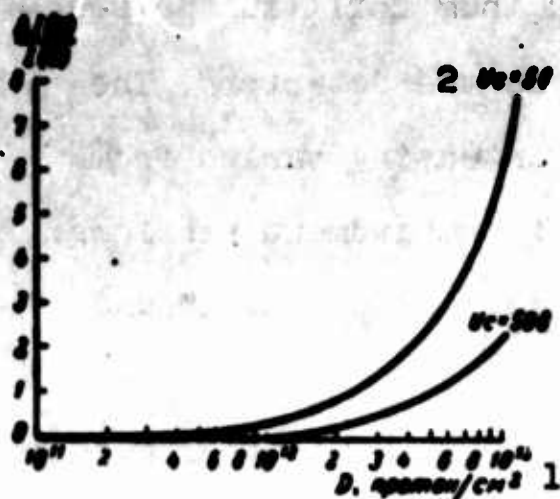
Fig. 2. Detector back-current measurement as a function of radiation dose that it has received. 1) D, protons/cm^2; 2) $U_s = 58$.

they had received a neutron dose D_n will appear when they are given a proton dose D_p, provided that

$$D_p(T_p) = \frac{W_n(T_n)}{W_p(T_p)} D_n(T_n).$$

Given neutron energies of 14 Mev and proton energies of 650 Mev, this leads, in agreement with the results of [3], to the relationship

$$D_p(650 \text{ Mev}) = 0.52 \, D_n \, (14 \text{ Mev}). \tag{2}$$

The changes in the detector characteristics as a result of bombardment are illustrated by Figs. 1-4, whose construction took into ac-
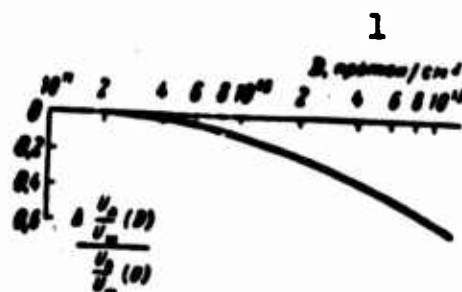
Fig. 3. Optimum value of ratio $\Delta\frac{U_A}{U_m}(D)\Big/\frac{U_A}{U_m}(0)$ as a function of radiation dose received by counter. 1) D, protons/cm^2. $U_m = U_{sh}$.
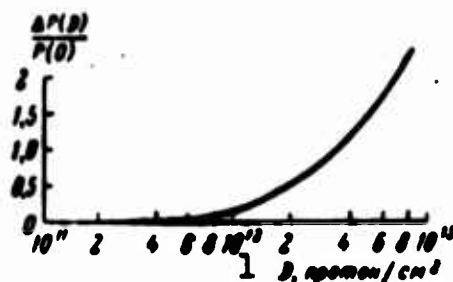
Fig. 4. Energy resolution of detector as a function of radiation dose that it has received. 1) D, protons/cm^2.

count not only our data, which were averaged over all of the irradiated specimens, but also the results of References [1, 2], which were devoted to neutron bombardment of semiconductor detectors. The resulting data can be characterized briefly as follows.
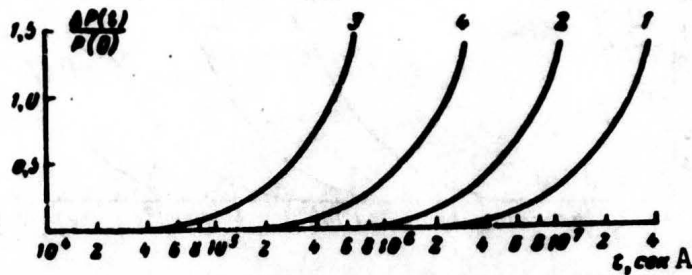
Fig. 5. Energy resolution of detector as a function of its time of res-
idence in maximum-intensity zones of the earth's radiation belts: 1)
Effect of protons with spectrum (3) and $T_0 = 10$ Mev; 2) same with $T_0 = 5$ Mev; 3) same with $T_0 = 1$ Mev; 4) effect of electrons with spectrum
given in Reference [5]. A) t, sec.
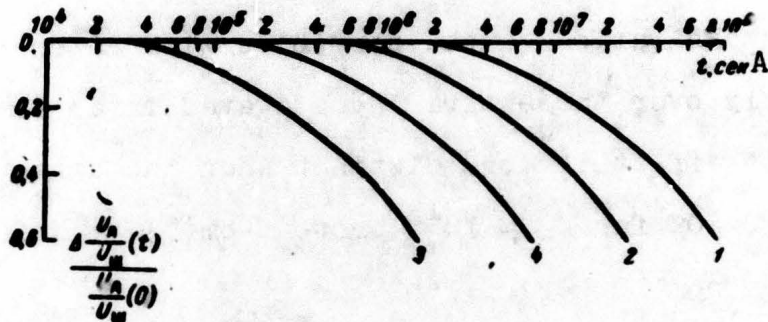
Fig. 6. Ratio $\Delta \frac{U_A}{U_{\blacksquare}}(t) / \frac{U_A}{U_{\blacksquare}}(0)$ as a function of counter's residence time in

maximum-intensity zones of the earth's radiation belts: 1) Effect of
protons with spectrum (3) and $T_0 = 10$ Mev; 2) same with $T_0 = 5$ Mev; 3)
same with $T_0 = 1$ Mev; 4) effect of electrons with the spectrum given
in Reference [5]. A) t, sec. $U_{\blacksquare} = U_{sh}$.

1. No marked difference is observed between the radiation stabil-
ities of specimens in whose preparation chemical and electrochemical
surface-polishing techniques had been used. Semiconductor detectors
with a tin-oxide film showed the same radiation stability as ordinary
specimens.

2. All parameters of the detectors change rather slightly under
doses $D_p(650) \approx 5 \cdot 10^{11} - 10^{12}$ protons·cm^{-2}. When doses in excess of this
value are received, the characteristics of the detectors begin to
change considerably more rapidly as the dose is increased.

3. The amplitude of the pulses (see Fig. 1) put out by the counter
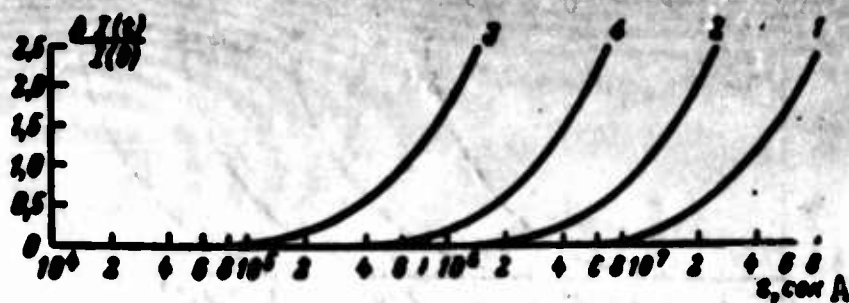
Fig. 7. Counter back current as a function of counter residence time in maximum-intensity zones of the earth's radiation belts: 1) Effect of protons with spectrum (3) and $T_0 = 10$ Mev; 2) same with $T_0 = 5$ Mev; 3) same with $T_0 = 1$ Mev; 4) effect of electrons with spectrum given in (5). Bias on detector: 50 v. A) t, sec.

under standard excitation (alpha-particles with an energy of 4.8 Mev) changes slightly over the entire investigated interval of radiation doses; here, this effect is more distinct when the detector works without bias ($\Delta U/U \approx 20\text{-}30\%$ for $D_p \approx 10^{13}$ protons·cm^{-2}) and is virtually absent at biases from 10-15 v.

4. The changes in the detector back currents (Fig. 2) are found to be considerably sharper for small bias values (0-5 v) than for large ones (20-50 v).

5. The optimum U_A/U_{sh} (signal/noise) ratio is shown in Fig. 3 as a function of radiation dose. It is interesting to note that the bias corresponding to the optimum value of this ratio changes slightly with radiation dose.

6. The change in energy resolution of the detectors upon bombardment is shown in Fig. 4. A marked deterioration of resolution begins at doses $D_p \approx 10^{12}$ and $1.5\text{-}2\cdot10^{13}$ protons·cm^{-2}. This loss in resolution may reach 250-300%. The bias at which the detector resolution is found to be optimum also changes to some extent with increasing dose received by the specimen. However, as in the case of the ratio U_A/U_{sh}, it is not possible to discern any regularity in this change between specimens.

7. The change in the capacitance of the detectors was insignifi-

- 190 -

cant over the entire range of radiation doses studied. The only tendency detected was one toward a slight decrease in the capacitance of the irradiated specimens. A sharp drop in capacitance was noted only for a single specimen, which, after receiving a dose of $1.6 \cdot 10^{13}$, showed a considerable deterioration in all of its characteristics.

A question raised on more than one occasion in the literature of recent years is that of the expediency of using semiconductor detectors in investigation of cosmic rays. In fact, the portability, small power requirements and high resolving ability of these devices make their use under the specific conditions prevailing aboard artificial earth satellites so attractive that we may confidently expect widespread use in future space research.

For this reason, it is of interest even now to estimate the possible length of service life and the basic property changes of semiconductorized detectors during prolonged residence in the earth's radiation belts. The calculation methods described in the above-cited work [3] and the experimental data secured in the present study were used to obtain such estimates.

In making the calculations, it was assumed, as in [3], that the spectrum of the protons in the inner radiation belt is described approximately by the function

$$I_p \approx T^{-1.84},\tag{3}$$

while the electron spectrum of the outer belt takes the form given in [4]. The calculations were made on the assumption that the lower limit T_{min} of the proton spectrum assumes one of the values $T_{min} = 1, 5$ or 10 Mev. The results of the calculations are presented in Figs. 5-7.

If the detector is subjected to simultaneous bombardment by protons with spectrum (3) and electrons with the spectrum of [5], then the change in its parameters for $T_{min} = 5$-10 Mev will be determined basi-

cally by the detrimental effect of the electrons. For $T_{min} = 1$ Mev, on the other hand, the damaging effect of the electrons may be disregarded.

The authors are indebted to V.P. Dzhelepov for his unflagging interest in the study and his assistance in carrying it out, and to N.G. Zaytseva for her assistance in determining the proton-beam intensity.

Received

3 February 1964

REFERENCES

1. S.A. Matveyev, S.M. Ryvkin, N.V. Strokan. Materialy soveshchaniya po poluprovodnikovym detektoram yadernykh izlucheniy [Data of Conference on Semiconductorized Nuclear-Radiation Detectors], Dubna, April, 1962.

2. R.W. Klingensmith, IRE Trans. Nucl. Sci., NS-8, No. 1, 112, 1961.

3. B.M. Golovin, A.P. Landsman, G.M. Grigor'yeva, B.P. Osipenko. Preprint OIYaI [United Nuclear Research Institute (OIYaI) Preprint], P-1247, 1963.

4. R. Takaki, M. Perkins, A. Turzolino. IRE Trans. Nucl. Sci., NS-8, No. 1, 64, 1961.

5. B.J. O'Brien, J.A. Van Allen, C.D. Laughlin, L.A. Frank. J. Geophys. Res., 67, 397, 1962.

Manuscript Page No.	[Transliterated Symbols]
188	ш = sh = shum = noise
187	c = s = smeshcheniye = bias

UDK 621.383.8:536.248

ANTIREFLECTION COATING AND TEMPERATURE STABILIZATION OF SILICON
PHOTOELECTRIC CELLS INTENDED FOR WORK UNDER CONDITIONS OF
RADIANT HEAT TRANSFER

M. M. Koltun and A. P. Landsman

A two-layered coating that makes it possible to combine effective
antireflection coating with a sharp improvement in the radiation char-
acteristics of the receiving surfaces of silicon photoelements is pro-
posed and calculations made for it. An increase in the short-circuit
currents and efficiencies of the photoelements by 40-42% was obtained
experimentally by antireflection coating, with a simultaneous drop in
the coefficient ratio α_c/ε to 0.94-0.98, which signifies temperature
stabilization of the photoelements at the $44-45°$ level in operation
aboard automatic interplanetary stations.

The temperature dependence of the efficiency of silicon photoele-
ments is defined by the relationship $d\eta/dT = 0.06\%/°C$. For photoelements
mounted on flat panels deployed perpendicular to the sunlight and car-
ried on interplanetary stations receding from the earth (which makes it
possible to disregard heating by solar radiation reflected from the
earth and the thermal radiation proper to the earth itself), the value
of the equilibrium working temperature can be figured from Formula [1]

$$T = \left[(1-\eta)\frac{S}{\sigma}\frac{A_{\alpha_c}}{A_\varepsilon}\frac{\alpha_c}{\varepsilon}\right]^{1/4};\qquad(1)$$

where η is the efficiency of the photoeletric generator, S is the power
of the incident sunlight, σ is the Stefan-Boltzmann constant ($5.67\cdot10^{-8}$
watt$^{-2}\cdot$degree^{-4}), A_{α_c} and A_ε are, respectively, the areas of the ab-
sorbing and radiating surfaces of the photogenerator, α_c is the inte-

- 193 -

gral coefficient of absorption of solar radiation by the photogenerator and ε is the integral coefficient of intrinsic emission by the receiving surface of the photogenerator.

For silicon photoelements with a clean polished surface ($\alpha_c = 0.69$; $\varepsilon = 0.24$; $S = 1400$ watts·m^{-2}; $A_\alpha/A_\varepsilon = 0.5$ since the dark surface of the panel is only a radiator with high ε; $\eta = 10\%$), the equilibrium temperature is 150-170°. This means that photoelements without temperature-regulating coatings on the receiving surface will be put out of commission in practice under the conditions of circumterrestrial cosmic space, since their efficiencies will drop to 0.1-0.2 of the value at 30°.

In developing coatings for photoelements, the necessity of combining good radiation characteristics in the coating with high antireflection properties presents particular complexity, since a consequence of the relatively high refractive index of silicon is that reflection from the polished surface reaches 34-35% in the spectral sensitivity region of the photoelement (0.4-1.1 μ) and, consequently, produces a corresponding efficiency loss.

As was indicated in [1], temperature-regulating coatings for silicon photoelements (which increase ε sharply at 30°) must have a low index of refraction and must be sufficiently thick as compared to the wavelength at the body's emission maximum at 30° (10 μ) in order to increase absorption in this region of the spectrum. This requirement means that a single-layer coating that improves the radiation characteristics of the surface cannot be used as an effective antireflection coating in the region from 0.4-1.1 μ, since the optimum antireflection-coating parameters [2]

$$d = \lambda/4 \text{ and } n = (n_{semicond.material})^{1/2}$$

(where $\underline{d}$ is the optical thickness and $\underline{n}$ is the refractive index) are not

maintained in this case.

The best temperature-regulating coatings that we produced (inorganic films, glass, silicones) have refractive indices n = 1.45-1.55. Consequently, the basic reflection losses in the region from 0.4-1.1 μ take place at the boundary between the temperature-regulating coating and the silicon, due to the great difference between the refractive indices of these media (at λ = 0.6 μ, n_{Si} = 4.05 and $n_{t.p.}$ ≈ 1.5), while reflection from the air-coating boundary amounts to no more than 4-5%. From this we can understand why the attempt made in [3] to improve the antireflection properties of a temperature-regulating coating by reducing reflection from the top boundary of the coating (by applying an antireflection layer of MgF_2 over a thick temperature-regulating Si_2O_3 film) was crowned with very modest success.

The authors investigated the possibility of reducing reflection at the boundary between the silicon and the temperature-regulating coating by introducing between these media an antireflection coating with an index of refraction intermediate between n_{Si} and $n_{t.p.}$.

Assuming $n_{t.p.}$ = 1.5 (in the region from 0.4-1.1 μ), we find that for a maximum reduction of reflection from this boundary, the intervening antireflection layer for such a two-layered system must have a refractive index $n_{p.s.}$ of

$$\sqrt{1,5 \cdot 4,05} = 2,47 \quad \text{for 0.6 μ}$$
$$\sqrt{1,5 \cdot 3,67} = 2,34 \quad \text{for 0.8 μ}$$

Among the easily reproducible, transparent antireflection coatings with good adhesion to the surface of the silicon that we produced, films of cerium dioxide and zinc sulfide have refractive indices closest to those calculated above. For an antireflection layer of zinc sulfide ($n_{0.6μ}$ = 2.33 and $n_{0.8μ}$ = 2.3) between silicon and a temperature-regulating coating with $n_{t.p.}$ = 1.5, the reflection from the boundary

- 195 -

between these two media, as calculated by the formula $R_{min} = (n_2^2 - n_1 n_3)^2 /$

$(n_2^2 + n_1 n_3)^2$ [2], will be reduced from 17.5 to 0.041% at 0.8 μ (for an op-

tical thickness of the layer d_{ZnS} = 0.2 μ) and from 21 to 0.32% for

0.6 μ (for d_{ZnS} = 0.15 μ).

A detailed calculation of the coefficient of reflection in the

spectral region from 0.4 to 1.1 μ was carried out for this same case of

a two-layered coating with an antireflection underlayer of ZnS. The

scattering of the refractive index of the zinc sulfide film, together

with the values of n given above for the wavelengths 0.6 and 0.8 μ,

were taken from Reference [4]. The calculation was made for two optical

thicknesses of the ZnS film: d = 0.15 μ (λ_{min} = 0.6 μ) and 0.2 μ

(λ_{min} = 0.8 μ). The scattering of the refractive index of the tempera-

ture-regulating coating was not taken into consideration. In calculat-

ing the over-all reflection, a 4% reflection from the upper boundary of

the temperature-regulating coating was added to the coefficient of re-

flection from the antireflection-coated silicon, which was figured with

consideration of multiple reflections in the film using the formula [5]:

$$R = \frac{r_1^2 + 2r_1 r_2 \cos 4\pi d / \lambda + r_2^2}{1 + 2r_1 r_2 \cos 4\pi d / \lambda + r_1^2 r_2^2},$$

where

$$r_1 = (n_2 - n_1) / n_2 + n_1), \ r_2 = (n_3 - n_2) / (n_3 + n_2), \ n_3 = n_{Si},$$
$$n_2 = n_{ZnS}, \quad n_1 = n_{\text{т. п.}} = 1, 5.$$

The spectral coefficient of reflection from the clean polished n-type

surfaces (concentration N_S = $4 \cdot 10^{20}$ atoms·cm^{-3}) of silicon photoele-

ments, as used in the calculations, was measured on two instruments: an

SF-2m spectral photometer (0.4-0.75 μ) and an IKS-14 infrared spectro-

photometer (0.75-1.1 μ) with a special adapter for recording total re-

flection. For comparison, a calculation was made to determine the spec-

tral coefficient of reflection from a surface that had been antireflec-
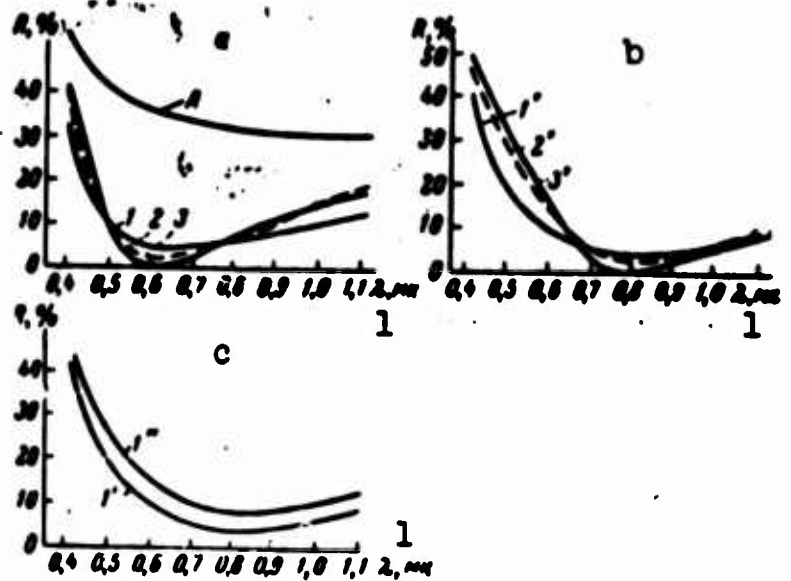
Fig. 1. Spectral reflection coefficients in the region 0.4-1.1 μ (cal-
culation): for two-layered coatings with an antireflection underlayer
of ZnS with d = 0.15 μ (1); ZnS with d = 0.2 μ (1') and SiO with d =
= 0.2 μ (1"); for single-layer antireflection coatings of ZnS with
d = 0.15 μ (2); ZnS with d = 0.2 μ (2'); SiO with d = 0.15 μ (3); SiO
with d = 0.2 μ (3'). The experimental curve A represents reflection
from a silicon photoelement with a clean polished surface (n-type, con-
centration $N_S = 4 \cdot 10^{20}$ atoms·cm-3). 1) λ, microns.

tion-coated with single layers of ZnS and silicon monoxide SiO, as well

as after application of a two-layered coating consisting of a tempera-

ture-regulating layer with n = 1.5 and an antireflection underlayer of

SiO (n = 1.9; the scattering of n_{SiO} was taken into account on the ba-

sis of the data in Reference [4]). The results obtained are shown in

Fig. 1.

It must be noted that although R_{min} was somewhat higher after ap-

plication of the two-layered coating (due to reflection from the upper

boundary of the temperature-regulating coating) than in the case of

purely antireflection films of ZnS and SiO, the reflection coefficient

R declined, on the whole, in the interval from 0.4 to 1.1 μ. Comparison

of curves 1' and 1" in Fig. 1c shows how heavily the effectiveness of

the double-layered coating depends on proper selection of the material

for the intermediate antireflection layer.

On the basis of experimental data on the absolute spectral sensi-

tivity of the photoelement without reflection coating (consisting of

- 197 -
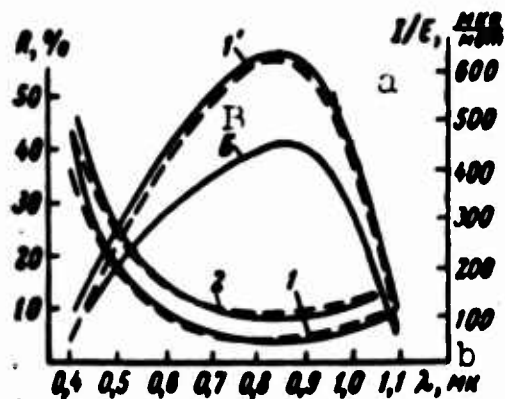
Fig. 2. Comparison of experimental (dashed curves) and calculated (solid curves) spectral reflection coefficients (R) and the absolute sensitivity (I/E) of a silicon photoelement with a polished surface before (I/E — curve B) and after application of two-layered coatings with an antireflection underlayer of ZnS with d = 0.2 μ (R is indicated by curves 1 and I/E by curves 1') and of SiO with d = 0.2 μ (R indicated by curves 2). a) I/E, μ a/mw; b) λ, microns.
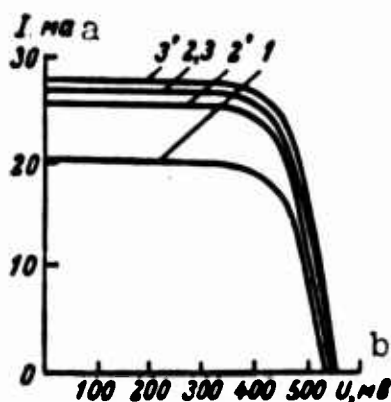
Fig. 3. Load current-voltage characteristic of a silicon photoelement with a polished surface: before antireflection coating (1); after antireflection coating with a single layer of SiO with d = 0.2 μ (2) and ZnS with d = 0.2 μ (3) and two-layered coatings with an antireflection underlayer of SiO with d = 0.2 μ (2') and ZnS with d = 0.2 μ (3'). Measurements made on a device simulating the extraatmospheric radiation of the sun with S = 1375 watts·m^{-2}. Area of photoelement receiver surface 0.72 cm^{-2} [sic]. a) I, ma; b) U, mv.

the short-circuit currents $I_{k.z.}$ of the photoelement in μa, measured

for each wavelength and then converted to mw of power of the incident

radiation), a calculation was made, using the reflection curves ob-

tained, to determine the spectral sensitivity of the same photoelement

after application of the double-layered and single-layered coatings.

Conversion of the spectral-sensitivity curves into the spectral dis-

tribution of the illumination created by the extraatmospheric sun made

it possible to obtain the spectral distribution of the $I_{k.z.}$ of the an-

- 198 -

1 Покрытие на полированной поверхности кремниевого фотоэлемента	2 Полученные расчетным путем токи короткого замыкания фотоэлемента при работе на Солнце (S = 1400 вт/м²), ма	
	3 Оптическая толщина просветляющего слоя, мм	
	0,15	0,2
4 Двуслойное покрытие (просветляющая пленка ZnS и поверх нее теплорегулирующее покрытие с n=1,5)	28,6	28,0
5 Однослойное просветляющее покрытие ZnS	27,9	27,2
6 Однослойное просветляющее покрытие SiO	28,8	28,1
7 Покрытие отсутствует	20	20

1) Coating on polished surface of silicon photoelement; 2) calculated short-circuit currents of photoelement in operation on sun (S = 1400 watts/m², ma; 3) optical thickness of antireflection coating, μ; 4) two-layered coating (antireflection film of ZnS under a temperature-regulating coating with n = 1.5); 5) single-layer antireflection coating of ZnS; 6) single-layer antireflection coating of SiO; 7) no coating.

tireflection-coated photoelement in operation on the same radiation, while figuring the areas bounding these curves enabled us to compare the short-circuit points [sic; tochki, points is probably an error for toki, currents] exhibited by the photoelectric cell after application of two-layered and single-layer coatings, for operation on sunlight. The results of the calculations are listed in the table. It follows from the table that even on the basis of antireflection properties considered alone, the two-layered coating of the type that we have proposed not only surpasses the ZnS antireflection coating, but is almost equivalent (d = 0.15 μ) or superior (d = 0.2 μ) to the single-layered antireflection coating of silicon monoxide, which is the optimum for antireflection coating of silicon photoelements.

The experimental results shown in Fig. 2 correspond almost perfectly with the results of calculation. A silicone coating with $n_{0.6\mu}$ = = 1.51 and a thickness ~ 80 μ, which is stable against the solar ultraviolet radiation and transparent in the region from 0.4-1.1 μ was selected as the upper temperature-regulating layer. Measurements of the

load volt/ampere characteristics of the photoelements showed that anti-reflection coating results not only in an increase in $I_{k.z.}$ close to that calculated, but also in a sharp increase in the efficiencies of the photoelements (Fig. 3). It is clear from Fig. 3 that the large (40-42%) increase in the $I_{k.z.}$ and efficiency as a result of antireflection coating is retained and even improved when the single-layer coating is replaced by a double-layer coating with an antireflection ZnS underlayer (curve 3', Fig. 3). Simultaneously with the rise in $I_{k.z.}$ and efficiency, the integral radiation coefficient ε increased from the values of 0.19-0.27, which are characteristic for a photoelement antireflection-coated with a single layer, to 0.92-0.94. The coefficient α_c of photoelements with a two-layered coating including a ZnS underlayer with d = 0.2 μ is 0.865, while it is 0.915 with a ZnS underlayer having d = 0.15 μ.* As a result, the ratio α_c/ε is 0.94-0.98, which indicates temperature stabilization of photoelements at the 44-45° level in outer space.

The merits of a double-layered coating of this type also include protection of the antireflection coating from attack by the environment and the absence of additional heating of the photoelement due to the "hothouse" effect.

Received

22 February 1964

Manu-
script
Page   [Footnote]
No.

200   The coefficients α_c and ε were evaluated with reference to
           direct measurements and by calculation [3].

REFERENCES

1. A. Thelen. Conf. Paper 1296-60, ARS Conf., Santa Monica, California, Sept. 27. 30, 1960.

2. I.V. Grebenshchikov, A.G. Vlasov, B.S. Neporent, N.V. Suykovskaya. Prosvetleniye optiki [Antireflection Coating of Optical Systems], OGIZ [State United Publishing Houses], Moscow-Leningrad., 1946.

3. C.A. Escoffery and W. Lift. Solar Energy, 4, No. 4, 1, 1960.

4. G.V. Rozenberg. Optika tonkosloynykh pokrytiy [Optics of Thin-Layered Coatings], Fizmatgiz [State Publishing House for Physico-mathematical Literature], Moscow, 1958, pages 54-60.

5. O.S. Heavens. Optical Properties of Thin Solid Films. London, 1955, page 58.

Manu- script Page No.	[Transliterated Symbols]
195	т.п. = t.p. = teploreguliruyushcheye pokritiye = temperature-regulating coating
195	п.с. = p.s. = promezhutochnyy sloy = intermediate layer
198	к.з. = k.z. = korotkoye zamykaniye = short circuit

INVESTIGATION OF RADIATION WITH THE FLIGHTS

OF THE "MARS-1" AND "LUNA-4" INTERPLANETARY AUTOMATIC STATIONS

S.N. Vernov, A.Ye. Chudakov, P.V. Vakulov, Ye.V. Gorchakov,
Yu.I. Logachev, G.P. Lyubimov, A.G. Nikolayev

A brief description of the equipment carried aboard the "Mars-1" and "Luna-4" stations is given, this equipment intended for the recording of radiation, and there is a discussion of the derived results. It has been observed that at a distance of 0.24 astronomical unit from the earth, the intensity of cosmic radiation remains virtually constant.

Data are also presented on the intensity of cosmic rays for various periods of the solar-activity cycle.

During the flight of the "Luna-4" station, slow, smooth changes in cosmic-ray intensity were recorded, and these are associated with a change in the magnetic conditions in the solar system. On being launched from the earth the "Mars-1" station cut through the radiation belts and data about these are presented.

The flights of automatic interplanetary stations to the moon and the neighboring planets of the earth make it possible to carry out an investigation of the primary cosmic radiation beyond the limits of the terrestrial magnetic field. This is particularly important for the study of the low-energy parts of cosmic radiation that play such an important role in a number of effects. Thus the change in the intensity of cosmic radiation during the 11-year cycle of solar activity occurs primarily as a result of low-energy particles; solar flares generate cosmic rays of similar low energies and these serve to explain the various variations in intensity that are associated with the change in the magnetic conditions of the solar system.

The determination of the change in cosmic-radiation intensity with a change in distance from the sun is also of interest.

Below we examine the results obtained in the recording of cosmic-radiation intensity outside of the terrestrial magnetic field during the flight of the "Mars-1" automatic interplanetary station during the period from 20 November 1962 through 25 January 1963, and during the flight of the "Luna-4" automatic station in the period from 2 through 14 April 1963. Data are also presented on the radiation belts of the earth, these data having been obtained by means of the equipment aboard the "Mars-1" station at the time of its launch from the earth on 1 November 1963 [sic].

Apparatus. The interplanetary automatic "Mars-1" station carried apparatus for the study of cosmic radiation in interplanetary space and in the radiation belts of the earth along the near-earth segment of the flight trajectory of the station. This apparatus consisted of two scintillation and two gas-discharge counters. One of the scintillation counters, carried inside the interplanetary station, was fitted out with a cylindrical NaI crystal 20 mm in diameter and 20 mm high. By means of this counter the total ionization produced by the radiation in the crystal was measured, and this counter also provided a record of the number of events in which energies above a given level were liberated in the crystal, and namely: above 30 kev and above 2.5 Mev.

A second scintillation counter with a cylindrical CsI crystal having a diameter of 20 mm and 3 mm thick was mounted on the outside of the station container. The crystal of this counter was covered by a thin sheet of aluminum foil (~ 2.2 mg$\cdot$cm^{-2}) on the free-space side through a solid angle of about 3 steradians. In other directions the crystal and photomultiplier were covered by a layer of aluminum ~ 1 g$\cdot$cm^{-2} thick. This scintillation counter recorded the total energy
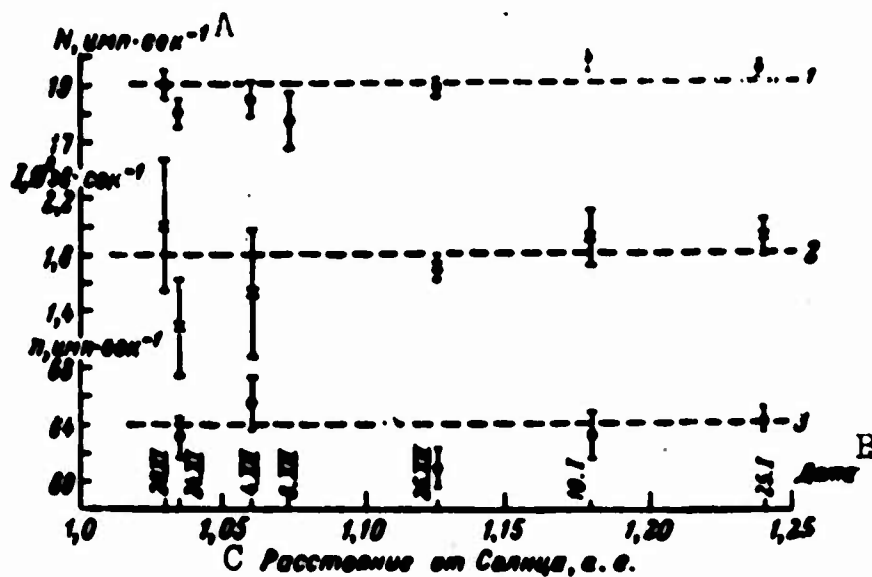
Fig. 1. The intensity of cosmic radiation during the flight of the "Mars-1" station as a function of the distance r from the sun. 1) According to the Geiger counter; 2) ionization of internal scintillation counter; 3) according to the 30 kev threshold of the internal scintilation counter; A) pulses·sec^{-1}; B) date; C) distance from sun, astronomical units.

liberated by radiation in the crystal and the number of particles liberating energy in the crystal in excess of 30 kev. Electrons with an energy $\geq$ 70-80 kev and protons with an energy $\geq$ 500 kev might have served as such particles.

Geiger counters (working length 50 mm, diameter 10 mm) were mounted in the interplanetary station.

The measurement of ionization and of the counting rates of the scintillation gas-discharge counters was carried out by the same methods as in the previous Soviet satellites and space rockets [1].

A gas-discharge counter (length 50 mm, diameter 10 mm) was mounted in the "Luna-4" automatic station launched on 2 April 1963 toward the moon for the purpose of studying radiation. The counter was mounted inside the station close to the shell under a material layer of about 1 g·cm^{-2}. The counter was heavily shielded on the remaining side (> 10 g·cm^{-2} of material). The continuous measurement of cosmic-radiation intensity was carried out by means of this counter, with continu-

ous transmission to the ground of the total number of counts between periods of communication. A statistical accuracy of about 0.1% was achieved for the measurement days. The accuracy achieved in the measurement of the number of counts and of the time was several times higher.

Cosmic-ray intensity as a function of distance from the sun. During the flight of the "Mars-1" station it proved possible to study the cosmic-ray intensity relationships for distances from the sun up to 1.24 astronomical units.

Fig. 2. Counting rate N of Geiger counters aboard the "Mars-1" station and n in the stratosphere at latitude 64° in the vicinity of Murmansk as a function of time. 1) pulses·sec⁻¹; 2) date; 3) November 1962; 4) December 1962; 5) January 1963.

The results obtained in the measurement of cosmic-radiation intensity by means of the Geiger counter, for ionization and for one threshold of the internal scintillation counter of the "Mars-1" station are shown in Fig. 1.

In order to account for the time variation in intensity a study has been conducted of the level of cosmic-ray intensity in the stratissphere at latitude 64° (at Murmansk). Figure 2 shows the counting rate of the single Geiger counter aboard the "Mars-1" station and the counting rate in the stratosphere (at the intensity maximum, height

- 205 -

50 g·cm^{-2}) for the period from November 1962 through January 1963.

As can be seen from the figures, no definite conclusions can be derived with respect to a change in cosmic-radiation intensity with increasing distance on the part of the "Mars-1" station.

Within the limits of the measurement errors (~2-3%) the intensity of the primary cosmic radiation remains constant at a distance of less than 1.24 astronomical units from the sun.

The intensity of cosmic rays as a function of distance to the sun was studied during the flights of the American "Pioneer-V" and "Mariner II" space vehicles. The "Pioneer-V" was launched in March of 1960 and approached the sun to a distance of 0.9 astronomical unit. A certain reduction in intensity was noted at that time, but it fell within the limits of error [2]. At the end of 1962 the "Mariner-II" space vehicle passed close to Venus, approaching the sun to a distance of 0.7 astronomical units. No changes in intensity were observed with approach to the sun [3].

Thus in a year close to the minimum of solar activity, in the vicinity of the earth's orbit at distances of 40 million km on the side away from the sun and on the side toward the sun the intensity of cosmic radiation remained constant with an accuracy to several per cent.

Intensity of cosmic rays as a function of the cycle of solar activity. In 1959, during the flight of Soviet space rockets, the most exact data were obtained on a stream of primary cosmic radiation beyond the terrestrial magnetosphere and on the average ionization capacity of cosmic-radiation particles [4]. Let us recall that a stream of cosmic rays in 1959 involved 1.98 $\pm$ 0.1 particles·cm^{-2}·sec^{-1} at an average ionizing capacity greater than the minimum by a factor of 2.5.

In 1963, during the flights of "Mars-1" and "Luna-4" data were also obtained on cosmic rays which can be compared with the data obtained

in 1959.

Table 1 shows the streams of cosmic radiation recorded by the Geiger counters mounted aboard the "Mars-1," "Luna-4" stations, and in Soviet space rockets, these data having been averaged over the time of flight.

The conditions under which the inside counters were shielded aboard the space vehicles and the "Mars-1" and "Luna-4" stations are approximately identical. Thus the stream of cosmic-radiation particles in 1963 exceeds the stream of particles in 1959 by a factor of almost 2.

TABLE 1

1 Космический аппарат	2 Дата старта ракет	3 Место расположения счетчика	4 Поток, см⁻²·сек⁻¹
1 космическая ракета [5]	2.1 1959 г. [11]	[17] Внутри контейнера	2,3 ± 0,1*
2 космическая ракета [6]	12. IX 1959 г. [12]	[18] То же	2,46 ± 0,1
2 космическая ракета [7]	12. IX 1959 г. [13]	[19] Вне контейнера	1,98 ± 0,1
3 космическая ракета [8]	4. X 1959 г. [14]	[20] На обшивке контейнера	2,12 ± 0,1
Станция «Марс-1» [9]	2.XI 1962 г. [15]	[21] Внутри контейнера	4,5 ± 0,1
Станция «Луна-4» [10]	2. IV 1963 г. [16]	[22] То же	4,45 ± 0,1

*The error is due to the indeterminacy of the geometric dimensions of the counter working volumes.

1) Space vehicle; 2) date of rocket launch; 3) position of counter; 4) stream, $cm^{-2} \cdot sec^{-1}$; 5) 1st space vehicle; 6) 2nd space vehicle; 7) 2nd space vehicle; 8) 3rd space vehicle; 9) the "Mars-1" station; 10) the "Luna-4" station; 11) 2 January 1959; 12) 12 September 1959; 13) 12 September 1959; 14) 4 October 1959; 15) 2 November 1962; 16) 2 April 1963; 17) inside the container; 18) the same; 19) outside of the container; 20) on the skin of the container; 21) inside the container; 22) the same.

The scintillation counters aboard the space rockets and the "Mars-1" station exhibited slightly varied characteristics from the standpoint of recording the ionization produced by emission in the crystal. Thus the instruments of the space rockets had NaI crystals 40 x x 40 mm in size, whereas the instrument aboard the "Mars-1" station operated on a crystal whose dimensions were 20 x 20 mm. Moreover, the

instruments aboard the space rockets recorded the energy liberation in the crystal without distortion, exceeding the average energy liberation of a relativistic proton by a factor of 200, while the instrument aboard the "Mars-1" station recorded without distortion energy liberation greater than the average energy liberation of a relativistic proton by a factor of only 3.

In 1959 the scintillation counters recorded a total energy liberation in the crystal of $1.5 \cdot 10^9$ ev$\cdot$sec^{-1} produced by cosmic rays, and a value of $1.8 \cdot 10^8$ ev$\cdot$sec^{-1} was obtained from the "Mars-1" station.

TABLE 2

1) максимную интенсив-ности в стратосфере			2) На расстоя-нии от 100 000 до 700 000 км от Земли
λ°=41	51	64	1,95
~1,1	1,25	1,45	

1) At the intensity maximum in the stratosphere; 2) at a distance from 100,000 to 700,000 km from the earth.

These values of energy liberation lead to various magnitudes of the mean ionizing capacity of the cosmic-radiation particles, differing by a factor of 2 between 1959 and 1963 (in 1959 it was greater by a factor of 2 than in 1963). However, consideration of the nonlinearity of the instrument aboard the "Mars-1" station significantly reduces the observed difference. With consideration of this correction factor we can draw the conclusion that in 1963 relative to 1959 the mean ionizing capacity of the particles of primary cosmic radiation had not increased.

All of the data on the change in the intensity of the cosmic radiation from 1959 through 1963 in the stratosphere at latitudes 41, 51, and 64°, as well as outside of the terrestrial magnetosphere, and the conclusion regarding the absence of an increase in the mean ionizing capacity of cosmic-ray particles make it possible to arrive at a conclusion regarding the average energy of the particles added in 1963 in comparison with 1959. Table 2 shows the ratios of cosmic-radiation intensity and mean ionizing capacity in 1963 and 1959 on the basis of

various data. The data for the stratosphere measurements have kindly been given by A.N. Charakhch'yan and T.N. Charakhch'yan.
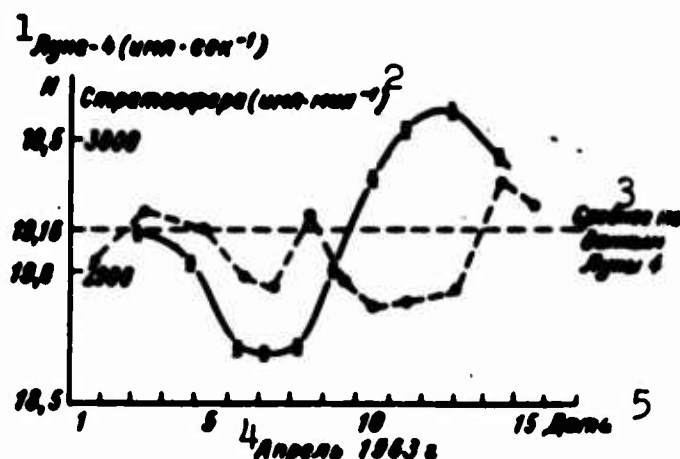
Fig. 3. Counting rate of Geiger counters during the flight of the "Luna-4" station (solid line) and balloonsondes in the stratosphere at latitude 64° in the vicinity of Murmansk (dashed line) during the period from 1 to 15 April 1963. 1) Luna-4 (pulses·sec^{-1}); 2) stratosphere pulses·min^{-1}; 3) average for Luna-4 data; 4) April 1963; 5) date.

This change in the number of particles at various latitudes may have been brought about by the additional particles of rather great energy (2-5 Bev) with a spectrum close to that of the primary cosmic radiation.

Variation in cosmic-radiation intensity recorded during flight of the "Luna-4" station. Figure 3 shows data derived during the operation of the "Luna-4" station. The average value of the counting rate for the counter comes to 19.161 ± 0.005 pulses·sec^{-1} (shown by the horizontal dashed line). The maximum deviations from the mean value are $\pm 2.5\%$ with an accuracy of about $\pm 0.1\%$ for each measurement. The voltage stability for the power sources employed by the apparatus during the course of the flight was maintained with high accuracy. The change in intensity as a result of fluctuations in the temperature inside of the station during this period amounted to no more than 0.5%.

We can see no other equipment factors for a change in intensity and it is our opinion that the recorded fluctuations in intensity are real.

This same figure also shows the results obtained in the measurements of intensity of cosmic radiation in the stratosphere in the vicinity of Murmansk for this same period of time.*

The change in intensity at Murmansk does not correlate with the change in intensity recorded aboard the "Luna-4" station. This leads to the conclusion that the fluctuations in intensity recorded during the flight of the "Luna-4" station were caused by particles exhibiting energies less than 2-3 Bev, not recorded in the maximum of the absorption curve at Murmansk (height 50 g·cm^{-2}). In any event, it may be stated that the spectrum of particles responsible for the variations in intensity recorded during the flight of the "Luna-4" station is softer than the spectrum of particles responsible for the 11-year change in cosmic-radiation intensity.

During the flight in interplanetary space of various space vehicles (the 3rd soviet space rocket, the "Pioneer V" rocket, the "Mariner-I," and the "Mars-1" station) time variations in intensity were noted, and these exhibited an amplitude of several per cent. Therefore, it is not the magnitude of the change in intensity recorded during the flight of the "Luna-4" station that is unanticipated, but rather the smooth manner of this change. It is not impossible that this is a result of the fact that during the period of minimum solar activity the sporadic processes taking place in the sun and leading to pronounced fluctuations in cosmic-ray intensity occur but infrequently or are entirely lacking, and that a change in the magnetic situation prevailing in near-earth outer space begins to play a role as a result of time changes in the solar wind. In this case the periodicity of the change in the magnetic situation in interplanetary space may be associated with the time required for the propagation of corpuscular streams in the solar system, i.e., with a time of the order 5-10 days. A perio-

dicity of this scale has been noted with the "Luna-4" station.
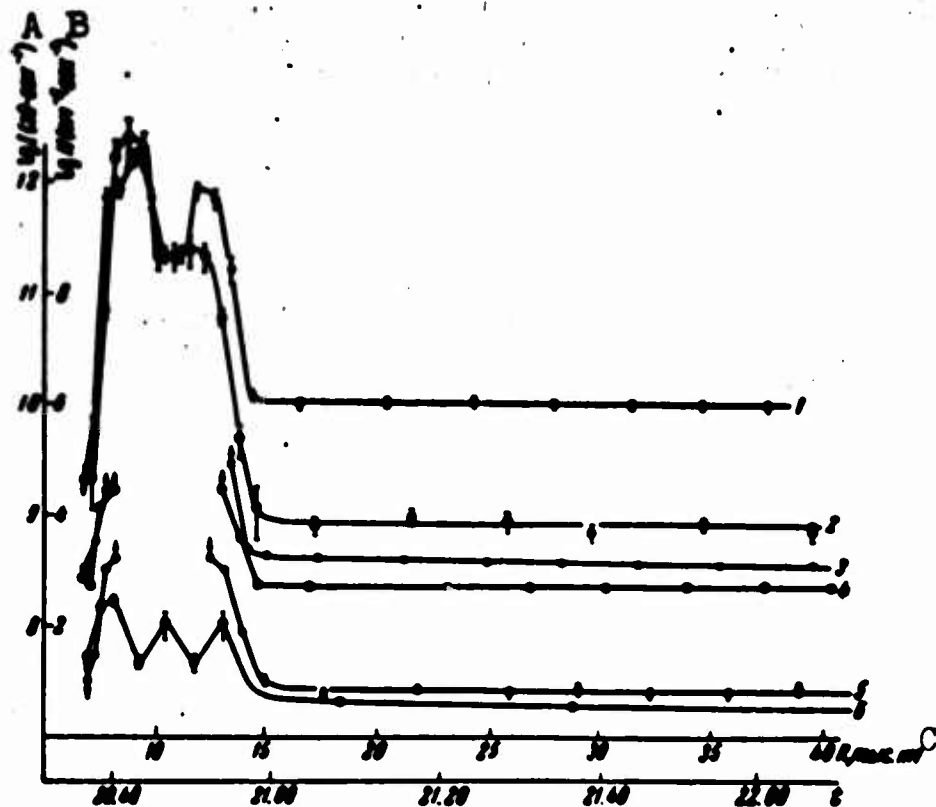
Fig. 4. Intensity of radiation recorded during the flight of the "Mars-1" station in the radiation belts around the earth on 1 November 1962 as a function of distance from the center of the earth. 1) Energy liberation per second in crystal of external scintillation counter; 2) energy liberation per second in crystal of internal scintillation counter; 3) counting rate of external scintillation counter; 4) counting rate of internal scintillation counter at 30 kev threshold; 5) counting rate for Geiger counter; 6) counting rate of internal scintillation counter at 2.5 Mev threshold; A) $\log I$ ev·sec^{-1}); B) $\log N$ $(cm^{-2} \cdot sec^{-1})$; C) R, thousand km.

Measurements in the radiation belts around the earth. The radiation in the radiation belts of the earth was recorded at the time the "Mars-1" station was launched from the earth. Figure 4 shows the radiation intensities as a function of distance from the center of the earth. Our attention is drawn first of all to the limited extent of the radiation belt. This is explained by the fact that the trajectory of the "Mars-1" station differed markedly from the trajectories of the first Soviet space rockets which cut through the outer radiation belt close to the equator. The "Mars-1" station, during its flight close to the equator, intersected the inner belt and then, moving away from the

- 211 -

earth, intersected the outer radiation belt at the higher geomagnetic latitudes.
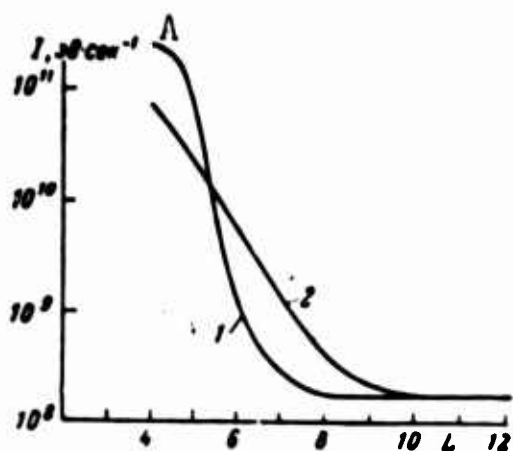
Fig. 5. Energy liberation in crystals of internal scintillation counters for the "Mars-1" station (1) and the second space rocket (2) as a function of L. A) I, ev·sec^{-1}.

Particularly surprising is the completely identical shape of the curves recorded by the various counters. For example, curve 5, showing the intensity of electrons with an energy of ≥ 70-80 kev (or of protons with an energy of ≥ 500 kev) is completely similar to the curve for the counting rate of the gas-discharge counter which effectively recorded electrons with an energy of ≥ 3 Mev (or protons with an energy of ≥ 50 Mev). During and prior to this flight there were no significant disturbances of the geomagnetic field. The passage through the outer boundary of the outer belt by the "Mars-1" station occurred at around midnight local time.

A comparison of the states of the belts in 1963 and 1959 is a difficult proposition because of the various flight trajectories for the space rockets and the "Mars-1" station. Figure 5 shows the values of energy liberation in the NaI crystals for the second space rocket and the "Mars-1" station as a function of the parameter L which characterizes the given magnetic shell [5]. The figure shows that the nature of the outer boundary of the outer radiation belt differed for the second space rocket from that of the "Mars-1" station. The second space rocket passed beyond the outer belt in the vicinity of the equatorial plane, while the "Mars-1" station passed out of the outer belt in the high latitudes. If it is maintained that the state of the belts during the time from September 1959 through November 1962 underwent no

change, it becomes possible to draw the conclusion that there exists
a more clearly delineated boundary of the outer radiation belt in the
high latitudes than is the case in the vicinity of the equatorial
plane. In other words, with large L there are no captured particles
with low points of reflection. However, it is most likely that the
change in the shape of the outer radiation belt should be ascribed to
temporal variations that were first detected in the flight of soviet
rockets [4] and studied in detail during the flight of the American
"Explorer-VII" satellite [6].

It is not out of the question that this difference in the shape
and position of the edge of the belt is associated with the variation
in the local time at which the flight through the edge of the belt
took place. A similar effect was first detected during the flights of
the American "Injun-I" satellite by means of a counter recording elec-
trons with an energy of >40 kev [7].

It turned out that at low flight altitudes (~1000 km) at noon lo-
cal time the edge of the belt is situated in the higher geomagnetic
latitudes than at midnight local time. Table 3 shows the instants (lo-
cal time) of flight through the edge of the outer radiation belt and
the parameter of the boundary magnetic shell from data produced by the
Soviet space rockets and the "Venus-1" and "Mars-1" stations. That mag-
netic shell at whose intersection the energy liberation in the crystal
exceeded the energy liberation from cosmic rays by a factor of 10 was
taken as the edge of the belt.

After leaving the radiation belts of the earth, all of the detec-
tors of penetrating radiation aboard the "Mars-1" station recorded a
virtually constant radiation intensity which, however, differs signifi-
cantly from primary cosmic radiation.

Table 4 shows the values of the streams of particles and energies

TABLE 3

1 Космический аппарат	2 Местное время пролета границы пояса			3 Граница пояса
	4 дата	5 часы	6 минуты	L
7 1-я космическая ракета	3.I 1959 г.	6	30	6,7
8 2-я космическая ракета	12.IX 1959 г.	20	30	6,5
9 3-я космическая ракета	4.X 1959 г.	14	30	--
10 Станция «Венера-1»	12.II 1961 г.	14	50	5,1
11 «Марс-1»	2.XI 1962 г.	21	30	6,0

1) Space vehicle; 2) local time of flight through boundary of belt; 3) belt boundary; 4) date; 5) hours; 6) minutes; 7) 1st space rocket; 8) 2nd space rocket; 9) 3rd space rocket; 10) the "Venus-1" station; 11) the "Mars-1" station; 12) 3 January 1959; 13) 12 September 1959; 14) 4 October 1959; 15) 12 February 1961; 16) 2 November 1962.

TABLE 4

1 Внутренний сцинтилляционный счетчик			2 Наружный сцинтилляционный счетчик		3 Счетчик Гейгера
4 ионизация, эв/сек	5 порог 30 кэв. эв/сек	6 порог 2,5 Мэв. имп/сек	7 ионизация, эв/сек	8 порог 30 кэв. имп/сек	9 имп/сек
$8 \cdot 10^4$	$2,5 \cdot 10^3$	20	10^{10}	$4 \cdot 10^3$	30

1) Internal scintillation counter; 2) external scintillation counter; 3) Geiger counter; 4) ionization, ev/sec; 5) 30 kev threshold ev/sec; 6) 2.5 Mev threshold, pulses/sec; 7) ionization, ev/sec; 8) 30 kev threshold, pulses/sec; 9) pulses/sec.

recorded by all detectors after passage out of the radiation belt.

The average energy liberated in the crystal per single reading of the external scintillation counter amounts to approximately 2 Mev per reading. The count of the gas-discharge counter is smaller by a factor of approximately 10^3 than the count of the scintillation counters for the 30 kev threshold. This indicates that the recorded radiation is due to electrons with energies ~2 Mev, directly recorded by the external and internal scintillation counters and on the basis of the bremsstrahlung recorded by the Geiger counter. (The Geiger counter was more heavily shielded than the cyrstal of the internal scintillation counter).

Since the stream of recorded electrons proved to be extremely stable in time, it is natural to assume that these electrons are the pro-

duct of the decay of long-lived radioactive nuclei.* The irradiation
of the "Mars-1" station by protons from the inner belt results in the
appearance of induced radioactivity. On the other hand, radioactive
nuclei formed in the atmosphere as a result of nuclear explosions
shortly before the flight of the "Mars-1" station may have been depos-
ited on the surface of the "Mars-1" station. However, an estimate of
the number of radioactive nuclei arising during these effects shows
that there are two few to explain the observed counting rates of the
radiation detectors aboard the "Mars-1" station.

It is therefore not impossible that the observed effect is pro-
duced by the appearance of high-energy electrons of unknown origin in
the vicinity of the earth.

REFERENCES

1.   P.V. Vakulov, N.N. Goryunov, Yu.I. Logachev and E.N. Sosnoved,
      Geomagnetizm i aeronomiya [Geomagnetism and Aeronomy], 1, 880,
      1961.

2.   C.Y. Fan, P. Meyer and J.A. Simson, Phys. Rev. Letters, 5, 272,
      1960.

3.   NASA News Release, 26 Febr. 1963.

4.   S.N. Vernov, A.Ye. Chudakov, P.V. Vakulov, Yu.I. Logachev and A.G.
      Nikolayev, Dokl. AN SSSR [Proc. Acad. Sci. USSR], 130, 517, 1960.

5.   C.E. McIlwain, J. Geophys. Res., 66, 3681, 1961.

6.   S.B. Forbush, G. Pizzella and D. Venkatesan, J. Geophys. Res., 67,
      3651, 1962.

7.   B.J. O'Brien, J. Geophys. Res., 68, 989, 1963.

Manu-script Page No.	[Footnotes]
210	After data from A.N. Charakhch'yan and T.N. Charakhch'yan.
215	Within 1 hour of measurements the intensity of radiation diminished by less than 5%.

EFFECTIVENESS OF PHARMACOCHEMICAL PROTECTION IN GAMMA IRRADIATION AND IRRADIATION BY PROTONS WITH ENERGIES OF 660 AND 120 Mev

V.S. Shashkov, P.P. Saksonov, V.V. Antipov, V.S. Morozov, G.F. Murin,

B.L. Razgovorov, N.N. Suvorov and V.M. Fedoseyev

The comparative effects of gamma-rays from Co^{60} and 660- and 120-Mev protons were studied in experiments on 1360 white mice. At a γ-ray dose rate of 364 r/min, the $DL_{100/30}$ came to 850 r (720 rad). On irradiation in a pulsed beam of 660-Mev protons (dose rate 600-700 rad/min), the $DL_{100/30}$ amounted to ~ 1178 rad. Cystamine (150 mg/kg), aminoethyl-isothiuronium (150 mg/kg), serotonin (50 mg/kg) and 5-methoxytryptamine (75 mg/kg), injected intraabdominally 10-15 min before γ- or proton irradiation, protected 50-80% of the animals from death. The protective effects of tryptamine and 5-hydroxytryptophane came to 20-25%. The relative biological effectiveness of 660-Mev protons as compared to Co^{60} γ-rays is 0.75 with respect to the DL_{50} for mice, and 0.73 with respect to the DL_{100}.

The problem of the biological effect of cosmic rays on living organisms is not only of theoretical importance, but also of great practical importance in the era in which man is conquering cosmic space. Further mastery of the cosmic reaches requires comprehensive evaluation of the radiation hazard, with recourse to simulation of a number of radiation components under terrestrial conditions.

The cosmic radiation is one of the chief obstacles, particularly to long flights over great distances [1, 2]. According to modern conceptions, the cosmic radiation includes rays originating from the Galaxy (the primary cosmic radiation), protons with various energies

formed in solar flares, and the penetrating radiation of the circumter-restrial radiation belts. From the practical standpoint, that of the radiation hazard, the corpuscular radiation (high-energy protons, heavy multiply charged nuclei) are of special interest; these are formed in large quantities in solar chromospheric flares and are incorporated in-to the outer and inner radiation belts.

In view of the complexity of the cosmic radiation spectrum, the difficulty of calculating absorbed dose for high-energy particles, the nonuniform transformation by the tissues of the absorbed energy, which is expended on ionization, excitation of electrons, nuclear interac-tions, the generation of bremsstrahlung x-ray and γ-radiation, etc., determination of the dose and biological effect of the cosmic radiation components presents considerable difficulty.

It is customary to regard the absence of characteristics for the relative biological effect (OBE) of the cosmic radiation as the chief obstacle to approximate evaluation of the biological effects of cosmic radiation, even given the availability of adequate information on its physical constants and satisfactory dosimetry.

Study of the OBE, first of all for protons, heavy nuclei and neu-trons, is part of one of the fundamental radiobiological problems of space flight, which [will] acquire ever-increasing importance as space-ships are fitted with nuclear powerplants.

Elaboration of this problem entered a stepped-up phase after it had been found possible to use high-altitude sounding balloons, rockets, and, first and foremost, satellites and space vehicles capable of re-turning to the earth for purposes of studying the biological effects of cosmic radiation. However, altitude experiments involve the necessity of studying the complex effect of space-flight factors on the living organism and isolating the contribution of cosmic radiation from this

effect.

The ultimate result is that in order to determine the contribution of ionizing radiation to the biological effect of space-flight factors, it is necessary to resort to laboratory experiments with the radiation levels registered in flight artificially reproduced, a task that sometimes involves considerable additional difficulties.

Determination of the OBE of the heavy cosmic-radiation component under laboratory conditions is impossible at the present time, since there is no apparatus available to generate particles of such high energies, and if there were such devices, they would not be adaptable for biological experimentation. Here we must make the reservation that even if we had information pertaining to the OBE of all cosmic radiation components, it would hardly be possible to draw inferences as to the biological effect of the complex-spectrum radiation on the basis of the summed influence of the individual components [3-5]. This purpose would obviously require the construction of special apparatus to produce a mixed beam of particles with an established spectrum and definite energies in its individual components.

As we have already noted, the OBE of various forms of radiation, including the corpuscular radiation, depend on many factors. The ionization density and linear energy losses on passage through a substance are important factors in this respect. Thus, an increase in the specific ionization from 3 to 100 ion pairs per 1 μ of path has little effect on the OBE, which remains approximately equal to unity. An increase in the ionization density from 100 to 1000 ion pairs per 1 μ gives an increase in the OBE in proportion to the logarithm of the specific ionization [6].

Various authors [6-13] consider the OBE as ranging from 2 to 30 for a specific ionization above 1000 ion pairs per 1 μ.

As we know, protons are the form of penetrating radiation most commonly encountered in outer space. They compose 85% of the primary cosmic radiation and are generated in large numbers in solar chromospheric flares, forming parts of the outer and inner radiation belts.

The first steps have recently been taken toward determining the OBE for protons. According to [14-16], the OBE of protons with an energy of 660 Mev with reference to Co^{60} γ-rays is 0.5-0.6 for mice, and 0.6-0.7 for rats. OBE for protons with an energy of 510 Mev have been established for dogs (1.2) and for rats (0.8) [17].

The above coefficients were determined from consideration of the survival times of the animals, the survival rates and the distinctness of the changes in the indicators investigated.

In experiments on monkeys, the OBE was 2 for protons with an energy of 730 Mev, with reference to γ-rays [18]. The OBE of protons with an energy of 157 Mev is 0.77 ± 0.1 for mice, with x-rays as the reference [19].

On the basis of the literature data, it is important to note that the OBE of any given type of radiation depends on what criterion was used as a basis for deriving it. The OBE of the identical form of radiation is often found to differ for different biological systems or organs [7-9, 12, 13, 19-23].

Thus, the radiation injuries caused by protons and neutrons are less reversible than those due to exposure to x-rays. As regards genetic consequences and injury to the crystalline lens, a certain cumulative effect has been noted for corpuscular radiation.

The OBE increase considerably with increasing irradiation time and time of observation after irradiation by high-energy particles [3, 5].

Neutron irradiation produces more pronounced changes in the chromosome apparatus than in the structures of the cell that are not related

to them. This relationship is reversed for x-rays [24, 25-33].

The OBE also depends on radiation dose, the functional state of the organism, and so forth. The irreversibility of changes governed by corpuscular radiation must be kept in mind in studying the biological effect of cosmic radiation, which has a complex, heterogeneous spectrum [25].

In evaluating the genetic effects of cosmic radiation, it is necessary to take into account both the hazard to the descendants and the somatic and cytogenetic changes in the irradiated organism, which result in shortening of the lifespan, disorders of the blood, malignant neoplasms and other pathological manifestations [31, 32].

While acknowledging that we deal, under laboratory conditions, with particles that simulate individual components of the cosmic radiation, we must nevertheless point out that thanks to devices capable of generating definite forms of radiation, it is possible to form some idea of their biological effectiveness.

The present paper was concerned with the influence of 660- and 120-Mev protons on animals and the prophylactic effect of radioprotective agents that are known to be effective in x-ray and γ-irradiation.

Experiments were conducted on 1360 mongrel male white mice weighing 18-21 g. The animals were subjected to Co^{60} γ-irradiation with protons having energies of 660 and 120 Mev.

The animals were γ-irradiated on the GUBE-800 experimental installation at the Biophysics Institute of the Academy of Sciences USSR at a dose rate of 264 r/min. Proton bombardment of the animals was accomplished in the pulsed beam of the OIYaI* synchrocyclotron (at Dubna) with a density of 10^8-10^9 protons per 1 cm^2/sec.

The number of pulses per second was 100, each lasting 200-400 μsec. Determination of the dose of protons with the 660-Mev energy and the

irradiation technique were as described in [16]. The dose rate determined from the induced activity in carbon plates was 500-700 rad/min in our experiments. Irradiation of the animals was accomplished in either case in plastic chambers, 10 mice at a time (5 controls and 5 animals that had been protected with the prophylactic agents).

It must be acknowledged that definite data do not exist for calculating the dose to be attributed to a single proton. On the basis of calculations in [16], it was found that in a beam of protons with energies of 660 Mev with the above intensity and a section diameter of 10 cm there are $(5.3 \pm 0.18) \cdot 10^{-8}$ rad/proton. According to information from staff members of the IBF MZ, the same value is $4.3 \cdot 10^{-8}$ rad/proton. According to foreign authors [34], the dose contribution in a beam of protons with energies of 500 Mev is $5 \cdot 10^{-8}$ rad/proton. In our experiments, we used $4.3 \cdot 10^{-8}$ rad/proton in calculating the dose.

TABLE 1

OBE for Various Doses of 660-Mev Protons With Reference to Co60 γ-rays

1 γ-лучи Co60					2 Протоны 660 Мэв					9 ОБЭ
3 доза, рэб*	4 число животных	5 выжило к 30-м суткам	6 % выживаемости	7 сред. продолжительность жизни, дни	3 доза, рэб	4 число животных	5 выжило к 30-м суткам	6 % выживаемости	8 средняя продолжительность жизни, дни ±m	
400	40	40	100	--	400	40	40	100	—	—
500	40	28	80	18,6	500	40	40	100	—	—
—	—	—	—	—	560	40	38	95	12,8 ± 5,3	—
600	40	24	60	12,1	650	40	32	80	14,2 ± 4,2	—
700	40	16	40	11,8	750	40	28	70	14,1 ± 3,2	0,75**
800	40	6	15	8,4	850	40	22	55	16,3 ± 3,1	—
—	—	—	—	—	950	40	12	30	12,4 ± 3,3	—
850	40	0	0	7,8	1178	160	3	1,7	11,7 ± 2,9	0,73***

*The coefficient used in converting r to rad was 1 r = 0.93 rad.
** From DL_{50}.
*** From DL_{100}.

1) Co60 γ-rays; 2) 660-Mev protons; 3) dose, rad*; 4) number of animals; 5) survived for 30 days; 6) % of survival; 7) average survival time, days; 8) average survival time, days ± m; 9) OBE.

The energy of the protons was lowered from 660 to 120 Mev by the

use of polyethylene blocks 1.5 m thick with an additional 6 cm of lead. The flux intensity and dose of the protons were determined from the activity induced in carbon indicators, which were read using a type B instrument with an MST-17 end-window counter. The intensity variations of the beam were checked with a monitor. The dose rate at the proton energy of 120 Mev came to 60 ± 10 rad/min.

Determination of the proton OBE was not part of the purpose of our experiments.

However, since we did have at our disposal a considerable number of animal control groups, we do have an opportunity to present data on the OBE here as well. Judgements were made as to the OBE of the 660-Mev protons from the influence that the various radiation doses had on the survival rates of the animals during the 30-day observation period and the weight change. The data from these experiments are given in Table 1.

Thus, the table indicates that the $DL_{50/30}$ of Co^{60} γ-rays in our experiments is 650 r (600 rad), while that of 660-Mev protons is ~ 900 rad. The $DL_{100/30}$ with reference to Co^{60} γ-rays is 850 r (790 rad), and that of 660-Mev protons is 1178 rad. The OBE of the protons, based on $DL_{50/30}$, is 0.75, while it is 0.73 on the basis of $DL_{100/30}$. These data are in fair agreement with those obtained in [16] on conversion of the dose by a coefficient of $4.3 \cdot 10^{-8}$ rad/proton.

As we know, the differences in the OBE for the different forms of radiation are linked to the differences in the spatial distribution of the ions (ionization density) or to the linear energy losses (LPE) in the tissues, by which this quantity is generally defined.

On interaction of 660-Mev protons with matter, a complex spectrum of secondary particles is formed, some with rather high LPE. Their contribution to the injurious effect will obviously come more strongly to the fore when we consider remote consequences, to judge from which the

proton OBE will be unity at the smallest.

The problem of pharmacochemical and biological protection from ionizing radiation forms a special offshoot of radiobiology, radiation medicine and space radiobiology. Some authors have concluded [35], with reference to literature data, that the various pharmacochemical substances that are effective in x-ray and γ-ray irradiation will not have such an effect for bombardment by corpuscular radiation, particularly as regards the genetic effect of this radiation.

It is also known that when antiradiation agents are used for protection from densely ionizing rays, we observe a lowering of their activity on neutron bombardment [36, 37] or the complete absence of any radio protective effect on α-irradiation [4].

TABLE 2

Protective Effect of Pharmacochemical Agents on Co^{60} γ-irradiation in Dose of 850 r (DL_{100})

1 Препараты	2 Количество мышей	3 Дожившие до 30-м суткам	4 % выживаемости	5 Средняя продолжительность жизни, погибших животных, дни ± m
6 Цистамин	40	22	55	13,8 ± 3,7
7 АЭТ	40	30	75	15,3 ± 4,2
8 Серотонин	40	24	60	12,4 ± 3,5
9 5-метокситриптамин	40	28	70	14,9 ± 3,7
10 Триптамин	20	8	20	8,3 ± 3,3
11 5-окситриптофан	20	8	20	8,0 ± 3,5
12 Контроль	40	0	0	7,5 ± 2,8
13 Биологический контроль	20	20	100	—

1) Preparation; 2) number of mice; 3) surviving after 30 days; 4) % of survival; 5) average survival time of animals that died, days $\pm$ m; 6) cystamine; 7) AET; 8) serotonin; 9) 5-methoxytryptamine; 10) tryptamine; 11) 5-hydroxytryptophane; 12) control; 13) biological control.

As was first shown by the several authors of [38-40], however, the prophylactic effect of certain radioprotective agents manifests on bombardment by 660-Mev protons to at least the same degree as on exposure to x-rays or Co^{60} γ-rays, if not more strongly. The most convincing data on the question as to the comparative radioprotective effects of prophylactic agents for bombardment with 660-Mev protons and γ-rays are

TABLE 3

Protective Effect of Preparations on Whole-Body Irradiation of Mice by 660-Mev Protons in a Dose of 1178 rad (DL_{100})

1 Препараты	2 Количество мышей	3 Выжило к 30-суткам	4 % выживаемости	5 Средняя продолжительность жизни погибших животных, дни ±m
6 Цистамин	80	41	51.2	15,3 ± 3,8
7 АЭТ	60	49	81,1	14,5 ± 2,9
8 Серотонин	30	15	50	12,8 ± 3,5
9 5-метокситриптамин	30	21	70	14,2 ± 3,3
10 Триптамин	20	5	25	10,9 ± 2,2
11 5-окситрипто-фан	20	4	20	11,0 ± 2,4
12 Контроль	160	3	1,7	11,7 ± 2,9
13 Биологический контроль	80	59	98,4	24

1) Preparation; 2) number of mice; 3) surviving after 30 days; 4) % of survival; 5) average survival time of animals that died, days $\pm$ m; 6) cystamine; 7) AET; 8) serotonin; 9) 5-methoxytryptamine; 10) tryptamine; 11) 5-hydroxytryptophane; 12) control; 13) biological control.

presented in [40].

We conducted tests to study the radioprotective effects of cystamine dichlorohydrate (150 mg/kg), S, β-aminoethylisothiuronium bromide dihydrobromide (AET, 150 mg/kg), serotonin creatinine sulfate (50 mg/ /kg), 5-methoxytryptamine chlorohydrate (75 mg/kg), tryptamine chloro-hydrate (100 mg/kg) and 5-hydroxytryptophane (250 mg/kg) in γ-irradia-tion from Co^{60} and irradiation by 660- and 120-Mev protons. The prepar-ation doses taken were converted to the base. All preparations were in-jected intraabdominally 10-15 min prior to irradiation.

The data from these experiments are given in Tables 2-4.

It follows from Table 2 that AET, 5-methoxytryptamine, serotonin and cystamine show the strongest radioprotective activity among the substances tested for Co^{60} γ-irradiation in an absolutely lethal dose. The protective effects of tryptamine and 5-hydroxytryptophane (the ini-tial product in the synthesis of serotonin in the organism) are consid-erably weaker.

Protective Action of Preparations
in Whole Body Irradiation by 120-
Mev Protons in doses of 1200 ± 100
rad (DL_{100})

1 Препарат	2 Количество животных	3 Выжило к 30-м суткам	4 % выживаемости	5 Средняя продолжительность жизни погибших животных, дни ± m
6) Цистамин	40	24	60	13,5 ± 4,3
7) АЭТ	40	30	75	16,3 ± 4,6
8) Серотонин	40	22	35	12,7 ± 3,5
9) 5-метокситриптамин	40	28	70	13,8 ± 3,2
10) Контроль	60	2	3,3	9,5 ± 3,1
11) Биологический контроль	20	20	100	—

1) Preparation; 2) number of animals; 3) surviving after 30 days; 4) %
of survival; 5) average survival time of animals that died, days ± m;
6) cystamine; 7) AET; 8) serotonin; 9) 5-methoxytryptamine; 10) control;
11) biological control.

Data on the radioprotective effects of the substances for whole-body irradiation by 660-Mev protons are given in Table 3.

On analysis of the experimental results presented in Table 3, it can be seen that AET and 5-methoxytryptamine were found most effective for irradiation both by protons and by γ-rays. The protective effects of cystamine and serotonin on exposure to 660-Mev protons are similar to their prophylactic properties for γ-irradiation. It is interesting to note that in the experiments of [40], the high protective effect of AET is retained even on irradiation by protons in superlethal doses (1600 rad).

We have not succeeded in finding data in the literature on the radioprotective action of certain effective antiradiation agents for irradiation of animals by 120-Mev protons. The results of our experiments in this direction are assembled in Table 4. It is seen from Table 4 that the effectiveness of the radioprotective preparations studied, which possess antiradiation properties for x-ray, γ-ray and 660-Mev proton irradiation are also retained fully for exposure to 120-Mev pro-

tons.

Thus, in summarizing the results of the experiments described, it might be supposed that the OBE of 660- and 120-Mev protons for mice do not exceed 1 at any rate and may even be lower, with reference to the electromagnetic radiation types. Here it is very important that certain radioprotective substances that are effective with respect to x- or γ-rays also retain their prophylactic properties when the organism is exposed to high-energy protons.

We do not consider here the mechanisms by which the pharmacochemical agents secure their radioprotective effects — mechanisms that remain unclear to the present day. In any event, they would appear to be of the same type for both exposure to electromagnetic radiation and exposure to high-energy corpuscular radiation with low ionization density.

The discovery of protective properties for exposure to corpuscular radiation in a number of pharmacochemical agents justifies a search for means of biological and chemical protection of the human crew and the entire biocomplex of the spacecraft. This necessitates further study of the principals of pharmacochemical protection for various energies, doses and dose rates of the corpuscular radiation, with emphasis on protons, and calls for investigation of the effect of radiation in combination with the other factors operating in space flight; this will make possible at least partial evaluation of the radiation hazard, determination of the admissible cosmic-radiation levels and adoption of effective protective measures against it.

Received

17 February 1964

REFERENCES

1.   Yu.M. Volynkin, P.P. Saksonov. Nauchnaya sessiya, posvyashchenna-

ya 5-y godovshchine zapuska l-go iskusstvennogo sputnika Zemli [Scientific Session Devoted to the 5th Anniversary of the Launching of the 1st Artificial Earth Satellite], Tez. dokl., Izd-vo AN SSSR [Topics of Reports, Academy of Sciences USSR Press], 1962 page 12.

2.   V. V. Antipov, N. N. Dobrov, P. P. Saksonov. Ibid., page 54.

3.   T. Ivens. Collection entitled "Radiobiologiya" [Radiobiology], IL [Foreign Literature Press], Moscow, 1955, page 400.

4.   A. C. Brige. Aviat. Med., 25, 326, 1954.

5.   T. S. Evans. Phys. and Med. Upp. Atm. New Mexico, 1952 page 533.

6.   L. R. Shepherd. J. Brit. Interplan. Soc., 30, 410, 1959.

7.   R. E. Zirkle. Radiation Biology, I, McGraw Hill Book Co., N. Y. – Toronto – London, 1954, page 315.

8.   J. B. Storer, P. S. Harris, A. F. Krebs. J. Aviat. Med., 25, 368, 1954.

9.   J. B. Storer, P. S. Harris, J. I. Furchuer, W. H. Langham. Rad. Res., 6, 188, 1957.

10. R. Colitz, H. Tibuana, C. Gros, B. Pierguem. J. Dutreix. Radiol. Electrol., Med. Nucl., 40, 413, 1959.

11. C. A. Tobias, T. Brustand. Phys. and Med. Atm. and Space, J. Wiley and Sons, N. Y.–London, 1960, page 193.

12. H. J. Schafer. J. Aviat. Med., 25, 338, 1954.

13. H. J. Schafer. J. Aviat. Med., 25, 392, 1954.

14. E. B. Kurlyandskaya et al. Dokl. AN SSSR [Proceedings of the Academy of Sciences USSR], 143, No. 3, 702, 1962.

15. E. B. Kurlyandskaya In collection entitled "Materialy po biologicheskomu deystviyu protonov vysokikh energiy" [Data on the Biological Effect of High-Energy Protons], Moscow, 1962, page 5.

16. G. A. Avrunina. Ibid., page 10.

17. A.V. Lebedinskiy, Yu.G. Nefedov, N.N. Ryzhov et al. Nauchnaya ses-
siya, posvyashchennaya 5-y godovshchine zapuska 1-go iskusstvenno-
go sputnika Zemli [Scientific Session Devoted to the 5th Anniver-
sary of the Launching of the 1st Artificial Satellite], Tez. dokl.,
Izd-vo AN SSSR [Topics of Reports, Academy of Sciences USSR Press],
1962, page 57.

18. R.W. Zellmer. Aerospace Med., 32, 942, 1961.

19. P. Bonet-Mayru, A. Deysine, M. Trilley, C. Stepan. Compt. rend.
Acad. Sci. [Proceedings of the Academy of Sciences at Paris], 251,
No. 25, 3088, 1960.

20. L.R. Langham. Aerospace Med., 30, 410, 1959.

21. K.A. Tobias. In collection entitled "Radiobiologiya" [Radiobiology],
IL [Foreign Literature Press], Moscow, 1955, page 364.

22. Recommendation of the International Commission on Radiological
Protection. Pergamon Press. London — N.Y. — Paris — Los-Angeles,
1959.

23. A.R. Sheferd. Issledovaniye mirovogo prostranstva [Investigation
of Outer Space], Fizmatgiz [State Publishing House for Physicomath-
ematical Literature], 1959, page 84.

24. M.A. Arsen'yeva, M.A. Bel'govskiy, N.L. Delone. In collection en-
titled "Radiobiologiya" [Radiobiology], Izd-vo AN SSSR [Academy of
Sciences USSR Press], 1957, page 329.

25. N.P. Dubinin. Problemy radiatsionnoy genetiki [Problems of Radia-
tion Genetics], Moscow, 1961.

26. G.A. Avrunina, N.M. Karamazina et al. Byul. eksperim. biol. i med.
[Bulletin of Experimental Biology and Medicine], No. 8, 52, 1961.

27. Ye.S. Shchepot'yeva, S.N. Ardashnikov et al. Izv. AN SSSR. Seriya
biol. [Bulletin of the Academy of Sciences USSR, Biology Series],
4, 642, 1961.

28. G. P. Parfenov. In collection entitled "Iskusstvennyye sputniki Zemli" [Artificial Earth Satellites], No. 10, Izd-vo AN SSSR [Academy of Sciences USSR Press], 1961, page 69.

29. Ya. L. Glembotskiy, E. A. Abeleva, Yu. A. Lapkin, G. P. Parfenov. In collection entitled "Iskusstvennyye sputniki Zemli" [Artificial Earth Satellites], No. 10, Izd-vo AN SSSR [Academy of Sciences USSR Press], 1961, page 61.

30. M. A. Arsen'yeva, V. V. Antipov, V. G. Petrukhin et al. In collection entitled "Iskusstvennyye sputniki Zemli" [Artificial Earth Satellites], No. 10, Izd-vo AN SSSR [Academy of Sciences USSR Press], 1961, page 82.

31. A. T. Krebs. J. Aviat. Med., 21, 481, 1950.

32. A. T. Krebs. J. Aviat. Med., 25, 331. 1954.

33. L. N. Breslavets. In collection entitled "Ocherki po radiobiologii" [Outlines of Radiobiology], Izd-vo AN SSSR [Academy of Sciences USSR Press], 1956, page 233.

34. R. Madey, A. Dunir, J. Krikger. Amer. Astr. Soc., 22, 39, 1962.

35. A. A. Gyurdzhian. In collection entitled "Iskusstvennyye sputniki Zemli" [Artificial Earth Satellites], No. 12, Izd-vo AN SSSR [Academy of Sciences USSR Press], page 77. 1962.

36. H. M. Patt, I. W. Clark, H. H. Vogle, H. H. Patt. Proc. Soc. Exp. Biol. Med., 84, 189, 1953.

37. R. L. Straube. Rad. Res., 1, No 2, 226, 1954.

38. S. P. Yarmonenko, G. A. Avrunina, V. S. Shashkov, R. D. Govorun. Radiobiologiya [Radiobiology], 2, No. 1, 125, 1962.

39. S. P. Yarmonenko, G. A. Avrunina. V. S. Shashkov, R. D. Govorun. Collection entitled "Problemy kosmicheskoy biologii" [Problems of Space Biology], 2. Izd-vo AN SSSR [Academy of Sciences USSR Press], 1962, page 388.

40. S.P. Yarmonenko. In collection "Materialy po biol. deystv. proto-
    nov vysokikh energiy" [Data on the Biology Effects of High-Energy
    Protons], Moscow, 1962, page 50.

Manu- script Page No.	[Transliterated Symbols]
218	ОБЭ = OBE = otnositel'naya biologicheskaya effektivnost' = relative biological effectiveness
221	ОИЯИ = OIYaI = Ob"yedinennyy Institut Yadernykh Issledovaniy = United Nuclear Research Institute
222	ИБФ МЗ = IBF MZ = Institut Biologicheskoy Fiziki Ministerstva Zdravookhraneniya = Biophysics Institute of the Ministry of Public Health
223	ЛПЗ = LPE = Lineynyye poteri energii = linear energy losses

OCCURRENCE OF CROSSING OVER IN DROSOPHILA MALES UNDER THE INFLUENCE OF VIBRATION, ACCELERATION AND γ-IRRADIATION

G. P. Parfenov

The influence of vibration, acceleration and γ-irradiation on the incidence of crossing over in Drosophila males is examined. It is customary to assume that this class of hereditary changes is governed by rebuilding of homologous chromosomes in the meiotic stages. This test was also used aboard artificial earth satellites to indicate the biological effect of cosmic radiation, and spotty results were obtained. To analyze the differences that arose, experiments were run with Drosophila specimens subjected to acceleration, vibrations, γ-irradiation and combinations of these factors. The data obtained are discussed.

One of the most hazardous and difficult-to-eliminate environmental factors in space flight is ionizing radiation. Although the mutagenic effects of certain types of ionizing radiation have been thoroughly studied, certain difficulties are encountered in the use of genetic material (the test objects for biological do？ ？？, of cosmic radiation). The conduct of experiments for these purposes necessitates disregarding one of the basic rules of genetic research, that which requires "purity" of the experimental and control groups. According to this rule, the content of the experimental material must differ from the control content only as regards the factor being studied, with absolute identity of all other conditions. In flights aboard artificial earth satellites, however, the biological objects are subjected, simultaneously with the cosmic radiation, to a number of other factors whose action, together or in isolation, on the hereditary structures has not

been studied or has been studied with inadequate thoroughness. These include acceleration, vibration, the state of weightlessness, temperature fluctuations and the composition of the atmosphere.

Some of the physical factors enumerated above (temperature and vibration) may affect the results of the experiments both in and for themselves [1, 2] and in concerted action with ionizing radiation [3]. As regards acceleration and atmospheric changes, they have not been shown to have a mutagenic effect of their own; however, they can modify substantially the effect of the ionizing radiation [4, 5].

We employed a test for the induction of crossing over in Drosophila males on the flights of the 5th satellite spacecraft and the "Vostok-1" and "Vostok-2" [6]. The results of this investigation were in many respects not particularly clear, since the effect was observed in one case (the 5th satellite spacecraft) and not observed in the two others ("Vostok-1" and "Vostok-2"), although the conditions would appear to have been the same for the 5th satellite spacecraft and the "Vostok-1." The flight of the "Vostok-2" was approximately 15 times as long. We suggested that in the two flights in which the effect did not appear, the analysis referred to male rudimentary cells that were in the premeiotic or postmeiotic stages during the flight, and since crossing over takes place preferentially in spermatocytes, crossover individuals could not be found.

Our hypothesis was based on the fact that for some time after the spacecraft had been recovered, the flies in the various series of experiments were not kept under identical temperature conditions. This could have been the reason why, in analyzing the descendants of the experimental males only 10-12 days after landing, we came upon the meiotic stages in some cases and did not catch them in others, since it is known that the duration of spermatogenesis in Drosophila is a function

of temperature. In the present study, we examined the frequency of occurrence of crossovers under the influence of γ-irradiation as a function of the time since exposure with the flies stored at a stable temperature.

It was noted in the preceding communication that crossovers may arise in Drosophila under the influence of vibration. We conducted a more complete study of this phenomenon and, furthermore, ascertained the effectiveness of the combined action of vibration and γ-irradiation and acceleration and γ-irradiation, as well as the effect of acceleration taken alone.

Technique of Experiment

The occurrence of crossing over was detected in chromosome 2 of hybrid males produced by crossing Domodededovo 32 ♀ and ♂ b cn vg. Thus, one 2 chromosome was marked in the hybrids by the genes black (b), cinnobar (cn), vestigial (vg); the other was obtained from wild-strain flies. All of the marker genes are recessive and possess distinct phenotypic effects in the homozygous state. The first affects the coloration of the body, the second the color of the eye, and the third the structure of the wings. The crossovers were taken into account in an analyzing crossing in the descendants of the hybrids described above and b cn vg/b cn vg females. All of the crossovers detected were checked individually in allelomorphism tests. Since the percentage ratios were calculated from the total number of crossovers, they may be somewhat on the high side. The basic crossings were made on a large scale: four males and six brood females were placed in each test tube. All experiments were conducted at $25 \pm 1^{\circ}$ C. The age of the males at the beginning of exposure did not exceed two days.

The frequency with which crossovers appeared as a function of time after exposure was studied in two experiments. In the first experiment,

the males were irradiated with a dose of 2000 r and crossed immediately after irradiation. Every two days thereafter, the males were removed from the cultures and crossed with fresh females. A total of 9 series was run, so that data were obtained on the appearance of crossovers from the 1st through the 18th day after irradiation. The second experiment was run on the same design, but the flies were irradiated with a dose of 1000 r and the series were renewed every day.

Since the maximum incidence of crossovers took place on the 9th-10th day after irradiation, the males were kept with a 3-4-fold excess of females until the 9th day after exposure in all subsequent experiments in order to deplete the sperm, and were then used for three days in an analyzing crossing. Five series were set up with a radiation dose of 1000 r, three series with vibration (4 and 2 hours) and two series with acceleration applied for 20 min. The combined action of vibration and irradiation was studied in three experiments. In two of these, vibration (4 and 2 hours) preceded irradiation. In the third experiment, the four-hour vibration phase followed after irradiation. The combined effect of acceleration and irradiation was studied in two experiments. In one, 20 minutes of acceleration preceded irradiation, while in the other it came afterward. In all experiments in which combined disturbances were used, the pause between them was about one hour.

We used Co^{60} γ-rays to irradiate the flies at a dose rate of 350-385 r/min in gelatin capsules in which 200-300 of the males had been placed. The flies were vibrated in glass test tubes lashed securely to the plate of the vibrating stand. The amplitude of the vibrations was 0.4 mm in all experiments, and the frequency was 70 cycles per second. The accelerations were set up in a biochemical (arm radius 15 cm) at a speed of 5000 rpm. The flies were not etherized for the exposure to vibration and acceleration.

Results of Experiments and Discussion

The results of the experiments are presented in Tables 1-4 and the figure. In the four control series, 11,268 F_1 flies were examined and no crossovers found among them. In the earlier study, inspection of 10,282 F_1 flies had also failed to detect a single crossover. Since, on the whole, there had been no exceptional individuals among the 21,550 flies examined, we took zero as the spontaneous percentage incidence of crossing over in our calculation of the difference between the experimental groups and the control.
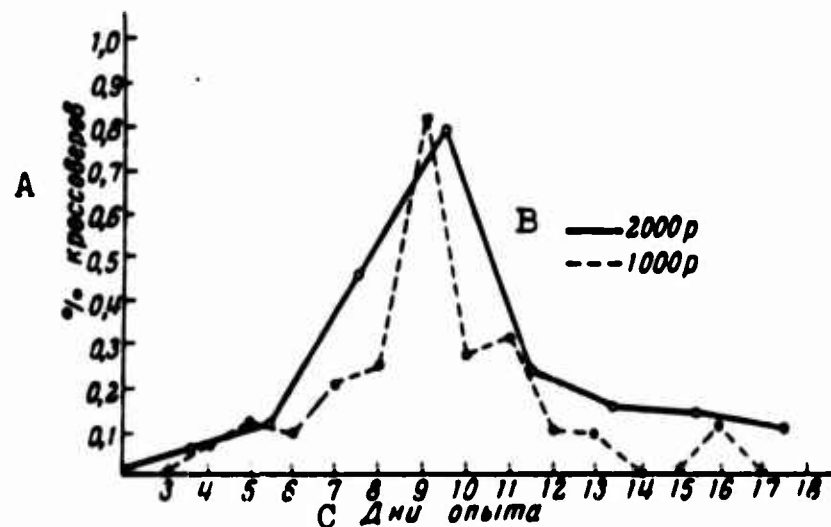
Incidence of crossovers after irradiation of males with γ-rays. A) % of crossovers; B) 2000 r; C) days of experiment.

The crossover yield after irradiation can be assigned quite rigorously to specific days. This comes particularly clearly to the fore in the experiment in which the series were renewed daily (Fig, Table 1). On the 9th day after irradiation, the curve in either experiment shows a sharp peak, in either direction from which the yield of crossovers drops off sharply. Thus, the stages at which crossing over in the males takes place with noticeable frequency occupy a very short time interval, and minor variations in the technique (storage temperature, less rapid depletion of sperm) can shift the results sharply. After irradiation

- 236 -

with a dose of 2000 r, the peak is less distinct, an effect undoubtedly due to the procedure of crossing at two-day intervals in this experiment.

The percentage of crossovers induced by irradiation at the 9th-11th days is the same, within the limits of error, in the six experimental series conducted (Table 2). The average crossover frequency, based on the six experiments, was 0.43 ± 0.05%. The relatively low sensitivity of this class of genetic changes to irradiation makes the test unsuitable for biological dosimetry of small ionizing-radiation doses. However, it can be used as an auxiliary indicator in other tests, to provide a sharp determination of the meiotic stages.

TABLE 1

Incidence of Crossing Over after γ-irradiation

1 Доза, р		2 Дни после облучения															
		3	4	5	6	7	8	9	10	• 11	12	13	14	15	16	17	18
2000	Количество мух 3 4 Количество кроссоверов % ± m	3140 2(0) 0,06 ± 0,04		1774 2(1) 0,11 ± 0,08		443 2(1) 0,45 ± 0,32		2570 20(12) 0,78 ± 1,17		2662 6(4) 0,23 ± 0,09		2642 4(1) 0,15 ± 0,07		2160 3(1) 0,14 ± 0,08		1991 2(0) 0,10 ± 0,07	
1000	Количество мух 3 4 Количество кроссов.рев % + m		1919 1(0) 0,06 ± ± 0,06	1848 2(2) 0,11 ± ± 0,07	2115 2(1) 0,09 ± ± 0,07	988 2(2) 0,20 ± ± 0,14	1673 4(3) 0,24 ± ± 0,11	2012 16(9) 0,80± ±0,20	2640 7(3) 0,27 ± ± 0,10	1934 6(3) 0,31 ± ± 0,12	1904 2(0) 0,10 ± ± 0,07	2226 2(2) 0,09 ± ± 0,06	1754 0 0,00	1584 0 0,00	1791 2(1) 0,11 ± ± 0,08		

Note. The figures in parentheses indicate the number of individuals checked genetically.

1) Dose, r; 2) days after irradiation; 3) number of flies; 4) number of crossovers.

The appearance of crossing over under the influence of vibration was observed in all of the experimental series run (Table 3). This is confirmed by the data of the communication [6]. It is necessary, however, to note the absence of a distinct dependence of the effect on the time of vibration, which represents a departure from the results of the first study. Moreover, the magnitude of the effect in the present experiments was found to be considerably smaller. The differences noted

could hardly be explained by the use of a different strain of flies
(D-32 instead of D-18) and (or) by the absence of a rest period in the
vibration. The origin of these differences – and the same applies to
the entire process in which crossovers emerge under the influence of
vibration – is not clear at the present time. However, the very fact
that crossovers do appear suggests that crossing over in the ♂ takes
place not as a consequence, or not simply as a consequence, of true
chromosome ruptures, but on less essential disturbances in the cell nu-
cleus. There are data indicating that the most common class of muta-
tions – recessive lethals – do not arise under the influence of vibra-
tion [7].

It is interesting that of the 26 crossovers obtained after subjec-
tion to vibration, 20 (77%) appeared as a result of exchange of chrom-
osome segments between the genes b and cn, i.e., in the interval in
which the centromere is located, while the distances, in units of the
chromosome map, between the genes b cn and vg are approximately the
same. No such selectivity was observed under irradiation: of the 69 ex-
ceptional individuals, 31 (45%) appeared as a result of exchanges be-
tween the genes cn and vg. Thus, crossing over arises in more proximal
parts of the chromosome under the influence of vibration.

TABLE 2

Occurrence of Crossing Over Un-
der the Influence of γ-irradia-
tion in a Dose of 1000 r

№ серии 1	Количест- во мух 2	Количест- во кросс- оверов 3	% ± m
1	6325	27(15)	0,43 ± 0,08
2	2305	8(4)	0,35 ± 0,12
3	530	2(1)	0,38 ± 0,27
4	3526	17(11)	0,48 ± 0,12
5	1969	9(7)	0,46 ± 0,15
6	1351	6(3)	0,44 ± 0,18
Итого 4	16006	69 (41)	0,43 ± 0,05

1) Series No.; 2) number of flies;
3) number of crossovers; 4) Total.

TABLE 3

Occurrence of Crossing Over Under the Influence of Vibration and Acceleration

1 Условия опыта	2 Количество мух	3 Количество кроссоверов	% ± m
4 вибрация 5 1-я серия (4 часа)	1429	4(3)	0,28 ± 0,14
6 2-я серия (4 часа)	4207	13(5)	0,31 ± 0,09
7 Итого	5536	17(8)	0,30 ± 0,07
3-я серия (2 часа) 9	3477	9(6)	0,26 ± 0,09
8 ускорение 1-я серия 10	4568	0	0,00
2-я серия 11	3736	1(0)	0,03 ± 0,03
7 Итого	8304	1(0)	0,01±0,01

1) Conditions of experiment; 2) number of flies; 3) number of crossovers; 4) vibration; 5) 1st series (4 hours); 6) 2nd series (4 hours); 7) total; 8) acceleration; 9) 3rd series (2 hours); 10) 1st series; 11) 2nd series.

TABLE 4

Occurrence of Crossing Over On Combined Application of Vibration and Acceleration with γ-irradiation

1 Условия опыта	2 Количество мух	3 Количество кроссоверов	% ± m
4 Вибрация (4 часа) + 1000 p	2993	8(3)	0,27 ± 0,09
5 Вибрация (2 часа) + 1000 p	1118	3(3)	0,27 ± 0,16
6 1000 p + вибрация (4 часа)	2813	19(9)	0,68 ± 0,15
7 Ускорение + 2000 p	3681	31(21)	0,84 ± 0,15
8 1000 p + ускорение	4325	19(10)	0,44 ± 0,10

1) Conditions of experiment; 2) number of flies; 3) number of crossovers; 4) vibration (4 hours) + 1000 r; 5) vibration (2 hours) + 1000 r; 6) 1000 r + vibration (4 hours); 7) acceleration + 2000 r; 8) 1000 r + acceleration.

In our experiments, the acceleration did not induce crossing over in males (Table 3). Among the 8304 individuals examined, one exceptional case was found ($\female + cn\,vg$), but could not be verified genetically. Nor does this treatment produce recessive lethal mutations [8].

On combined subjection to vibration and subsequent irradiation, the number of crossovers that appeared was exactly the same as that observed when vibration was applied alone (Table 4). In all probability, the vibration may, while preserving the injurious effect proper, con-

- 239 -

tribute to a placement of the chromosomes — which persists for at least 1 hour — that favors restitutions of the chromosomes ruptureu by the ionizing radiation and interferes with their recombination. With the disturbances applied in this order, the vibration may be regarded as a protective factor. When they are applied in the reverse order (irradiation first, and then vibration), the extent of the total effect is approximately equal to the sum of the effect produced by each factor in isolation. Thus, vibration has no influence whatsoever on processes related to recovery from premutation injuries.

With one essential difference, the same general relationships prevailed for combined application of acceleration and irradiation. In the experiment in which acceleration preceded irradiation, the modifying influence of the mechanical factor was manifested clearly. Unlike vibration, however, acceleration amplified the effect of irradiation in a dose of 1000 r by a factor of approximately two. In this case, it may be assumed that the acceleration is modifying the effect of subsequent irradiation by affecting the positioning of homologous chromosomes. Acceleration following irradiation or applied alone had no influence whatsoever.

Conclusions. I. The frequency of crossing over in chromosome 2 of Drosophila melanogaster males under the influence of γ-irradiation, vibration and acceleration was studied.

2. The maximum incidence of crossovers, which indicates action upon rudimentary cells in the meiotic stages, occurred on the 9th day after γ-irradiation when the cultures were stored at a temperature of $25 + 1°$ C.

3. Vibration with an amplitude of 0.4 mm, a frequency of 70 cycles and duration up to 4 hours induced crossing over, showing greater effectiveness in the more proximal regions of the chromosome.

- 240 -

4. Acceleration to 4000 g was found to have no effect.

5. Vibration reduced the subsequent effect of γ-irradiation, while acceleration, on the contrary, increased the irradiation effect.

6. The effects add when vibration and acceleration are administered after γ-irradiation.

REFERENCES

1.   S. Zimmering. Genetics, 48, No. 1, 138, 1963.

2.   G.P. Parfenov. Collection entitled "Iskusstvennyye sputniki Zem-
      li" [Artificial Earth Satellites], No. 10. Izd-vo AN SSSR [Academy
      of Sciences Press], 1961, page 69.

3.   M.M. Tikhomirova. Collection entitled 'Issledovaniya po genetike"
      [Researches in Genetics], 1, Izd-vo LGU [Leningrad State Univer-
      sity Press], 1961, page 19.

4.   R. Savhagen. Hereditas, 47, No. 1, 44, 1961.

5.   S. Wolff and R. Borstel, Proc. Nat. Acad. Sci. USA, 40, No. 12,
      1938, 1954.

6.   E.A. Abeleva, G.P. Parfenov, Yu.A. Lapkin. Collection entitled
      "Iskusstvennyye sputniki Zemli" [Artificial Earth Satellites],
      No. 13, Izd-vo AN SSSR [Academy of Sciences USSR Press], 1962,
      page 119.

7.   Ya.L. Glembotskiy, G.P. Parfenov. Collection entitled "Problemy
      Kosmicheskoy biologii" [Problems of Space Biology], 2. Izd-vo AN
      SSSR [Academy of Sciences USSR Press], 1962, page 98.

8.   O. Reddi. Nature, 198, No. 4877, 316, 1963.

DISTRIBUTION LIST

DEPARTMENT OF DEFENSE	Nr. Copies	MAJOR AIR COMMANDS	Nr. Copies
		DDC	20
		AFSC	
		SCFDD	1
		TDBDP	10
		TDBTL	5
		TDGS	1
		TDC	1
HEADQUARTERS USAF		TDF	3
		TDEWG	2
AFNINDE	1	TDEWT	1
ARL (ARB)	1	TDFS	5
AFCIN-M	1	TDEEC (Minshall)	2
		AEDC (AEY)	1
		AFETR (MTW)	1
		AFFTC (FTF)	1
OTHER AGENCIES		AFMDC (MDF)	1
		AFWL (WLF)	1
AEC	2	AMD (AMRF)	1
ARMY (FSTC)	3	APGC (PGF)	1
ATD	2	ASD (ASFA)	25
CIA	1	BSD (BSF)	1
DIA	4	ESD (ESY)	1
NAFEC	1	RADC (RAY)	1
NASA (ATSS-T)	73	SSD (SSFI)	2
NAVY	3		
NSA	6		
OAR	1		
OTS	2		
PWS	1		
PGE	15		
RAND	1		
AFCRL (CRXLR)	1		
SPECTRUM	1		